

Analysis and Synthesis of Self-Synchronizing Chaotic Systems

Kevin M. Cuomo

RLE Technical Report No. 582

February 1994

**Research Laboratory of Electronics
Massachusetts Institute of Technology
Cambridge, Massachusetts 02139-4307**

This work was supported in part by the U.S. Air Force Office of Scientific Research under Grant AFOSR-91-0034-C, in part by the U.S. Navy Office of Naval Research under Grant N00014-93-1-0686, and in part by a subcontract from Lockheed Sanders, Inc. under the U.S. Navy Office of Naval Research Contract N00014-91-C-0125.



Analysis and Synthesis of Self-Synchronizing Chaotic Systems

by

Kevin M. Cuomo

Submitted to the Department of Electrical Engineering and Computer Science
on December 27, 1993, in partial fulfillment of the
requirements for the degree of
Doctor of Philosophy

Abstract

Chaotic systems provide a rich mechanism for signal design and generation, with potential applications to communications and signal processing. Because chaotic signals are typically broadband, noise-like, and difficult to predict, they can be used in various contexts, *e.g.*, as masks for information-bearing waveforms and as modulating waveforms in spread spectrum systems. Of practical significance are chaotic systems that possess the self-synchronization property. This property allows two identical chaotic systems to synchronize when the second system (receiver) is driven by the first (transmitter). A potential drawback to utilizing self-synchronizing chaotic systems in applications is that the analysis and synthesis of these systems is not well-understood due to their highly nonlinear nature. This thesis focuses on both of these critical areas.

In this thesis, we develop a systematic approach for *analyzing* the self-synchronization properties of general nonlinear systems. To further conceptualize the self-synchronization property, we exploit an identified equivalence between self-synchronization and stable error dynamics between the transmitter and receiver systems. We use this conceptualization to prove that self-synchronization in the Lorenz system is a result of globally stable error dynamics. We then address robustness of self-synchronizing chaotic systems and develop an approximate analytical error model that quantifies and explains the sensitivity of synchronization in the Lorenz system to perturbation of the drive signal.

The ability to *synthesize* new chaotic systems enhances their usefulness for practical applications. We develop and illustrate several systematic procedures for synthesizing new classes of high-dimensional dissipative chaotic systems that possess the self-synchronization property. The procedures vary in the number of drive signals required for synchronization and the resulting complexity of the system dynamics. Finally, the practical implications of this work are explored. Two techniques for embedding an information-bearing waveform in a chaotic carrier signal and for recovering the information at the receiver are developed and demonstrated using a Lorenz-based transmitter and receiver circuit.

Thesis Supervisor: Alan V. Oppenheim

Title: Distinguished Professor of Electrical Engineering

Acknowledgments

I would like to thank my advisor, Professor Alan V. Oppenheim, for his persistent encouragement and guidance during the course of this thesis. To have known him in his teaching, leadership, and mentorship roles, and to have had the opportunity to work closely with him has meant a great deal to me.

I thank my reader Professor S. H. Strogatz of the M.I.T. Mathematics Department for his motivational teachings of nonlinear dynamics, for his enthusiastic collaboration during the course of this thesis, and for inviting me to present my research to his nonlinear dynamics and chaos class.

I thank my readers Professor A. S. Willsky, and Professor G. W. Wornell of the M.I.T. Electrical Engineering and Computer Science Department for many helpful and motivating discussions during various stages of this work.

Thanks also to the entire M.I.T. Digital Signal Processing Group for providing a fun and stimulating research environment. I am very grateful for being a part of it.

I thank my supervisors Dr. D. Willner and Dr. K. Roth of M.I.T. Lincoln Laboratory for their patience and support during the time period of this degree. The financial support of the M.I.T. Lincoln Laboratory Staff Associate Program is also gratefully acknowledged.

Finally, a special thanks to my wife, Dr. Donna L. Cuomo, for her boundless love, patience, and support. Her many personal sacrifices over the past three years have enabled me to pursue and complete this thesis.

Contents

1	Introduction	15
1.1	Outline of the Thesis	18
2	Nonlinear Dynamics and Chaos	21
2.1	Equilibrium Points and Local Stability	22
2.2	Lyapunov's Direct Method	24
2.3	Quantifying Chaotic Behavior	29
2.3.1	Lyapunov Exponents	29
2.3.2	Attractor Dimension	32
3	Self-Synchronization in Chaotic Systems	37
3.1	Decomposing Chaotic Systems into Drive and Response Subsystems .	38
3.2	Determining the Stable Response Subsystems for General Nonlinear Systems	42
3.3	Equivalence Between Self-Synchronization and Asymptotic Stability .	53
4	Self-Synchronization and Nonlinear State Estimation	57
4.1	State Estimation of the Lorenz System	58
4.1.1	Continuous EKF	59
4.1.2	Linearized EKF	60
4.1.3	Process Noise	62
4.2	Performance Comparisons	63
5	Robustness and Signal Recovery in a Synchronized Chaotic System	69
5.1	Experiments to Demonstrate Robustness and Signal Recovery	70
5.1.1	Sensitivity of Synchronization to Additive White Noise	72
5.1.2	Sensitivity of Synchronization to Additive Speech	73
5.2	Determining the Synchronization Error Moment Equations	75
5.2.1	Approximate Approach	76
5.2.2	Exact Approach via Stochastic Calculus	79
5.3	Development of an Approximate Synchronization Error Model	87
5.3.1	Error Model Performance with Additive White Noise	95
5.3.2	Error Model Performance with Additive Speech	96
5.4	Summary	98

6	Synthesizing Self-Synchronizing Linear Feedback Chaotic Systems	103
6.1	x -Input/ x -Output LFBCSs	105
6.1.1	Conditions for Global Self-Synchronization	106
6.1.2	Conditions for Global Stability	107
6.1.3	A Systematic Synthesis Procedure	109
6.1.4	Linear Stability Analysis	110
6.1.5	Numerical Example	115
6.2	z -Input/ z -Output LFBCSs	119
6.2.1	Conditions for Global Self-Synchronization	122
6.2.2	Conditions for Global Stability	123
6.2.3	A Systematic Synthesis Procedure	125
6.2.4	Numerical Example	127
6.3	Summary	129
7	Synthesizing Self-Synchronizing Chaotic Arrays	135
7.1	Conditions for Global Self-Synchronization	138
7.2	Conditions for Global Stability	140
7.3	A Systematic Synthesis Procedure	142
7.4	Linear Stability Analysis	144
7.5	Numerical Example	153
7.6	Summary	157
8	Synthesizing a General Class of Synchronizing Chaotic Systems	161
8.1	Conditions for Global Self-Synchronization	163
8.2	Conditions for Global Stability	166
8.3	A Systematic Synthesis Procedure	168
8.4	Linear Stability Analysis	170
8.5	Numerical Examples	171
8.5.1	The Lorenz System	171
8.5.2	A Four-Dimensional Synchronizing Chaotic System	173
8.5.3	A Five-Dimensional Synchronizing Chaotic System	176
8.6	Summary	183
9	Applications of Self-Synchronizing Chaotic Systems	185
9.1	Lorenz-Based Circuit Implementations	186
9.1.1	The Transmitter Circuit	186
9.1.2	The Receiver Circuit	190
9.2	Chaotic Signal Masking and Recovery	194
9.2.1	Concept	195
9.2.2	Circuit Experiment	196
9.2.3	Model-Based Signal Recovery	197
9.3	Chaotic Binary Communications	202
9.3.1	Concept	202
9.3.2	Synchronization Error Analysis and Detection	203

9.3.3	Circuit Experiments	207
9.4	Summary	210
10	Conclusions and Suggestions for Future Research	213
10.1	Summary and Contributions	213
10.2	Future Research Directions	215
A	Linear Stability Analysis of z-Input/z-Output LFBCSs	217
B	Lorenz Transmitter and Receiver Circuit Components	221
C	Voltage-Controlled Resistor Circuit	223

List of Figures

2-1	<i>Illustration of Lyapunov's Direct Method.</i>	25
2-2	<i>Positive Definite Functions.</i>	26
2-3	<i>A Trapping Region for the Lorenz Flow.</i>	28
2-4	<i>Lyapunov Exponents of the Lorenz System.</i>	33
2-5	<i>Lyapunov Dimension of the Lorenz System.</i>	35
3-1	<i>Decomposing a Chaotic System into Drive and Response Subsystems.</i>	39
3-2	<i>Lorenz Synchronizing Receiver Representations: (a) Decomposed Form. (b) Cascade Form. (c) Combined (3-D) Form.</i>	41
3-3	<i>Synchronization of Transmitter and Receiver Signals in the Lorenz System. (a) $x(t)$ vs. $x_r(t)$. (b) $y(t)$ vs. $y_r(t)$. (c) $z(t)$ vs. $z_r(t)$.</i>	43
3-4	<i>SRS Tree for the Lorenz System.</i>	48
3-5	<i>SRS Tree for the Double Scroll System.</i>	51
3-6	<i>SRS Tree for the Rössler System.</i>	52
3-7	<i>Block Diagram of the Lorenz Synchronizing Receiver.</i>	56
4-1	<i>Block Diagram of the Continuous EKF for the Lorenz System.</i>	60
4-2	<i>Block Diagram of the Linearized EKF.</i>	61
4-3	<i>Numerical Experiment to Evaluate the Output CER vs. Input CPR.</i>	65
4-4	<i>Performance Comparison: Lorenz Receiver vs. Continuous EKF.</i>	66
4-5	<i>Performance Comparison: Lorenz Receiver vs. Linearized EKF.</i>	67
4-6	<i>Sensitivity to Modeling Errors: Lorenz Receiver and Continuous EKF.</i>	68
5-1	<i>Output CER_x, CER_y, and CER_z vs. Input CPR for the Lorenz Synchronizing Receiver.</i>	73
5-2	<i>True Power Spectra of the Error Signals: (a) $E_x(\omega)$. (b) $E_y(\omega)$. (c) $E_z(\omega)$.</i>	74
5-3	<i>Power Spectra of $x(t)$ and $p(t)$ when the Perturbation is a Speech Signal.</i>	75
5-4	<i>Power Spectra of $p(t)$ and $\hat{p}(t)$ when the Perturbation is a Speech Signal.</i>	76
5-5	<i>(a) Original Speech. (b) Received Signal. (c) Recovered Speech.</i>	77
5-6	<i>Cascade System Representation of the Second Moment Equations.</i>	82
5-7	<i>Prediction of the Output CER From the Second Moment Equation.</i>	85
5-8	<i>(a) Prediction of the Synchronization Error Variances From the Second Moment Equation. (b) Synchronization Error Correlation Coefficients.</i>	86

5-9	(a) <i>Perturbation-to-Error Ratio vs. Lorenz System Parameter σ (Input CPR=10 dB).</i> (b) <i>Perturbation-to-Error Ratio vs. Lorenz System Parameter b (Input CPR=10 dB).</i>	88
5-10	(a) <i>A Sample Function of $x(t)$.</i> (b) <i>A Sample Function of $y(t)$.</i> (c) <i>Power Spectra of $x(t)$ and the Piecewise Constant Approximation of $x(t)$.</i>	91
5-11	<i>Spread Spectrum Model of the Lorenz Error Dynamics.</i>	92
5-12	<i>Equivalent Linear Time-Invariant Model of the Lorenz Error Dynamics.</i>	94
5-13	(a) <i>Pole-Zero Plot for $H_{11}(s)$.</i> (b) <i>Pole-Zero Plot for $H_{12}(s)$.</i> (c) <i>Magnitude Response of $H_{11}(s)$ and $H_{12}(s)$.</i> (d) <i>Phase Response of $H_{11}(s)$ and $H_{12}(s)$.</i>	95
5-14	<i>True and Estimated Power Spectra of the Error Signals: (a) $E_x(\omega)$.</i> (b) $E_y(\omega)$. (c) $E_z(\omega)$	96
5-15	<i>Dynamical System Representation of the Message Recovery Process.</i>	97
5-16	(a) <i>Power Spectrum of $p(t)$ and the True and Estimated Power Spectrum of $e_x(t)$.</i> (b) <i>Power Spectrum of $p(t)$ and the True and Estimated Power Spectrum of $\hat{p}(t)$.</i>	99
5-17	<i>Speech Waveforms: (a) True Recovered Message.</i> (b) <i>Recovered Message using the Equivalent Linear Time-Invariant Model.</i>	100
6-1	<i>Communicating with Linear Feedback Chaotic Systems.</i>	104
6-2	(a) <i>Eigenfrequency Diagram for a 5-Dimensional x-input/x-output LFBCS.</i> (b) <i>Graphical Determination of the Bifurcation Parameter.</i> (c) <i>Bifurcation Diagram.</i>	117
6-3	<i>Lyapunov Exponents for a 5-Dimensional x-input/x-output LFBCS.</i>	118
6-4	<i>Lyapunov Dimension for a 5-Dimensional x-input/x-output LFBCS.</i>	118
6-5	<i>Chaotic Attractor for a 5-Dimensional x-input/x-output LFBCS.</i>	120
6-6	<i>Self-Synchronization in a 5-Dimensional x-input/x-output LFBCS.</i>	121
6-7	(a) <i>Eigenfrequency Diagram for a 5-Dimensional z-input/z-output LFBCS.</i> (b) <i>Graphical Determination of the Bifurcation Parameter.</i> (c) <i>Bifurcation Diagram.</i>	128
6-8	<i>Lyapunov Exponents for a 5-Dimensional z-input/z-output LFBCS.</i>	130
6-9	<i>Lyapunov Dimension for 5-Dimensional LFBCSs.</i>	130
6-10	<i>Chaotic Attractor for a 5-Dimensional z-input/z-output LFBCS.</i>	131
6-11	<i>Self-Synchronization in 5-Dimensional LFBCSs.</i>	132
7-1	<i>Communicating with Chaotic Arrays.</i>	136
7-2	<i>Stability Diagram for a 7-Dimensional Chaotic Array.</i>	155
7-3	<i>Lyapunov Exponents for a 7-Dimensional Chaotic Array.</i>	156
7-4	<i>Lyapunov Dimension for a 7-Dimensional Chaotic Array.</i>	156
7-5	<i>Self-Synchronization in a 7-Dimensional Chaotic Array.</i>	158
8-1	<i>Communicating with a General Class of Synchronizing Chaotic Systems.</i>	162
8-2	<i>Lyapunov Exponents for a 4-Dimensional Chaotic System.</i>	175
8-3	<i>Lyapunov Dimension for a 4-Dimensional Chaotic System.</i>	176
8-4	<i>Chaotic Attractor Projections for a 4-Dimensional Chaotic System ($r = 60$).</i>	177

8-5	<i>Self-Synchronization in a 4-Dimensional Chaotic System.</i>	178
8-6	<i>Lyapunov Exponents for a 5-Dimensional Chaotic System.</i>	181
8-7	<i>Lyapunov Dimension for a 5-Dimensional Chaotic System.</i>	181
8-8	<i>Chaotic Attractor Projections for a 5-Dimensional Chaotic System ($r = 90$).</i>	182
8-9	<i>Self-Synchronization in a 5-Dimensional Chaotic System.</i>	183
9-1	<i>Lorenz-Based Chaotic Circuit.</i>	187
9-2	<i>Circuit Data: (a) A sample function of $u(t)$. (b) Averaged power spectrum of $u(t)$. (c) A sample function of $v(t)$. (d) Averaged power spectrum of $v(t)$.</i>	189
9-3	<i>Circuit Data: (a) Chaotic attractor projected onto uv-plane. (b) Chaotic attractor projected onto uw-plane.</i>	190
9-4	<i>Circuit Data: (a) Autocorrelation functions $R_{uu}(\tau)$ and $R_{vv}(\tau)$. (b) Probability density of $u(t)$. (c) Probability density of $v(t)$.</i>	191
9-5	<i>Circuit Data: Poincaré section.</i>	192
9-6	<i>Circuit Data: First return map.</i>	192
9-7	<i>Self-Synchronizing Receiver Circuit.</i>	193
9-8	<i>Circuit Data: Synchronization of transmitter and receiver signals.</i>	194
9-9	<i>Chaotic Signal Masking and Recovery System.</i>	195
9-10	<i>Circuit Data: Power spectra of $u(t)$ and $p(t)$ when the perturbation is a speech signal.</i>	196
9-11	<i>Circuit Data: Power spectra of $p(t)$ and $\hat{p}(t)$ when the perturbation is a speech signal.</i>	197
9-12	<i>(a) Recovered Speech (simulation) (b) Recovered Speech (circuit).</i>	198
9-13	<i>Model-Based Signal Recovery.</i>	199
9-14	<i>Communicating Binary-valued Bit Streams with Self-Synchronizing Chaotic Systems.</i>	203
9-15	<i>Normalized Synchronization Error vs. Parameter Mismatch (percent).</i>	206
9-16	<i>Circuit Data: (a) Binary waveform used to modulate the b parameter of the Lorenz transmitter equations. (b) Averaged power spectrum of the drive signal with and without parameter modulation.</i>	209
9-17	<i>Circuit Data: (a) Binary modulation waveform. (b) Synchronization error power. (c) Recovered binary waveform.</i>	211
C-1	<i>Voltage-Controlled Resistor Circuit.</i>	224

Chapter 1

Introduction

For many years, there has been tremendous interest in the study of nonlinear dynamical systems that exhibit chaotic behavior. It is now well-understood that chaotic solutions of purely deterministic systems are an inherent feature of many nonlinear systems. Chaotic behavior has been reported in a broad range of scientific disciplines, including astronomy, biology, chemistry, ecology, engineering, and physics. Much of this research has focused on dissipative chaotic systems. Such systems are characterized by limiting trajectories that are attracted to a region in state space that has zero volume and fractional dimension. Trajectories on this limiting set are locally unstable, yet remain bounded within some region of state space. These sets are termed *strange attractors* and exhibit a *sensitive dependence on initial conditions* in the sense that any two arbitrarily close initial conditions will lead to trajectories that rapidly diverge. This inherent instability makes long term predictability of chaotic signals difficult because small uncertainties in the initial state will be exponentially amplified.

Synchronization of dynamical systems possessing these properties would seem to be counter-intuitive. In 1990, however, it was discovered that a certain class of dissipative chaotic systems possess a self-synchronization property [1, 2, 3]. This property allowed two identical chaotic systems to synchronize when the second system was driven by the first. In certain communication contexts, the first system can be viewed as the transmitter and the second system as the receiver.

The phenomenon of synchronization has been of longstanding interest and studied

extensively. However, these studies had typically focused on the complex interactions among mutually coupled oscillator systems. The best known example is the motion of the earth and moon. Other more recent examples include: spatially distributed nonlinear systems such as coupled lasers [4], phase-locked loops [5], neural networks [6], and biological systems [7, 8]. There is, however, a fundamental difference between synchronization in mutually coupled systems and self-synchronizing systems. For the latter systems the coupling is one-way, *i.e.*, only from the transmitter to the receiver.

The concepts of self-synchronization and chaos from purely deterministic systems suggest some potential applications - - one of the main motivating forces behind this thesis. Because chaotic signals are typically broadband, noise-like, and difficult to predict, we have proposed their use in various contexts, *e.g.*, as masks for information-bearing waveforms and as modulating waveforms in spread spectrum systems [9, 10]. These proposed applications exploit the self-synchronization property to faithfully recover the information at the receiver. A major drawback to utilizing self-synchronizing chaotic systems in communication applications is that the *analysis* and *synthesis* of these systems is not well-understood due to their highly nonlinear nature. This thesis focuses on both of these critical areas.

With respect to analysis, we first develop a systematic approach for examining the self-synchronization properties of general nonlinear systems. Although this approach provides a valuable analysis tool, it does not provide much insight for understanding the mechanism underlying the self-synchronization property. To overcome this limitation, we reformulate our analysis approach from the viewpoint of nonlinear stability theory. This approach enables us to identify an equivalence between self-synchronization in chaotic systems and asymptotically stable error dynamics between the transmitter and receiver systems. We then prove the global self-synchronization property of the Lorenz system and provide a clear mathematical framework for our subsequent analysis and synthesis techniques.

To utilize the Lorenz system in applications, it is important to examine the sensitivity of synchronization when a perturbation signal is added to the synchronizing drive signal. We establish an analogy between synchronization in chaotic systems,

nonlinear observers for deterministic systems, and state estimation in probabilistic systems. Then we show numerically that the performance of the Lorenz receiver as a nonlinear observer compares favorably with two well-known extended Kalman filter algorithms when the perturbation is white noise. The normalized error in synchronization of each state variable is significantly less than the normalized error in the drive signal, provided that the input chaos-to-perturbation ratio (CPR) is larger than some critical value. We use stochastic calculus to determine the exact first and second moments of the synchronization error signals when the perturbation is white noise. This analysis explains the observed threshold effect at low input CPRs. In addition, the development of an equivalent linear time-invariant error model quantifies the sensitivity of synchronization in terms of the spectral characteristics of the perturbation signal. This model explains why the synchronization is robust to wideband perturbations, and why low-level speech signals or other narrowband perturbations can be accurately recovered at the receiver even though the synchronization error is comparable in power to the message itself.

We next turn our attention to the synthesis problem. In [11], it was demonstrated that it is possible to create a five-dimensional chaotic system by augmenting the Lorenz system with additional states. That approach, however, involves considerable trial and error. In this thesis, we develop several *systematic* procedures for synthesizing new classes of high-dimensional dissipative chaotic systems that possess the self-synchronization property. The first class of systems that we introduce are referred to as *linear feedback chaotic systems* (LFBCSs). LFBCSs are composed of a low-dimensional chaotic system and a linear feedback system. We focus on LFBCSs that utilize the Lorenz system as the chaotic system component and develop systematic synthesis procedures for this type of LFBCS. A second class of systems generalizes the LFBCS concept by allowing for multiple Lorenz systems and a linear system to be combined into a *chaotic array*. A systematic procedure for synthesizing this class of systems is also developed. The third class of systems represent a further generalization of these concepts; they eliminate the necessity of the linear system and, therefore, consist of an entirely nonlinear system. A systematic synthesis capability

is provided which allows high-dimensional non-Lorenz self-synchronizing chaotic systems to be designed. The synthesis techniques vary in the number of drive signals required for synchronization and the resulting complexity of the system dynamics. The flexibility afforded by the various synthesis techniques enhances the usefulness of synchronized chaotic systems for communications and signal processing.

Having a strong theoretical understanding of the concept of self-synchronization in chaotic systems, we next consider some applied aspects of these systems. First, we show that the Lorenz transmitter and receiver systems can be implemented as simple analog circuits using commercially available hardware. The performance of these circuits is shown to be in excellent agreement with numerical and theoretical predictions. The desire to utilize the Lorenz circuits for private communications led us to develop two techniques for embedding an information-bearing waveform in the chaotic drive signal, and for recovering the information with the synchronizing receiver. With the first approach, we show that low-level speech signals can be privately transmitted and recovered with the receiver circuit. The second approach allows binary-valued bit streams to privately transmitted and recovered. While these two approaches do not represent the ultimate in privacy or practicality, they do mark an important starting point for the field.

1.1 Outline of the Thesis

The thesis is organized as follows. In Chapter 2, we summarize some relevant topics in nonlinear dynamics and chaos, and establish the notation used throughout the thesis. The emphasis of this summary is on the local stability analysis of equilibrium points, Lyapunov's direct method for examining global stability, and the concepts of Lyapunov exponents and attractor dimension for chaotic systems. Each of these topics plays a useful role throughout the thesis and the inclusion of this chapter makes the thesis self-contained. The reader can, however, omit this chapter without loss of continuity.

In Chapter 3, we generalize the ideas of chaotic system decomposition and self-

synchronization, and develop a systematic approach for determining all of the stable subsystems of general nonlinear systems. We then identify an equivalence between self-synchronization and stable error dynamics. This equivalence allows us to prove the global self-synchronization property of the Lorenz system and forms the basis for our analysis and synthesis techniques discussed in subsequent chapters.

In Chapter 4, we perform numerical experiments that quantify the sensitivity of synchronization in the Lorenz system when white noise is added to the drive signal. To calibrate the performance of the Lorenz receiver, we compare its performance against two well-known extended Kalman filter algorithms.

In Chapter 5, we perform a theoretical analysis of self-synchronization robustness and signal recovery in the Lorenz system. We use stochastic calculus to determine the exact first and second moments of the synchronization error signals when the drive signal is perturbed by white noise. An approximate analytical error model explains both the robustness of synchronization to wideband perturbations and why speech or other narrowband perturbations can be faithfully recovered at the receiver.

In Chapter 6, we synthesize a new class of chaotic systems called linear feedback chaotic systems (LFBCSs). The LFBCSs that we consider are composed of the Lorenz system and an N -dimensional linear feedback system. Our primary theoretical results include the development of self-synchronization and global stability conditions for this class of systems. Linear stability analysis leads to an approach for estimating the critical value of the bifurcation parameter at the onset of chaotic behavior. We also suggest a systematic procedure for synthesizing new LFBCSs.

In Chapter 7, we develop an approach for synthesizing chaotic arrays that consist of an arbitrary number of Lorenz oscillators and an N -dimensional linear system. The theoretical results include: *(i)* the development of self-synchronization conditions for this class of systems, *(ii)* the development of global stability conditions for this class of systems, and *(iii)* a systematic synthesis procedure.

In Chapter 8, we develop an approach for synthesizing *a general class of self-synchronizing chaotic systems*. A systematic synthesis procedure is used to show that the Lorenz system is only one member of a more general class of three-dimensional

chaotic systems which possess the self-synchronization property. To further illustrate the simplicity and generality of the synthesis procedure, the design of higher dimensional chaotic systems is performed.

In Chapter 9, an analog circuit implementation of the Lorenz system is used to demonstrate two potential approaches to private communications based on synchronized chaotic signals and systems.

Chapter 10 summarizes the main contributions of this thesis and suggests some directions for future research.

Chapter 2

Nonlinear Dynamics and Chaos

In the main part of the thesis, we will need to utilize various well-known analysis techniques in nonlinear dynamics and chaos. In particular, local stability analysis, Lyapunov's direct method, and the concepts of Lyapunov exponents and attractor dimension play key roles throughout the thesis. This chapter summarizes each of these topics, with emphasis on nonlinear systems represented by a set of first-order ordinary differential equations. While the inclusion of this chapter makes the thesis self-contained, the reader can, however, omit this chapter without loss of continuity.

We begin by discussing the local stability analysis of nonlinear systems near the equilibrium points. This analysis proves useful in later chapters where it is necessary to find conditions on the system's parameters such that all of the equilibrium points will be unstable. We then discuss Lyapunov's direct method. This method is useful for examining the global stability of nonlinear systems and for determining trapping regions for a dissipative chaotic flow. Finally, we discuss some useful measures of chaotic behavior, in particular, the notions of Lyapunov exponents and attractor dimension. These measures are useful for confirming and comparing chaotic behavior for the various nonlinear systems that we consider.

2.1 Equilibrium Points and Local Stability

Throughout this thesis, we will focus our analysis and synthesis efforts on nonlinear systems which are representable by a set of ordinary differential equations of the form

$$\dot{\mathbf{x}} = \mathbf{f}(\mathbf{x}), \quad \mathbf{x} \in R^N . \quad (2.1)$$

For simplicity, we will always assume that $\mathbf{f}(\mathbf{x})$ is a smooth function so that the basic existence-uniqueness theorems for ordinary differential equations apply to (2.1).

A typical starting point for the analysis of (2.1) is to determine the equilibrium (fixed) points and to perform a local stability analysis. The fixed points, \mathbf{x}_0 , satisfy $\mathbf{f}(\mathbf{x}_0) = 0$. Unfortunately, the determination of the zeros of a nonlinear function is often not analytically tractable. There are, however, well-known numerical techniques, such as the Newton-Raphson method, which are well-suited to this problem.

For the purpose of discussion, let us assume that the fixed points of (2.1) have been determined. The behavior of solutions near \mathbf{x}_0 can be examined by linearizing (2.1) at \mathbf{x}_0 . The linearized system is given by

$$\delta\dot{\mathbf{x}} = D\mathbf{f}(\mathbf{x}_0)\delta\mathbf{x}, \quad \delta\mathbf{x} \in R^N , \quad (2.2)$$

where $\delta\mathbf{x} = \mathbf{x} - \mathbf{x}_0$ and where $D\mathbf{f} = [\partial f_i / \partial x_j]$ is the system's Jacobian matrix. Because equation (2.2) is linear in $\delta\mathbf{x}$, the local stability of this system can be easily determined from the eigenvalues of the Jacobian matrix. Moreover, if $D\mathbf{f}(\mathbf{x}_0)$ has no zero or purely imaginary eigenvalues, then the local stability of solutions to (2.1) near \mathbf{x}_0 is determined by the linearization [12]. This result is particularly useful in later chapters where it is necessary to determine the critical parameter values for which the fixed points of a nonlinear system undergo an abrupt change in stability. To illustrate these concepts, the fixed points of the chaotic Lorenz system are determined and a local stability analysis is performed.

The Lorenz equations, first introduced by E. N. Lorenz as a simplified model of

fluid convection [13], are given by

$$\begin{aligned} \dot{x} &= \sigma(y - x) \\ \dot{y} &= rx - y - xz \\ \dot{z} &= xy - bz \end{aligned} \quad (2.3)$$

where σ , r , and b are positive parameters. By varying r , the qualitative behavior of solutions to (2.3) can change abruptly. Abrupt changes in the qualitative behavior of a dynamical system are referred to as *bifurcations* and, in the case of the Lorenz system, r is commonly referred to as the *bifurcation parameter*. The critical values of r for which local bifurcations occur can be determined through linear stability analysis.

The first step is to determine the fixed points of the Lorenz system - - the origin is clearly a fixed point for all parameter values. Additionally, a pair of nontrivial fixed points exists when $r \geq 1$. The state space location of these fixed points is given by $\mathbf{x}_p = (\pm\sqrt{b(r-1)}, \pm\sqrt{b(r-1)}, (r-1))$. The Jacobian matrix of the Lorenz system evaluated at the origin ($\mathbf{x}_0 = \mathbf{0}$) is given by

$$D\mathbf{f}(\mathbf{0}) = \begin{bmatrix} -\sigma & \sigma & 0 \\ r & -1 & 0 \\ 0 & 0 & -b \end{bmatrix} .$$

The eigenvalue at $-b$ represents a stable mode since $b > 0$. The characteristic polynomial for the upper 2×2 block is given by

$$\lambda^2 + (\sigma + 1)\lambda + \sigma(1 - r) = 0.$$

The two roots of this characteristic polynomial are in the left-half plane for $r < 1$. For $r > 1$, one root is in the right-half plane and represents an unstable mode at the origin. Thus, r is a bifurcation parameter for the Lorenz system because a slight variation in r can abruptly alter the system's local stability.

The Jacobian matrix of the Lorenz system evaluated at the fixed point pair ($\mathbf{x}_0 =$

\mathbf{x}_p) is given by

$$Df(\mathbf{x}_p) = \begin{bmatrix} -\sigma & \sigma & 0 \\ 1 & -1 & \mp\sqrt{b(r-1)} \\ \pm\sqrt{b(r-1)} & \pm\sqrt{b(r-1)} & -b \end{bmatrix} .$$

The characteristic polynomial of $Df(\mathbf{x}_p)$ is given by

$$\lambda^3 + (\sigma + b + 1)\lambda^2 + b(\sigma + r)\lambda + 2b\sigma(r - 1) = 0 . \quad (2.4)$$

The critical value of r , when a root of (2.4) crosses from the left-half plane to the right-half plane, can be determined by applying the Routh-Hurwitz criterion. This critical value, r_c , is given by

$$r_c = \frac{\sigma(\sigma + b + 3)}{\sigma - b - 1} . \quad (2.5)$$

As r is varied, a local bifurcation occurs when $r = r_c$. For $r > r_c$, the fixed point pair is unstable. Thus, for $r > \max(1, r_c)$ all fixed points of the Lorenz equations are unstable. Assuming that the trajectories remain bounded, either limit cycles or a chaotic attractor will exist. In Section 2.2, we utilize Lyapunov's direct method to show that all trajectories of the Lorenz system remain bounded for all positive parameter values. The interested reader may consult [12, 13, 14] for a more in-depth analysis of the Lorenz equations.

2.2 Lyapunov's Direct Method

Lyapunov's direct method involves determining a family of closed curves ($N = 2$) or closed surfaces ($N > 2$) in state space such that the general behavior of nearby trajectories of a dynamical system can be examined. The best way to show how this works is by example.

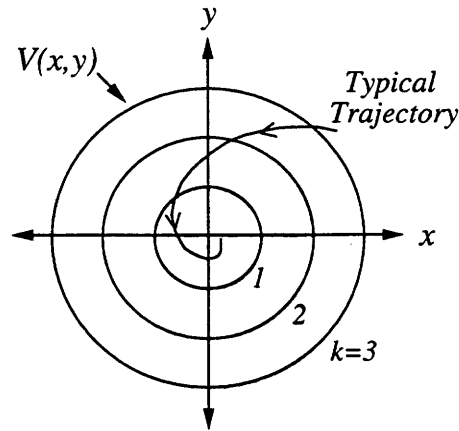


Figure 2-1: *Illustration of Lyapunov's Direct Method.*

Example (Jordan and Smith [15])

In this example, consider the global stability of the origin for the system

$$\dot{x} = -y - x^3, \quad \dot{y} = x - y^3 .$$

To solve this problem, consider the family of closed curves $V(x, y) = x^2 + y^2 = k$, where k is a positive scalar. For each fixed $k > 0$, $V(x, y)$ defines a circle enclosing the origin in the xy -plane as illustrated in figure 2-1. We wish to show that for any point on any of these circles, the state space trajectory through this point is directed toward the interior of the circle. If this property holds for all $k > 0$, then the origin is globally asymptotically stable. To show that this property holds, the total derivative of $V(x, y)$ is evaluated along trajectories. Specifically,

$$\frac{dV(x(t), y(t))}{dt} = \frac{\partial V}{\partial x} \dot{x} + \frac{\partial V}{\partial y} \dot{y} = -2(x^4 + y^4) .$$

Since $\dot{V}(x, y)$ is negative for all $(x, y) \neq 0$, the trajectories move continuously to smaller and smaller circles and eventually approach the origin. This shows that the origin is globally asymptotically stable.

In higher dimensional problems, $V(\mathbf{x})$ is a positive definite scalar function of N components (x_1, \dots, x_N) . By evaluating the total derivative of $V(\mathbf{x})$, we can examine

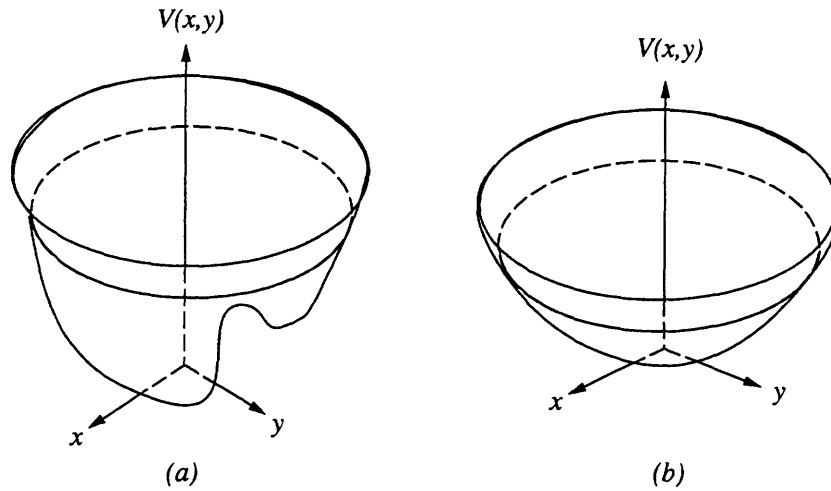


Figure 2-2: *Positive Definite Functions.*

the behavior of trajectories in high-dimensional state spaces. Specifically, the total derivative of $V(\mathbf{x})$ along trajectories is given by

$$\frac{dV(\mathbf{x}(t))}{dt} = \sum_{i=1}^N \frac{\partial V}{\partial x_i} f_i(\mathbf{x}) ,$$

where $f_i(\mathbf{x})$ is the component of the vector field associated with the i^{th} state equation of the nonlinear system. If $\dot{V}(\mathbf{x})$ is a negative definite function, then the origin in state space is globally asymptotically stable. In general, positive definite functions may have multiple extrema as illustrated in figure 2-2(a). If, however, $\dot{V}(\mathbf{x})$ is negative definite, then $V(\mathbf{x})$ exhibits a single global minimum at the origin as illustrated in figure 2-2(b). Functions $V(\mathbf{x})$ with this property are called *Lyapunov functions*. In later chapters, we will find Lyapunov functions particularly useful for examining the global stability of nonlinear systems.

In problems of a more general nature, it is often the case that stable fixed points do not exist, yet all trajectories remain bounded in state space. To examine the global behavior of trajectories in these systems, we consider quadratic positive definite functions of the form

$$V(\mathbf{x}) = \frac{1}{2}(\mathbf{x} - \mathbf{c})^T P(\mathbf{x} - \mathbf{c}) = k, \quad (2.6)$$

where P is a symmetric $N \times N$ positive definite matrix and k is a positive scalar. Geometrically, (2.6) represents a family of ellipsoids in state space with \mathbf{c} defining the location of its center. Of particular importance for global stability analysis is the determination of a closed surface S for which $\dot{V}(\mathbf{x}) = 0$. If $\dot{V}(\mathbf{x}) < 0$ for all \mathbf{x} outside S , then any ellipsoid T from the family (2.6) that contains S will suffice as a global *trapping region* for the N -dimensional flow. This means that all trajectories will eventually enter T and remain in T for all time thereafter. Finding a trapping region may be a difficult task; however, if one can be found then it can be used to prove that all trajectories remain bounded for all $t > 0$.

It is well-known that the Lorenz system provides an example of a nonlinear system for which an ellipsoidal trapping region can be analytically determined. As we show below, an ellipsoid from the family

$$V(\mathbf{x}) = \frac{1}{2} (rx^2 + \sigma y^2 + \sigma(z - 2r)^2) = k, \quad k > 0 \quad (2.7)$$

will determine a trapping region for the Lorenz flow for k sufficiently large.

The total derivative of $V(\mathbf{x})$ is given by

$$\dot{V}(\mathbf{x}) = -\sigma r x^2 - \sigma y^2 - \sigma(z - r)^2 + \sigma b r^2 .$$

By setting $\dot{V}(\mathbf{x}) = 0$ and rearranging terms, we obtain

$$\frac{x^2}{br} + \frac{y^2}{br^2} + \frac{(z - r)^2}{r^2} = 1 . \quad (2.8)$$

Equation (2.8) represents an ellipsoid in state space. This ellipsoid plays the role of the closed surface S . Since $\dot{V} < 0$ for all \mathbf{x} outside of S , any ellipsoid T from the family (2.7) which contains S will suffice as a trapping region for the Lorenz flow. Figure 2-3 illustrates the trapping region T and the $\dot{V}(\mathbf{x}) = 0$ ellipsoid S .

Another key feature of the Lorenz flow is that it is highly dissipative. This can be shown by computing the divergence of the vector field for the Lorenz equations as

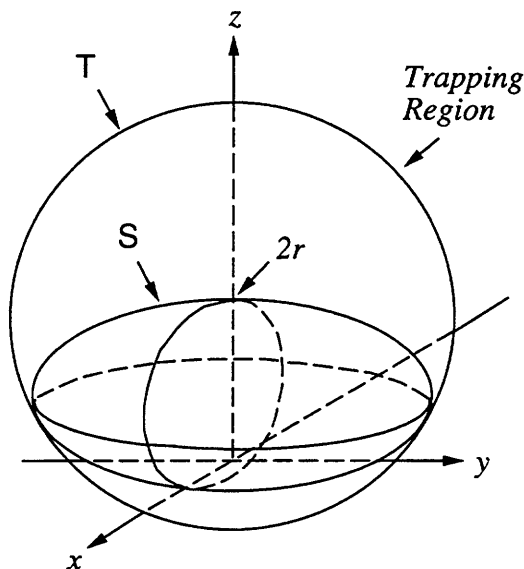


Figure 2-3: A Trapping Region for the Lorenz Flow.

follows,

$$\nabla \cdot \dot{\mathbf{x}} = \frac{\partial \dot{x}}{\partial x} + \frac{\partial \dot{y}}{\partial y} + \frac{\partial \dot{z}}{\partial z} = -(\sigma + 1 + b) .$$

Since the divergence is a negative constant, it follows that any volume in state space will contract exponentially fast [14]. The use of the divergence operator will be shown in Chapters 6-8 to be important for ensuring that our synthesis procedures produce chaotic systems which are dissipative.

In summary, linear stability analysis of the Lorenz system (Section 2.1) showed that for $r > \max(1, r_c)$ all of the fixed points are unstable and therefore the motion is non-trivial. Lyapunov's direct method was then used to illustrate that the Lorenz flow is confined to an ellipsoidal region in state space for all positive parameter values. Furthermore, invariant tori are not possible in the Lorenz system, because the divergence of the vector field is a negative constant. This property ensures that the Lorenz system is dissipative with exponentially fast volume contraction. This analysis alone does not guarantee the existence of chaotic behavior since the possibility for limit cycles exists. A dynamical system which behaves chaotically must exhibit a positive Lyapunov exponent. This issue is discussed in the next section.

2.3 Quantifying Chaotic Behavior

In this section, we discuss the concepts of Lyapunov exponents and attractor dimension for dissipative chaotic systems. These concepts are used to measure and quantify the chaotic behavior of the various nonlinear systems that we consider in subsequent chapters of this thesis.

2.3.1 Lyapunov Exponents

Lyapunov exponents are the average exponential rates of divergence or convergence of nearby trajectories in a dynamical system. Positive Lyapunov exponents correspond to diverging trajectories in state space and set the time scale for reliable prediction of future states. Negative Lyapunov exponents correspond to converging trajectories in state space and set the time scale on which transient motion will decay [16]. In between these two extremes are the zero Lyapunov exponents which correspond to flow along the trajectory. If at least one Lyapunov exponent of a dynamical system is positive, then a volume element in state space will expand in some direction and nearby trajectories will diverge. The exponential expansion of a chaotic flow implies that diverging trajectories must experience a repeated *folding* process in order for the motion to remain bounded. Loosely speaking, each positive Lyapunov exponent reflects a “direction” for which the folding process takes place and trajectories become decorrelated. This dynamical behavior leads to a sensitive dependence on initial conditions and is a primary feature of every chaotic system.

Lyapunov exponents are most easily understood by considering a one-dimensional discrete-time map of the form

$$x_{n+1} = f(x_n), \quad x \in R .$$

Suppose that the initial state of this system is given by $x'_0 = x_0 + \delta x_0$, where δx_0 represents an infinitesimal error in the true initial state x_0 . The error in specifying

x_n is given by

$$\begin{aligned}\delta x_n &= x'_n - x_n = f^n(x'_0) - f^n(x_0) \\ &\approx Df^n(x_0)\delta x_0 ,\end{aligned}$$

where f^n denotes the n -fold composition, $f^n = f \circ \dots \circ f$. Applying the chain rule for differentiation we can write

$$Df^n(x_0) = Df(x_{n-1})Df(x_{n-2}) \cdots Df(x_0) ,$$

and therefore, the average rate of exponential growth of δx_n is given by

$$\left| \frac{\delta x_n}{\delta x_0} \right| = \prod_{i=0}^{n-1} |Df(x_i)| = e^{\lambda n} .$$

The Lyapunov exponent, λ , can then be expressed as

$$\lambda = \lim_{n \rightarrow \infty} \frac{1}{n} \sum_{i=0}^{n-1} \log |Df(x_i)| .$$

Lyapunov exponents can also be interpreted in information-theoretic terms [17]. Specifically, the positive exponents reflect the average rate at which predictive ability is lost, or equivalently, the average rate of information gained by observing the current state of the system. The well-known Hénon map [18], for example, exhibits a positive exponent equal to 0.4. If the initial condition is known to a precision of 16 bits, then the ability to predict beyond approximately 40 iterations is lost.

The concept of Lyapunov exponents also applies to continuous-time dynamical systems. To illustrate this, we denote the general solution of the dynamical system $\dot{x}(t) = f(x(t))$, $x \in R$, by $x(t) = \phi_t(x(0))$. Analogous to the discrete-time case, the initial state of the system is assumed to be given by $x'(0) = x(0) + \delta x(0)$, with the resulting error at time t given by

$$\delta x(t) = x'(t) - x(t) = \phi_t(x'(0)) - \phi_t(x(0)) \approx D\phi_t(x(0))\delta x(0) .$$

By periodically sampling the linearized flow, $D\phi_t$, the Lyapunov exponents for a continuous-time system can be defined as those of a discrete-time system generated by the mapping $D\phi_{nT} = Df^n$.

Several notable properties of continuous-time chaotic systems are:

- all continuous-time chaotic systems have at least one zero Lyapunov exponent corresponding to the direction tangent to the flow;
- the sum of the Lyapunov exponents is equal to the time averaged divergence of the vector field;
- any continuous-time dissipative chaotic system has at least one negative exponent, the sum of the exponents is negative, and the limiting trajectories evolve on an attracting set having zero volume in state space; and
- the minimum dimension of a continuous-time chaotic system is three.

Using a symbolic notation, the spectrum of Lyapunov exponents for a three-dimensional chaotic system has the unique representation $(+, 0, -)$, whereas in four-dimensions there are three possible types, with representations given by $(+, 0, -, -)$, $(+, 0, 0, -)$ and $(+, +, 0, -)$.

In dynamical systems with the state space dimension greater than one, the existence and computation of Lyapunov exponents relies on the multiplicative ergodic theorem of Oseledec [19]. This theorem states that if a matrix product is defined as

$$Df^n(\mathbf{x}) = Df(f^{n-1}(\mathbf{x})) \cdots Df(f(\mathbf{x}))Df(\mathbf{x}) \quad ,$$

then under some general ergodicity conditions, the following limit exists

$$\lim_{n \rightarrow \infty} \frac{1}{2n} \log \left([Df^n(\mathbf{x})]^T [Df^n(\mathbf{x})] \right) = \Lambda \quad ,$$

where Λ is a diagonal $N \times N$ matrix. Furthermore, the Lyapunov exponents correspond to the diagonal elements of Λ .

Unfortunately, a direct application of the multiplicative ergodic theorem is numerically unstable, especially when positive Lyapunov exponents exist. This difficulty has been overcome by the QR decomposition approach suggested by Eckmann and Ruelle [20], which is based on decomposing the matrix product $Df^n(\mathbf{x})$ into triangular factors. Their approach begins by defining $Df(\mathbf{x}) = Q_1 R_1$, where Q_1 is an orthogonal matrix and R_1 is an upper triangular matrix. For $j > 1$, the matrices $T^j(\mathbf{x}) = Df(f^{j-1}(\mathbf{x}))Q_{j-1}$ are successively defined and decomposed according to $T^j(\mathbf{x}) = Q_j R_j$. It is straightforward to show that $Df^n(\mathbf{x}) = Q_n R_n \cdots R_1$. It can also be shown that the diagonal elements $\lambda_{ii}^{(n)}$ of the triangular matrix product $R_n \cdots R_1$ obtained from this algorithm satisfy

$$\lim_{n \rightarrow \infty} \frac{1}{n} \log \lambda_{ii}^{(n)} = \lambda_i ,$$

where λ_i corresponds to the i^{th} largest Lyapunov exponent.

The QR method provides a numerically stable approach for computing the Lyapunov exponents of a dynamical system defined by a set of state equations. Using the QR method, we show in figure 2-4 the computed Lyapunov exponents for the Lorenz system. For this case, the parameter values $\sigma = 16$ and $b = 4$ were fixed, and the parameter r was varied over the range $20 < r < 100$. Note that the onset of chaotic behavior occurs near $r = 34$ as evidenced by the existence of a positive Lyapunov exponent. The large negative exponent is due to the highly dissipative nature of the Lorenz chaotic attractor and, as expected, a zero Lyapunov exponent is also apparent. Note also that equation (2.5) determines that all of the fixed points will be unstable for $r > 33.5$. From figure 2-4, we see that this critical value closely predicts when chaotic motion will occur.

2.3.2 Attractor Dimension

Long term chaotic motion in dissipative systems is confined to a strange attractor whose geometric structure is invariant to the evolution of the dynamics. Typically, a strange attractor is a fractal object and, consequently, there are many possible notions

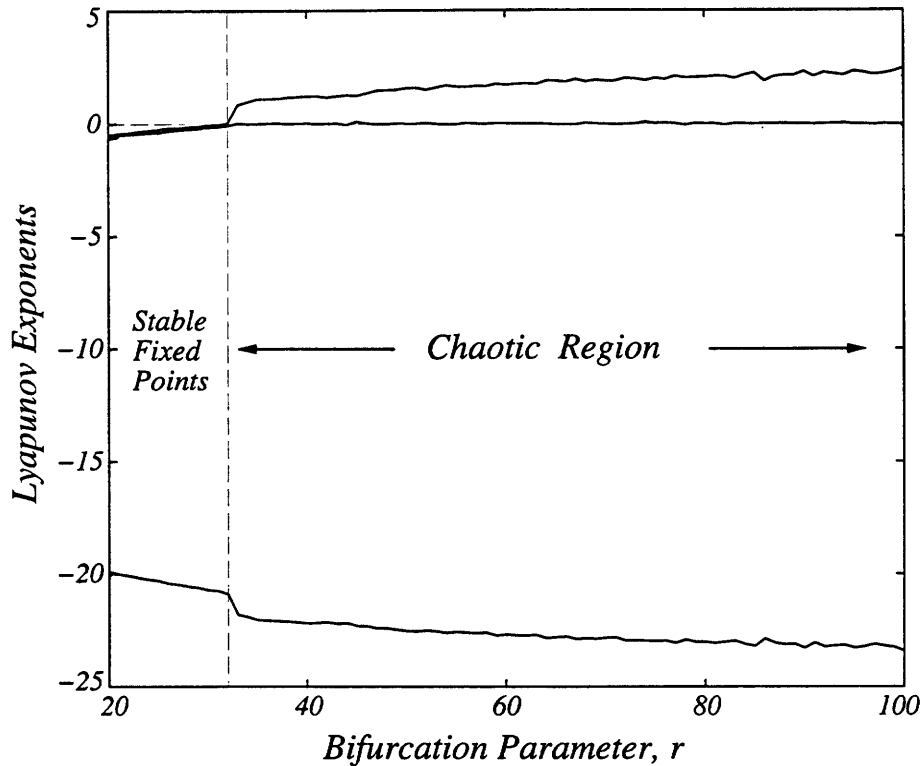


Figure 2-4: *Lyapunov Exponents of the Lorenz System.*

of dimension for strange attractors. In this section, we discuss some well-known and widely accepted definitions of attractor dimension. We also discuss a simple relationship to Lyapunov exponents and provide a numerical example to further emphasize some useful aspects of these concepts.

Dissipative chaotic systems are typically ergodic. All initial conditions within the system's basin of attraction lead to a chaotic attractor in state space which can be associated with a time-invariant probability measure, $\rho(\mathbf{x})$. Intuitively, the dimension of the chaotic attractor should reflect the amount of information required to specify a location on the attractor with a certain precision. This intuition is formalized by defining the *information dimension*, $\dim_H \rho$, of the chaotic attractor as

$$\dim_H \rho = \lim_{\epsilon \rightarrow 0} \frac{\log \rho[B_{\mathbf{x}}(\epsilon)]}{\log \epsilon} ,$$

where $\rho[B_{\mathbf{x}}(\epsilon)]$ denotes the mass of the measure ρ contained in a ball of radius ϵ , centered at the point \mathbf{x} in state space [20, 21]. Information dimension is important

from an experimental viewpoint because it is straightforward to estimate. The mass, $\rho[B_{\mathbf{x}}(\epsilon)]$, can be estimated by

$$\rho[B_{\mathbf{x}}(\epsilon)] \approx \frac{1}{M} \sum_{i=1}^M U(\epsilon - |\mathbf{x}_i - \mathbf{x}|) ,$$

where $U(\cdot)$ is the unit step function. In typical experiments, the state vectors \mathbf{x} are estimated from a time delay embedding of an observed time series [22].

Information dimension will, in general, depend on the particular point \mathbf{x} in state space being considered. Grassberger and Procaccia's approach [23] eliminates this dependence by defining the quantity

$$C(\epsilon) = \frac{1}{M^2} \sum_{i=1}^M \sum_{j=1}^M U(\epsilon - |\mathbf{x}_i - \mathbf{x}_j|) ,$$

and then defining the *correlation dimension*, $\dim_C \rho$, as

$$\dim_C \rho = \lim_{\epsilon \rightarrow 0} \frac{\log C(\epsilon)}{\log \epsilon} .$$

In practice, one usually plots $\log C(\epsilon)$ as a function of $\log \epsilon$ and then measures the slope of the curve to obtain an estimate of $\dim_C \rho$. It is often the case that $\dim_H \rho$ and $\dim_C \rho$ are approximately equal.

There is also a meaningful relationship between information dimension and Lyapunov exponents for chaotic systems [21, 24, 25]. If $\lambda_1, \dots, \lambda_N$ are the Lyapunov exponents of a chaotic system, then the *Lyapunov dimension*, $\dim_L \rho$, is defined as

$$\dim_L \rho = k + \frac{\lambda_1 + \dots + \lambda_k}{|\lambda_{k+1}|} , \quad (2.9)$$

where $k = \max\{i : \lambda_1 + \dots + \lambda_i > 0\}$. Equation (2.9) suggests that only the first $k+1$ Lyapunov exponents are important for specifying the dimensionality of the chaotic attractor. Kaplan *et al.* [24, 25] conjecture that $\dim_H \rho = \dim_L \rho$ in "almost" all cases. Clearly, if this is correct then equation (2.9) provides a straightforward way to estimate the attractor dimension when the dynamical equations of motion are known.

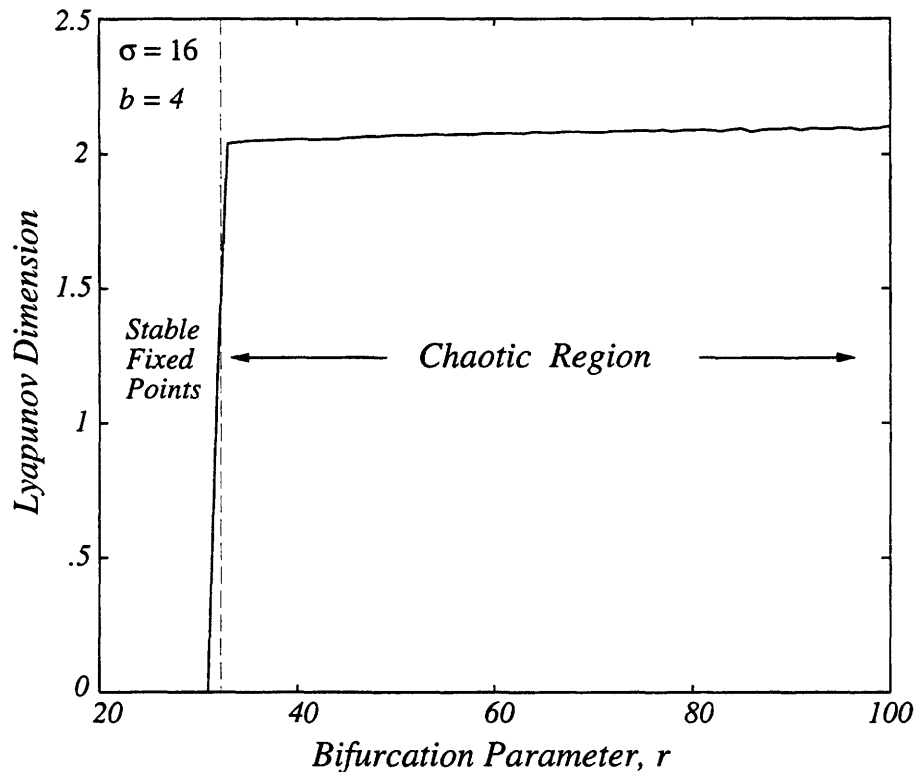


Figure 2-5: *Lyapunov Dimension of the Lorenz System.*

In figure 2-5, we show the computed Lyapunov dimension of the Lorenz attractor as the parameter r is varied over the range $20 < r < 100$. Note that for $r > 34$, the Lyapunov dimension is nearly constant with an average value of approximately 2.06. This value is consistent with the correlation dimension of the Lorenz attractor given in [26]. Similar numerical experiments with the Hénon, Rössler, and double scroll [27] systems show a similar consistency. Since $\dim_{L\rho}$ is relatively straightforward to determine, we will use this approach throughout the thesis to obtain meaningful estimates of the attractor dimension for the various chaotic systems that we consider.

Chapter 3

Self-Synchronization in Chaotic Systems

The concept of chaotic synchronization is intriguing, and until recently, had not received much attention. It is now well-known that dissipative chaotic systems of a certain class possess a self-synchronization property. This property allows two identical chaotic systems to synchronize when the second system is driven by the first. The ability to synchronize remote chaotic systems by linking them with a common drive signal suggests new and potentially interesting approaches to private communications. Some applied aspects of synchronized chaotic systems will be discussed and demonstrated in Chapter 9.

Self-synchronization in chaotic systems is not well-understood due to the highly nonlinear nature of these systems. The analysis presented in this chapter provides a major step toward further understanding this remarkable property, and is organized as follows. In Section 3.1, we discuss the concept of chaotic system decomposition and demonstrate the self-synchronization property of the Lorenz system. In Section 3.2, we formalize this concept and develop a systematic approach for examining the self-synchronization properties of general nonlinear systems. In Section 3.3, we establish an equivalence between self-synchronization in chaotic systems and asymptotically stable error dynamics. We then use Lyapunov functions to provide an analytical explanation of self-synchronization in a class of chaotic systems.

3.1 Decomposing Chaotic Systems into Drive and Response Subsystems

In 1990, Pecora and Carroll [1, 2] reported that certain chaotic systems could be decomposed into drive and response subsystems that synchronize when coupled by a common drive signal. Specifically, they decomposed a nonlinear system of the form

$$\dot{\mathbf{x}} = \mathbf{f}(\mathbf{x}), \mathbf{x} \in R^N ,$$

into subsystems, *i.e.*, expressed it as

$$\dot{\mathbf{d}}_1 = \mathbf{D}_1(\mathbf{d}_1, \mathbf{d}_2), \mathbf{d}_1 \in R^{N-m} \quad (3.1)$$

$$\dot{\mathbf{d}}_2 = \mathbf{D}_2(\mathbf{d}_1, \mathbf{d}_2), \mathbf{d}_2 \in R^m . \quad (3.2)$$

This decomposition can be performed by simply partitioning the state variables into two groups, one associated with \mathbf{D}_1 and the other with \mathbf{D}_2 . However, only certain partitions of the state variables will produce a stable \mathbf{D}_2 subsystem in the sense that all of the *conditional Lyapunov exponents* associated with \mathbf{D}_2 are negative. If a stable decomposition is achieved, then a stable response subsystem can be formed by duplicating \mathbf{D}_2 and replacing the state variables \mathbf{d}_2 by new state variables \mathbf{r} . This leads to a response subsystem of the form

$$\dot{\mathbf{r}} = \mathbf{D}_2(\mathbf{d}_1, \mathbf{r}), \mathbf{r} \in R^m . \quad (3.3)$$

Viewed as a single system, equations (3.1) and (3.2) can be interpreted as a transmitter or drive system with (3.3) forming a receiver or response subsystem that is driven by \mathbf{d}_1 . Figure 3-1 illustrates the approach.

In [1, 2], it was shown numerically that if the conditional Lyapunov exponents associated with \mathbf{D}_2 are all negative, then the state variables \mathbf{r} will synchronize to the state variables \mathbf{d}_2 . The term *conditional* is applied to emphasize that the dynamics of \mathbf{D}_2 depend on the drive variable \mathbf{d}_1 . In typical cases, an analytical determination of

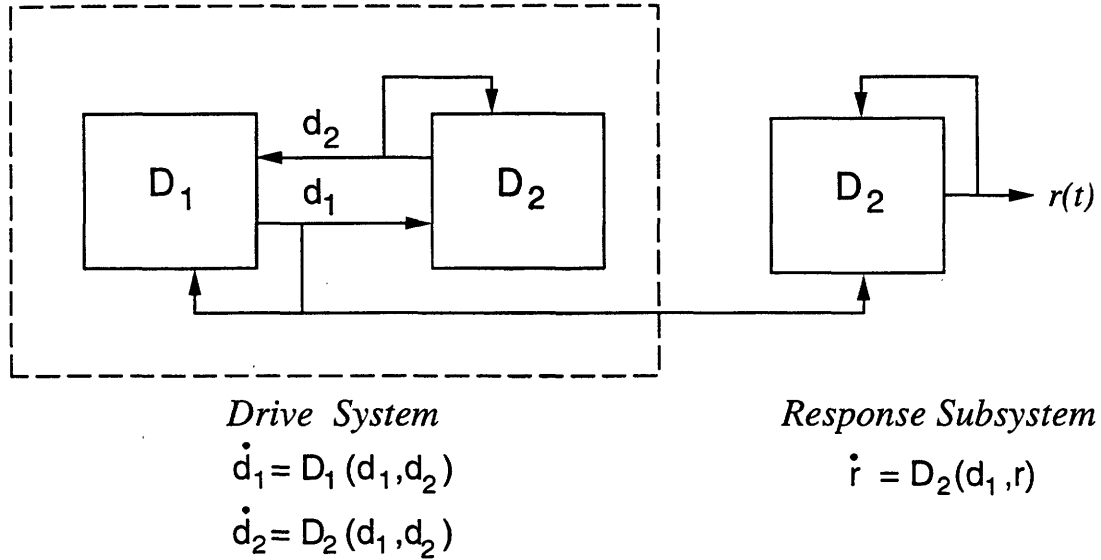


Figure 3-1: *Decomposing a Chaotic System into Drive and Response Subsystems.*

the conditional Lyapunov exponents is not possible and numerical approaches, such as the QR decomposition method (Section 2.3), are necessary to calculate them.

The Lorenz system (2.3) provides an example of a chaotic system for which stable decompositions are possible. For example, a stable (y_1, z_1) response subsystem can be defined by

$$\begin{aligned} \dot{y}_1 &= rx(t) - y_1 - x(t)z_1 \\ \dot{z}_1 &= x(t)y_1 - bz_1, \end{aligned} \quad (3.4)$$

and a stable (x_2, z_2) response subsystem by

$$\begin{aligned} \dot{x}_2 &= \sigma(y(t) - x_2) \\ \dot{z}_2 &= x_2y(t) - bz_2. \end{aligned} \quad (3.5)$$

Equations (3.4) and (3.5) represent dynamical response systems which are driven by the transmitter signals $x(t)$ and $y(t)$ respectively. It can be shown numerically that the conditional Lyapunov exponents of the (y_1, z_1) response subsystem are both negative and thus $|y_1 - y|$ and $|z_1 - z| \rightarrow 0$ as $t \rightarrow \infty$ [1, 3]. Also, the eigenvalues of the Jacobian matrix for the (x_2, z_2) response subsystem are both negative and thus $|x_2 - x|$ and $|z_2 - z| \rightarrow 0$ as $t \rightarrow \infty$.

The two response subsystems can be cascaded to regenerate the full-dimensional

dynamics which are evolving at the transmitter [9, 10, 28, 29]. If the input signal to the (y_1, z_1) subsystem is $x(t)$, then the output $y_1(t)$ can be used to drive the (x_2, z_2) subsystem. This subsequently generates a “new” $x(t)$ in addition to having obtained, through synchronization, $y(t)$ and $z(t)$. It is also possible to regenerate the full-dimensional dynamics of the transmitter by reversing the order of the response subsystems and using $y(t)$ as the drive signal. The advantage of using $x(t)$ as the drive signal is that the two response subsystems given by equations (3.4) and (3.5) can be *combined* into a single system having a three-dimensional state space [30, 31, 32]. This produces a full-dimensional receiver system given by

$$\begin{aligned}\dot{x}_r &= \sigma(y_r - x_r) \\ \dot{y}_r &= rx(t) - y_r - x(t)z_r \\ \dot{z}_r &= x(t)y_r - bz_r .\end{aligned}\tag{3.6}$$

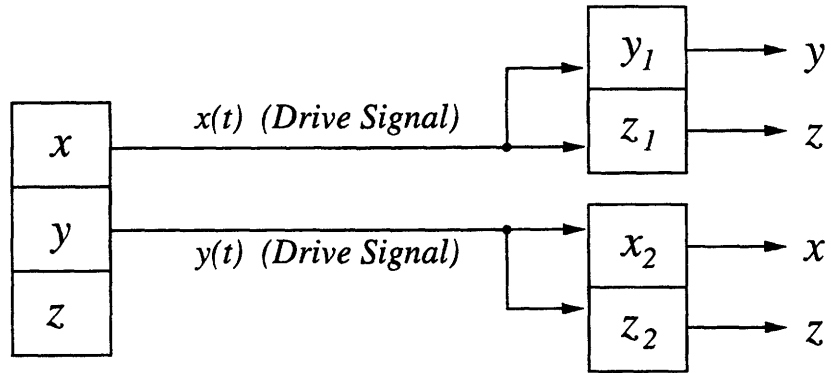
An interesting feature of the receiver equations (3.6) is that they are algebraically similar to the transmitter equations (2.3), except that the drive signal $x(t)$ replaces $x_r(t)$ in the second and third equations.

In figure 3-2(a), (b), and (c), we show the decomposed, cascade, and combined representations respectively, for a receiver system that can regenerate the full-dimensional dynamics of the Lorenz system. Note that the receiver depicted in figure 3-2(a) is four-dimensional and requires that two drive signals be communicated. The receiver depicted in figure 3-2(b) eliminates the need for two drive signals but is also four-dimensional. In an analog circuit implementation of the receiver systems, the state space dimension corresponds to the number of integrators and is, therefore, related to system complexity. The combined representation (figure 3-2(c)) requires the fewest integrators and is preferable in certain applications. For the remainder of the thesis, we will refer to the combined representation as the *Lorenz receiver* in light of the potential applications.

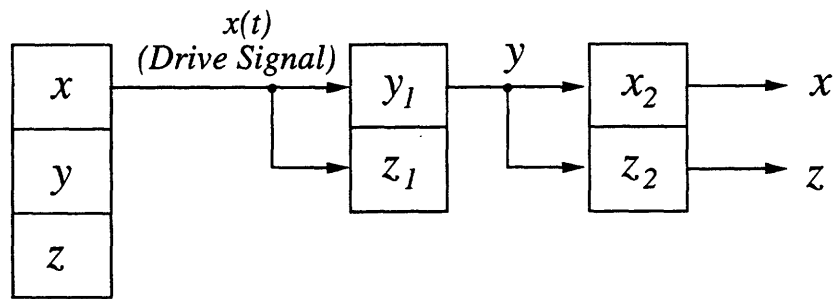
To illustrate the self-synchronization property of the Lorenz receiver, we show in figure 3-3(a) a comparison between the transmitter signal $x(t)$ (dashed line) and the corresponding receiver signal $x_r(t)$ (solid line), when the receiver is initialized from the

*Chaotic
Transmitter*

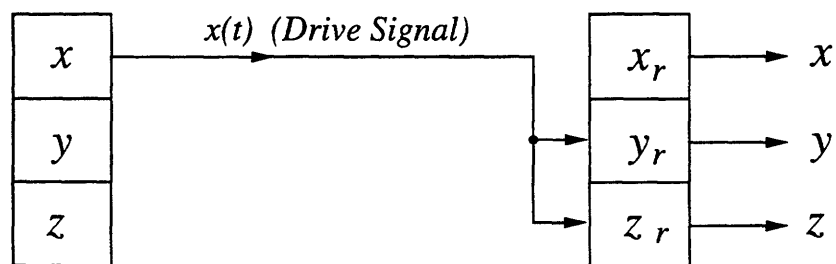
*Synchronizing
Receiver*



(a) Decomposed Representation



(b) Cascade Representation



(c) Combined Representation

Figure 3-2: Lorenz Synchronizing Receiver Representations: (a) Decomposed Form. (b) Cascade Form. (c) Combined (3-D) Form.

zero-state. Figures 3-3(b) and (c) show a similar comparison between the $y(t)$ and $z(t)$ transmitter and receiver signals, respectively. Synchronization is clearly rapid and maintained. Furthermore, the synchronization of the transmitter and receiver is global, *i.e.*, the receiver can be initialized in any state and the synchronization still occurs. This important result will be proven analytically in Section 3.3.

The ability to decompose the Lorenz equations into cascading subsystems that regenerate the full-dimensional transmitter dynamics suggests an interesting approach for studying the self-synchronization properties of general nonlinear systems. This approach relies on determining the stable response subsystems for general nonlinear systems and is discussed in Section 3.2.

3.2 Determining the Stable Response Subsystems for General Nonlinear Systems

The first step is to formalize the concepts of chaotic system decomposition and self-synchronization. We can then develop a systematic approach for determining all of the stable response subsystems for general nonlinear systems and show how to cascade these subsystems in an optimal way. While this analysis is presented using a continuous-time framework, the approach also applies to discrete-time systems.

The class of nonlinear systems that we consider is represented by a set of N first-order ordinary differential equations of the form

$$\begin{aligned} \dot{x}_1 &= f_1(x_1, \dots, x_N) \\ &\vdots \\ \dot{x}_N &= f_N(x_1, \dots, x_N) . \end{aligned} \tag{3.7}$$

The functions f_1, \dots, f_N map $R^N \rightarrow R^1$ and are assumed to be smooth. In our subsequent analysis of chaotic system decomposition and self-synchronization, the following definition of driven subsystems will be useful.

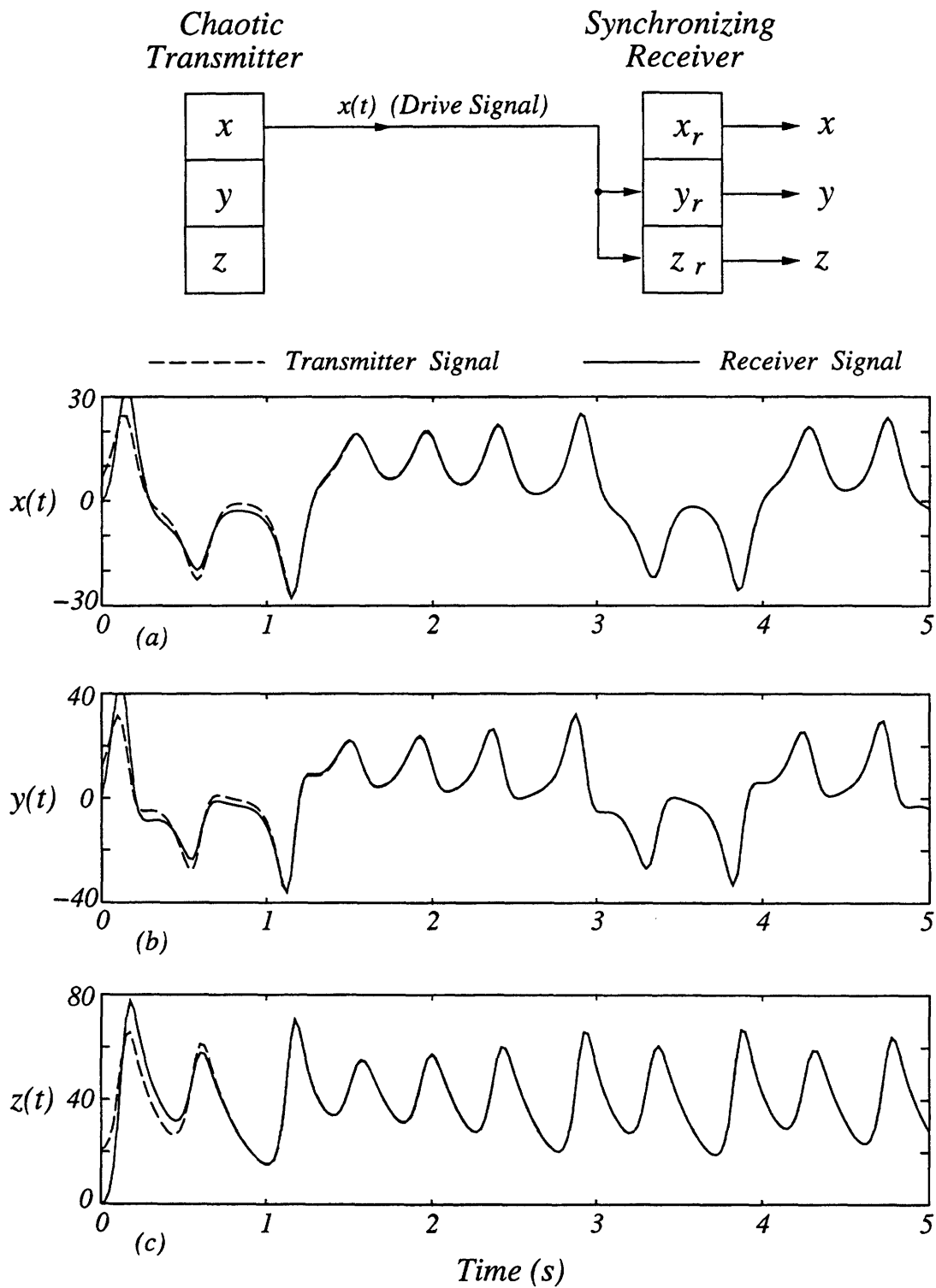


Figure 3-3: Synchronization of Transmitter and Receiver Signals in the Lorenz System. (a) $x(t)$ vs. $x_r(t)$. (b) $y(t)$ vs. $y_r(t)$. (c) $z(t)$ vs. $z_r(t)$.

Definition 3.1 For any positive integer N , let J_N be the set whose elements are the integers, $1, 2, \dots, N$. Fix a proper subset $\mathbf{j} \subset J_N$. Let $x_{\mathbf{j}}$ denote the set of state variables with indices that range over the elements of \mathbf{j} . We say that a state x_i , for $i \in J_N$, drives a subsystem composed of states $x_{\mathbf{j}}$ if and only if

$$\dot{x}_{\mathbf{j}} = f_{\mathbf{j}}(x_i, x_{\mathbf{j}}), \quad i \notin \mathbf{j} .$$

Applying Definition 3.1 to the Lorenz equations (2.3), we can conclude that:

- y drives the x subsystem, but that x does not drive the y subsystem because the equation for \dot{y} also depends on the state z ;
- neither x nor y alone drive the z subsystem by the same definition; and
- every two-dimensional subsystem of (2.3) satisfies Definition 3.1. Specifically, x drives the (y, z) subsystem, y drives the (x, z) subsystem, and z drives the (x, y) subsystem.

In fact, any system of the form (3.7) can be *drive decomposed* into subsystems, where each subsystem is driven by a single state variable. As discussed above, we see that exactly four driven subsystems exist for the Lorenz system. They are listed below.

1. x drives (y, z) .
2. y drives (x, z) .
3. z drives (x, y) .
4. y drives x .

This approach to drive decomposition can be readily extended to N -dimensional systems. There are exactly N possible one-dimensional subsystems in the single drive variable case, *i. e.*, one subsystem corresponding to each state variable. Equivalently,

the number of one-dimensional subsystems S_1 is given by the combination,

$$S_1 = \binom{N}{1} = \frac{N!}{(N-1)!1!} = N .$$

In general, the number of m -dimensional subsystems S_m is given by

$$S_m = \binom{N}{m} .$$

The total number of subsystems S of any order is obtained by summing S_m , for $m = 1, \dots, N - 1$,

$$S = \sum_{m=1}^{N-1} S_m = 2^N - 2 .$$

Observe that S has an exponential dependence on N . For $N = 3$, there are at most 6 subsystems, and for $N = 10$, there are at most 1022. However, the number of subsystems which satisfy Definition 3.1 is usually much less because some of the state equations may depend on only a few state variables. A simple approach for identifying the various subsystems which satisfy Definition 3.1 is discussed below.

The number of unique N -bit binary words, excluding the zero-string and one-string, is exactly $2^N - 2$. Therefore, a two-dimensional subsystem that is composed of states x_j , for $j = \{1, 2\}$, can be represented by the binary word $B(x_j)$ given by

$$B(x_j) = (1, 1, 0, \dots, 0) .$$

In this case, the 1's occur in the two leftmost bit positions, corresponding to the x_1 and x_2 states respectively. The binary representation makes it clear why the zero-string and one-string are omitted. The former would correspond to a zero-dimensional subsystem and the latter would correspond to an N -dimensional subsystem. Both of these cases are excluded by Definition 3.1.

The binary representation is an orderly way of identifying the various subsystems

Response $B(x_j)$	Drive			Satisfy Def. 3.1?	Stable?
	x	y	z		
(0 0 1)	1	1	0	No	No
(0 1 0)	1	0	1	No	No
(0 1 1)	1	0	0	Yes	Yes
(1 0 0)	0	1	0	Yes	Yes
(1 0 1)	0	1	0	Yes	Yes
(1 1 0)	0	0	1	Yes	No

Table 3.1: *Drive Decomposition of the Lorenz System.*

for a general system of differential or difference equations. In table 3.1, we show the *drive decomposition table* for the Lorenz system. This table is constructed by assigning each drive variable to a column, and every possible subsystem to a row. The rows follow the standard binary ordering. Since table 3.1 represents a three-dimensional system, it has 6 rows. An N -dimensional system would have a table with $(2^N - 2)$ rows. A “1” entry in the table indicates that the corresponding drive variable couples into the subsystem and that the drive variable is not a state variable of that subsystem. A “0” entry in the table indicates that the corresponding subsystem is not driven by that drive variable. The table also indicates which subsystems satisfy Definition 3.1. These are the response subsystems and they will be represented notationally by conditioning them with respect to the drive variable. For example, if x drives the (y, z) response subsystem then it will be denoted by $(y, z|x)$.

The drive decomposition table provides a systematic approach for identifying the response subsystems from the algebraic structure of the transmitter equations. State variables which belong to stable response subsystems (SRSs) can be regenerated by a self-synchronizing receiver and those belonging to unstable subsystems can not. Table 3.1 shows that the Lorenz system contains exactly four response subsystems, as expected. Three of these are two-dimensional and one is one-dimensional. Of these four response subsystems, only the $(y, z|x)$, $(x, z|y)$ and $(x|y)$ are stable in the sense of having a complete set of negative conditional Lyapunov exponents. The stable response subsystems are indicated in the last column of table 3.1.

The SRSs are of primary interest in our subsequent analysis because they can be used in cascade to regenerate the transmitter dynamics. One way of regenerating the three-dimensional dynamics of the Lorenz system is to use the cascade

$$x \longrightarrow (y, z|x) \longrightarrow (x|y) .$$

With $x(t)$ as the drive signal, the $(y, z|x)$ response subsystem allows $y(t)$ and $z(t)$ to be reconstructed through synchronization. Subsequent use of $y(t)$ to drive the $(x|y)$ response subsystem allows $x(t)$ to be regenerated. A systematic approach for determining an appropriate cascade of SRSs can be obtained by using *trees*. A brief description of trees as used in this context is given below.

To describe trees, we first introduce some terminology. A tree consists of nodes and branches, where each node represents a SRS. Every branch has exactly two nodes associated with it. The upper node corresponds to the l^{th} level of the tree and the lower node to the $(l + 1)^{\text{st}}$ level of the tree. A path consists of an interconnection of branches arranged from the highest node of the tree to the lowest node of the tree. The lowest level node of any path is called a terminal node.

To construct an SRS tree, we begin by listing each state variable, x_1, \dots, x_N , at the top level of the tree. Then we treat the state variable x_1 as the drive variable and locate the “1” entries in column 1 of the drive decomposition table which correspond to SRSs. Each of these SRSs becomes a level 2 node and a branch is drawn connecting it to x_1 . This procedure is repeated for state variables x_2, \dots, x_N by considering columns 2 through N , respectively. If no SRSs correspond to the “1” entries in a given column of the drive decomposition table then the corresponding drive variable is terminal. At level 2 of the tree, we treat the SRS state variables as drive variables and repeat the above procedure. In general, the SRS state variables at the l^{th} level of the tree become drive variables for the $(l + 1)^{\text{st}}$ level SRSs. From this construction, it is clear that every SRS is driven by a state variable from the previous level. We say that a l^{th} level **state** variable is terminal if:

1. it is also a state variable of some SRS at a higher level of the tree along the same path, or

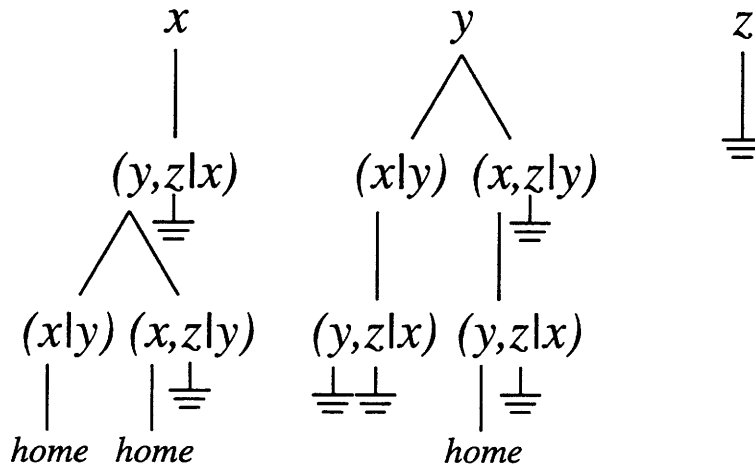


Figure 3-4: *SRS Tree for the Lorenz System.*

2. it was terminated at some higher level node of the tree.

The tree construction is complete when every path reaches a terminal node. A **node** is terminal if:

1. all of the SRS state variables are terminal, or
2. the union of the SRS state variables along the same path comprise a complete set of state variables (also called the home path).

In figure 3-4, we show the complete SRS tree for the Lorenz system. The SRS tree clearly indicates which transmitter states are recoverable through synchronization and which SRSs to use to recover those states. In this figure, we see that there are exactly three cascades of SRSs which can be used to regenerate the full-dimensional transmitter dynamics. These cascades correspond to the three “home” paths and are listed below.

1. $x \rightarrow (y, z|x) \rightarrow (x|y)$
2. $x \rightarrow (y, z|x) \rightarrow (x, z|y)$
3. $y \rightarrow (x, z|y) \rightarrow (y, z|x)$

It is possible that several cascades of SRSs may correspond to a home path. To help choose an optimal cascade, we define the path length as the overall dimensionality

of the SRSs representing that path. In an analog circuit realization of the SRSs, the path length corresponds to the total number of integrators and is therefore related to system complexity. It is advantageous from an implementation viewpoint to select the cascade corresponding to the shortest path length. For the case of the Lorenz system, cascade 1 has a length of three whereas cascades 2 and 3 have a length of four. Therefore, cascade 1 represents the minimum length. If more than one home path shares the minimum length, we can further distinguish between these home paths by choosing the cascade which minimizes a certain cost function. In the context of state estimation, each home path can be viewed as a full-dimensional *observer*, and we can base our optimization approach on a cost function which reflects the overall stability of the observer. One such cost function is based on the sum of the largest conditional Lyapunov exponents of each SRS in the cascade. We denote this cost function by J_{max} and define it as

$$J_{max} = \sum_i \max \{CL(SRS_i)\} \quad , \quad (3.8)$$

where $CL(\cdot)$ denotes the conditional Lyapunov exponents.

In the Lorenz system with parameters $\sigma = 16$, $r = 45.6$, and $b = 4$, the conditional Lyapunov exponents of the three SRSs are given by

$$\begin{aligned} CL(x|y) &= (-16) \quad , \\ CL(x, z|y) &= (-16, -4) \quad , \\ CL(y, z|x) &= (-2.5, -2.5) \quad . \end{aligned} \quad (3.9)$$

Evaluating J_{max} for cascades 1, 2, and 3, we obtain -18.5, -6.5, and -6.5, respectively. In this case, cascade 1 minimizes J_{max} and also has the minimum length. Cascade 1 would be the optimal choice based on these criteria.

We observe that the SRS tree construction procedure must terminate after, at most, N levels. These N levels correspond to N SRSs which can be used in cascade as a full-dimensional observer. This result is summarized in Theorem 3.1.

Response $B(x_j)$	Drive			Satisfy	Stable?
	x	y	z	Def. 3.1?	
(0 0 1)	0	1	0	Yes	No
(0 1 0)	1	0	1	No	No
(0 1 1)	1	0	0	Yes	Yes
(1 0 0)	0	1	0	Yes	Yes
(1 0 1)	0	1	0	Yes	No
(1 1 0)	0	0	1	Yes	No

Table 3.2: *Drive Decomposition of the Double Scroll System.*

Theorem 3.1 *If a stable decomposition of an N -dimensional system produces a full-dimensional observer, then the observer consists of a cascade of, at most, N single-input stable response subsystems.*

As a second example of drive decomposition, consider the double scroll equations [27]

$$\begin{aligned}
 \dot{x} &= \alpha(y - h(x)) \\
 \dot{y} &= x - y + z \\
 \dot{z} &= -\beta y ,
 \end{aligned} \tag{3.10}$$

where $h(x)$ is a piecewise linear function

$$h(x) = \begin{cases} a_1x + (a_0 - a_1) & x > 1 \\ a_0x & -1 \leq x \leq 1 \\ a_1x - (a_0 - a_1) & x < -1 \end{cases}$$

The drive decomposition table for this system is given in table 3.2. For the parameter values that we have chosen, $\alpha = 9, \beta = 100/7, a_0 = -1/7$, and $a_1 = 2/7$, the conditional Lyapunov exponents for the SRSs are given by

$$\begin{aligned}
 CL(x|y) &= (-1.0) , \\
 CL(y, z|x) &= (-.5, -.5) .
 \end{aligned} \tag{3.11}$$

In figure 3-5, we show the complete SRS tree for the double scroll system. Note that there are two ways to regenerate the full-dimensional dynamics of this system.

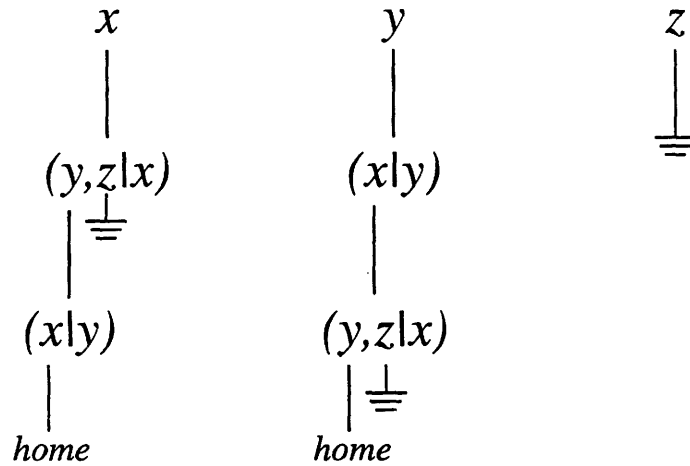


Figure 3-5: *SRS Tree for the Double Scroll System.*

Response $B(x_j)$	Drive			Satisfy Def. 3.1?	Stable?
	x	y	z		
(0 0 1)	1	0	0	Yes	Yes
(0 1 0)	1	0	0	Yes	No
(0 1 1)	1	0	0	Yes	No
(1 0 0)	0	1	1	No	No
(1 0 1)	0	1	0	Yes	Yes
(1 1 0)	0	0	1	Yes	No

Table 3.3: *Drive Decomposition of the Rössler System.*

Because the two home paths represent a re-ordering of the SRSs, our optimality criteria will not distinguish between them.

The Rössler system, given by

$$\begin{aligned}
 \dot{x} &= -y - z \\
 \dot{y} &= x + ay \\
 \dot{z} &= b + z(x - c) ,
 \end{aligned}
 \tag{3.12}$$

provides an example of a chaotic system for which the full-dimensional dynamics can not be regenerated by a cascade of single-input SRSs. The drive decomposition table for this system is given in table 3.3. For the parameter values that we have chosen, $a = .2$, $b = .2$, and $c = 11$, the conditional Lyapunov exponents for the SRSs are given

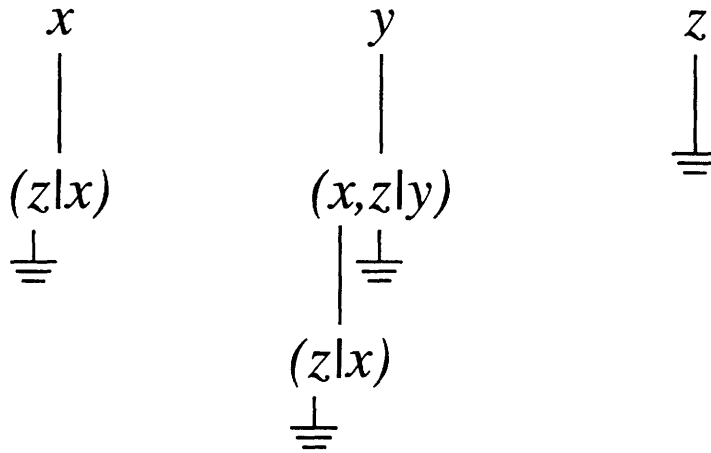


Figure 3-6: *SRS Tree for the Rössler System.*

by

$$\begin{aligned}
 CL(z|x) &= (-10.9) , \\
 CL(x, z|y) &= (-.04, -10.9) .
 \end{aligned}
 \tag{3.13}$$

In figure 3-6, we show the complete SRS tree for the Rössler system. The $(x, z|y)$ response subsystem allows $x(t)$ and $z(t)$ to be regenerated with $y(t)$ as the drive signal. The $(z|x)$ response subsystem allows $z(t)$ to be regenerated with $x(t)$ as the drive signal. This figure suggests, however, that it is not possible to regenerate the full-dimensional dynamics of the Rössler system with this approach.

It should be emphasized that drive decomposition tables and SRS trees are particularly useful for examining the self-synchronizing properties of higher dimensional systems. The relatively low-order systems discussed in this section were chosen to illustrate the approach, rather than to suggest limitations. Two potential drawbacks of this approach are:

- it requires considerable computation to determine the conditional Lyapunov exponents of each response subsystem; and
- the approach does not provide much insight for understanding the self-synchronization property. It also does not suggest a systematic procedure for synthesizing new chaotic systems which possess the self-synchronization property.

In Section 3.3, we analyze self-synchronization from the viewpoint of nonlinear

stability theory. A major advantage of this approach is that it provides a clear mathematical framework for analyzing and synthesizing a large class of self-synchronizing chaotic systems.

3.3 Equivalence Between Self-Synchronization and Asymptotic Stability

The main theme of this section is the relationship between self-synchronization and asymptotic stability. We will focus our attention on chaotic systems which possess the *complete* self-synchronization property, *i.e.*, systems for which it is possible to regenerate all of the transmitter signals. For simplicity, we also assume that the transmitter and receiver systems have the same state space dimension, as was the case for the combined representation of the Lorenz receiver (Section 3.1). In Chapters 6-8, we develop synthesis techniques for this class of systems and in Chapter 9 we discuss some applied aspects.

Below, we give a mathematical definition of self-synchronization which is useful in our subsequent analysis.

Definition 3.2 Two dynamical systems, a transmitter $\dot{\mathbf{x}} = \mathbf{f}(\mathbf{x})$ and a receiver $\dot{\mathbf{x}}_r = \mathbf{f}(\mathbf{x}, \mathbf{x}_r)$, where \mathbf{x} and $\mathbf{x}_r \in R^N$, and $\mathbf{f} : R^N \rightarrow R^N$, are said to possess the self-synchronization property if there exists a domain Ω in R^N such that if $\mathbf{x}(0)$ and $\mathbf{x}_r(0) \in \Omega$, then $\|\mathbf{x}(t) - \mathbf{x}_r(t)\| \rightarrow 0$ as $t \rightarrow \infty$. The self-synchronization is termed global if Ω spans R^N .

Definition 3.2 in effect states that the concept of self-synchronization is equivalent to the concept of asymptotically stable error dynamics between the transmitter and receiver systems. If we define the synchronization errors by $\mathbf{e}(t) = \mathbf{x}(t) - \mathbf{x}_r(t)$, then Definition 3.2 implies that $\|\mathbf{e}(t)\| \rightarrow 0$ as $t \rightarrow \infty$. This is equivalent to our definition of asymptotically stable error dynamics.

In Section 2.2, we showed that Lyapunov's direct method is useful for examining

the asymptotic stability of general nonlinear systems. When the error system is linear, we can restrict our attention to quadratic Lyapunov functions of the form

$$E = \frac{1}{2} \mathbf{e}^T R \mathbf{e} ,$$

where \mathbf{e} denotes any vector in the error system's state space, and where R is a symmetric $N \times N$ positive definite matrix. Geometrically, E represents an ellipsoid in the error system's state space with the center of the ellipsoid located at the origin. If \dot{E} is negative definite, then Lyapunov's theorem (Theorem 10.2 in [15]) ensures that the origin is globally asymptotically stable. Thus, the transmitter and receiver systems will synchronize regardless of the initial conditions.

To show that self-synchronization in the Lorenz system is a result of stable error dynamics, we first define the error signals as

$$\begin{aligned} e_x(t) &= x(t) - x_r(t) \\ e_y(t) &= y(t) - y_r(t) \\ e_z(t) &= z(t) - z_r(t) . \end{aligned}$$

Assuming that the Lorenz transmitter and receiver parameters are identical, a set of equations which govern their error dynamics is given by

$$\begin{aligned} \dot{e}_x &= \sigma(e_y - e_x) \\ \dot{e}_y &= -e_y - x(t)e_z \\ \dot{e}_z &= x(t)e_y - be_z . \end{aligned} \tag{3.14}$$

Using a more concise notation, these error equations can be written as a linear time-dependent system of the form

$$\dot{\mathbf{e}} = A(t)\mathbf{e} ,$$

where $\mathbf{e} = (e_x, e_y, e_z)$. A sufficient condition for the error equations to be globally

asymptotically stable at the origin can be determined by considering a Lyapunov function of the form

$$E(\mathbf{e}) = \frac{1}{2} \left(\frac{1}{\sigma} e_x^2 + e_y^2 + e_z^2 \right) .$$

Note that $E(\mathbf{e})$ is positive definite provided that $\sigma > 0$. The time rate of change of $E(\mathbf{e})$ along trajectories is given by

$$\begin{aligned} \dot{E}(\mathbf{e}) &= \frac{1}{\sigma} e_x \dot{e}_x + e_y \dot{e}_y + e_z \dot{e}_z \\ &= - \left(e_x - \frac{1}{2} e_y \right)^2 - \frac{3}{4} e_y^2 - b e_z^2 . \end{aligned}$$

Provided that $b > 0$, $\dot{E}(\mathbf{e})$ is negative definite. Since σ and b in the Lorenz equations are both assumed to be positive, E is positive definite and \dot{E} is negative definite. It then follows from Lyapunov's theorem that $\mathbf{e}(t) \rightarrow 0$ as $t \rightarrow \infty$. Therefore, synchronization occurs as $t \rightarrow \infty$ regardless of the initial conditions imposed on the transmitter and receiver systems.

Note also that the Lorenz transmitter and receiver systems do not have to operate chaotically for synchronization to occur. By appropriately choosing the parameters σ , r , and b , the motion can, in principle, be confined to limit cycles and yet synchronization between the transmitter and receiver will still occur. This shows that the self-synchronization property exhibited by certain chaotic systems does not depend on chaotic behavior; rather it should be viewed as a result of stable error dynamics between the transmitter and receiver systems.

A drawback of the Lyapunov approach for analysis problems is that it is usually difficult to define an appropriate Lyapunov function for examining the stability of general nonlinear systems. For synthesis problems, however, we can assume that a suitable Lyapunov function exists, and determine the constraints that this assumption places on the system's algebraic structure. In Chapters 6-8, we use this approach to propose several systematic procedures for synthesizing self-synchronizing chaotic systems.

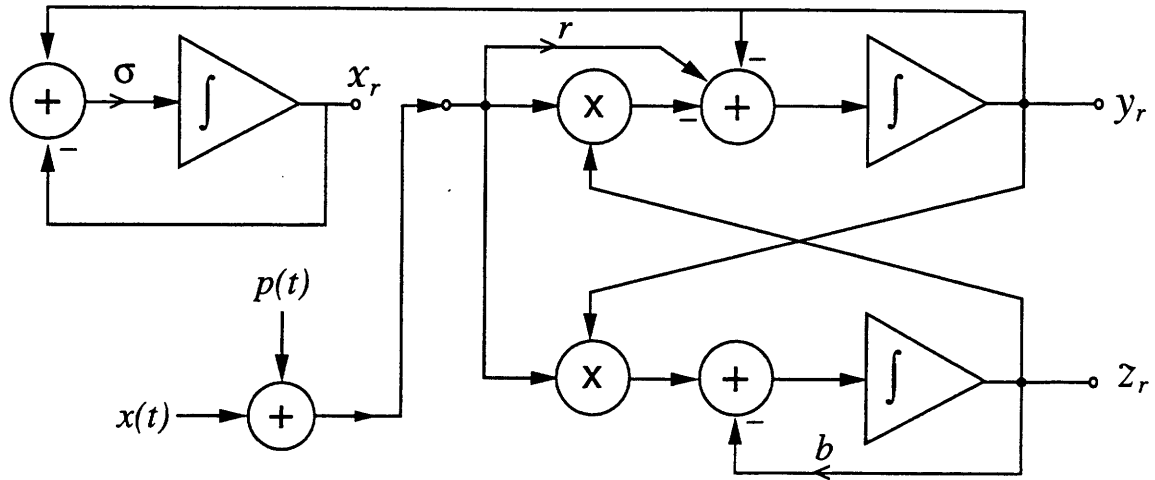


Figure 3-7: *Block Diagram of the Lorenz Synchronizing Receiver.*

Another issue concerns the sensitivity of the synchronization when a perturbation signal $p(t)$ is added to the synchronizing drive signal $x(t)$. Clearly, this is an important practical issue for realistic systems that utilize chaotic synchronization. As a step toward further addressing this issue, Chapter 4 establishes an analogy between synchronization in chaotic systems and nonlinear state estimation in probabilistic systems. This analogy is possible because synchronized chaotic systems can be viewed as performing the role of a nonlinear observer. For example, consider figure 3-7 which shows a block diagram representation of the Lorenz receiver equations (3.6). The Lorenz receiver can be viewed as an open-loop nonlinear observer. It would seem that this system would not make a highly robust observer because of the open-loop structure. Chapter 4 addresses this issue by comparing the performance of the Lorenz receiver to two well-known extended Kalman filter algorithms when white noise is added to the transmitter's drive signal.

Chapter 4

Self-Synchronization and Nonlinear State Estimation

In Chapter 3, we showed that synchronization in the Lorenz system is a result of stable error dynamics between the transmitter and receiver systems. In effect the Lorenz receiver is a type of nonlinear state estimator. This interpretation suggests an analogy between self-synchronization in chaotic systems and nonlinear state estimation in probabilistic systems using extended Kalman filters (EKFs). The performance of EKFs in state estimation problems is well-documented, whereas studies of the sensitivity of synchronization in chaotic systems has only recently been explored [33, 34].

In this chapter, we numerically examine the sensitivity of synchronization in the Lorenz system when a white noise perturbation signal $p(t)$ is added to the synchronizing drive signal $x(t)$. In this case, the Lorenz receiver equations are given by

$$\begin{aligned}\dot{x}_r &= \sigma(y_r - x_r) \\ \dot{y}_r &= rs(t) - y_r - s(t)z_r \\ \dot{z}_r &= s(t)y_r - bz_r .\end{aligned}\tag{4.1}$$

The received drive signal $s(t)$ is given by

$$s(t) = x(t) + p(t) .$$

With $s(t)$ equal to the transmitter signal $x(t)$, the receiver state variables x_r, y_r , and z_r will asymptotically synchronize to the transmitter variables x, y , and z . The receiver variables, however, will not exactly synchronize to the transmitter variables when $p(t)$ is non-zero. To calibrate the performance of the Lorenz receiver as a nonlinear state estimator, we will compare its performance to the well-known continuous and linearized EKF algorithms.

In Section 4.1, we discuss the implementation of the EKFs for the Lorenz system. In Section 4.2, we present the numerical experiments and performance comparisons.

4.1 State Estimation of the Lorenz System

Probabilistic state estimates of the Lorenz system can be obtained by expressing the Lorenz system dynamics and received signal as a dynamical system of the form

$$\begin{aligned}\dot{\mathbf{x}}(t) &= \mathbf{f}(\mathbf{x}(t)) + \mathbf{w}(t) \\ s(t) &= H\mathbf{x}(t) + p(t) .\end{aligned}\tag{4.2}$$

The vector \mathbf{x} denotes the Lorenz state variables, *i.e.*, $\mathbf{x} = (x, y, z)$. The process noise $\mathbf{w}(t)$ and measurement noise $p(t)$ are assumed to be zero-mean, white, and uncorrelated. We denote by $Q(t)$ and σ_p^2 the spectral densities of $\mathbf{w}(t)$ and $p(t)$, respectively. Because the received signal is given by $s(t) = x(t) + p(t)$, the observation matrix H is equivalent to the row vector $(1, 0, 0)$.

In Section 4.1.1, we discuss the continuous EKF algorithm for obtaining state estimates of the Lorenz system. In Section 4.1.2, we discuss an alternative state estimation approach, the linearized EKF algorithm. In Section 4.1.3, we determine an appropriate spectral density $Q(t)$ for use in the EKF algorithms.

4.1.1 Continuous EKF

The continuous EKF state estimation equation corresponding to the dynamical system model represented by (4.2) is given by

$$\dot{\hat{\mathbf{x}}}(t) = \mathbf{f}(\hat{\mathbf{x}}(t)) + K(t)[s(t) - H\hat{\mathbf{x}}(t)] . \quad (4.3)$$

The Kalman gain $K(t)$ is determined by linearizing (4.2) about the current state estimate, *i.e.*, by expressing $\mathbf{x}(t)$ as

$$\mathbf{x}(t) = \hat{\mathbf{x}}(t) + \delta\mathbf{x}(t) .$$

The linearized system, which is valid for small $\delta\mathbf{x}(t)$, is given by

$$\begin{aligned} \delta\dot{\mathbf{x}}(t) &= D\mathbf{f}(\hat{\mathbf{x}}(t))\delta\mathbf{x}(t) + \mathbf{w}(t) \\ \nu(t) &= s(t) - H\hat{\mathbf{x}}(t) = H\delta\mathbf{x}(t) + p(t) . \end{aligned} \quad (4.4)$$

The time-dependent matrix $D\mathbf{f}(\hat{\mathbf{x}}(t))$ corresponds to the Jacobian matrix of the Lorenz system evaluated at the current state estimate. Since equation (4.4) represents a linear time-dependent system, the Kalman filter error covariance matrix $P(t)$ and Kalman gain $K(t)$ are governed by the matrix Riccati equation given below.

$$\begin{aligned} \dot{P}(t) &= D\mathbf{f}(\hat{\mathbf{x}}(t))P(t) + P(t)D\mathbf{f}^T(\hat{\mathbf{x}}(t)) + Q(t) \\ &\quad - \frac{1}{\sigma_p^2}P(t)H^T H P(t) \\ K(t) &= \frac{1}{\sigma_p^2}P(t)H^T \end{aligned} \quad (4.5)$$

Equations (4.3) and (4.5) determine the continuous EKF state estimates for the Lorenz system. In figure 4-1, we show a block diagram of the continuous EKF. In comparison with the block diagram of the Lorenz receiver (figure 3-7), we see that the EKF has a closed-loop structure whereas the Lorenz receiver has an open-loop structure.

Although the state estimation equation (4.3) captures the exact nonlinear dynamics of the Lorenz system, the state estimates will diverge if $K(t)$ becomes small. This

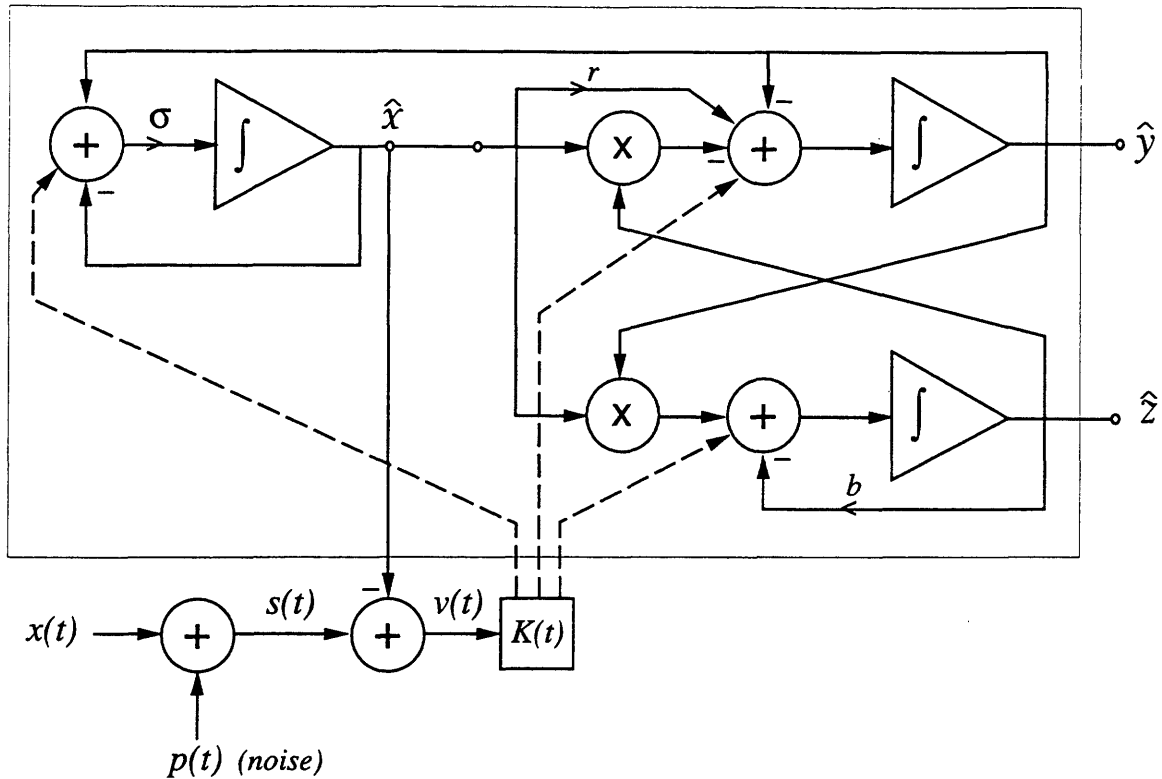


Figure 4-1: *Block Diagram of the Continuous EKF for the Lorenz System.*

follows from the fact that chaotic systems are sensitive to initial conditions and any error in the current state estimate will increase exponentially fast if $K(t)$ is small. To avoid the filter divergence, the spectral density $Q(t)$ must be appropriately adjusted. This issue is discussed further in Section 4.1.3. We next discuss the linearized EKF algorithm for obtaining state estimates of the Lorenz system.

4.1.2 Linearized EKF

The linearized EKF algorithm is based on the assumption that the actual system state is given by

$$\mathbf{x}(t) = \bar{\mathbf{x}}(t) + \delta\mathbf{x}(t) , \quad (4.6)$$

where the nominal trajectory $\bar{\mathbf{x}}(t)$ is assumed to be known. The quality of the linearized EKF's state estimates depends on having an accurate nominal trajectory. In many applications, however, an accurate nominal trajectory may not be available.

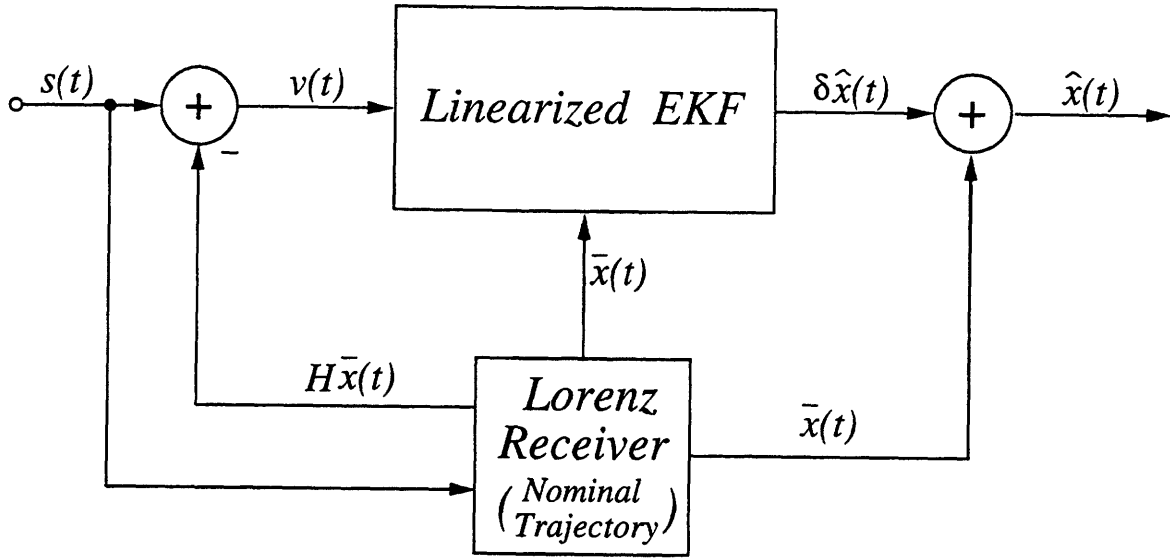


Figure 4-2: Block Diagram of the Linearized EKF.

For the Lorenz system, our approach for obtaining the nominal trajectory “on-line” is to use the state estimates from the Lorenz receiver. This approach is illustrated in figure 4-2.

The dynamics governing $\delta \mathbf{x}(t)$ are determined by substituting equation (4.6) into (4.2) and expanding $\mathbf{f}(\mathbf{x}(t))$ in a Taylor series through linear terms. The resulting linearized system is given by

$$\begin{aligned} \delta \dot{\mathbf{x}}(t) &= D\mathbf{f}(\bar{\mathbf{x}}(t))\delta \mathbf{x}(t) + \mathbf{w}(t) \\ \nu(t) &= s(t) - H\bar{\mathbf{x}}(t) = H\delta \mathbf{x}(t) + p(t) . \end{aligned} \quad (4.7)$$

The Kalman filter for estimating $\delta \mathbf{x}(t)$ is given by

$$\delta \dot{\hat{\mathbf{x}}}(t) = D\mathbf{f}(\bar{\mathbf{x}}(t))\delta \hat{\mathbf{x}}(t) + K(t)[\nu(t) - H\delta \hat{\mathbf{x}}(t)] . \quad (4.8)$$

The error covariance matrix $P(t)$ and Kalman gain $K(t)$ are governed by the matrix Riccati equation given below.

$$\begin{aligned} \dot{P}(t) &= D\mathbf{f}(\bar{\mathbf{x}}(t))P(t) + P(t)D\mathbf{f}^T(\bar{\mathbf{x}}(t)) + Q(t) \\ &\quad - \frac{1}{\sigma_p^2}P(t)H^T H P(t) \\ K(t) &= \frac{1}{\sigma_p^2}P(t)H^T \end{aligned} \quad (4.9)$$

A useful feature of the Riccati equation is that the Jacobian matrix $D\mathbf{f}(\bar{\mathbf{x}}(t))$ depends on the nominal trajectory rather than the current state estimate, as was the case for the continuous EKF. Since the nominal trajectory is assumed to be known a priori, the Kalman gain and error covariance matrix can be computed “off-line.”

4.1.3 Process Noise

Determining an appropriate spectral density $Q(t)$ of the process noise $\mathbf{w}(t)$ is an important issue. One might conclude that $Q(t)$ should be very small due to our complete knowledge of the system model that we wish to simulate. However, rapid filter divergence occurs in this case. The local instability of chaotic systems creates “new” uncertainties about the eventual evolution of the system state which must be accounted for by appropriately adjusting $Q(t)$. If $Q(t)$ is too small, then the Kalman filter rejects the received data and favors the model, thus leading to rapid filter divergence.

One approach to identifying a good first estimate of $Q(t)$ for the Lorenz system is by observing that $Q(t)$ and Lyapunov exponents have the same units (s^{-1}). Intuitively, positive Lyapunov exponents affect the evolution of future states in a deterministic system in much the same way that $Q(t)$ affects the uncertainty of future states in a probabilistic system. It seems plausible that $Q(t)$ could be, in some sense, related to Lyapunov exponents. A simple argument to support this intuition is given below.

Over short time intervals the exponential divergence of nearby trajectories in a chaotic system is dominated by the largest positive Lyapunov exponent λ_{max} . If $\delta x(0)$ represents a small perturbation from $x(t)$ at $t = 0$, then the trajectories diverge at a rate given by

$$\frac{|\delta x(t)|}{|\delta x(0)|} = e^{\lambda_{max}t} \approx 1 + \lambda_{max}t \quad . \quad (4.10)$$

This divergence creates uncertainty in the current state of the chaotic system. Now consider the situation of a first-order integrator driven by white noise. The dynamical

system is represented by

$$\dot{x}(t) = w(t) , \quad (4.11)$$

where $w(t)$ has a constant spectral density equal to Q . The Lyapunov equation governing the uncertainty in the current state of (4.11) is given by

$$\dot{P}(t) = Q . \quad (4.12)$$

Equation (4.12) has the solution $P(t) = P(0) + Qt$. For $P(0) = 1$ and $Q = \lambda_{max}$, the evolution of uncertainty in the first-order integrator is equivalent to the evolution of uncertainty in the chaotic system. This argument suggests a connection between Q and the largest positive Lyapunov exponent.

The largest Lyapunov exponent for the Lorenz system, with parameter values $\sigma = 16, r = 45.6$, and $b = 4$, is approximately 1.5. Using $Q(t) = 1.5Ic$, where I is the 3×3 identity matrix and c is a positive scalar, extensive simulations of both the continuous and linearized EKF were run. We determined that a small range for c exists which produces acceptable performance for both EKFs. We selected a value near the middle of this range, specifically $c = 2$.

In the next section, a set of experiments is conducted to evaluate the performance of the Lorenz receiver and EKFs when the perturbation $p(t)$ is Gaussian white noise.

4.2 Performance Comparisons

In this set of experiments, we denote by $\sigma_x^2, \sigma_y^2, \sigma_z^2$, and σ_p^2 the average power in $x(t), y(t), z(t)$, and $p(t)$, respectively. The input chaos-to-perturbation ratio (CPR) reflects the perturbation in the drive signal and is given by

$$\text{Input CPR} = 10 \log_{10} \left[\frac{\sigma_x^2}{\sigma_p^2} \right] .$$

The output chaos-to-error ratio (CER) associated with $x(t)$ reflects the error between $x(t)$ and $x_r(t)$ and is defined as

$$\text{Output CER}_x = 10\log_{10} \left[\frac{\sigma_x^2}{\sigma_{ex}^2} \right] .$$

The output CER for the state variables $y(t)$ and $z(t)$ are similarly defined as

$$\begin{aligned} \text{Output CER}_y &= 10\log_{10} \left[\frac{\sigma_y^2}{\sigma_{ey}^2} \right] , \\ \text{Output CER}_z &= 10\log_{10} \left[\frac{\sigma_z^2}{\sigma_{ez}^2} \right] . \end{aligned}$$

In figure 4-3, we illustrate the numerical experiment used to evaluate the output CER of the Lorenz receiver and EKFs as a function of the input CPR. Each state estimator receives the identical input sample values, *i.e.*, the received signal $s(t)$ is simultaneously observed by the Lorenz receiver and EKFs. An initial rest condition is imposed on the Lorenz receiver while the EKFs are initialized using the true state of the transmitter at $t = 0$. State estimates were computed for several seconds and the first few seconds of output data were discarded to eliminate start-up transients. The output CER was then computed for the state estimates from the remaining output data.

In figure 4-4, we compare the performance of the Lorenz receiver (solid curves) and the continuous EKF (dashed curves). The performance of these two state estimators is similar over a wide range of input CPRs. Near -10 dB input CPR, the Lorenz receiver exhibits a sharp threshold effect. However, above this threshold, the Lorenz receiver achieves an output CER which is approximately 10 dB greater than the input CPR. We should emphasize that the performance of the Lorenz receiver is insensitive to initial conditions. The EKF, on the other hand, requires accurate initial conditions or the state estimates may rapidly diverge. The EKF also has a disadvantage at high input CPRs. Because the EKF algorithm inverts the noise density σ_p^2 , a lower bound was placed on σ_p^2 in order to avoid numerical problems at high input CPRs. This limits the quality of the EKF state estimates at high input CPRs.

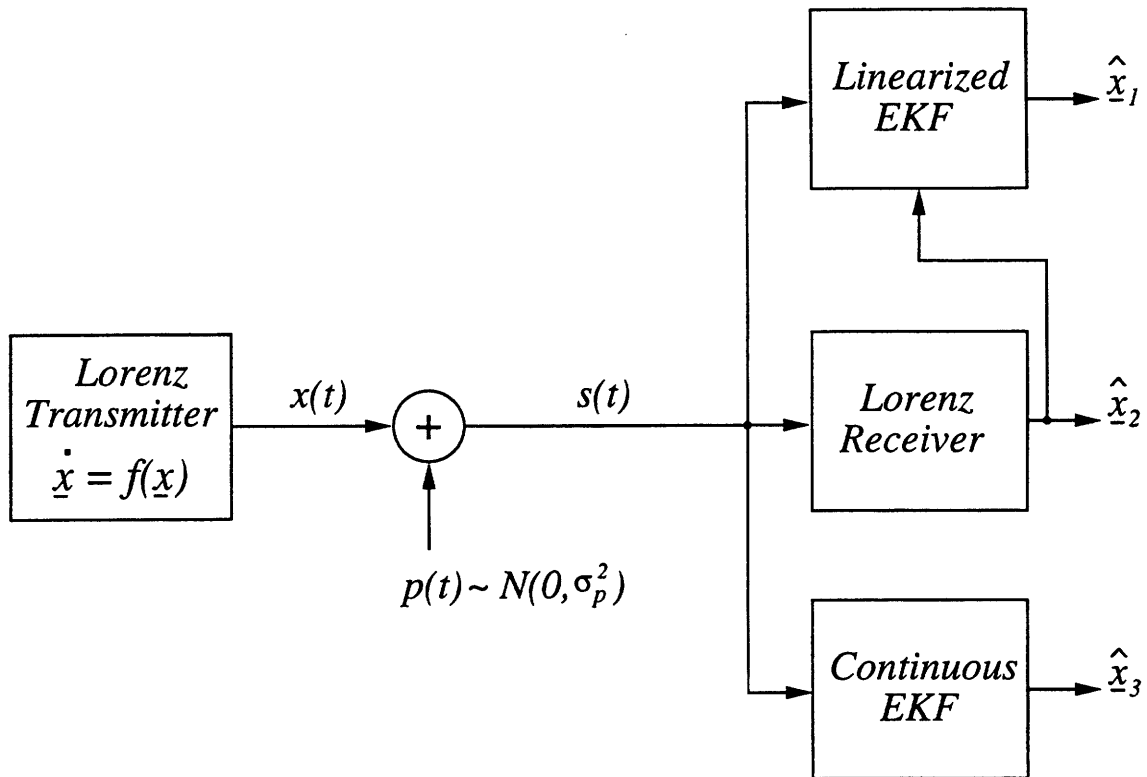


Figure 4-3: Numerical Experiment to Evaluate the Output CER vs. Input CPR.

In figure 4-5, we show the performance curves for the Lorenz receiver and linearized EKF. Although the performance of these two state estimators is very similar, the linearized EKF has an important advantage over the continuous EKF. The linearized EKF can be initialized with a wide range of initial conditions and not diverge, which was not the case for the continuous EKF. The linearized EKF's insensitivity to initial conditions is due to the ability of the Lorenz receiver to provide meaningful state estimates even at low input CPRs. These state estimates provide an accurate nominal trajectory for the linearized EKF.

In an informal experiment, we numerically evaluated the sensitivity of the Lorenz receiver and continuous EKF to parameter modeling errors at the receiver. The transmitter parameters were fixed at their nominal values while each receiver parameter was treated as a uniformly distributed random variable. The mean value of the receiver parameters equaled the value of the corresponding transmitter parameter. The variance of the receiver parameters reflected the percent modeling error being tested, where modeling error was defined as the ratio of the standard deviation to the mean

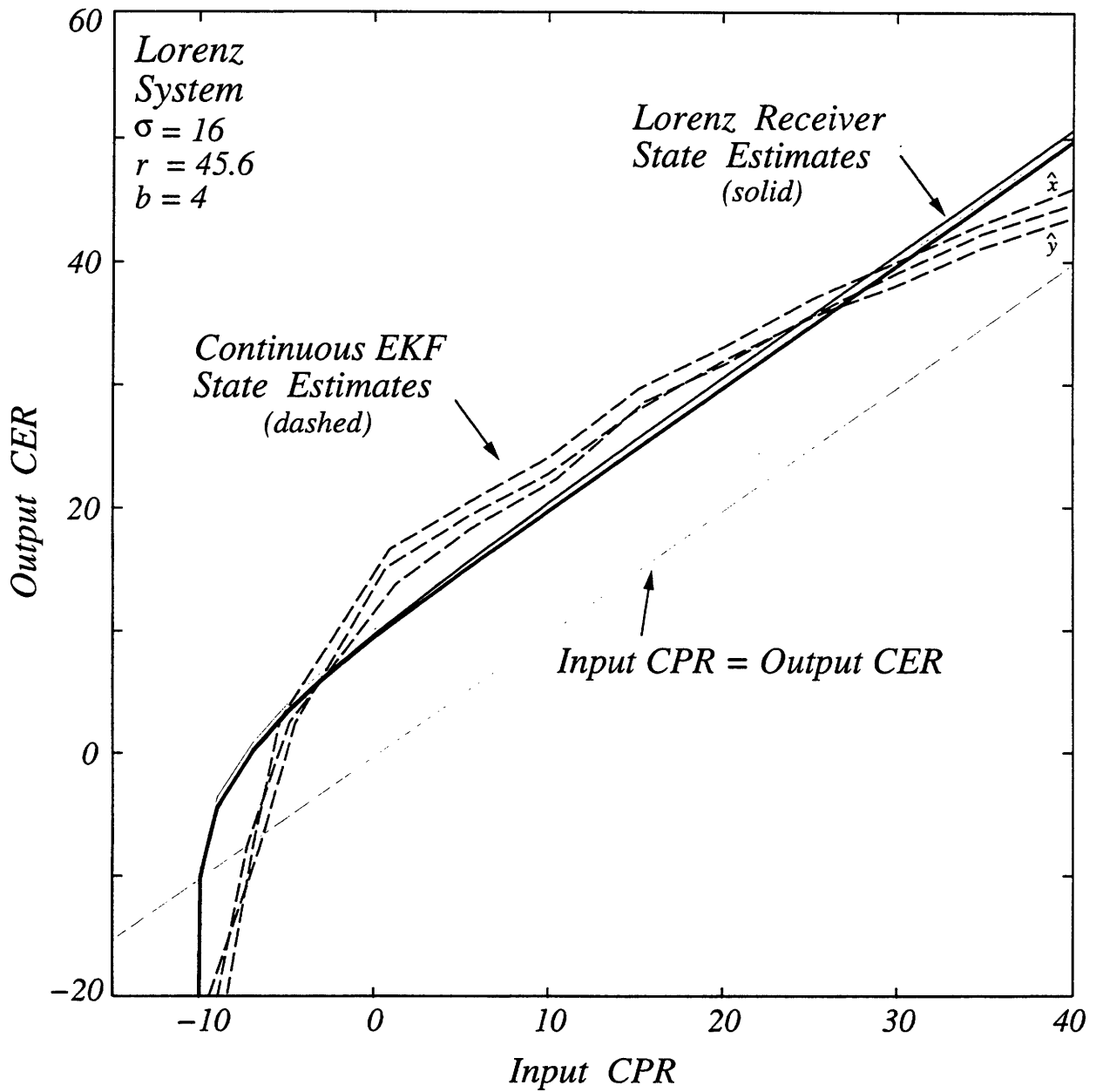


Figure 4-4: Performance Comparison: Lorenz Receiver vs. Continuous EKF.

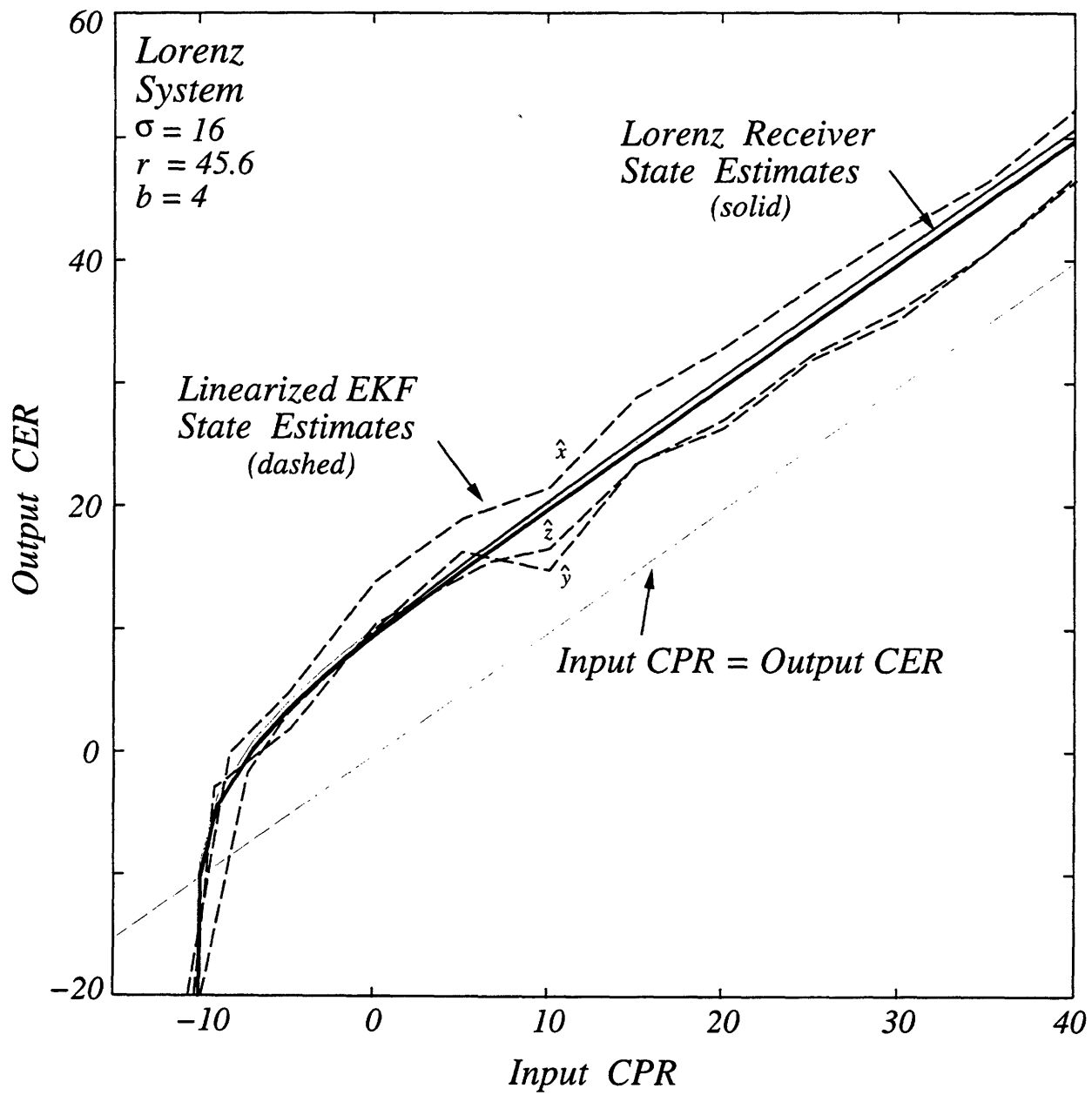


Figure 4-5: Performance Comparison: Lorenz Receiver vs. Linearized EKF.

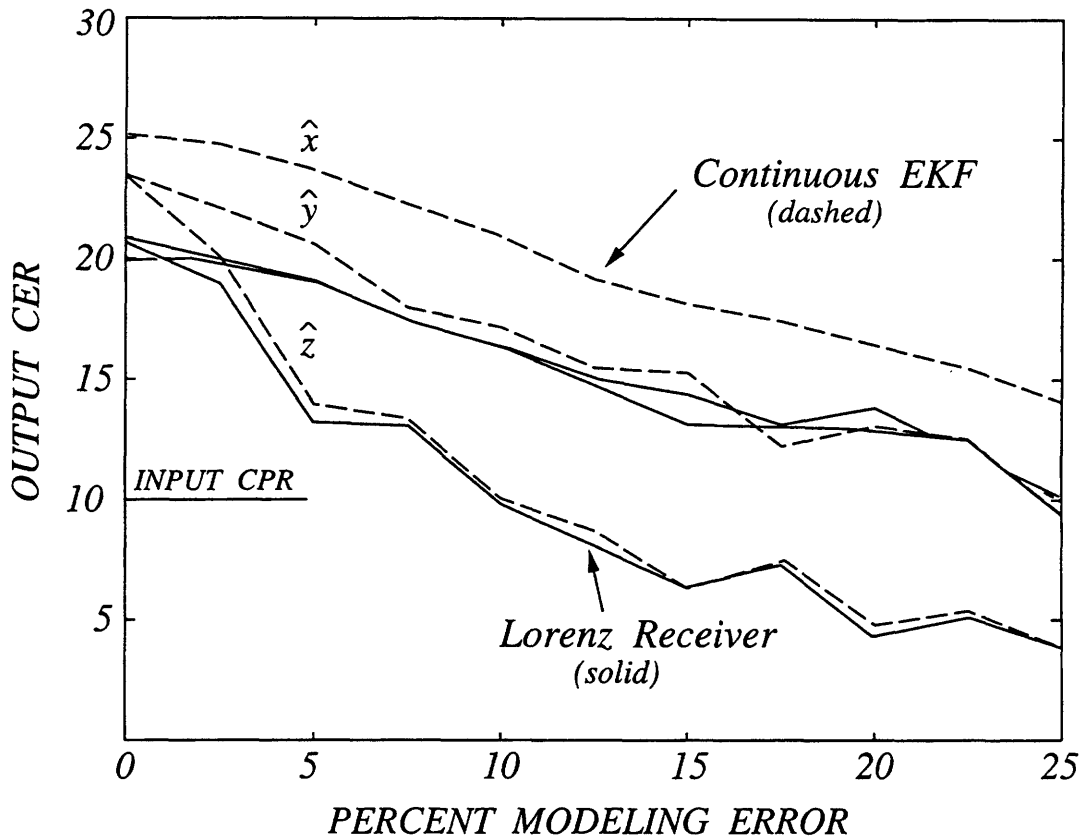


Figure 4-6: *Sensitivity to Modeling Errors: Lorenz Receiver and Continuous EKF.*

value of the receiver parameters. A wide range of modeling errors was tested, with the input CPR fixed at 10 dB throughout the experiment. In figure 4-6, we summarize the results of the experiment. The performance curves were averaged over several independent trials. The slopes of these curves indicate that the sensitivity of the Lorenz receiver and EKF are comparable over the range of modeling errors tested.

In summary, the performance of the Lorenz receiver for obtaining state estimates of the Lorenz system is comparable to the corresponding continuous and linearized EKF algorithms when white noise is added to the drive signal. Two notable characteristics of the output CER vs. input CPR curves for the Lorenz receiver are:

- a threshold effect is evident at a critical value of input CPR; and
- above the threshold, the normalized error in synchronization of each state variable is significantly smaller than the perturbation.

In Chapter 5, these characteristics are explored in greater detail.

Chapter 5

Robustness and Signal Recovery in a Synchronized Chaotic System

In Chapter 4, we showed that the Lorenz receiver produces robust state estimates when the drive signal is perturbed by additive white noise. The normalized error in synchronization of each state variable is approximately 10 dB less than the normalized error in the drive signal, provided that the input CPR is larger than some critical value. These observations pose the question of whether the synchronization is also robust to speech or other narrowband perturbations. This chapter is motivated by the desire to answer this question as well as the related questions listed below.

- Why does the Lorenz receiver exhibit a threshold effect at low input CPRs?
- Are the synchronization errors correlated, and if so, is it a linear or nonlinear dependency?
- Does the sensitivity of the synchronization depend on the spectral characteristics of the perturbation signal? If so, can it be explained?
- Suppose that the received signal consists of the sum of a low-level speech signal, or other narrowband message, and the synchronizing drive signal. Can the message be accurately recovered by subtracting the regenerated drive signal at the receiver from the received signal? Why or why not?

When a message or other perturbation is added to the chaotic drive signal, the receiver does not regenerate a perfect replica of the drive; there is always some syn-

chronization error. By subtracting the regenerated drive signal from the received signal, successful message recovery would result if the synchronization error was small relative to the perturbation itself. One of the main results presented in this chapter is that for the Lorenz system, the synchronization error is not small compared to a narrowband perturbation; nevertheless, the message can be recovered because the synchronization error turns out to be nearly coherent with the message. We will present experimental evidence for this effect, along with an explanation in terms of an approximate analytical model.

In Section 5.1, we present the results of several experiments which demonstrate the robustness of synchronization to white noise perturbations and the ability to recover speech perturbations. In Section 5.2, we use stochastic calculus to determine the first and second moments of the synchronization error signals when the perturbation is white noise. A dynamical system interpretation of the second moment equation explains the threshold effect observed at low input CPRs. This equation also provides an analytical means for quantifying the correlation between the error signals. In Section 5.3, we develop an approximate analytical model that quantifies and explains the sensitivity of the synchronization in terms of the spectral characteristics of the perturbation. We also explain why speech and other narrowband perturbations can be recovered faithfully, even though the synchronization error is comparable in power to the message itself. In Section 5.4, we summarize the primary contributions of this chapter.

5.1 Experiments to Demonstrate Robustness and Signal Recovery

In this section, we conduct a series of experiments to demonstrate the robustness of synchronization to white noise perturbations and the ability to recover speech perturbations. These experiments focus on the synchronizing properties of the Lorenz

transmitter equations,

$$\begin{aligned}\dot{x} &= \sigma(y - x) \\ \dot{y} &= rx - y - xz \\ \dot{z} &= xy - bz \ ,\end{aligned}\tag{5.1}$$

and the corresponding receiver equations,

$$\begin{aligned}\dot{x}_r &= \sigma(y_r - x_r) \\ \dot{y}_r &= rs(t) - y_r - s(t)z_r \\ \dot{z}_r &= s(t)y_r - bz_r \ .\end{aligned}\tag{5.2}$$

Previously, we showed that with $s(t)$ equal to the transmitter signal $x(t)$, the signals x_r, y_r , and z_r will asymptotically synchronize to x, y , and z , respectively.

In our notation for the transmitter and receiver equations, we have established the convention that \dot{x}, \dot{y} , and \dot{z} denote $dx/d\tau, dy/d\tau$, and $dz/d\tau$ respectively where $\tau = t/T$ is normalized time and T is a time scale factor. This convention provides the flexibility for adjusting the time scale of the signals. It is also convenient to define the normalized frequency $\omega = \Omega T$, where Ω denotes the angular frequency in units of rad/s. The parameter values used in our experiments are $\sigma = 16, r = 45.6$, and $b = 4$. For the experiments which use a speech segment as the perturbation signal, the value of T is $400 \mu\text{sec}$, otherwise $T = 1 \text{ sec}$.

The use of the Lorenz system for practical applications requires that the receiver approximately synchronizes when a perturbation $p(t)$ is added to $x(t)$, *i.e.*, when $s(t)$ is given by

$$s(t) = x(t) + p(t) \ .$$

In Section 5.1.1, we experimentally examine the error between the state variables x, y , and z in the transmitter, and the state variables x_r, y_r , and z_r in the receiver when $p(t)$ is white noise. The corresponding errors will be denoted as e_x, e_y , and e_z

respectively, *i.e.*,

$$\begin{aligned}e_x(t) &= x(t) - x_r(t) \\e_y(t) &= y(t) - y_r(t) \\e_z(t) &= z(t) - z_r(t) .\end{aligned}$$

By subtracting the regenerated drive signal $x_r(t)$ from the received signal $s(t)$, the recovered message is

$$\hat{p}(t) = s(t) - x_r(t) = p(t) + [x(t) - x_r(t)] .$$

In this context, $e_x(t)$ corresponds directly to the error in the recovered message. In Section 5.1.2, we experimentally examine this error when $p(t)$ is a speech signal.

5.1.1 Sensitivity of Synchronization to Additive White Noise

In figure 5-1, we plot the output chaos-to-error ratio (CER) for each state variable as the input chaos-to-perturbation ratio (CPR) is varied over a wide range. Two relevant characteristics of the output CER curves are: *(i)* a threshold effect is evident at low input CPRs, and *(ii)* above the threshold the normalized synchronization error of each of the state variables is approximately 10 dB less than the normalized error in the drive signal $x(t)$. We analytically determine an exact moment equation which closely predicts both of these characteristics later in Section 5.2.

In figure 5-2, we plot the message and error spectra for each of the three state variables vs. normalized frequency ω . Note that at relatively low frequencies, the error in reconstructing $x(t)$ slightly exceeds the perturbation of the drive but that for normalized frequencies above 20 the situation quickly reverses. The analytical model developed in Section 5.3 closely predicts and explains this behavior. These figures suggest that the sensitivity of synchronization depends on the spectral characteristics of the perturbation signal. For signals which are bandlimited to the frequency range $0 < \omega < 10$, we would expect that the synchronization errors will be larger than

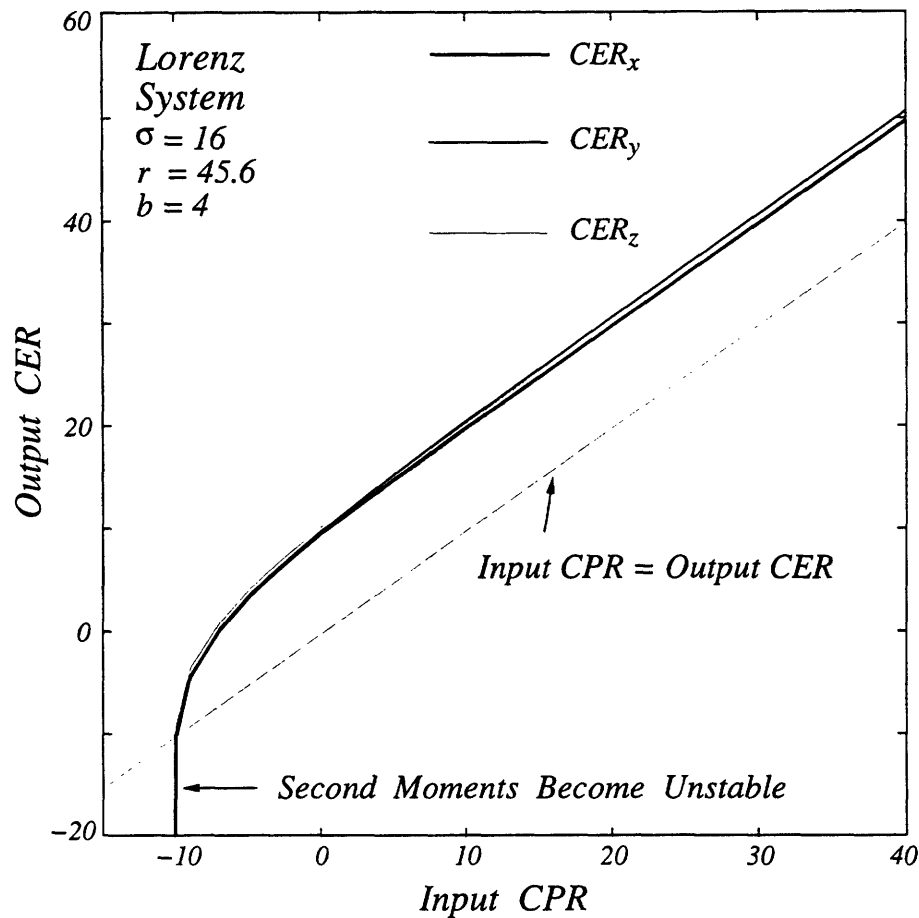


Figure 5-1: Output CER_x , CER_y , and CER_z vs. Input CPR for the Lorenz Synchronizing Receiver.

the perturbation itself. This turns out to be the case, although the next experiment shows there are additional interesting characteristics as well.

5.1.2 Sensitivity of Synchronization to Additive Speech

In this experiment, $p(t)$ is a low-level speech signal (the message to be transmitted and recovered). The normalizing time parameter is $400\ \mu sec$ and the speech signal is bandlimited to 4 kHz or, equivalently, to a normalized frequency ω of 10. Figure 5-3 shows the power spectrum of a representative speech signal and the chaotic signal $x(t)$. The overall CPR in this experiment is approximately 20 dB.

To recover the message, we subtract the regenerated drive signal at the receiver

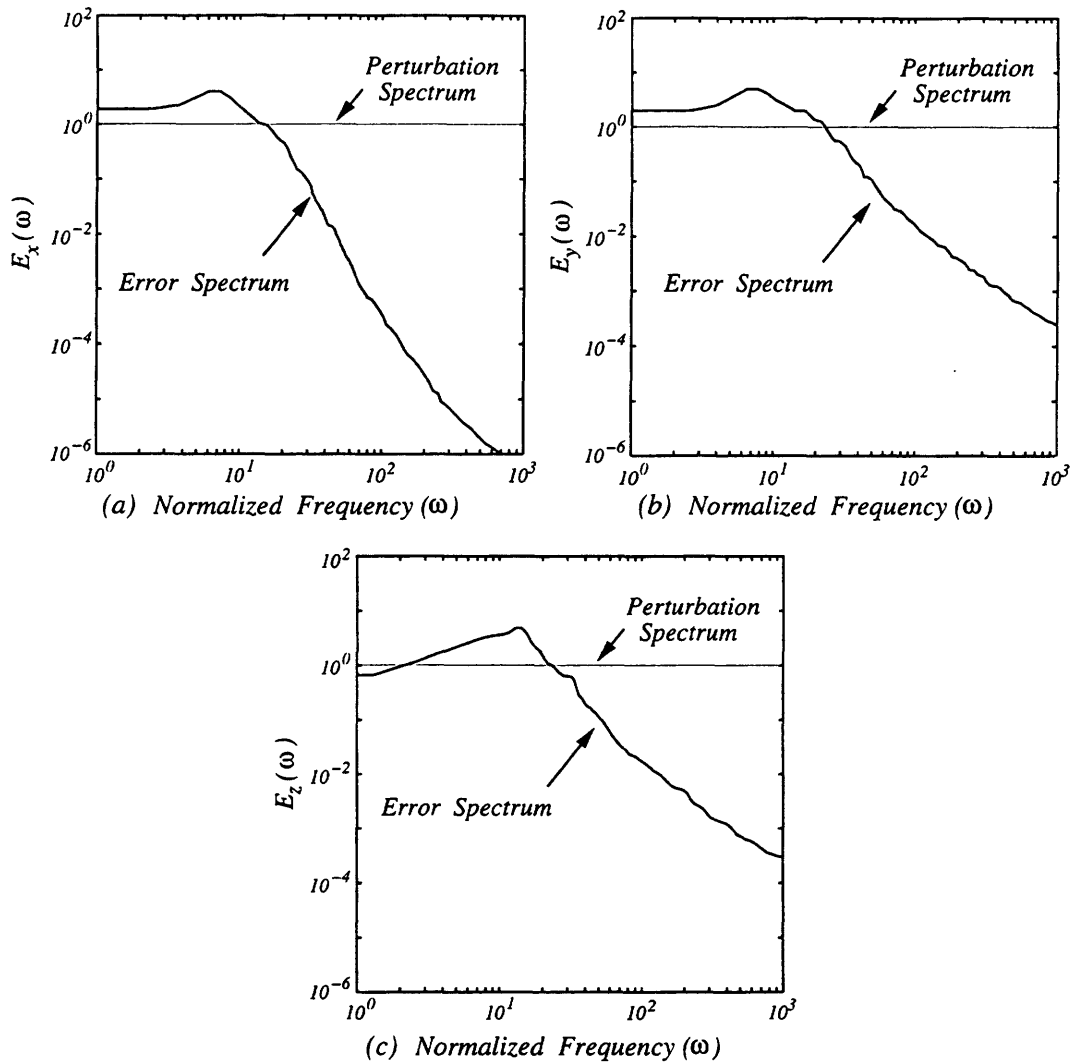


Figure 5-2: True Power Spectra of the Error Signals: (a) $E_x(\omega)$. (b) $E_y(\omega)$. (c) $E_z(\omega)$.

from the received signal. In this case, the recovered message is

$$\hat{p}(t) = p(t) + e_x(t) .$$

It would be expected that successful message recovery would result if $e_x(t)$ was small relative to the perturbation signal. For the Lorenz system, however, we will show that although the synchronization error is not small compared to the perturbation, the message can be recovered because $e_x(t)$ is nearly coherent with the message. Experimental evidence for this effect is presented below and an explanation in terms

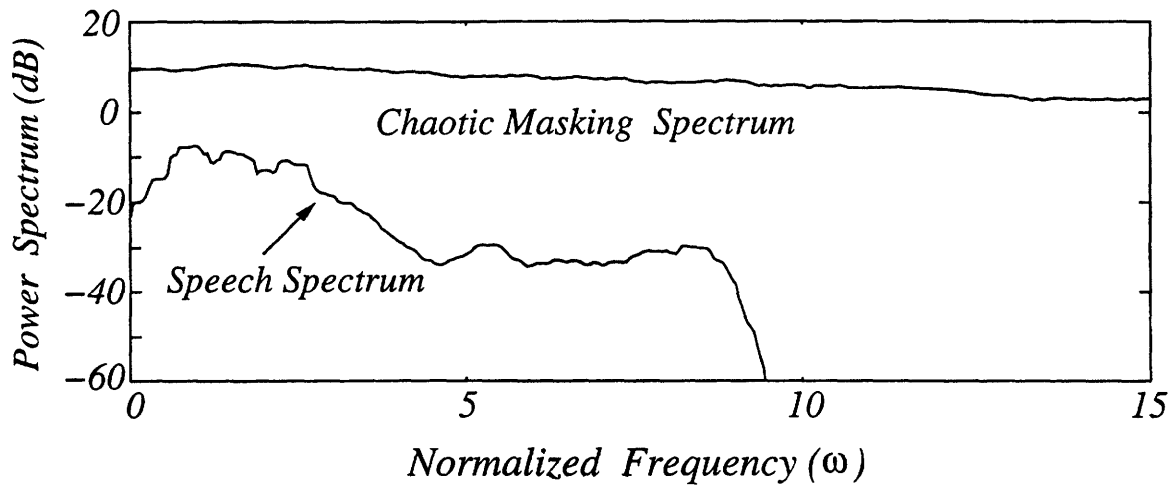


Figure 5-3: *Power Spectra of $x(t)$ and $p(t)$ when the Perturbation is a Speech Signal.*

of an approximate analytical model is presented in Section 5.3.

In figure 5-4, we show the spectrum of $\hat{p}(t)$ for this same example. Notice that $\hat{p}(t)$ includes considerable energy beyond the bandwidth of the speech. Furthermore, $\hat{p}(t)$ resembles a scaled version of the message at low frequencies. Later, we show that these observations are consistent with the synchronization error $e_x(t)$ being nearly coherent with the message at low frequencies and noise-like at high frequencies. Consequently, the speech recovery can be improved by lowpass filtering $\hat{p}(t)$. We denote the lowpass filtered version of $\hat{p}(t)$ by $\hat{p}_f(t)$. In figure 5-5(a)-(c), we show $p(t)$, $s(t)$, and $\hat{p}_f(t)$ respectively. With this lowpass filtering, the message-to-error ratio is approximately 10 dB.

5.2 Determining the Synchronization Error Moment Equations

In this section, we analytically determine the first and second moments of the synchronization error signals when the perturbation is white noise to help explain the threshold effect observed at low input CPRs. We start with an approximate approach (Section 5.2.1) and then use stochastic calculus to obtain an exact result (Section 5.2.2).

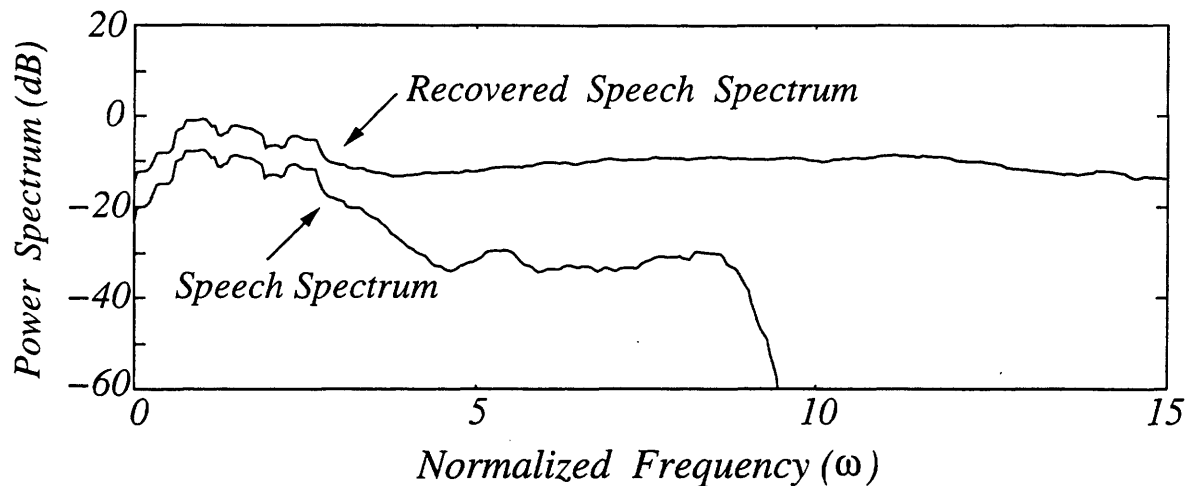


Figure 5-4: Power Spectra of $p(t)$ and $\hat{p}(t)$ when the Perturbation is a Speech Signal.

5.2.1 Approximate Approach

By subtracting the receiver equations (5.2) from the transmitter equations (5.1), the following set of error equations is obtained.

$$\dot{\mathbf{e}} = \begin{bmatrix} -\sigma & \sigma & 0 \\ 0 & -1 & -s(t) \\ 0 & s(t) & -b \end{bmatrix} \mathbf{e} + \begin{bmatrix} 0 \\ z(t) - r \\ -y(t) \end{bmatrix} p(t) \quad (5.3)$$

These error equations represent a linear time-dependent system of the form

$$\dot{\mathbf{e}} = A(s(t))\mathbf{e} + \mathbf{b}(t)p(t) . \quad (5.4)$$

If we assume that the perturbation $p(t)$ is small, then we can approximate (5.4) by a linear time-dependent system of the form

$$\dot{\mathbf{e}} = A(x(t))\mathbf{e} + \mathbf{b}(t)p(t) . \quad (5.5)$$

By using augmented state models, it is possible to analyze the statistical properties of (5.5) when $p(t)$ is temporally correlated. We will assume, however, that $p(t)$ is a zero-mean white noise process with covariance function $K_p(t, \tau) = \sigma_p^2 \delta(t - \tau)$ to simplify the presentation of our error analysis approach.

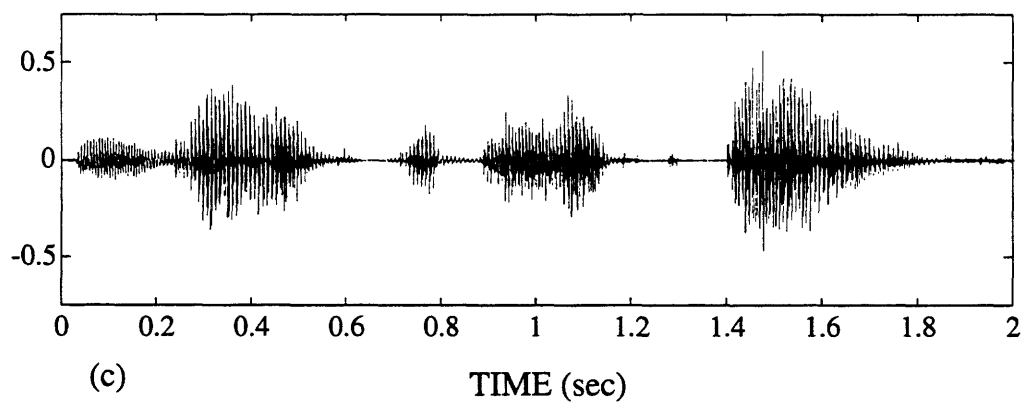
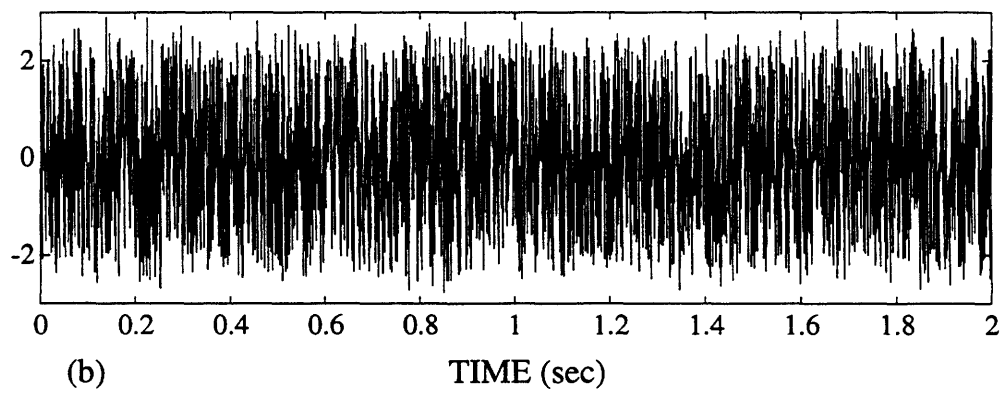
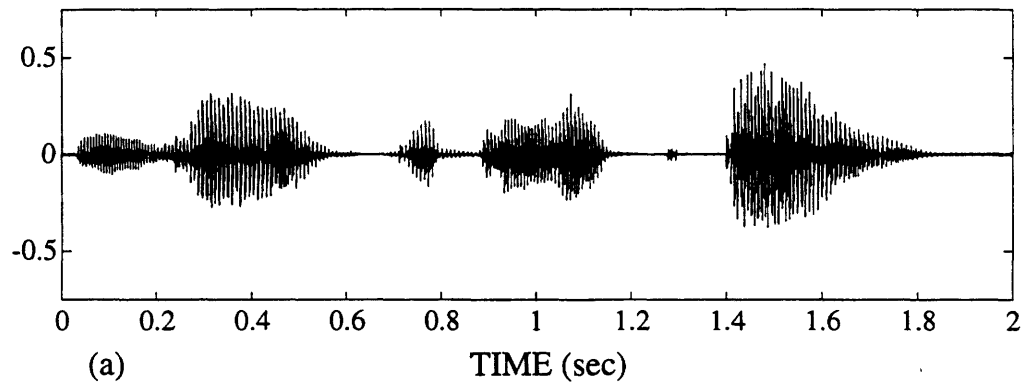


Figure 5-5: (a) Original Speech. (b) Received Signal. (c) Recovered Speech.

From (5.5), the first moment of $\mathbf{e}(t)$ is governed by a differential equation of the form

$$\dot{\eta}_e(t) = A(x(t))\eta_e(t) . \quad (5.6)$$

Previously, we showed that equations of this form are asymptotically stable at the origin (see equation (3.14)). Thus, $\eta_e(t) \rightarrow 0$ as $t \rightarrow \infty$. This shows that the Lorenz receiver produces unbiased state estimates of x , y , and z when $p(t)$ is a small zero-mean white noise process. We show later that this result holds even when $p(t)$ is not small.

The error covariance matrix $P_e(t)$ corresponding to (5.5) is governed by the matrix Lyapunov equation

$$\dot{P}_e(t) = A(x(t))P_e(t) + P_e(t)A^T(x(t)) + \sigma_p^2 \mathbf{b}(t)\mathbf{b}^T(t) . \quad (5.7)$$

This equation shows that $P_e(t)$ depends linearly on the noise intensity σ_p^2 . For small σ_p^2 (large input CPRs), the numerical estimates of output CER vs. input CPR, shown in figure 5-1, are consistent with this observation. However, due to the linear dependence on σ_p^2 , equation (5.7) does not predict the threshold effect observed at low input CPRs. In the threshold region, σ_p^2 is relatively large and equation (5.7) is no longer a valid approximation of the true error covariance matrix. In the next section, we use stochastic calculus to determine exact moment equations which overcome this limitation.

5.2.2 Exact Approach via Stochastic Calculus

The exact error equations (5.3) can be represented by a *bilinear system* having a four-dimensional state space. Specifically, we define the augmented vector ζ by

$$\zeta = \begin{bmatrix} e_x \\ e_y \\ e_z \\ 1 \end{bmatrix},$$

and determine the dynamics of ζ below.

$$\dot{\zeta} = \left\{ \begin{bmatrix} -\sigma & \sigma & 0 & 0 \\ 0 & -1 & -x(t) & 0 \\ 0 & x(t) & -b & 0 \\ 0 & 0 & 0 & 0 \end{bmatrix} + \begin{bmatrix} 0 & 0 & 0 & 0 \\ 0 & 0 & -1 & z(t) - r \\ 0 & 1 & 0 & -y(t) \\ 0 & 0 & 0 & 0 \end{bmatrix} p(t) \right\} \zeta \quad (5.8)$$

Equation (5.8) has the form $\dot{\zeta} = \{A_0(t) + A_1(t)p(t)\}\zeta$, *i.e.*, it represents a bilinear system which is driven by the stochastic process $p(t)$. Methods based on the theory of stochastic differential equations and Lie algebras have been developed for the analysis of this class of systems [36, 37, 38]. As shown below, we can utilize these theories to determine the first and second moments of $e(t)$. We will also assess the stochastic stability of these moments.

The Ito differential equation corresponding to (5.8) is given by

$$d\zeta = \{A_0(t)dt + A_1(t)\sigma_p dw(t)\}\zeta, \quad (5.9)$$

where the stochastic process $w(t)$ is the integral of white noise, *i.e.*, $w(t)$ is a Brownian motion or Wiener process. Ito equations are particularly useful for computing expectations. They are awkward, however, for performing differential computations because the rules of Ito calculus do not conform to the rules of ordinary calculus. On the other hand, Stratonovich equations obey the rules of ordinary calculus but

expectations are more difficult to calculate. A common approach is to convert the Ito equation to Stratonovich form, perform the necessary differential calculations, and convert back to Ito form.

The Stratonovich equation corresponding to (5.9) is given by

$$d_s \zeta = \{[A_0(t) - \frac{\sigma_p^2}{2} A_1^2(t)]dt + A_1(t) \sigma_p d_s w(t)\} \zeta . \quad (5.10)$$

Following Willsky and Marcus [38], the “ n^{th} -power” of (5.10) is given by

$$d_s \zeta^{[n]} = \{[A_0^{[n]}(t) - \frac{\sigma_p^2}{2} A_1^2(t)^{[n]}]dt + A_1^{[n]}(t) \sigma_p d_s w(t)\} \zeta^{[n]} , \quad (5.11)$$

where the vector $\zeta^{[n]}$ consists of the elements

$$\sqrt{\binom{n}{n_1} \binom{n-n_1}{n_2} \cdots \binom{n-n_1-\cdots-n_{i-1}}{n_i}} e_x^{n_1} e_y^{n_2} e_z^{n_3} \mathbf{1}^{n_4}, \quad \sum_{i=1}^4 n_i = n ,$$

ordered lexicographically. Converting (5.11) back to Ito form, we obtain

$$d\zeta^{[n]} = \{[A_0^{[n]}(t) - \frac{\sigma_p^2}{2} (A_1^2(t)^{[n]} - A_1^{[n]}(t)^2)]dt + A_1^{[n]}(t) \sigma_p dw(t)\} \zeta^{[n]} . \quad (5.12)$$

The moment equations for $\zeta^{[n]}$ are obtained by taking expected values of (5.12). The result of this calculation is given by

$$\frac{d}{dt} E\{\zeta^{[n]}\} = \{[A_0^{[n]}(t) - \frac{\sigma_p^2}{2} (A_1^2(t)^{[n]} - A_1^{[n]}(t)^2)]\} E\{\zeta^{[n]}\} . \quad (5.13)$$

For $n = 1$, equation (5.13) reduces to

$$\frac{d}{dt} E\{\zeta(t)\} = A_0(t) E\{\zeta(t)\} . \quad (5.14)$$

We now utilize the following definition to assess the stochastic stability of (5.14).

Definition 5.1 (Willsky and Marcus [38]) A vector random process, ξ , is n^{th} -order

asymptotically stable if

$$\lim_{t \rightarrow \infty} E\{\xi^{[n]}(t)\} = 0 .$$

Applying this definition to equation (5.14) we see that the Lorenz error dynamics are first-order asymptotically stable, *i.e.*, $E\{\mathbf{e}(t)\} \rightarrow 0$ as $t \rightarrow \infty$. Equivalently, the Lorenz receiver produces state estimates with the following property.

Theorem 5.1 *The Lorenz receiver produces unbiased state estimates when zero-mean white noise of arbitrary intensity is added to the drive signal $x(t)$.*

While Theorem 5.1 is an important property from certain state estimation perspectives, it does not explain the threshold effect observed at low input CPRs. To further investigate this effect, we will determine the second moment of ζ .

Evaluating the moment equation (5.13) for $n = 2$ we obtain

$$\begin{aligned} \frac{d}{dt} E \left\{ \begin{bmatrix} e_x^2 \\ e_x e_y \\ e_x e_z \\ e_y^2 \\ e_y e_z \\ e_z^2 \end{bmatrix} \right\} &= \begin{bmatrix} -2\sigma & 2\sigma & 0 & 0 & 0 & 0 \\ 0 & -1 - \sigma & -x(t) & \sigma & 0 & 0 \\ 0 & x(t) & -b - \sigma & 0 & \sigma & 0 \\ 0 & 0 & 0 & -2 & -2x(t) & \sigma_p^2 \\ 0 & 0 & 0 & x(t) & -b - 1 - \sigma_p^2 & -x(t) \\ 0 & 0 & 0 & \sigma_p^2 & 2x(t) & -2b \end{bmatrix} E \left\{ \begin{bmatrix} e_x^2 \\ e_x e_y \\ e_x e_z \\ e_y^2 \\ e_y e_z \\ e_z^2 \end{bmatrix} \right\} \\ &+ \sigma_p^2 \begin{bmatrix} 0 \\ 0 \\ 0 \\ (z(t) - r)^2 \\ -y(t)(z(t) - r) \\ y(t)^2 \end{bmatrix} . \end{aligned}$$

This six-dimensional system can be represented by a cascade of two three-dimensional subsystems as illustrated in figure 5-6. The dynamical equations defining these subsystems are given below.

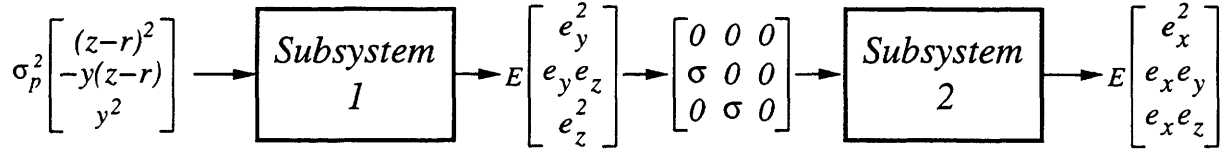


Figure 5-6: Cascade System Representation of the Second Moment Equations.

Subsystem 1:

$$\frac{d}{dt} E \left\{ \begin{bmatrix} e_y^2 \\ e_y e_z \\ e_z^2 \end{bmatrix} \right\} = \begin{bmatrix} -2 & -2x(t) & \sigma_p^2 \\ x(t) & -b-1-\sigma_p^2 & -x(t) \\ \sigma_p^2 & 2x(t) & -2b \end{bmatrix} E \left\{ \begin{bmatrix} e_y^2 \\ e_y e_z \\ e_z^2 \end{bmatrix} \right\} + \sigma_p^2 \begin{bmatrix} (z(t)-r)^2 \\ -y(t)(z(t)-r) \\ y(t)^2 \end{bmatrix}$$

Subsystem 2:

$$\frac{d}{dt} E \left\{ \begin{bmatrix} e_x^2 \\ e_x e_y \\ e_x e_z \end{bmatrix} \right\} = \begin{bmatrix} -2\sigma & 2\sigma & 0 \\ 0 & -1-\sigma & -x(t) \\ 0 & x(t) & -b-\sigma \end{bmatrix} E \left\{ \begin{bmatrix} e_x^2 \\ e_x e_y \\ e_x e_z \end{bmatrix} \right\} + \sigma E \left\{ \begin{bmatrix} 0 \\ e_y^2 \\ e_y e_z \end{bmatrix} \right\}$$

It is important to recognize that subsystem 2 does not depend on σ_p^2 , and its stability can be assessed by considering the positive definite function¹,

$$E_2 = \frac{1}{2} \left(\frac{1}{2\sigma} \overline{e_x^2} + \overline{e_x e_y} + \overline{e_x e_z} \right) .$$

Evaluating the time rate of change of E_2 , we obtain

$$\dot{E}_2 = - \left(\overline{e_x^2} - \frac{1}{2} \overline{e_x e_y} \right)^2 - \left(\frac{3}{4} + \sigma \right) \overline{e_x e_y}^2 - (b + \sigma) \overline{e_x e_z}^2 .$$

Because E_2 is positive definite and \dot{E}_2 is negative definite, it follows from Lyapunov's theorem that subsystem 2 is globally asymptotically stable. For any bounded input, subsystem 2 produces bounded outputs.

Subsystem 1 clearly depends on σ_p^2 and is stable for σ_p^2 less than some critical value.

¹In our subsequent notation, the overbars will denote statistical averages.

This critical value can be determined by considering the positive definite function,

$$E_1 = \frac{1}{2} \left(\overline{e_y^2} + 2\overline{e_y e_z} + \overline{e_z^2} \right) .$$

Evaluating the time rate of change of E_1 , we obtain

$$\dot{E}_1 = -2 \left(\overline{e_y^2} - \frac{\sigma_p^2}{2} \overline{e_z^2} \right)^2 - 2(b+1+\sigma_p^2) \overline{e_y e_z} - 2 \left(b - \frac{\sigma_p^4}{4} \right) \overline{e_z^2} .$$

Observe that \dot{E}_1 is negative definite if the following condition is satisfied.

$$b - \frac{\sigma_p^4}{4} > 0$$

This condition shows that subsystem 1 is stable for values of σ_p^2 that satisfy the inequality

$$\sigma_p^2 < 2\sqrt{b} = \gamma . \quad (5.15)$$

Equation (5.15) identifies a threshold γ for which subsystem 1 is stable; thus, the second moment equations produce bounded outputs. For values of σ_p^2 which exceed this threshold, subsystem 1 will lose stability and cause the second moment equations to be unstable.

Before confirming this analysis by numerical experiment, it is useful to write the second moment equations in the form

$$\dot{P}_e(t) = A(x(t))P_e(t) + P_e(t)A^T(x(t)) + \sigma_p^2 \mathbf{b}(t)\mathbf{b}^T(t) + \sigma_p^2 S P_e(t) S^T , \quad (5.16)$$

where S is a constant skew-symmetric matrix given by

$$S = \begin{bmatrix} 0 & 0 & 0 \\ 0 & 0 & 1 \\ 0 & -1 & 0 \end{bmatrix} .$$

Equation (5.16) is a type of Lyapunov equation that is similar to the approximate version given by equation (5.7). The only difference is that (5.16) contains the higher order term $\sigma_p^2 S P_e(t) S^T$. This term destabilizes (5.16) at low input CPRs. The results of our second moment analysis are summarized below.

Theorem 5.2 *The exact synchronization error covariance matrix $P_e(t)$ of the Lorenz receiver is governed by the matrix Lyapunov equation*

$$\dot{P}_e(t) = A(x(t))P_e(t) + P_e(t)A^T(x(t)) + \sigma_p^2 \mathbf{b}(t)\mathbf{b}^T(t) + \sigma_p^2 S P_e(t) S^T ,$$

when zero-mean white noise of intensity σ_p^2 is added to the drive signal $x(t)$. Moreover, $P_e(t)$ is bounded for $\sigma_p^2 < 2\sqrt{b}$.

In figure 5-1, we showed a plot of output CER for each state variable as the input CPR is varied over a wide range. In figure 5-7 we reproduce these curves (dashed lines) together with a plot of the output CER as predicted by the Lyapunov equation (5.16) (solid curves). The analytical predictions are in excellent agreement with the numerical results.

In figure 5-8(a), we show a plot of the synchronization error variances (diagonal elements of $P_e(t)$) vs. σ_p^2 . For small σ_p^2 , the error variances depend linearly on σ_p^2 as expected. For $\sigma_p^2 \geq 4$ ($2\sqrt{b} = 4$), the error variances become unbounded. This critical value of instability is in excellent agreement with the value predicted by equation (5.15). This analysis confirms that the threshold effect is due to an inherent instability of the second moment equation at low input CPRs.

In figure 5-8(b), we show a plot of the synchronization error correlation coefficients vs. σ_p^2 . The correlation coefficient ρ_{xy} reflects the correlation between e_x and e_y and is defined by

$$\rho_{xy} = \frac{\sigma_{e_x e_y}}{\sigma_{e_x} \sigma_{e_y}} ,$$

where $\sigma_{e_x e_y}$ denotes the covariance of e_x and e_y . An analogous definition is used for ρ_{xz} and ρ_{yz} . The coefficient ρ_{xy} suggests a strong linear dependence between e_x and e_y .

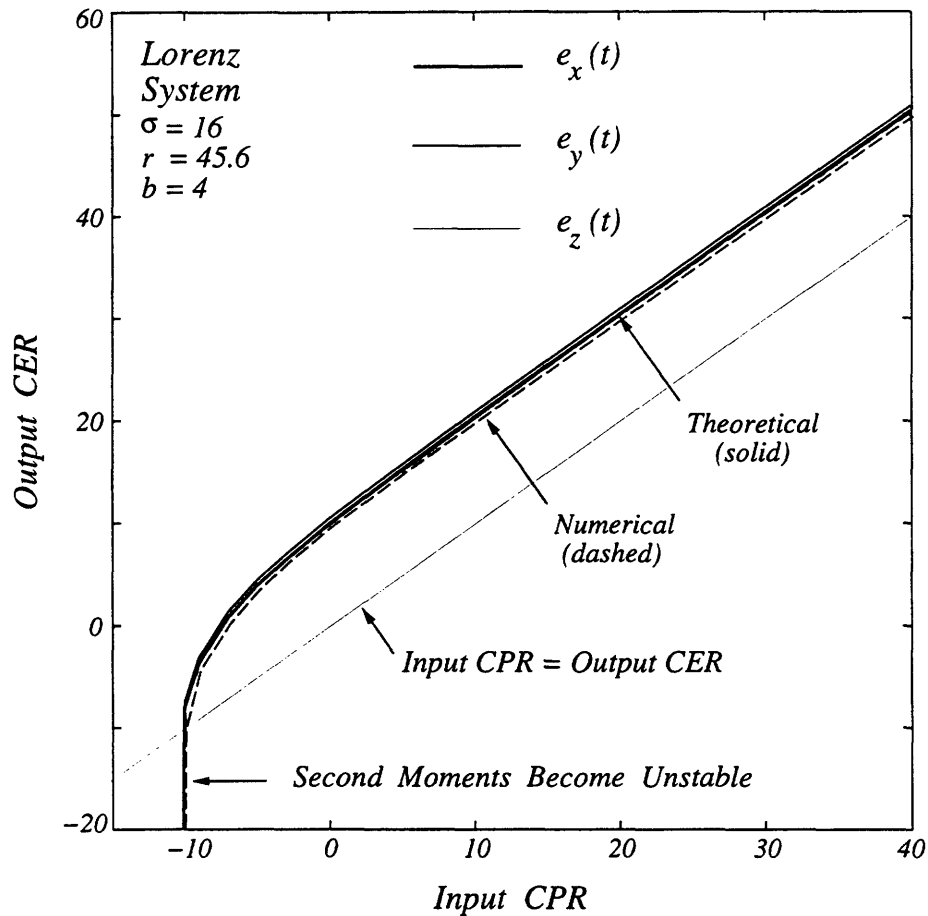


Figure 5-7: Prediction of the Output CER From the Second Moment Equation.

This dependence is consistent with the exact error equations (5.3) which indicate that e_x is the result of processing e_y with a lowpass filter having a cutoff frequency ω equal to σ . The coefficients ρ_{xz} and ρ_{yz} indicate that both e_x and e_y are nearly uncorrelated with e_z . This may not be obvious from the exact error equations, however, in Section 5.3 we develop an approximate error model which provides further insight into why this is the case.

It is also of interest to determine whether the robustness of synchronization in the Lorenz system is sensitive to the parameter values used in the implementation of the transmitter and receiver equations. One way to measure the sensitivity is by defining the perturbation-to-error ratio (PER) for each state variable. The PER associated

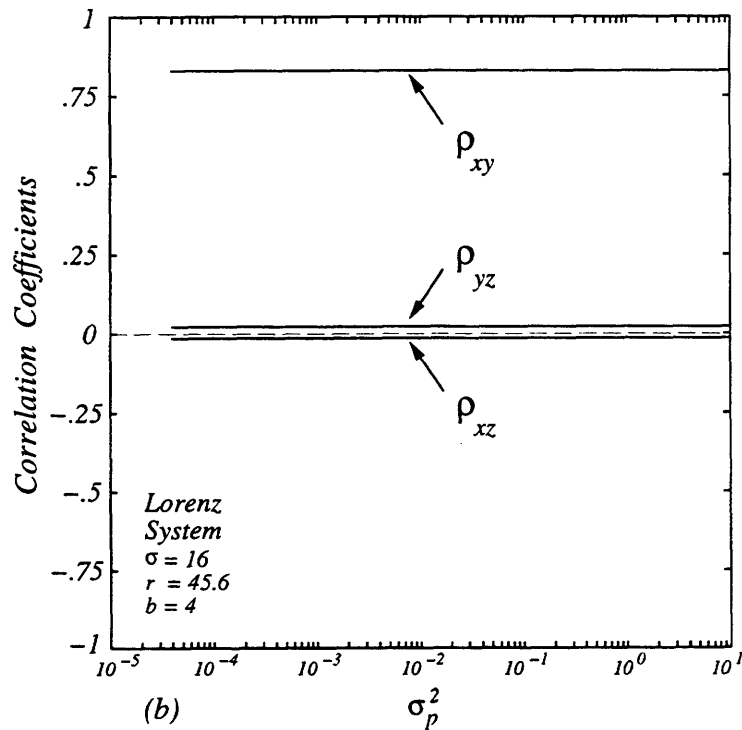
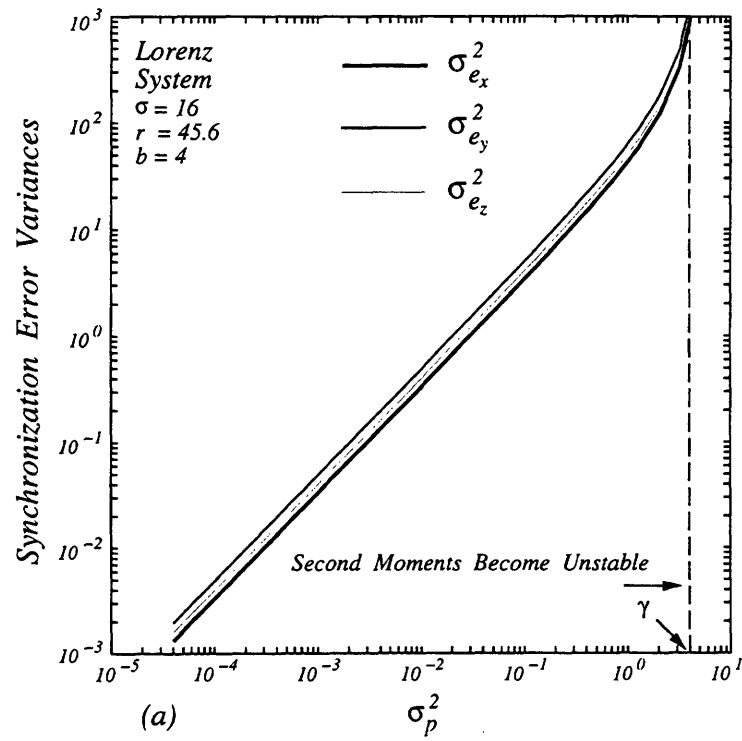


Figure 5-8: (a) Prediction of the Synchronization Error Variances From the Second Moment Equation. (b) Synchronization Error Correlation Coefficients.

with $x(t)$ is defined by

$$\text{PER}_x = \text{Output CER}_x - \text{Input CPR} .$$

The PER associated with $y(t)$ and $z(t)$ is defined analogously. An informal experiment was run in which the Lorenz parameter r is held fixed while σ and b are varied individually, and the input CPR is fixed at 10 dB. The Lyapunov equation (5.16) was then used to provide analytical predictions of the output CER for each state variable.

In figure 5-9(a), we show a plot of the PER for each state variable vs. σ . A small improvement in PER_x and PER_y is obtained by decreasing σ from its nominal value of 16. This is consistent with the lowpass filtering interpretation of the error equations; reducing σ narrows the passband of the lowpass filter. A small improvement in PER_z is obtained by increasing σ . In figure 5-9(b) we show a plot of the PER for each state variable vs. b . Variations in the b parameter have little effect on the PER of each state variable. This experiment suggests that the robustness of synchronization in the Lorenz system is not sensitive to the parameters tested.

5.3 Development of an Approximate Synchronization Error Model

In Section 5.1.1, we showed numerically that when the perturbation is white noise, the normalized error in each state variable is approximately 10 dB less than the normalized error in the drive signal. Also, the error in reconstructing the state variables slightly exceeds the perturbation of the drive signal at low frequencies, but for normalized frequencies above 20 the situation quickly reverses. In Section 5.1.2, we demonstrated that a low-level speech signal could be added to the drive signal and accurately recovered at the receiver. In this section, we develop an approximate analytical error model which is consistent with and explains these observations [34].

It is useful in our subsequent analysis to rewrite the error equations (5.3) in the

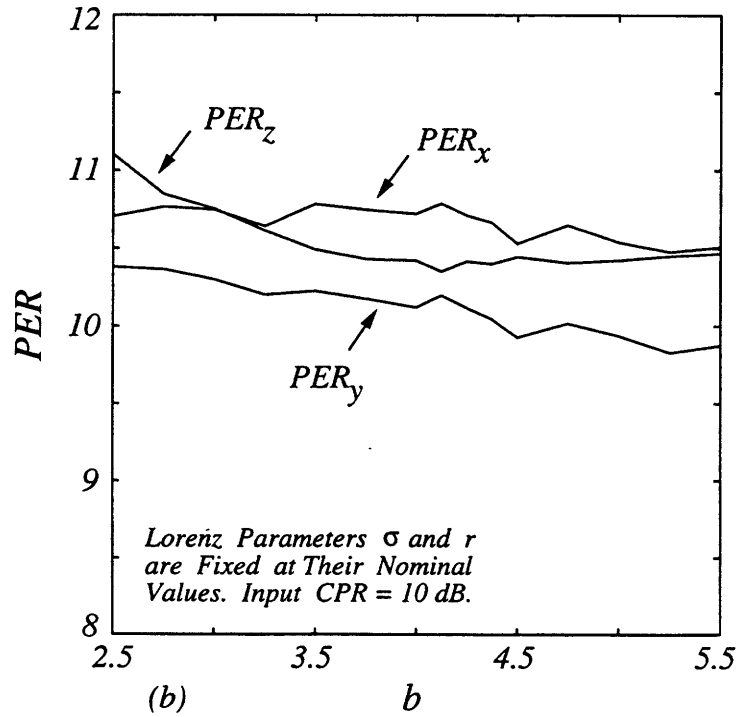
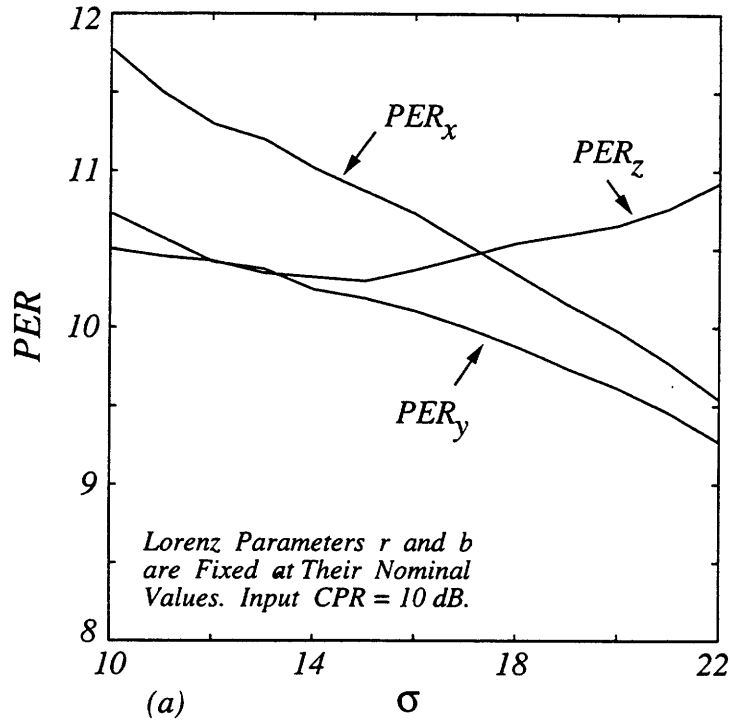


Figure 5-9: (a) Perturbation-to-Error Ratio vs. Lorenz System Parameter σ (Input CPR=10 dB). (b) Perturbation-to-Error Ratio vs. Lorenz System Parameter b (Input CPR=10 dB).

form

$$\dot{\mathbf{e}} = \begin{bmatrix} -\sigma & \sigma & 0 \\ 0 & -1 & 0 \\ 0 & 0 & -b \end{bmatrix} \mathbf{e} + \begin{bmatrix} 0 \\ -e_z \\ e_y \end{bmatrix} s(t) + \begin{bmatrix} 0 \\ \nu(t) + \bar{z} - r \\ -y(t) \end{bmatrix} p(t) , \quad (5.17)$$

where

$$\nu(t) = z(t) - \bar{z} .$$

The constant \bar{z} denotes the mean value of $z(t)$. For the parameter values that we have chosen, the value of $\bar{z} \approx 39$.

Our approach to analyzing the error system (5.17) is to assume that:

- the perturbation $p(t)$ is small, *i.e.*, $\sigma_p^2 \ll \sigma_x^2$;
- $\nu(t)$ is white noise; and
- $x(t)$ and $y(t)$ can be approximated by binary-valued functions with random transition times.

The first assumption is straightforward and allows us to approximate $s(t)$ by $x(t)$ in equation (5.17). The second assumption is justified by numerical experiment. While the third assumption may seem to be a very crude approximation, it is nevertheless a helpful heuristic. To make it more plausible, consider a sample function of $x(t)$ and $y(t)$ as illustrated in figure 5-10(a) and (b) respectively. A notable characteristic of these signals is that $x(t)$ resembles a scaled and slightly delayed version of $y(t)$. This similarity is consistent with the Lorenz equations (5.1) which indicate that $x(t)$ is the result of processing $y(t)$ with a lowpass filter having a cutoff frequency ω equal to σ . The binary-valued functions (dashed lines) in figure 5-10(a) and (b) emphasize the bipolar nature of these signals. The amplitude of these functions is scaled to reflect the standard deviation while the transition times occur at the zero crossings of the underlying waveform. The zero crossings of $x(t)$ and $y(t)$ appear to be randomly distributed and nearly coincide with each other. This suggests that we

can approximate $x(t)$ and $y(t)$ by

$$\begin{aligned}x(t) &\approx \sigma_x w(t) , \\y(t) &\approx \sigma_y w(t) ,\end{aligned}$$

where $w(t) = \pm 1$ with randomly distributed transition times. The power spectrum of $w(t)$ is broadband because of the random transition times and, as depicted in figure 5-10(c), reasonably approximates the power spectrum of the underlying waveforms. Because $w(t)$ is broadband, modulation of a narrowband signal with $w(t)$ will significantly increase the bandwidth of the narrowband signal. On the other hand, since $w^2(t) = 1$, the original narrowband signal can be exactly recovered by modulating with $w(t)$ a second time.

With these assumptions, equation (5.17) becomes

$$\dot{\mathbf{e}} = \begin{bmatrix} -\sigma & \sigma & 0 \\ 0 & -1 & 0 \\ 0 & 0 & -b \end{bmatrix} \mathbf{e} + \begin{bmatrix} 0 \\ -e_z \\ e_y \end{bmatrix} \sigma_x w(t) + \begin{bmatrix} 0 \\ \nu(t) + \bar{z} - r \\ -\sigma_y w(t) \end{bmatrix} p(t) . \quad (5.18)$$

In the context of spread spectrum communications, we refer to $w(t)$ as a *spreading function*. The resulting error model, which we refer to as the *spread spectrum error model*, is illustrated in figure 5-11. $H_1(s)$, $H_2(s)$, and $H_3(s)$ denote the transfer functions of linear time-invariant systems and are given by

$$H_1(s) = \frac{1}{s+1} , \quad H_2(s) = \frac{1}{s+b} , \quad H_3(s) = \frac{\sigma}{s+\sigma} .$$

An essential feature of this model is that it is driven by the scaled perturbation $(\bar{z} - r)p(t)$ and a white noise signal $n(t) = \nu(t)p(t)$ having an intensity that depends on $p(t)$. We are now going to make a plausibility argument that $s_{fb}(t)$ contains the message $p(t)$. First, observe that the modulated signals $-\sigma_y w(t)p(t)$ and $\sigma_x w(t)e_y(t)$ are also broadband because $p(t)$ and $e_y(t)$ are modulated by the broadband spreading function $w(t)$. If these modulated signals were directly modulated

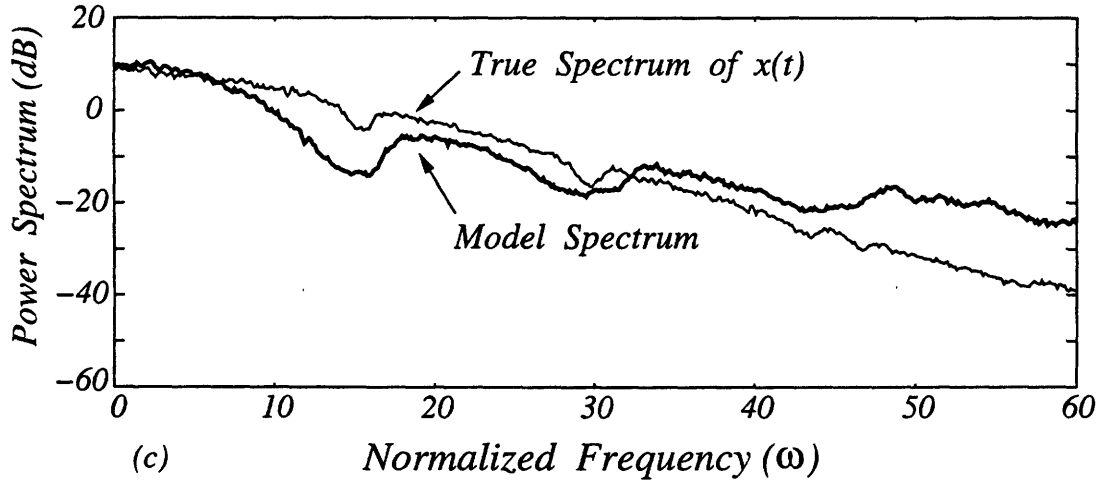
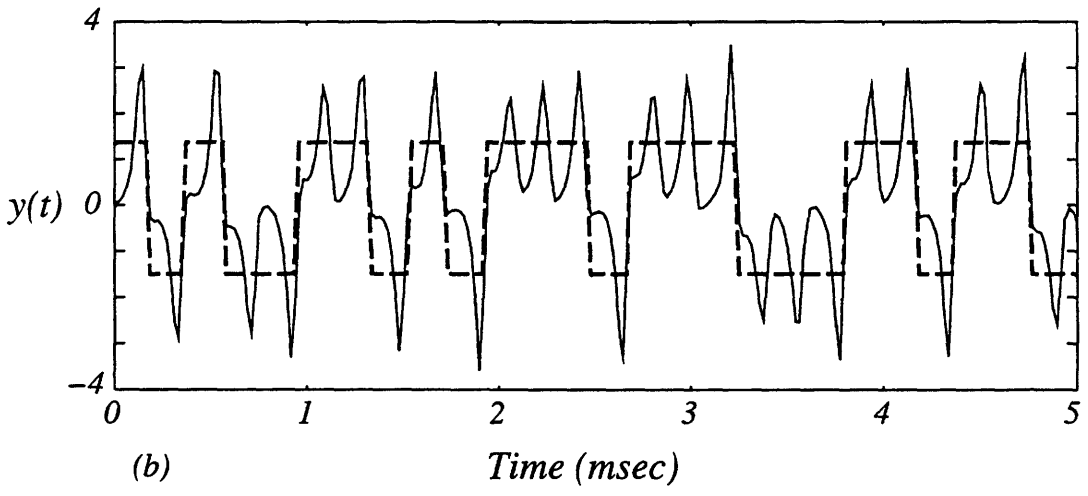
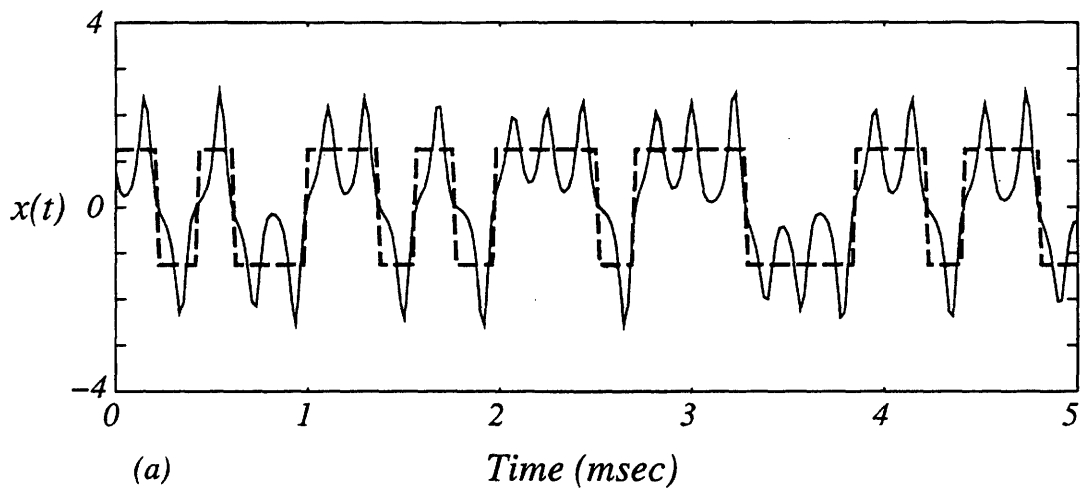


Figure 5-10: (a) A Sample Function of $x(t)$. (b) A Sample Function of $y(t)$. (c) Power Spectra of $x(t)$ and the Piecewise Constant Approximation of $x(t)$.

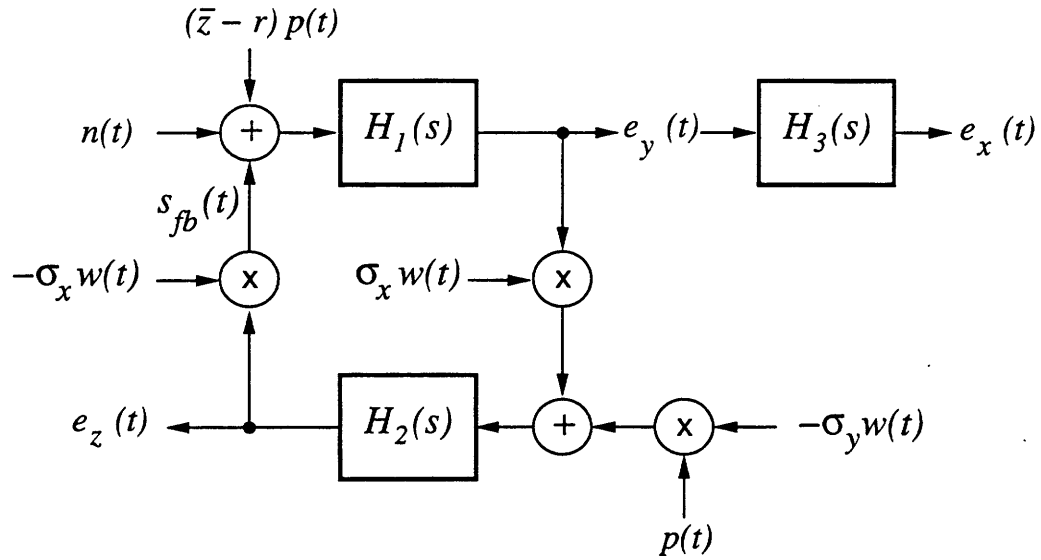


Figure 5-11: *Spread Spectrum Model of the Lorenz Error Dynamics.*

by $w(t)$ a second time, then it would be possible to exactly recover $p(t)$ and $e_y(t)$ respectively. In figure 5-11, we see that $e_z(t)$ is the result of lowpass filtering the sum $-\sigma_y w(t)p(t) + \sigma_x w(t)e_y(t)$ with $H_2(s)$. It seems reasonable that the feedback signal $s_{fb}(t) = -\sigma_x w(t)e_z(t)$ will approximate a weighted sum of $p(t)$ and $e_y(t)$. This heuristic argument is consistent with numerical experiments and allows the error signals $e_y(t)$ and $e_x(t)$ to be viewed as consisting of the sum of a noise component due to lowpass filtering $n(t)$ and a component due to lowpass filtering the perturbation $p(t)$. As we show below, this interpretation of the error signals can be made more rigorous by adding an additional constraint.

In our subsequent analysis, it is useful to view equation (5.18) as two subsystems:

$$\dot{e}_x = \sigma(e_y - e_x); \quad \text{and} \quad (5.19)$$

$$\begin{bmatrix} \dot{e}_y \\ \dot{e}_z \end{bmatrix} = \begin{bmatrix} -1 & -\sigma_x w(t) \\ \sigma_x w(t) & -b \end{bmatrix} \begin{bmatrix} e_y \\ e_z \end{bmatrix} + \begin{bmatrix} n(t) + (\bar{z} - r)p(t) \\ -\sigma_y w(t)p(t) \end{bmatrix}. \quad (5.20)$$

The first subsystem (5.19) is a linear time-invariant system. The second subsystem (5.20) is also linear but has a time-dependent coefficient $w(t)$. Exploiting the linearity of these subsystems, we can write the solution to (5.19) and (5.20) in terms of their free and forced response (more precisely, their zero-input and zero-state response).

We are now going to argue that $e_y(t)$ and $e_x(t)$ are dominated by their forced response, and that these responses are not affected by setting $w(t) = 1$ for all time.

Inspection of equation (5.20) shows that the forced response of $e_y(t)$ does not depend on the sign of $w(t)$. The same is true for $e_x(t)$, because $e_x(t)$ is the output of a linear time-invariant system which is driven by $e_y(t)$. Only the free responses of these error signals depend on the sign of $w(t)$. The contribution of the free response to the overall solution, however, is relatively small. This follows from the observation that the free response of $e_y(t)$ and $e_x(t)$ consists of brief transients; a new transient is induced each time $w(t)$ changes sign. Since the average time between sign changes of $w(t)$ is long compared to the decay time of the transients, the forced response dominates the overall solution. The corresponding argument for $e_z(t)$ is more difficult. However, our numerical experiments will clearly show that the constraint $w(t) = 1$ leads to an error model which is consistent with the exact error equations.

With $w(t) = 1$, the forced solution to (5.18) is given by

$$\begin{aligned} e_x(s) &= H_3(s)e_y(s) , \\ e_y(s) &= H_{11}(s)P(s) + H_{12}(s)N(s) , \\ e_z(s) &= H_{21}(s)P(s) + H_{22}(s)N(s) , \end{aligned} \tag{5.21}$$

where $e(s)$, $P(s)$, and $N(s)$ denote the Laplace transforms of $e(t)$, $p(t)$, and $n(t)$ respectively. The transfer functions $H_{ij}(s)$, for $i, j = 1, 2$, correspond to linear time-invariant systems and are given by

$$\begin{aligned} H_{11}(s) &= \frac{(\bar{z} - r)(s + b) + \sigma_x \sigma_y}{s^2 + (b + 1)s + b + \sigma_x^2} , \\ H_{12}(s) &= \frac{s + b}{s^2 + (b + 1)s + b + \sigma_x^2} , \\ H_{21}(s) &= \frac{\sigma_x(\bar{z} - r) - \sigma_y(s + 1)}{s^2 + (b + 1)s + b + \sigma_x^2} , \\ H_{22}(s) &= \frac{\sigma_x}{s^2 + (b + 1)s + b + \sigma_x^2} . \end{aligned}$$

Equation (5.21) represents an equivalent linear time-invariant error model which is driven by the perturbation $p(t)$ and white noise $n(t)$. A block diagram representation

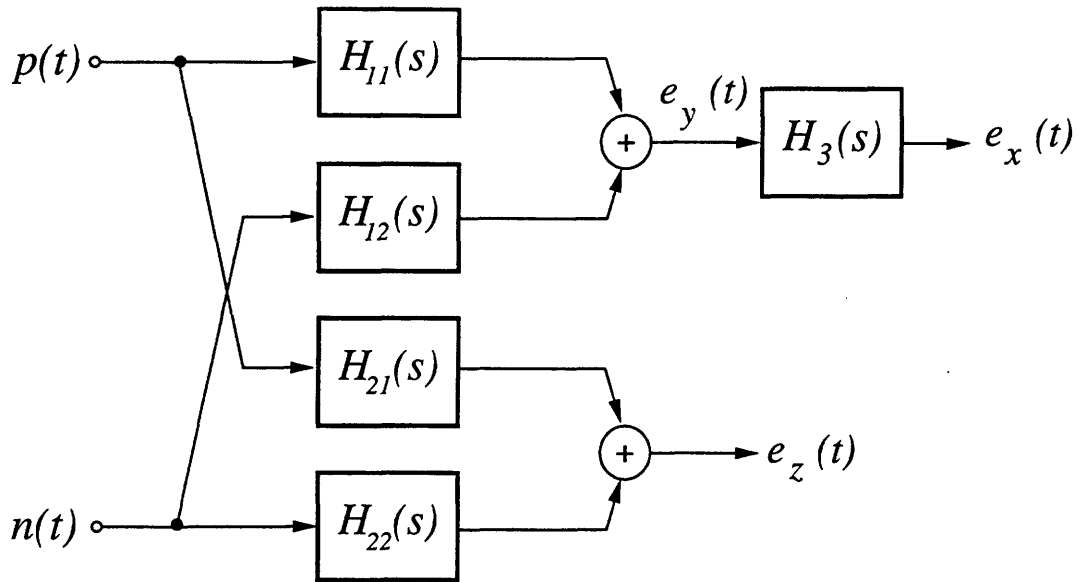


Figure 5-12: *Equivalent Linear Time-Invariant Model of the Lorenz Error Dynamics.*

of (5.21) is shown in figure 5-12. This system clearly shows that $e_y(t)$ and $e_x(t)$ can be viewed as consisting of the sum of a noise component due to lowpass filtering $n(t)$ and a component due to lowpass filtering the perturbation $p(t)$.

In the experiment where a low-level speech signal was added to the drive signal (Section 5.1.2), the recovered message was given by

$$\hat{p}(t) = p(t) + e_x(t) .$$

The error signal $e_x(t)$ depends on the properties of $H_{11}(s)$ and $H_{12}(s)$. In figure 5-13(a) and (b), we show pole-zero plots for $H_{11}(s)$ and $H_{12}(s)$ respectively. These transfer functions represent second-order lowpass filters having a cutoff frequency ω approximately equal to 13. The magnitude and phase response of these filters is shown in figure 5-13(c) and (d), respectively. Note that $H_{11}(s)$ slightly amplifies signal components within its passband $0 < \omega < 13$, whereas $H_{12}(s)$ attenuates signal components in this frequency range. For messages which are bandlimited to this frequency range, such as the speech sample illustrated in figure 5-3, the error signals $e_y(t)$ and $e_x(t)$ will resemble a slightly amplified and noise-corrupted version of the message. Furthermore, these error signals will be nearly coherent with the message

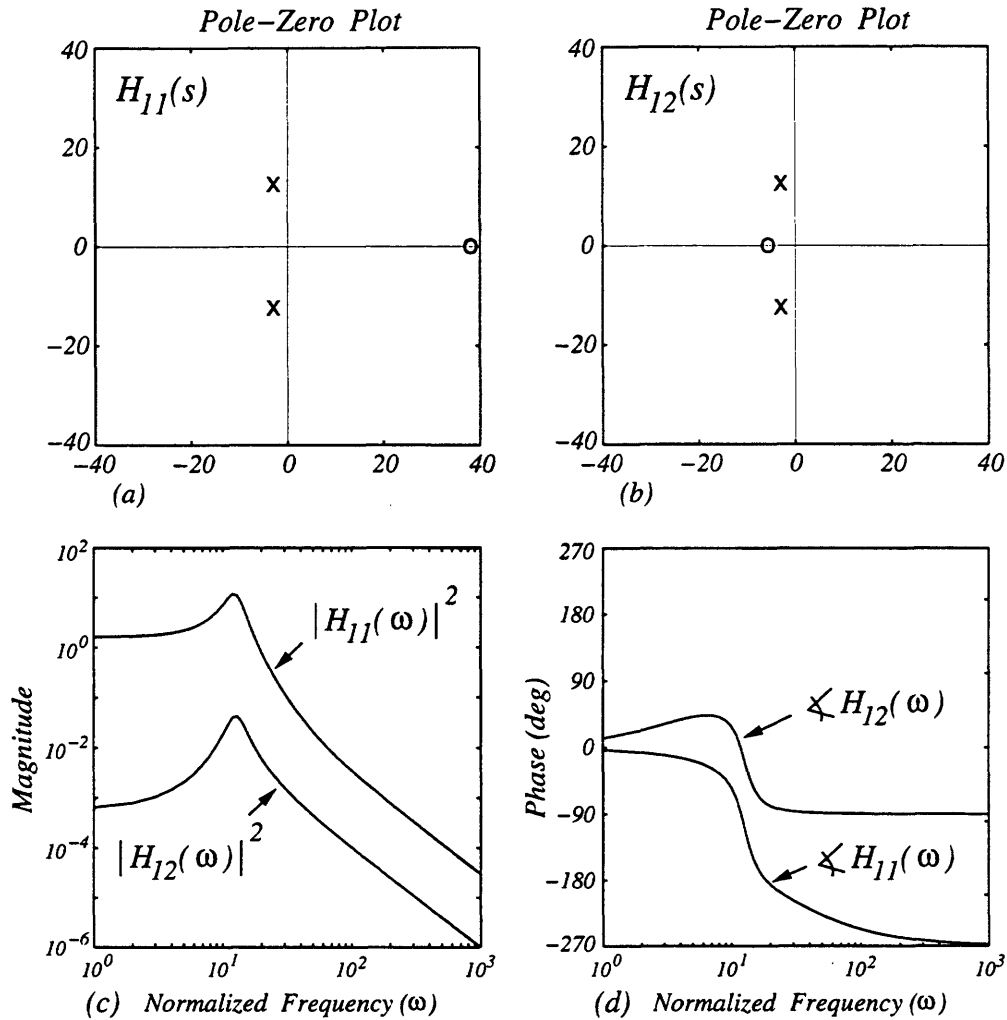


Figure 5-13: (a) Pole-Zero Plot for $H_{11}(s)$. (b) Pole-Zero Plot for $H_{12}(s)$. (c) Magnitude Response of $H_{11}(s)$ and $H_{12}(s)$. (d) Phase Response of $H_{11}(s)$ and $H_{12}(s)$.

because both $H_{11}(s)$ and $H_3(s)$ exhibit a small group delay in this frequency range.

Below, we compare the performance predicted by this error model with experimental results for both white noise and speech perturbations.

5.3.1 Error Model Performance with Additive White Noise

In figure 5-2, we showed the power spectrum of each of the error components as compared with the spectrum of the white noise perturbation and noted that most of the error power is contained in the low frequencies. The error model as depicted in figure 5-12 clearly indicates that each of the error components is the output of a

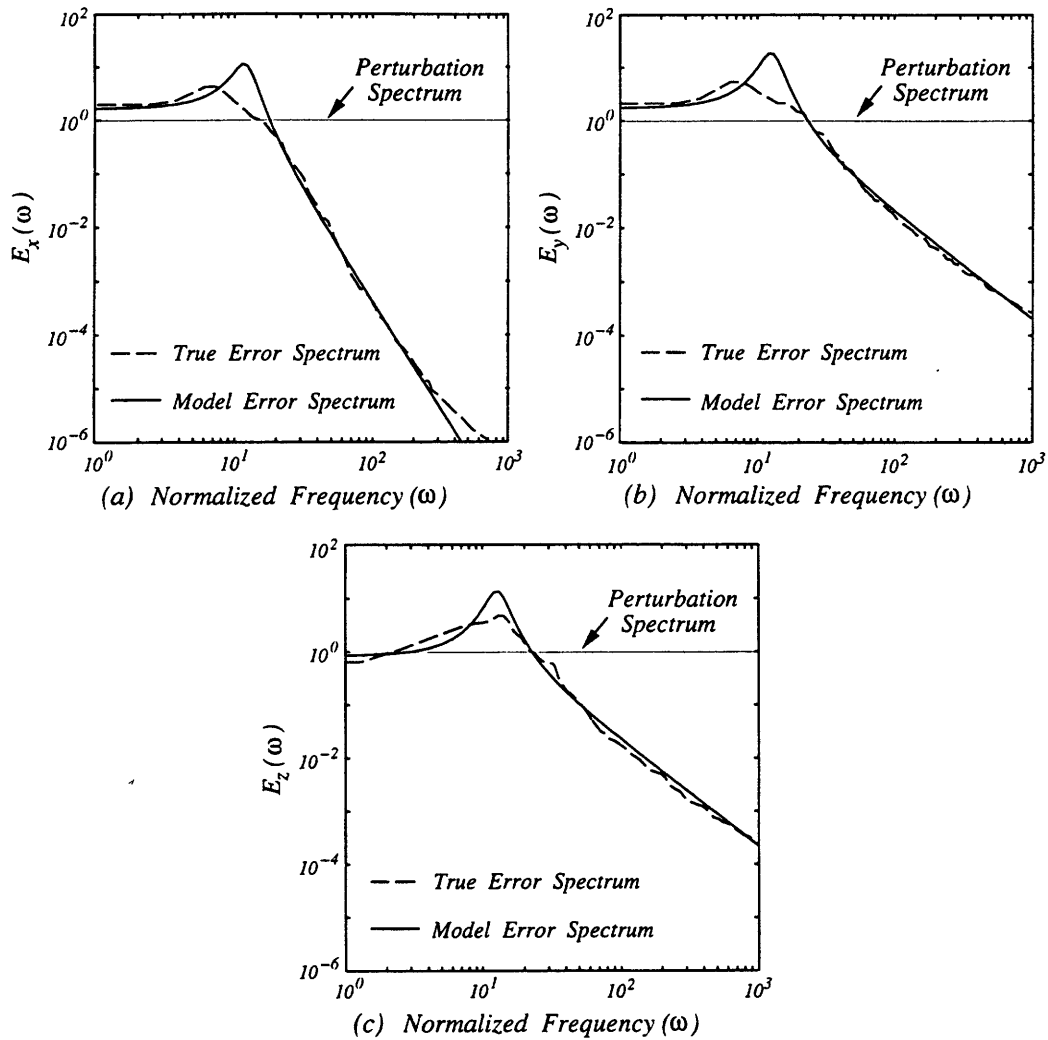


Figure 5-14: True and Estimated Power Spectra of the Error Signals: (a) $E_x(\omega)$. (b) $E_y(\omega)$. (c) $E_z(\omega)$.

lowpass filter. In figure 5-14, we reproduce figure 5-2 and include the power spectrum of the error components as predicted by the model of figure 5-12. As we see, the true results and the results predicted by the model are consistent.

5.3.2 Error Model Performance with Additive Speech

In this section, the performance predicted by the error model in figure 5-12 is compared with the experimental results when the perturbation is a speech signal.

In figure 5-15, we show a block diagram representation of the message recovery process. The recovered message $\hat{p}(t)$ consists of two components, one corresponding

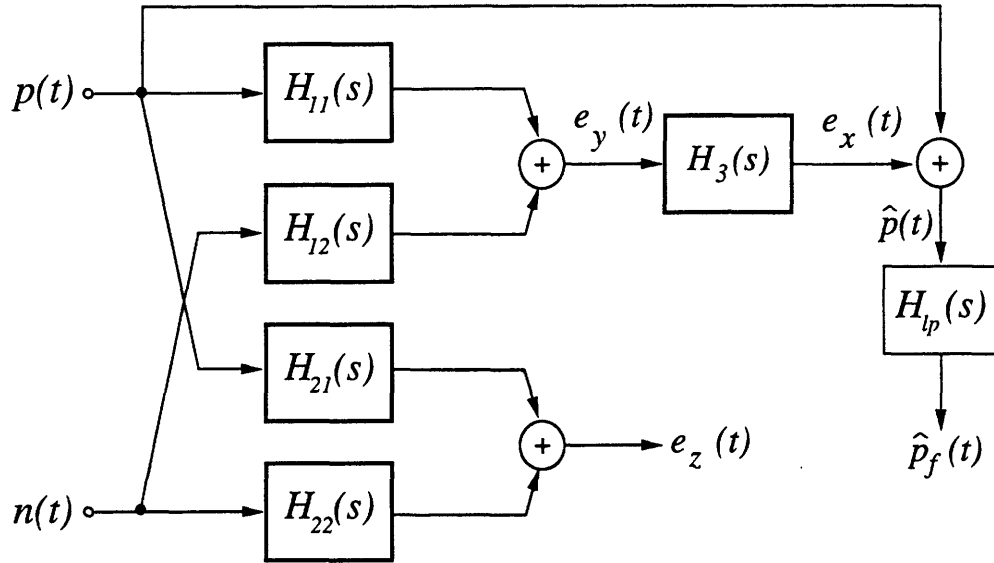


Figure 5-15: *Dynamical System Representation of the Message Recovery Process.*

directly to the message $p(t)$ and the other corresponding to the error signal $e_x(t)$. We know from the experimental results in Section 5.1.2 that $\hat{p}(t)$ represents a faithful recovery of $p(t)$. Clearly, if $e_x(t)$ is small relative to $p(t)$, then $\hat{p}(t) \approx p(t)$. However, the assumption that $e_x(t)$ is small is not correct because the low frequency components in $p(t)$ will produce a significant synchronization error. Instead, the explanation is that $e_x(t)$ is not small but is coherent with $p(t)$. This is plausible from figure 5-15 which indicates that $e_x(t)$ consists of the sum of a noise component due to $n(t)$ and a component due to $p(t)$. Because $p(t)$ is relatively low frequency, it can pass through $H_{11}(s)$ and $H_3(s)$ with little phase shift whereas the noise component will be significantly attenuated. Therefore, $e_x(t)$ will resemble a scaled version of $p(t)$ at low frequencies and be noise-like at higher frequencies. This analysis is verified below by numerical experiment.

In figure 5-16(a), we show a comparison of the true and estimated power spectrum of $e_x(t)$. These spectra are consistent and resemble the message spectrum in the frequency range $0 < \omega < 3$. In figure 5-16(b) we show a comparison of the true and estimated power spectrum of $\hat{p}(t)$. These spectra are also consistent and closely resemble the message spectrum in the frequency range $0 < \omega < 3$. Although the synchronization error $e_x(t)$ is larger than the message $p(t)$, the recovered message $\hat{p}(t)$

resembles a scaled version of $p(t)$ because the message and error are nearly coherent at these frequencies.

To improve the message-to-error ratio of $\hat{p}(t)$, an additional lowpass filter with a transfer function given by

$$H_{lp}(\omega) = \begin{cases} 1/2 & 0 \leq \omega \leq 3 \text{ rad} \\ 0 & \omega > 3 \text{ rad} \end{cases},$$

can be used to process $\hat{p}(t)$. Applying this filter to both the true and estimated $\hat{p}(t)$, we obtain the recovered speech waveforms shown in figure 5-17. The model estimate is in excellent agreement with the true result.

5.4 Summary

This chapter examined the questions of synchronization robustness and signal recovery in the Lorenz system. In Section 5.2, the use of stochastic calculus enabled us to determine the exact first and second moments of the synchronization error signals when the perturbation is white noise. Stability analysis of the second moment equation explains the threshold effect observed at low input CPRs. This equation also provides an exact analytical means for quantifying the correlation between the error signals. Some helpful insights gained from the analysis presented in Section 5.2 are given below.

- The Lorenz receiver exhibits a threshold effect at low input CPRs because the second moment equation loses stability at a critical value of σ_p^2 . Using Lyapunov functions, the critical value was predicted as $\sigma_p^2 = 2\sqrt{b}$.
- The synchronization errors e_x and e_y exhibit a strong linear dependence which is explained by the fact that e_x is the result of processing e_y with a lowpass filter having a cutoff frequency ω equal to σ . Also, the error variable e_z is nearly uncorrelated with both e_x and e_y .

In Section 5.3, the development of an approximate analytical error model has

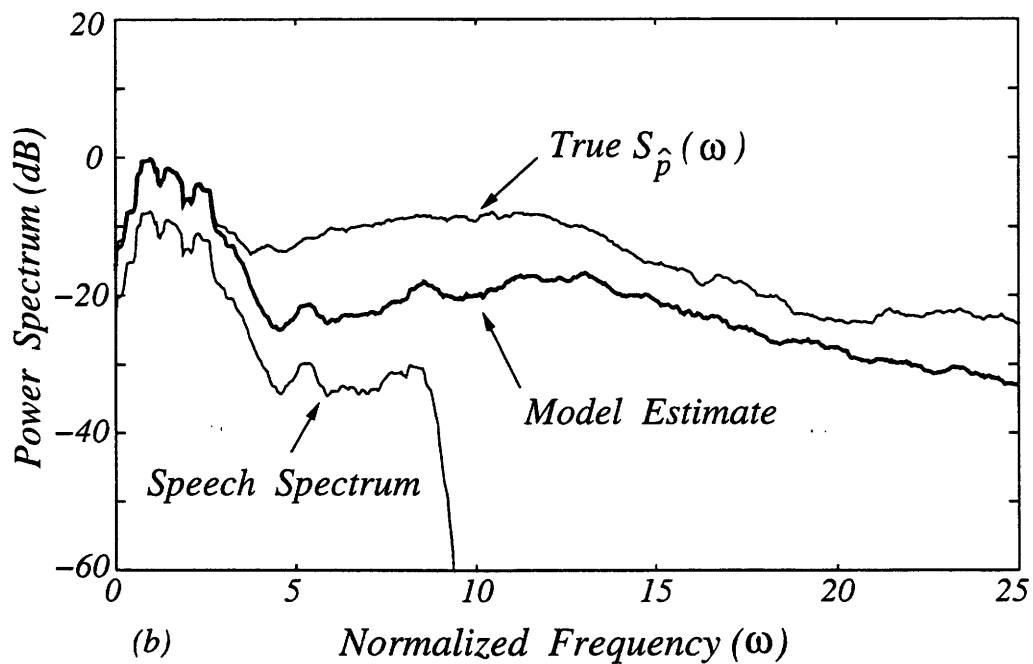
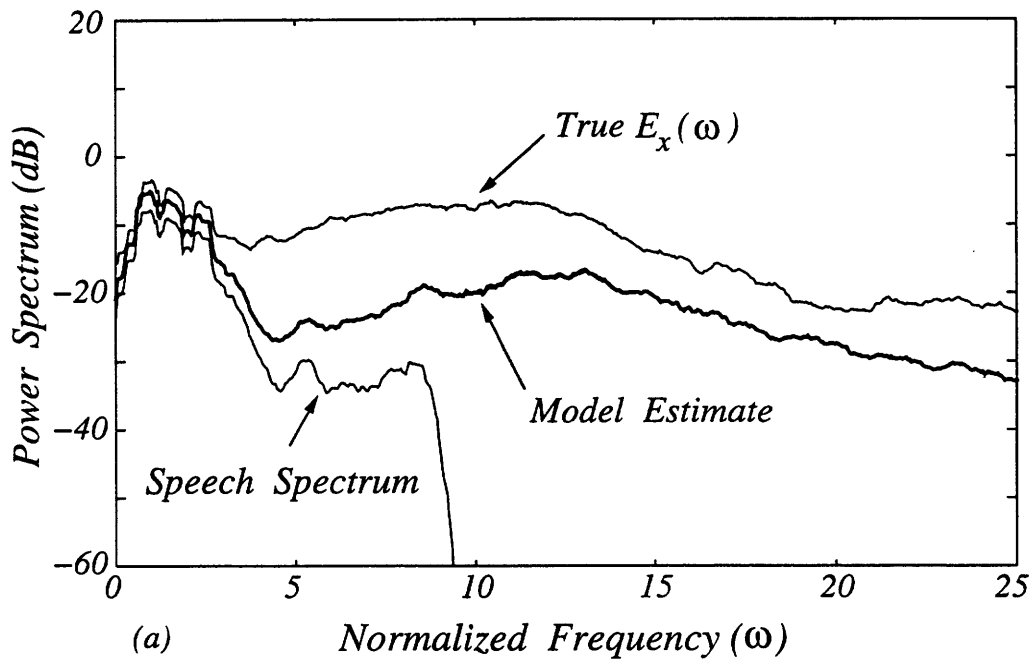


Figure 5-16: (a) Power Spectrum of $p(t)$ and the True and Estimated Power Spectrum of $e_x(t)$. (b) Power Spectrum of $p(t)$ and the True and Estimated Power Spectrum of $\hat{p}(t)$.

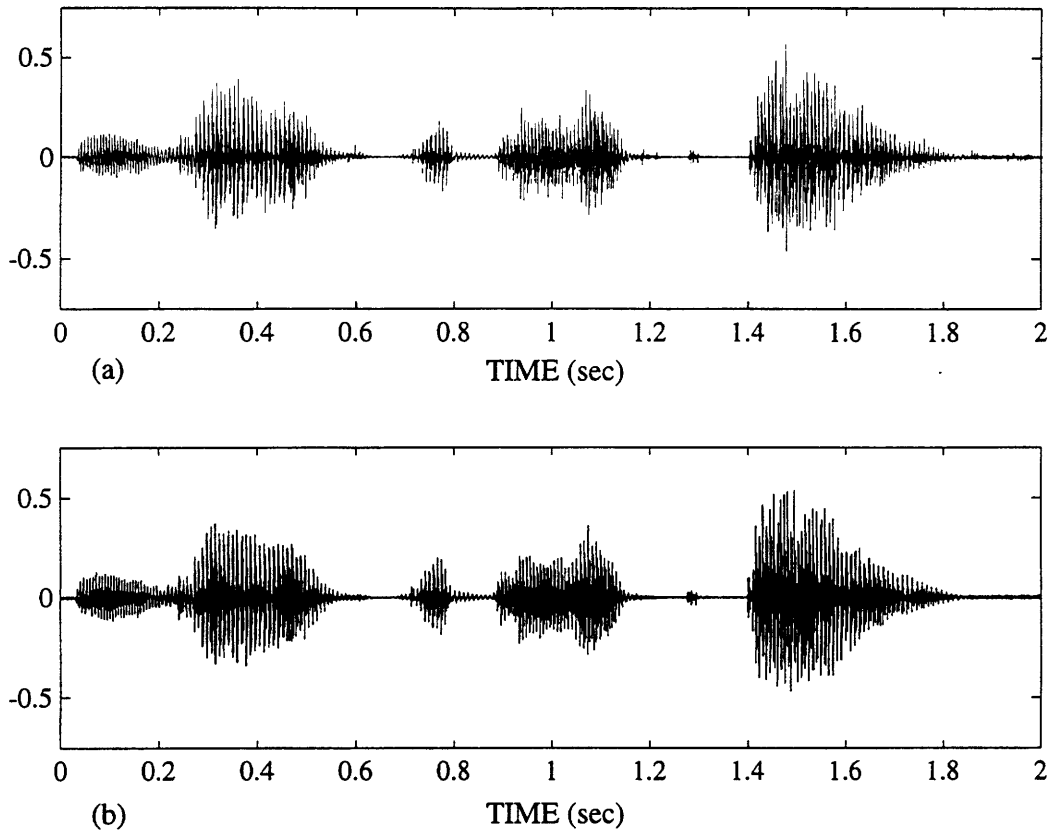


Figure 5-17: *Speech Waveforms: (a) True Recovered Message. (b) Recovered Message using the Equivalent Linear Time-Invariant Model.*

further enhanced our understanding of self-synchronization robustness and signal recovery. Some helpful insights gained from this model are given below.

- The Lorenz receiver can be viewed as a type of lowpass filter which slightly amplifies signals within its passband $0 < \omega < 13$ and rapidly attenuates signals outside of this frequency range. The sensitivity of synchronization, therefore, depends on the spectral characteristics of the perturbation. For example, the normalized error in synchronization is approximately 10 dB less than the normalized error in the drive signal when the perturbation is white noise. For perturbations having a lowpass characteristic, the receiver's synchronization error is larger than the perturbation; however, both e_x and e_y are nearly coherent with the perturbation at low frequencies. The analytical model explains why the synchronization is robust to wideband perturbations, and why the errors are nearly coherent with the message at low frequencies.
- We can now offer the explanation that a low-level speech signal can be faithfully recovered at the receiver because the synchronization error $e_x(t)$ is nearly coherent with the speech at low frequencies. Thus, the receiver's own syn-

chronization error reinforces the message to allow an accurate recovery of the original message. Additional lowpass filtering can then be used to improve the message-to-error ratio of the recovered message.

These results improve our understanding of the mechanisms underlying the synchronization in the Lorenz system. In certain communication applications, however, it is undesirable to be restricted to the Lorenz system; we need the ability to choose from a variety of synchronized chaotic systems. Unfortunately, there are currently no known systematic techniques for synthesizing chaotic systems which possess the self-synchronization property. In Chapter 6, we address this issue by synthesizing a class of chaotic systems which we refer to as *linear feedback chaotic systems*. Chapters 7 and 8 discuss alternative approaches which also provide for a systematic synthesis capability.

Chapter 6

Synthesizing Self-Synchronizing Linear Feedback Chaotic Systems

A potential drawback to utilizing synchronized chaotic systems in communications is that systematic synthesis procedures have not been developed. In fact, only a few chaotic systems which possess the self-synchronization property are currently known. In [11], it was shown that it is possible to create a five-dimensional chaotic system by augmenting the Lorenz system with additional states. However, that approach involved considerable trial and error.

This chapter is directed at a systematic approach for synthesizing high-dimensional dissipative chaotic systems which possess the self-synchronization property. To develop this approach, we begin by considering a class of chaotic systems which we refer to as *linear feedback chaotic systems* (LFBCSs). LFBCSs are composed of a low-dimensional chaotic system and a linear feedback system as illustrated in figure 6-1. Applying linear feedback to a chaotic system will increase its dimensionality, allowing for considerable flexibility in the design of new chaotic systems. Although this approach is applicable to any chaotic system, we will focus our attention on LFBCSs which utilize the Lorenz system. The advantages of applying linear feedback to the Lorenz system are that the resulting high-dimensional chaotic systems are analytically tractable and relatively easy to implement. Furthermore, this approach allows an unlimited number of self-synchronizing LFBCSs be designed, increasing the

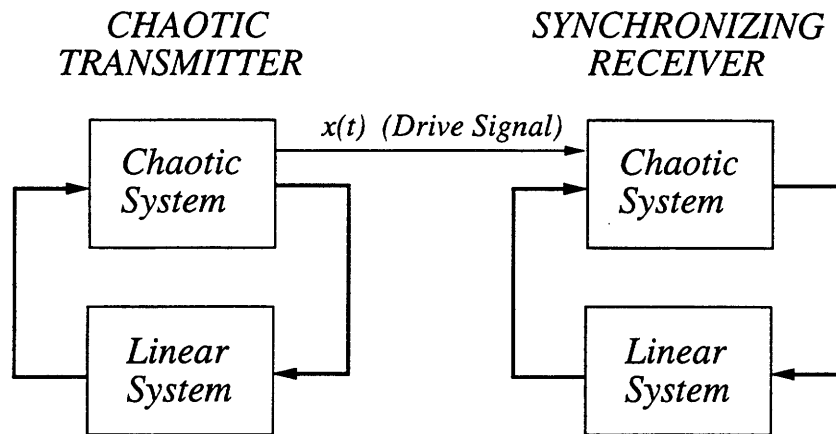


Figure 6-1: *Communicating with Linear Feedback Chaotic Systems.*

applicability of synchronized chaotic systems for practical applications.

In the communications scenario illustrated in figure 6-1, the LFBCS at the transmitter conveys the chaotic drive signal $x(t)$ to an identical LFBCS at the receiver. This drive signal provides a means for establishing and maintaining synchronization between the transmitter and receiver systems. Although these systems may operate chaotically, the self-synchronization property ensures complete coherence between the transmitter and receiver systems. In Chapter 9, we demonstrate some applied aspects of synchronized chaotic systems using an analog circuit implementation of the Lorenz system.

In Section 6.1, we examine a LFBCS in which the Lorenz signal $x(t)$ drives the linear system and the output of the linear system is added to the equation for \dot{x} in the Lorenz system (x -input/ x -output LFBCSs). Section 6.2 examines a LFBCS in which the Lorenz signal $z(t)$ drives the linear system and the output of the linear system is added to the equation for \dot{z} in the Lorenz system (z -input/ z -output LFBCSs). In both sections, we focus on:

- the development of self-synchronization and global stability conditions;
- a well-defined systematic synthesis procedure;
- a linear stability analysis of the fixed points to determine the critical values of the bifurcation parameter such that all of the fixed points will be unstable; and

— numerical examples to illustrate the theoretical results.

In Section 6.3, we summarize the results of this chapter.

6.1 x -Input/ x -Output LFBCSs

Although many types of LFBCSs are possible, consider the situation where the chaotic Lorenz signal $x(t)$ drives a single-input/single-output linear system and the output of the linear system is added to the equation for \dot{x} in the Lorenz system. In this case, the transmitter equations are given by

$$\begin{aligned}\dot{x} &= \sigma(y - x) + \nu \\ \dot{y} &= rx - y - xz \\ \dot{z} &= xy - bz \\ \dot{\mathbf{l}} &= A\mathbf{l} + Bx \\ \nu &= C\mathbf{l} + Dx \quad ,\end{aligned}\tag{6.1}$$

where \mathbf{l} and ν denote the state variables and output of the linear system, respectively. The linear system is N -dimensional, *i.e.*, A is $N \times N$, B is $N \times 1$, C is $1 \times N$, and D is 1×1 . For notational simplicity, we refer to the transmitter state variables collectively by the vector $\mathbf{x} = (x, y, z, \mathbf{l})$, when convenient.

Our first goal in this section is to develop sufficient conditions such that the transmitter (6.1) satisfies the requirements that:

- there exists an algebraically similar receiver system which possesses the global self-synchronization property; and
- the transmitter system is globally stable.

These two requirements are satisfied in Sections 6.1.1 and 6.1.2, respectively. Section 6.1.3 summarizes the various self-synchronization and global stability conditions and suggests a systematic procedure for synthesizing x -input/ x -output LFBCSs. In Section 6.1.4, we perform a linear stability analysis of the fixed points for this class of systems. In Section 6.1.5, we describe the results of several numerical experiments.

6.1.1 Conditions for Global Self-Synchronization

From certain theoretical and practical viewpoints, it is advantageous for the synchronizing receiver to have the same algebraic structure as the transmitter. The self-synchronization properties of the Lorenz system suggest a receiver system of the form

$$\begin{aligned}
 \dot{x}_r &= \sigma(y_r - x_r) + \nu_r \\
 \dot{y}_r &= rx(t) - y_r - x(t)z_r \\
 \dot{z}_r &= x(t)y_r - bz_r \\
 \dot{\mathbf{l}}_r &= A\mathbf{l}_r + Bx(t) \\
 \nu_r &= C\mathbf{l}_r + Dx(t) .
 \end{aligned} \tag{6.2}$$

Algebraically, the receiver system (6.2) is obtained from the transmitter (6.1) by renaming variables $\mathbf{x} \rightarrow \mathbf{x}_r$ and substituting the drive signal $x(t)$ for $x_r(t)$ in all state equations except the first.

We can study the self-synchronization properties of the transmitter and receiver equations by forming the error system. The error system is derived by defining the error variables

$$\begin{aligned}
 e_x &= x(t) - x_r(t) \\
 e_y &= y(t) - y_r(t) \\
 e_z &= z(t) - z_r(t) \\
 \mathbf{e}_l &= \mathbf{l} - \mathbf{l}_r ,
 \end{aligned}$$

and subtracting (6.2) from (6.1) to obtain

$$\begin{aligned}
 \dot{e}_x &= \sigma(e_y - e_x) + Ce_l \\
 \dot{e}_y &= -e_y - x(t)e_z \\
 \dot{e}_z &= x(t)e_y - be_z \\
 \dot{\mathbf{e}}_l &= A\mathbf{e}_l .
 \end{aligned} \tag{6.3}$$

Since the dynamics of \mathbf{e}_l are independent of $e_x, e_y,$ and $e_z,$ we can see that if A is

a stable matrix, then the e_l subsystem is globally asymptotically stable at the origin. The (e_y, e_z) subsystem is also decoupled from the rest of the system, and was shown previously (equation (3.14)) to be globally asymptotically stable at the origin. The error signal $e_x(t)$ must also go to zero as $t \rightarrow \infty$ because $e_x(t)$ is the output of a stable linear time-invariant system that is driven by $e_y(t)$ and $e_l(t)$. From this analysis, we conclude that the error system is globally asymptotically stable at the origin if A is a stable matrix. Equivalently, with A as a stable matrix, the transmitter and receiver are guaranteed to synchronize regardless of the initial conditions imposed on these systems. In the next section, we develop conditions sufficient to ensure that the transmitter is globally stable.

6.1.2 Conditions for Global Stability

A set of sufficient conditions for which all trajectories of the transmitter equations remain bounded can be determined by defining a family of ellipsoids

$$V(\mathbf{x}) = \frac{1}{2} (rx^2 + \sigma y^2 + \sigma(z - 2r)^2 + \mathbf{1}^T P \mathbf{1}) = k, \quad (6.4)$$

where P is a symmetric $N \times N$ positive definite matrix and k is a positive scalar. As we show below, for k sufficiently large, $V(\mathbf{x})$ will determine a trapping region for the transmitter's flow.

Evaluating $\dot{V}(\mathbf{x})$ we obtain

$$\dot{V}(\mathbf{x}) = -\sigma y^2 - \sigma b(z - r)^2 - \begin{bmatrix} x \\ \mathbf{1} \end{bmatrix}^T M \begin{bmatrix} x \\ \mathbf{1} \end{bmatrix} + \sigma r^2 b, \quad (6.5)$$

where the matrix M is given by

$$M = \begin{bmatrix} r(\sigma - D) & -\frac{1}{2}(B^T P + rC) \\ -\frac{1}{2}(PB + rC^T) & -\frac{1}{2}(PA + A^T P) \end{bmatrix}. \quad (6.5)$$

If M is positive definite, then $\dot{V}(\mathbf{x}) = 0$ determines an ellipsoid in state space. Suf-

cient conditions for M to be positive definite are given below.

- $PB + rC^T = \mathbf{0}$.
- $PA + A^T P$ is negative definite.
- $\sigma - D > 0$.

The first condition provides a constraint between the allowable B and C vectors. The second condition can be satisfied by choosing a stable A matrix such that $PA + A^T P$ is negative definite. The third condition provides an upper bound on D .

If these conditions are satisfied, then $\dot{V} = 0$ determines an ellipsoid in state space of the form

$$\frac{y^2}{br^2} + \frac{(z-r)^2}{r^2} + \frac{1}{\sigma br^2} \begin{bmatrix} x \\ 1 \end{bmatrix}^T M \begin{bmatrix} x \\ 1 \end{bmatrix} = 1 . \quad (6.6)$$

Since $\dot{V} < 0$ for all \mathbf{x} outside of the ellipsoid (6.6), any ellipsoid from the family (6.4) which contains (6.6) will suffice as a trapping region for the flow. This ensures global stability of the transmitter equations.

If the self-synchronization and global stability conditions are satisfied, the transmitter equations are dissipative. Specifically, the divergence of the vector field corresponding to (6.1) is given by

$$\begin{aligned} \nabla \cdot \dot{\mathbf{x}} &= \frac{\partial \dot{x}}{\partial x} + \frac{\partial \dot{y}}{\partial y} + \frac{\partial \dot{z}}{\partial z} + \sum_{i=1}^N \frac{\partial \dot{l}_i}{\partial l_i} \\ &= -(\sigma - D + 1 + b - \text{tr}(A)) . \end{aligned}$$

Exploiting the stability condition on A leads to the inequality

$$\text{tr}(A) = \sum_{i=1}^N \Re(\lambda_i) < 0 .$$

The stability condition on A , together with $\sigma - D > 0$, ensures that the divergence is a negative constant. A constant negative divergence implies that the transmitter equa-

tions are dissipative and that any volume in state space will go to zero exponentially fast.

6.1.3 A Systematic Synthesis Procedure

Sections 6.1.1 and 6.1.2 give sufficient conditions for the transmitter to be dissipative and globally stable and for the receiver system to possess the global self-synchronization property. These conditions are summarized below.

$$\begin{array}{l} \text{Self-Synchronization} \\ \text{Global Stability} \end{array} \left\{ \begin{array}{l} 1. \ A \text{ is stable.} \\ 2. \ PB + rC^T = 0, \text{ for some } N \times N \text{ positive} \\ \quad \text{definite matrix } P. \\ 3. \ PA + A^T P \text{ is negative definite.} \\ 4. \ \sigma - D > 0. \end{array} \right.$$

Condition 1 implies that there exists a positive definite solution P to the matrix Lyapunov equation

$$PA + A^T P + Q = 0, \quad Q > 0.$$

By choosing Q to be any symmetric positive definite matrix, condition 3 can always be satisfied. Exploiting this relationship, the following synthesis procedure is suggested.

Synthesis Procedure

1. Choose any stable A matrix and any $N \times N$ symmetric positive definite matrix Q .
2. Solve $PA + A^T P + Q = 0$ for the positive definite solution P .
3. Choose any vector B and set $C = -B^T P/r$.
4. Choose any D such that $\sigma - D > 0$.

Next, the stability of the fixed points needs to be addressed. We must determine conditions which ensure that all of the fixed points of the transmitter equations are

unstable so that non-trivial motion will occur. As shown below, this can be accomplished through a linear stability analysis of the transmitter equations.

6.1.4 Linear Stability Analysis

Inspection of the transmitter equations shows that the origin is always a fixed point. Two additional fixed points can be determined by setting the transmitter's vector field equal to zero and solving for the non-trivial stationary points. The equations to be solved are listed below¹.

1. $\sigma(y^* - x^*) + Cl^* + Dx^* = 0$,
2. $rx^* - y^* - x^*z^* = 0$,
3. $x^*y^* - bz^* = 0$,
4. $Al^* + Bx^* = 0$.

Combining equations 2 and 3, y^* and z^* can be determined in terms of x^* as

$$\begin{aligned} y^* &= \frac{rbx^*}{b + x^{*2}} \text{ ,} \\ z^* &= \frac{rx^{*2}}{b + x^{*2}} \text{ .} \end{aligned}$$

Equation 4 determines l^* as

$$l^* = -A^{-1}Bx^* \text{ ,}$$

and x^* is determined from equation 1 as

$$x^* = \pm \sqrt{b \left(\frac{\sigma r}{\sigma + CA^{-1}B - D} - 1 \right)} \text{ .} \quad (6.7)$$

¹State variables with star "*" superscripts denote fixed points in this analysis.

The term under the radical in (6.7) must be positive in order for these fixed points to exist. This suggests that a fixed point pair exists for $r \geq r_c$, where r_c is given by

$$r_c = 1 + \frac{CA^{-1}B - D}{\sigma} .$$

Observe that the scalar $H(0) = -CA^{-1}B + D$ is equivalent to the transfer function of the linear feedback system evaluated at the origin. Therefore, r_c can be conveniently written as

$$r_c = 1 - \frac{H(0)}{\sigma} . \quad (6.8)$$

Now that we have determined all of the fixed points and the critical value of r for which they exist, we are ready to perform a stability analysis.

Linear stability analysis of the fixed points can be performed by studying the Jacobian matrix corresponding to (6.1). Evaluating the Jacobian matrix at the origin we obtain

$$J(\mathbf{0}) = \begin{bmatrix} D - \sigma & \sigma & 0 & C \\ r & -1 & 0 & \mathbf{0}^T \\ 0 & 0 & -b & \mathbf{0}^T \\ B & \mathbf{0} & \mathbf{0} & A \end{bmatrix} .$$

If all of the eigenvalues of $J(\mathbf{0})$ are in the left-half plane, then the origin is stable. If at least one eigenvalue is in the right-half plane, then the origin will be unstable. In typical experiments, increasing the value of r above some critical value will cause the origin to lose stability. In practice, this critical value can always be determined numerically for a specific LFBCS. As shown below, an analytical analysis of the eigenvalues of $J(\mathbf{0})$ will provide additional conceptual insight and allow us to draw some general conclusions regarding the behavior of generic LFBCSs.

Using the matrix identity

$$\begin{vmatrix} A_{11} & A_{12} \\ A_{21} & A_{22} \end{vmatrix} = \left| A_{11} - A_{12}A_{22}^{-1}A_{21} \right| |A_{22}| \quad ,$$

the characteristic polynomial for $J(\mathbf{0})$ is determined as

$$|\lambda I - J(\mathbf{0})| = (\lambda + b) \prod_{i=1}^N (\lambda - \lambda_i) \begin{vmatrix} \lambda + \sigma - H(\lambda) & -\sigma \\ -r & \lambda + 1 \end{vmatrix} = 0. \quad (6.9)$$

The eigenvalues λ_i , for $i = 1, \dots, N$, belong to the A matrix and, therefore, represent stable modes. The eigenvalue $\lambda = -b$ also represents a stable mode. Unstable modes will exist for r sufficiently large. As shown below, the presence of unstable modes can be detected by determining the characteristic polynomial of the 2×2 determinant in (6.9).

The characteristic polynomial for the 2×2 determinant in (6.9) is given by

$$\lambda^2 + (\sigma + 1 - H(\lambda))\lambda + \sigma(1 - r) - H(\lambda) = 0 \quad . \quad (6.10)$$

As r is varied, a bifurcation occurs when a root of (6.10) crosses the imaginary axis in the complex plane. When this occurs, the critical value(s) of r can be determined by restricting our attention to solutions of (6.10) for values of $\lambda = jf$, for $f \geq 0$. Substituting $\lambda = jf$ into (6.10) and introducing the notation $H(jf) = H_R(f) + jH_I(f)$ we obtain

$$\left[\sigma(1 - r) - f^2 - H_R(f) + fH_I(f) \right] + j \left[f(\sigma + 1 - H_R(f)) - H_I(f) \right] = 0 \quad .$$

Setting the imaginary part of this expression equal to zero and solving for f in terms of $H_R(f)$ and $H_I(f)$ we obtain

$$f = \frac{H_I(f)}{\sigma + 1 - H_R(f)} = G(f) \quad . \quad (6.11)$$

Similarly, by setting the real part equal to zero we obtain

$$r = 1 - \frac{f^2 + H_R(f) - fH_I(f)}{\sigma} . \quad (6.12)$$

Equation (6.11) determines the *eigenfrequencies* where bifurcations occur and (6.12) determines the corresponding bifurcation parameter. The term “eigenfrequency” is used here to describe the point on the imaginary axis in the complex plane where the roots of a characteristic polynomial cross when traversing from the left-half plane to the right-half plane or vice versa.

The eigenfrequency equation (6.11) is written as $f = G(f)$, where $G(f)$ is determined by the frequency response of the linear feedback system. Note that $G(f)$ is an odd and continuous function. Because of these properties, we know that $G(0) = 0$ and therefore $f = 0$ is always a solution to the eigenfrequency equation. From (6.12), the value of r corresponding to $f = 0$ is given by $r = 1 - H(0)/\sigma$. This value of r also corresponds to the existence of the fixed point pair (compare with (6.8)). This analysis suggests that the fixed point pair is created when the origin loses stability (commonly referred to as a *pitchfork* bifurcation). This type of bifurcation is also exhibited at the origin in the Lorenz system (without feedback). Later in Section 6.1.5, numerical analysis of a specific LFBCS provides support for these observations.

Now that the stability of the origin is further understood, we turn our attention toward the stability of the fixed point pair. Evaluating the Jacobian matrix at the fixed point pair we obtain

$$J(\mathbf{x}_0) = \begin{bmatrix} D - \sigma & \sigma & 0 & C \\ r - z^* & -1 & -x^* & \mathbf{0}^T \\ y^* & x^* & -b & \mathbf{0}^T \\ B & \mathbf{0} & \mathbf{0} & A \end{bmatrix} .$$

Substituting the coordinates of the fixed point pair into $J(\mathbf{x}_0)$, and computing the resulting eigenvalues, provides a numerical approach for examining the linear stability of these fixed points. As was the case at the origin, however, additional conceptual

insight is gained by examining the eigenvalues of $J(\mathbf{x}_0)$ analytically.

The eigenfrequency and bifurcation equations corresponding to the fixed point pair can be determined through an analysis similar to that used at the origin. Omitting the algebraic details, the resulting eigenfrequency equation is given by

$$f = \frac{f^3 + H_I(f)(b + K(f) - f^2)}{K(f) + H(0) - H_R(f)(b + 1) + b(\sigma + 1)} = G'(f) , \quad (6.13)$$

where the function $K(f)$ is given by

$$K(f) = \frac{f^2(\sigma + b + 1) - bH(0) + H_R(f)(b - f^2) - fH_I(f)(b + 1)}{2\sigma - H(0) - H_R(f)} . \quad (6.14)$$

The bifurcation parameter can be shown to satisfy

$$r = \left(1 - \frac{H(0)}{\sigma}\right) \left(1 + \frac{K(f)}{b}\right) . \quad (6.15)$$

Solutions to the eigenfrequency equation (6.13) can be determined graphically for arbitrary $H(f)$ by plotting $f - G'(f)$ and locating the zero-crossings. The bifurcation equation (6.15) can then be used to determine the critical values of r for which the fixed point pair undergoes bifurcations. It is also interesting to note that the eigenfrequency and bifurcation equations determine the critical values of r in terms of the frequency response of any N -dimensional linear system.

To gain additional insight into the behavior of solutions to (6.13), observe that $G'(f)$ is an odd and continuous function. It then follows that $G'(0) = 0$ and, therefore, $f = 0$ is always a solution to (6.13). From (6.15), the corresponding value of r is given by

$$r = 1 - \frac{H(0)}{\sigma} .$$

Recall that this value of r predicts the pitchfork bifurcation at the origin when the origin loses stability and the fixed point pair is created. If the fixed point pair is stable when it is created, then its loss of stability occurs when a complex conjugate pair of

eigenvalues ($f > 0$) crosses into the right-half plane. This type of bifurcation is akin to a *Hopf* bifurcation. Using a specific LFBCS, we will demonstrate this behavior numerically in the next section.

6.1.5 Numerical Example

The synthesis procedure suggested in Section 6.1.3 allows an unlimited number of Lorenz-based x -input/ x -output LFBCSs to be designed. For the purpose of demonstration, consider the following five-dimensional LFBCS.

$$\begin{aligned}
 \dot{x} &= \sigma(y - x) + \nu \\
 \dot{y} &= rx - y - xz \\
 \dot{z} &= xy - bz \\
 \begin{bmatrix} \dot{l}_1 \\ \dot{l}_2 \end{bmatrix} &= \begin{bmatrix} -\frac{1}{2} & 10 \\ -10 & -\frac{1}{2} \end{bmatrix} \begin{bmatrix} l_1 \\ l_2 \end{bmatrix} + \begin{bmatrix} 1 \\ 1 \end{bmatrix} x \\
 \nu &= - \begin{bmatrix} 1 & 1 \end{bmatrix} \begin{bmatrix} l_1 \\ l_2 \end{bmatrix}
 \end{aligned} \tag{6.16}$$

In this system, the Lorenz signal $x(t)$ drives a two-dimensional linear system and the output of the linear system is added to the \dot{x} equation of the Lorenz system. It can be shown in a straightforward way that the linear system satisfies the self-synchronization and global stability conditions for suitable choices of P, Q , and R . For the numerical demonstrations presented below, the Lorenz parameters chosen are $\sigma = 16$ and $b = 4$; the bifurcation parameter r will be varied.

Using the eigenfrequency equation (6.13), we show in figure 6-2(a) a plot of $f - G'(f)$ vs. f . The zero-crossing of $f - G'(f)$, for $f > 0$, corresponds to the eigenfrequency where a Hopf bifurcation occurs and the fixed point pair becomes unstable. Substituting this critical frequency into the bifurcation equation (6.15) determines the critical value of r for which the bifurcation occurs. Alternatively, we can plot equation (6.15) vs. f and obtain the critical value of r graphically as illustrated in figure 6-2(b). As indicated, the critical value is $r_{Hopf} = 34$. From these figures, we

see that as r increases above r_{Hopf} , the fixed point pair remains unstable because no additional bifurcations occur in the indicated range for r .

In figure 6-2(c), we show the *bifurcation diagram* for the LFBCS. This diagram is generated by plotting the x -component of the fixed points as a function of the bifurcation parameter. The solid lines indicate that the corresponding fixed point is stable, whereas the dashed lines indicate that the fixed point is unstable. In the region where all the fixed points are unstable, the motion is confined to either limit cycles or a chaotic attractor. In typical numerical experiments, we observe that chaotic motion usually occurs for r slightly above r_{Hopf} .

In figure 6-3, we show the computed Lyapunov exponents as r is varied over the range $20 < r < 100$. Note that the onset of chaotic behavior occurs near $r = 34$, as evidenced by the existence of a positive Lyapunov exponent. This critical value of r is in excellent agreement with the value of r_{Hopf} predicted by the eigenfrequency and bifurcation diagrams. Other important characteristics of figure 6-3 are listed below.

- Two exponents equal to $-1/2$ are apparent. These exponents correspond to the real parts of the linear system poles.
- A large negative exponent is apparent. This exponent is due to the highly dissipative nature of the LFBCS.
- A zero exponent is also apparent. This exponent corresponds to motion tangent to the flow.

For comparison purposes, the computed Lyapunov exponents for the Lorenz system (without feedback) are also shown in this figure.

In figure 6-4, we show the computed Lyapunov dimension as r is varied over the same range, $20 < r < 100$. This figure demonstrates that the LFBCS achieves a greater Lyapunov dimension than the Lorenz system without feedback applied. The Lyapunov dimension could be increased by using more states in the linear system. However, numerical experiments suggest that a limit will be reached since the Lyapunov dimension depends more heavily on the most positive exponents and stable linear feedback creates only negative exponents.

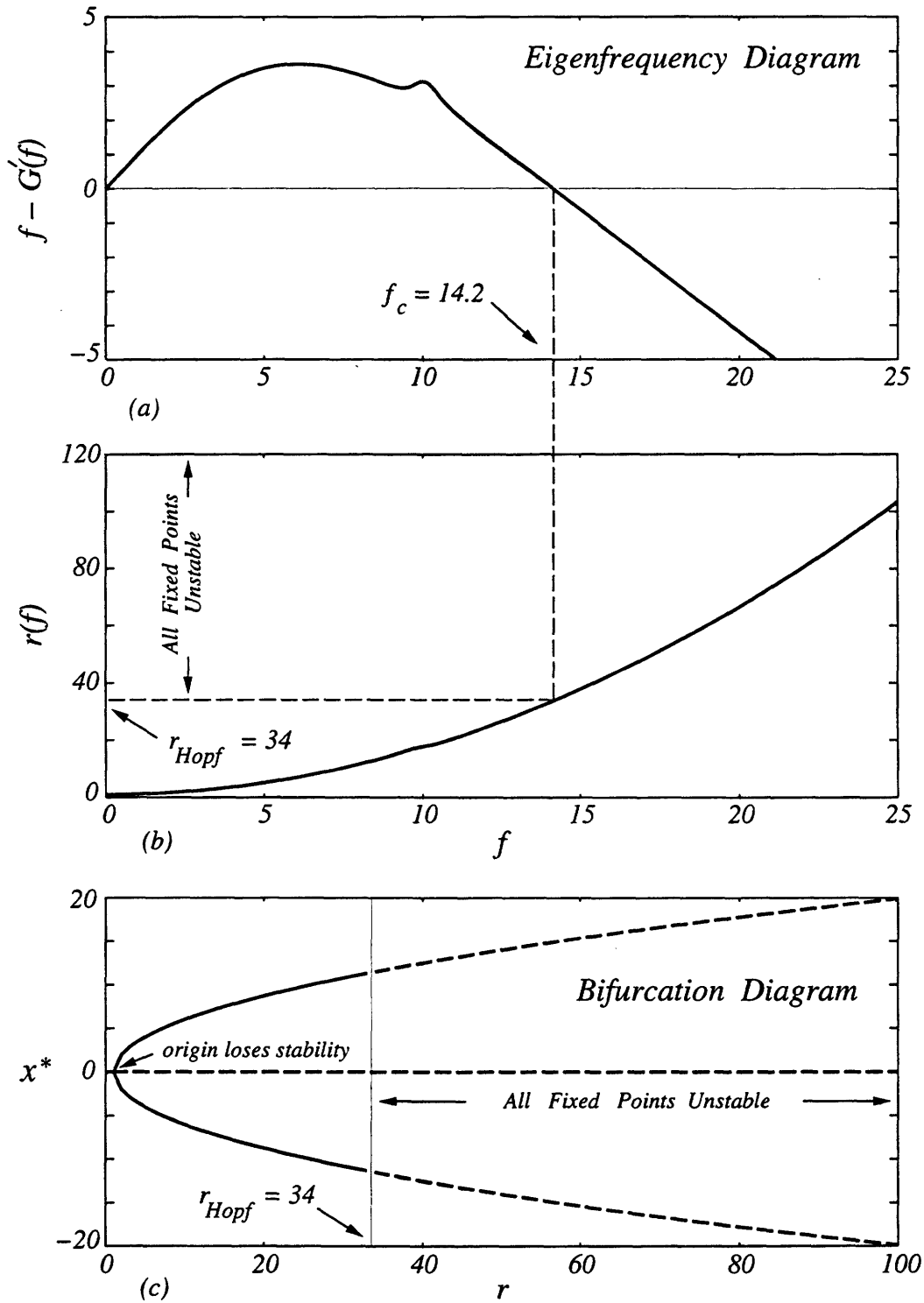


Figure 6-2: (a) Eigenfrequency Diagram for a 5-Dimensional x -input/ x -output LF-BCS. (b) Graphical Determination of the Bifurcation Parameter. (c) Bifurcation Diagram.

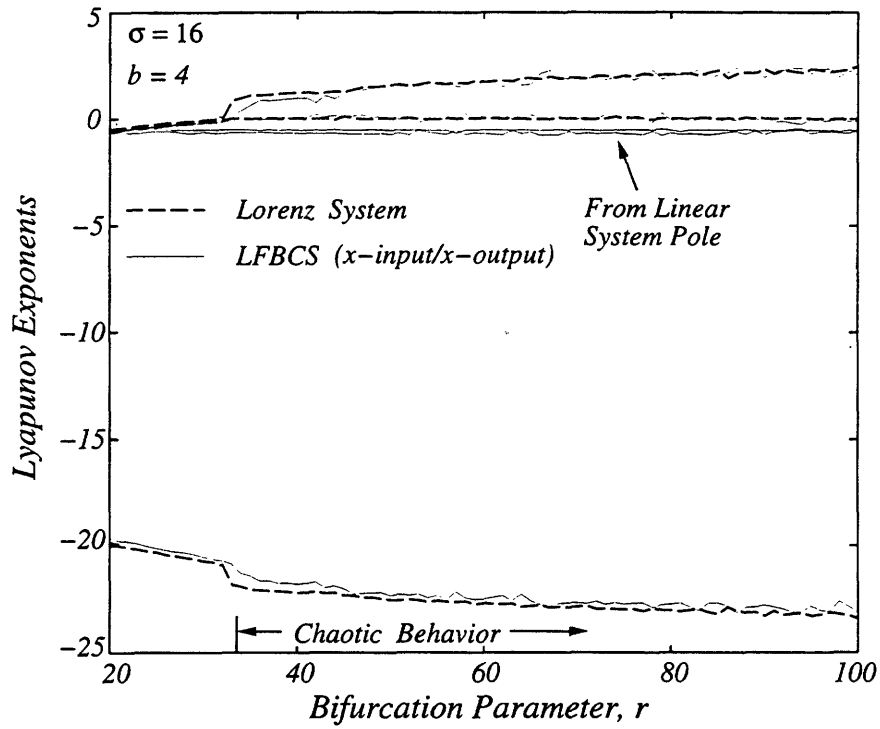


Figure 6-3: *Lyapunov Exponents for a 5-Dimensional x-input/x-output LFBCS.*

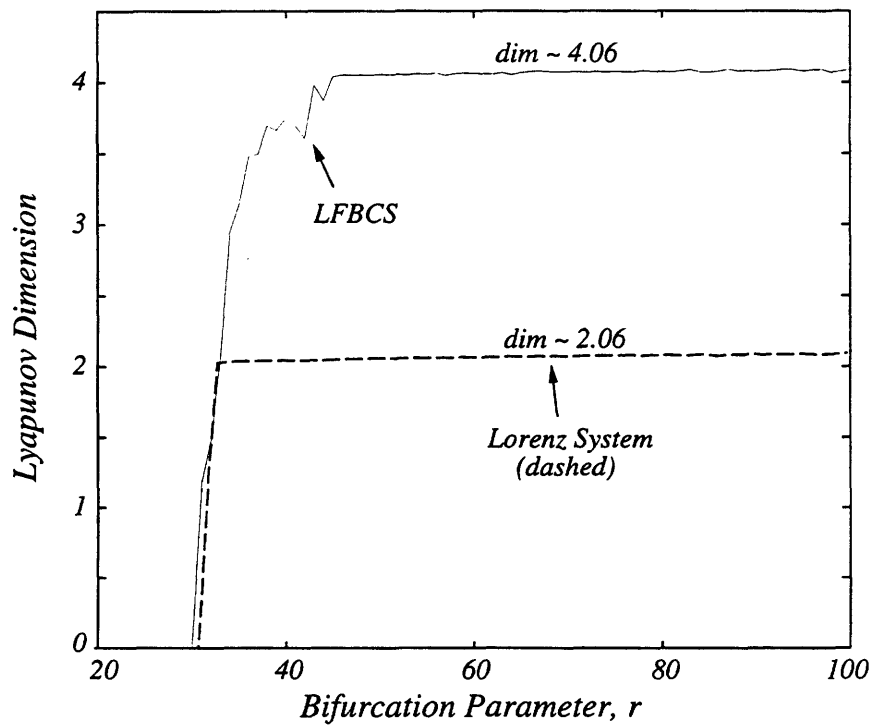


Figure 6-4: *Lyapunov Dimension for a 5-Dimensional x-input/x-output LFBCS.*

In figure 6-5, we show various projections of the LFBCS's chaotic attractor. The (x, y) and (x, z) projections are similar to the Lorenz system. The (x, l_1) and (x, l_2) projections, however, reveal a more complex structure and suggest that the trajectories evolve on a higher dimensional attractor in state space.

In figure 6-6, we demonstrate the rapid synchronization between the transmitter and receiver systems. The curve measures the distance in state space between the transmitter and receiver trajectories when the receiver is initialized from the zero state. Synchronization is maintained indefinitely.

In the next section, we examine a LFBCS where the Lorenz signal $z(t)$ drives an N -dimensional linear system and the output of the linear system is added to the \dot{z} equation of the Lorenz system. These systems, which we refer to as z -input/ z -output LFBCSs, provide additional insight into the behavior of different types of LFBCSs.

6.2 z -Input/ z -Output LFBCSs

The transmitter equations for this class of LFBCSs is given by

$$\begin{aligned}
 \dot{x} &= \sigma(y - x) \\
 \dot{y} &= rx - y - xz \\
 \dot{z} &= xy - bz + \nu \\
 \dot{\mathbf{l}} &= A\mathbf{l} + Bz \\
 \nu &= C\mathbf{l} + Dz \quad ,
 \end{aligned} \tag{6.17}$$

where \mathbf{l} and ν denote the state variables and output of the linear system, respectively. The linear system is N -dimensional, *i.e.*, A is $N \times N$, B is $N \times 1$, C is $1 \times N$, and D is 1×1 .

Following the development outlined in Section 6.1, we will first determine sufficient conditions such that the transmitter equations satisfy two requirements: *(i)* there exists an algebraically similar receiver system which possesses the global self-synchronization property, and *(ii)* the transmitter system is globally stable. Section 6.2.1 contains the self-synchronization analysis and Section 6.2.2 contains the global

x-Input/x-Output LFBCS

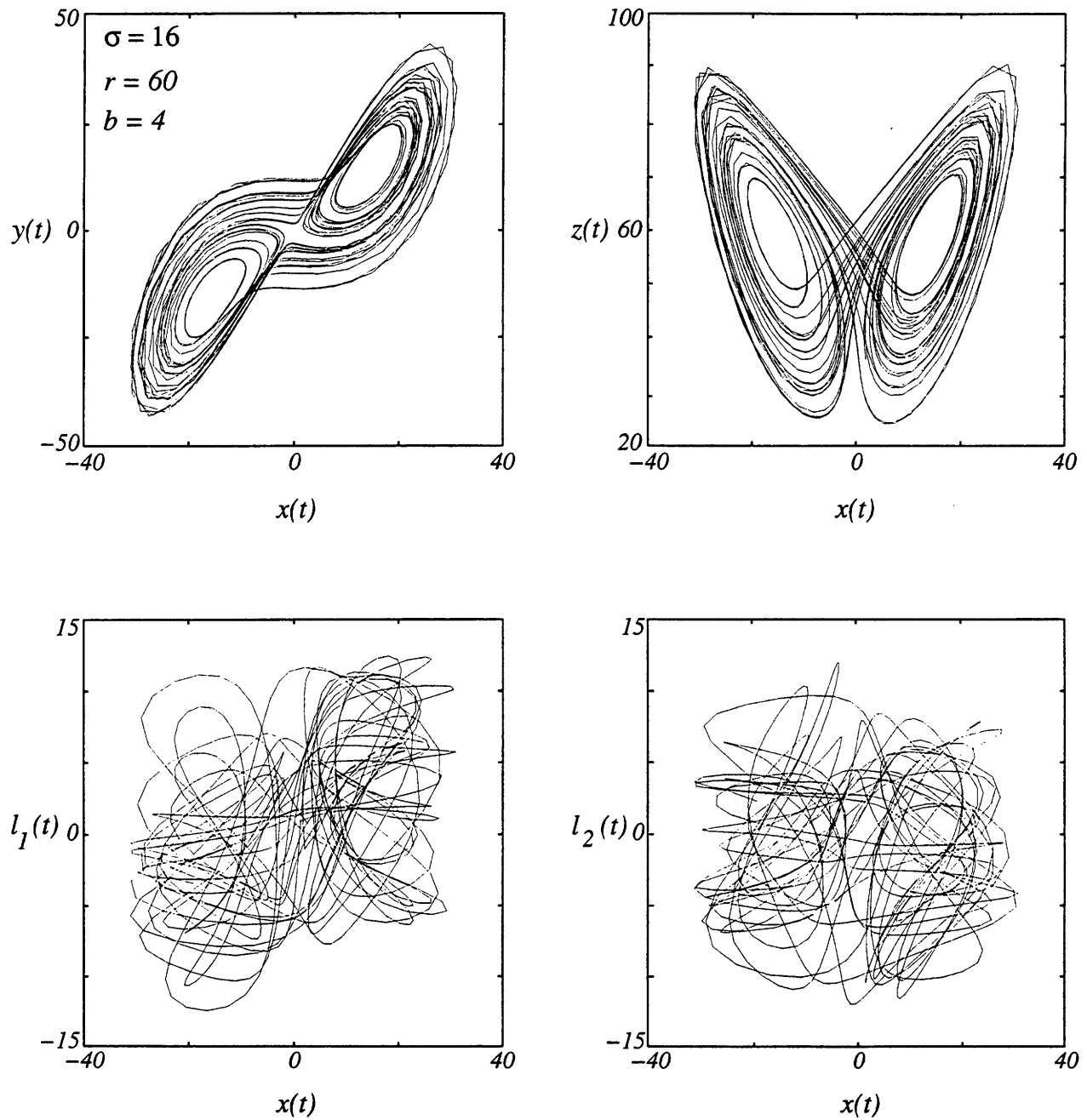


Figure 6-5: *Chaotic Attractor for a 5-Dimensional x-input/x-output LFBCS.*

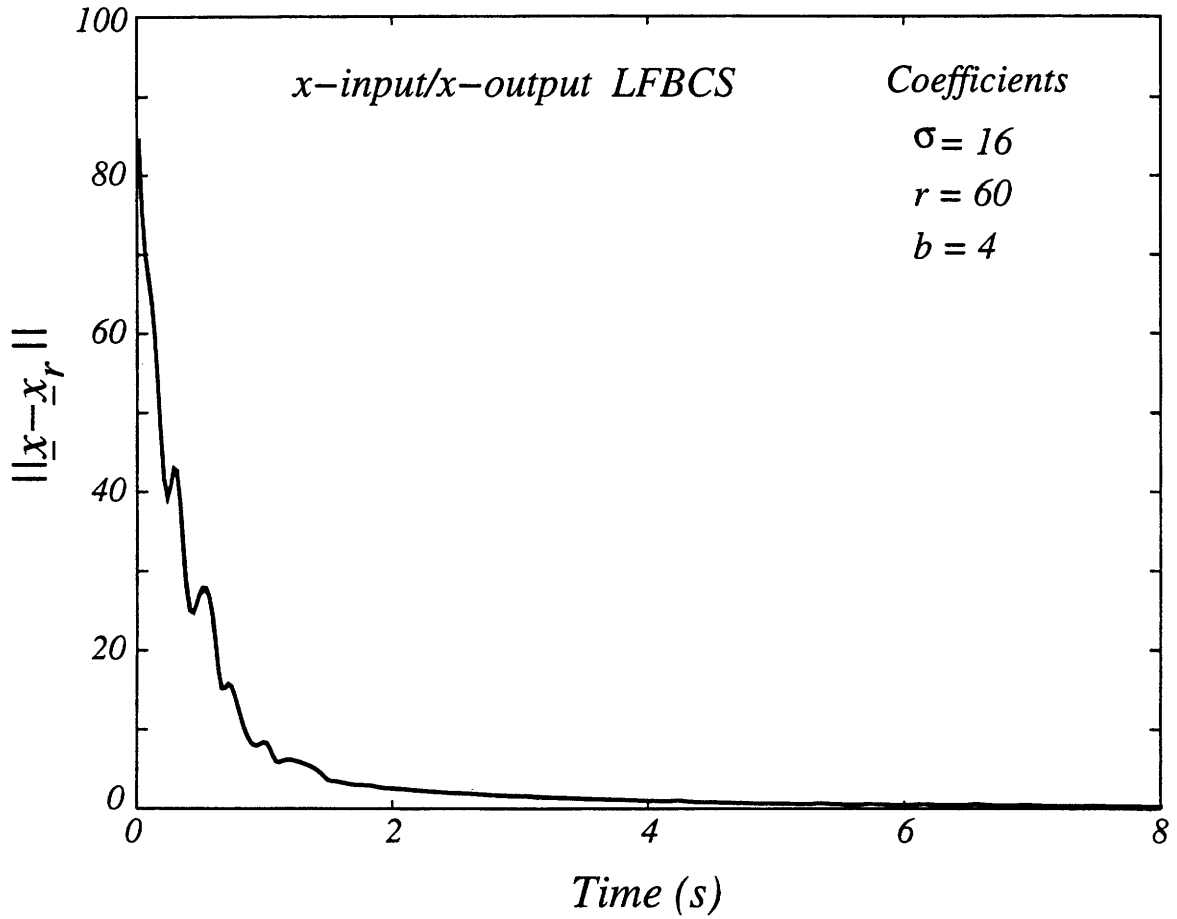


Figure 6-6: *Self-Synchronization in a 5-Dimensional x-input/x-output LFBCS.*

stability analysis. In Section 6.2.3, we suggest a systematic procedure for synthesizing z -input/ z -output LFBCSs. In Section 6.2.4, we describe the results of several numerical experiments which demonstrate the theoretical results. Appendix A contains the linear stability analysis for z -input/ z -output LFBCSs.

6.2.1 Conditions for Global Self-Synchronization

The synchronizing receiver equations for z -input/ z -output LFBCSs are given by

$$\begin{aligned}
 \dot{x}_r &= \sigma(y_r - x_r) \\
 \dot{y}_r &= rx(t) - y_r - x(t)z_r \\
 \dot{z}_r &= x(t)y_r - bz_r + \nu_r \\
 \dot{\mathbf{l}}_r &= A\mathbf{l}_r + Bz_r \\
 \nu_r &= C\mathbf{l}_r + Dz_r .
 \end{aligned} \tag{6.18}$$

This system is obtained from the transmitter by renaming variables $\mathbf{x} \rightarrow \mathbf{x}_r$ and substituting the drive signal $x(t)$ in place of $x_r(t)$ in the equations for \dot{y}_r and \dot{z}_r .

The corresponding error system is given by

$$\begin{aligned}
 \dot{e}_x &= \sigma(e_y - e_x) \\
 \dot{e}_y &= -e_y - x(t)e_z \\
 \dot{e}_z &= x(t)e_y - be_z + Ce_l + De_z \\
 \dot{\mathbf{e}}_l &= A\mathbf{e}_l + B\mathbf{e}_z .
 \end{aligned}$$

Note that the error variables \mathbf{e}_l do not decouple from the rest of the error system, which was the case for the x -input/ x -output LFBCSs studied in Section 6.1. In this case, a set of sufficient conditions for the error system to be globally asymptotically stable at the origin can be determined by considering a Lyapunov function of the form

$$E(\mathbf{e}) = \frac{1}{2} \left(\frac{1}{\sigma} e_x^2 + e_y^2 + e_z^2 + \mathbf{e}_l^T R \mathbf{e}_l \right) ,$$

where R is a symmetric $N \times N$ positive definite matrix. For conciseness, the error variables are denoted by the vector $\mathbf{e} = (e_x, e_y, e_z, \mathbf{e}_l)$.

The time rate of change of $E(\mathbf{e})$ along trajectories is given by

$$\dot{E}(\mathbf{e}) = -\left(e_x - \frac{1}{2}e_y\right)^2 - \frac{3}{4}e_y^2 - \begin{bmatrix} e_z \\ \mathbf{e}_l \end{bmatrix}^T T \begin{bmatrix} e_z \\ \mathbf{e}_l \end{bmatrix}, \quad (6.19)$$

where the matrix T is given by

$$T = \begin{bmatrix} b - D & -\frac{1}{2}(B^T R + C) \\ -\frac{1}{2}(RB + C^T) & -\frac{1}{2}(RA + A^T R) \end{bmatrix}.$$

Observe that \dot{E} is negative definite if T is positive definite. A sufficient set of conditions for T to be positive definite are given below.

- $RB + C^T = 0$, for some $N \times N$ positive definite matrix R .
- $RA + A^T R$ is negative definite.
- $b - D > 0$.

If these conditions are satisfied, then the transmitter and receiver systems are guaranteed to synchronize regardless of the initial conditions. In the next section, we develop the sufficient conditions which will guarantee that the transmitter is globally stable.

6.2.2 Conditions for Global Stability

A set of conditions sufficient for bounding all trajectories of the transmitter can be determined by defining a family of ellipsoids

$$V(\mathbf{x}) = \frac{1}{2} \left(r x^2 + \sigma y^2 + \sigma (z - 2r)^2 + \mathbf{l}^T P \mathbf{l} \right) = k, \quad (6.20)$$

where P is a symmetric $N \times N$ positive definite matrix and k is a positive scalar.

If we restrict $PB + \sigma C^T = \mathbf{0}$, then $\dot{V}(\mathbf{x})$ can be written in the form

$$\dot{V}(\mathbf{x}) = -\sigma r x^2 - \sigma y^2 - \begin{bmatrix} z - r \\ \mathbf{1} - \mathbf{q} \end{bmatrix}^T M \begin{bmatrix} z - r \\ \mathbf{1} - \mathbf{q} \end{bmatrix} + c ,$$

where the matrix M is given by

$$M = \begin{bmatrix} \sigma(b - D) & \mathbf{0}^T \\ \mathbf{0} & -\frac{1}{2}(PA + A^T P) \end{bmatrix} .$$

Also, the scalar c is given by

$$c = \sigma r^2(b - D) - \mathbf{q}^T \frac{(PA + A^T P)}{2} \mathbf{q} ,$$

and the vector \mathbf{q} is given by

$$\mathbf{q} = -r(PA + A^T P)^{-1}(PB - \sigma C^T) .$$

If M is positive definite and $c > 0$, then $\dot{V}(\mathbf{x}) = 0$ determines an ellipsoid in state space. Sufficient conditions for M to be positive definite and for $c > 0$ are given below.

- $PB + \sigma C^T = \mathbf{0}$.
- $PA + A^T P$ is negative definite.
- $b - D > 0$.

The first condition is simply the $PB + \sigma C^T = \mathbf{0}$ restriction. The second condition can be satisfied by choosing a stable A matrix such that $PA + A^T P$ is negative definite. The third condition provides an upper bound on D . Comparing these conditions with the self-synchronization conditions reveals some similarity between them.

If these conditions are satisfied, then $\dot{V} = 0$ determines an ellipsoid of the form

$$\frac{\sigma r x^2}{c} + \frac{\sigma y^2}{c} + \frac{1}{c} \begin{bmatrix} z - r \\ \mathbf{1} - \mathbf{q} \end{bmatrix}^T M \begin{bmatrix} z - r \\ \mathbf{1} - \mathbf{q} \end{bmatrix} = 1 . \quad (6.21)$$

Since $\dot{V} < 0$ for all \mathbf{x} outside of the ellipsoid (6.21), any ellipsoid from the family (6.20) which contains (6.21) will suffice as a trapping region for the flow.

The transmitter equations are dissipative if the self-synchronization and global stability conditions are satisfied. Specifically, the divergence of the vector field corresponding to (6.17) is given by

$$\begin{aligned} \nabla \cdot \dot{\mathbf{x}} &= \frac{\partial \dot{x}}{\partial x} + \frac{\partial \dot{y}}{\partial y} + \frac{\partial \dot{z}}{\partial z} + \sum_{i=1}^N \frac{\partial \dot{l}_i}{\partial l_i} \\ &= -(\sigma + 1 + b - D - \text{tr}(A)) . \end{aligned}$$

With A stable and $b - D > 0$, the divergence is a negative constant. This implies that all volumes in state space will go to zero exponentially fast.

6.2.3 A Systematic Synthesis Procedure

Sections 6.2.1 and 6.2.2 give sufficient conditions for the transmitter to be dissipative and globally stable and for the receiver system to possess the global self-synchronization property. These conditions are summarized below.

$$\begin{array}{l} \text{Self-Synchronization} \\ \text{Global Stability} \end{array} \left\{ \begin{array}{l} 1. \quad RB + C^T = \mathbf{0}, \text{ for some } N \times N \text{ positive} \\ \quad \text{definite matrix } R \\ 2. \quad RA + A^T R \text{ is negative definite} \\ 3. \quad b - D > 0 \\ 4. \quad PB + \sigma C^T = \mathbf{0}, \text{ for some } N \times N \text{ positive} \\ \quad \text{definite matrix } P \\ 5. \quad PA + A^T P \text{ is negative definite} \\ 6. \quad b - D > 0 \end{array} \right.$$

If we choose $P = \sigma R$, then conditions 1 and 4 and conditions 2 and 5 are equivalent. Furthermore, conditions 2 and 5 imply that A is stable. As a result, there exists a positive definite solution R to the matrix Lyapunov equation

$$RA + A^T R + Q = 0 ,$$

where Q is any positive definite matrix. In light of these simplifications, the following synthesis procedure is suggested.

Synthesis Procedure

1. Choose any stable A matrix and any $N \times N$ symmetric positive definite matrix Q .
2. Solve $RA + A^T R + Q = 0$ for the positive definite solution R .
3. Choose any vector B and set $C = -B^T R$.
4. Choose any D such that $b - D > 0$.

This synthesis procedure is nearly identical to the x -input/ x -output synthesis procedure developed in Section 6.1.

In the next section, a numerical example demonstrates the behavior of a z -input/ z -output LFBCS.

6.2.4 Numerical Example

For the purpose of demonstration, consider the following five-dimensional z -input/ z -output LFBCS.

$$\begin{aligned}
 \dot{x} &= \sigma(y - x) \\
 \dot{y} &= rx - y - xz \\
 \dot{z} &= xy - bz + \nu \\
 \begin{bmatrix} \dot{l}_1 \\ \dot{l}_2 \end{bmatrix} &= \begin{bmatrix} -\frac{1}{2} & 10 \\ -10 & -\frac{1}{2} \end{bmatrix} \begin{bmatrix} l_1 \\ l_2 \end{bmatrix} + \begin{bmatrix} 1 \\ 1 \end{bmatrix} z \\
 \nu &= - \begin{bmatrix} 1 & 1 \end{bmatrix} \begin{bmatrix} l_1 \\ l_2 \end{bmatrix}
 \end{aligned} \tag{6.22}$$

The linear system in this example is identical to the one used in Section 6.1.5. The overall dynamics of (6.22) will be different than the corresponding x -input/ x -output LFBCS, however, because the Lorenz signal $z(t)$ drives the linear system and the output of the linear system is added to the \dot{z} equation of the Lorenz system. The linear system can be shown to satisfy the self-synchronization and global stability conditions for suitable choices of P , Q , and R .

We performed a detailed linear stability analysis of the z -input/ z -output transmitter equations (see Appendix A) analogous to the one in Section 6.1.4 to derive the eigenfrequency and bifurcation equations for this class of systems. Using the eigenfrequency equation (A.5), we show in figure 6-7(a) a plot of $f - G'(f)$ vs. f . Figure 6-7(b) shows a plot of the corresponding bifurcation equation (A.6). As indicated, a Hopf bifurcation occurs at $r_{Hopf} = 34$. Figure 6-7(c) shows the bifurcation diagram for the LFBCS and illustrates that all of the fixed points are unstable for $r > r_{Hopf}$.

In figure 6-8, we show the computed Lyapunov exponents as r is varied over the range $20 < r < 100$. These exponents are remarkably similar to the x -input/ x -output example exponents (figure 6-3) even though the transmitter equations are different. In particular, the onset of chaotic behavior occurs near $r = 34$ and two exponents equal to $-1/2$ are evident. Another striking similarity between the two LFBCS types

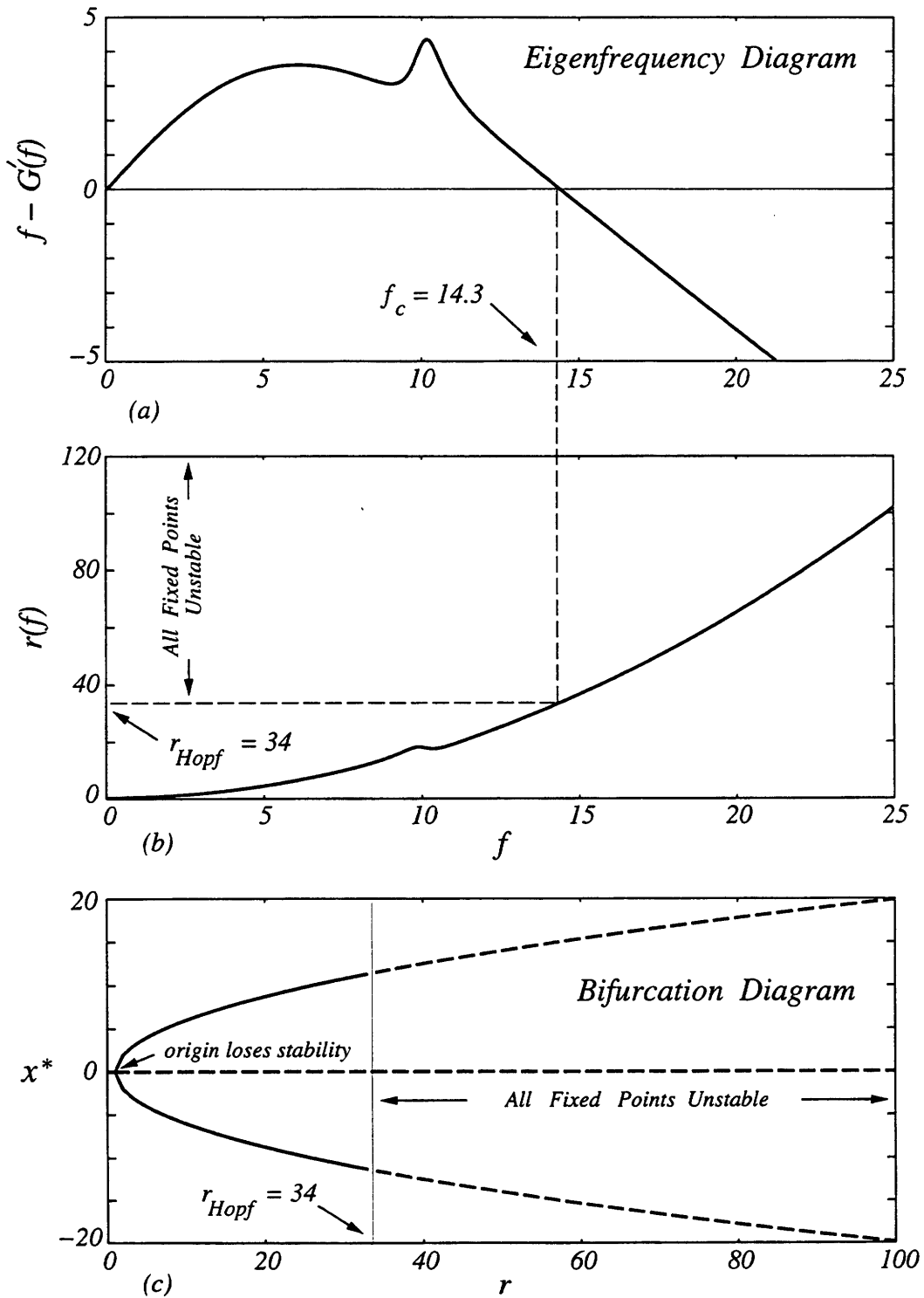


Figure 6-7: (a) Eigenfrequency Diagram for a 5-Dimensional z-input/z-output LF-BCS. (b) Graphical Determination of the Bifurcation Parameter. (c) Bifurcation Diagram.

is the computed Lyapunov dimensions as illustrated in figure 6-9.

In figure 6-10, we show various projections of the LFBCS's chaotic attractor. The (x, y) and (x, z) projections are similar to the Lorenz system as was also the case for the x -input/ x -output LFBCS. The (x, l_1) and (x, l_2) projections suggest that the trajectories evolve on a higher dimensional attractor in state space. Comparing the (x, l_1) and (x, l_2) projections in this figure with the corresponding projections in figure 6-5 shows that the two LFBCS types exhibit different spatial patterns.

In figure 6-11, we demonstrate the rapid synchronization between the transmitter and receiver systems for both LFBCS types. The curves measure the distance in state space between the transmitter and receiver trajectories when the receivers are initialized from the zero state. Synchronization is maintained indefinitely in both cases.

6.3 Summary

The analysis and synthesis results presented in this chapter have further enhanced our understanding of self-synchronization in a class of chaotic systems. The development of a systematic procedure for synthesizing high-dimensional chaotic systems which possess the self-synchronization property may serve a useful purpose for future communications applications. Some conjectures and insights gained from this work are listed below.

- Many of the qualitative properties of the Lorenz system are maintained after applying stable linear feedback. Specifically, there are at most three fixed points - - the origin plus a fixed point pair. In typical experiments, the origin loses stability via a pitchfork bifurcation and the fixed point pair loses stability via a Hopf bifurcation. This same behavior is known to occur in the Lorenz system.
- The Lyapunov spectrum for a LFBCS consists of the Lyapunov exponents for the Lorenz system plus additional negative exponents equal to the real part of the linear system poles. Therefore, LFBCSs exhibit only one positive Lyapunov exponent. These conjectures are supported by limited numerical experiments.

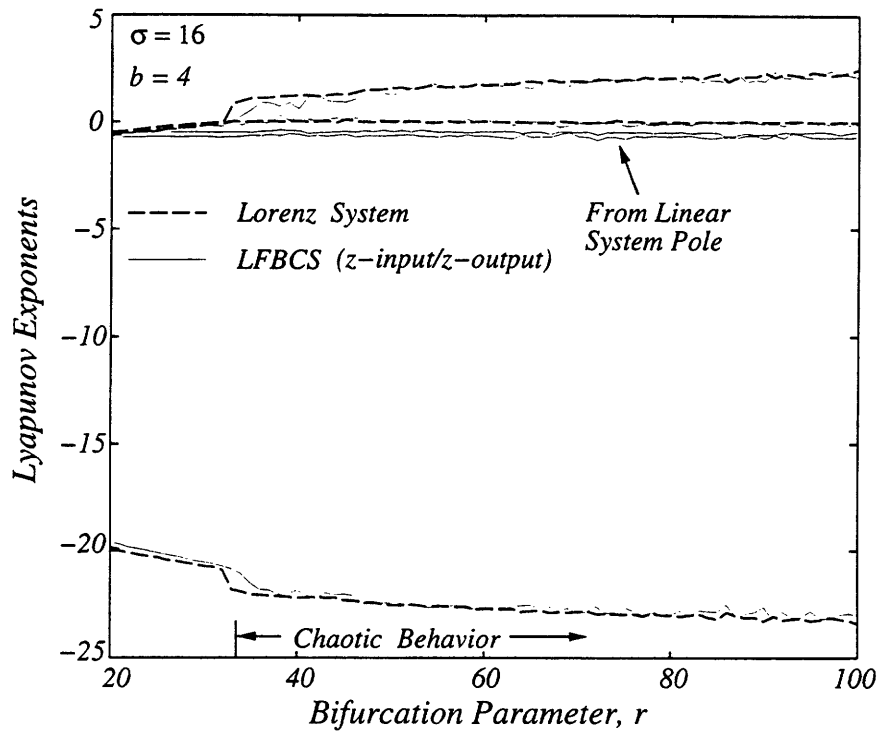


Figure 6-8: Lyapunov Exponents for a 5-Dimensional z -input/ z -output LFBCS.

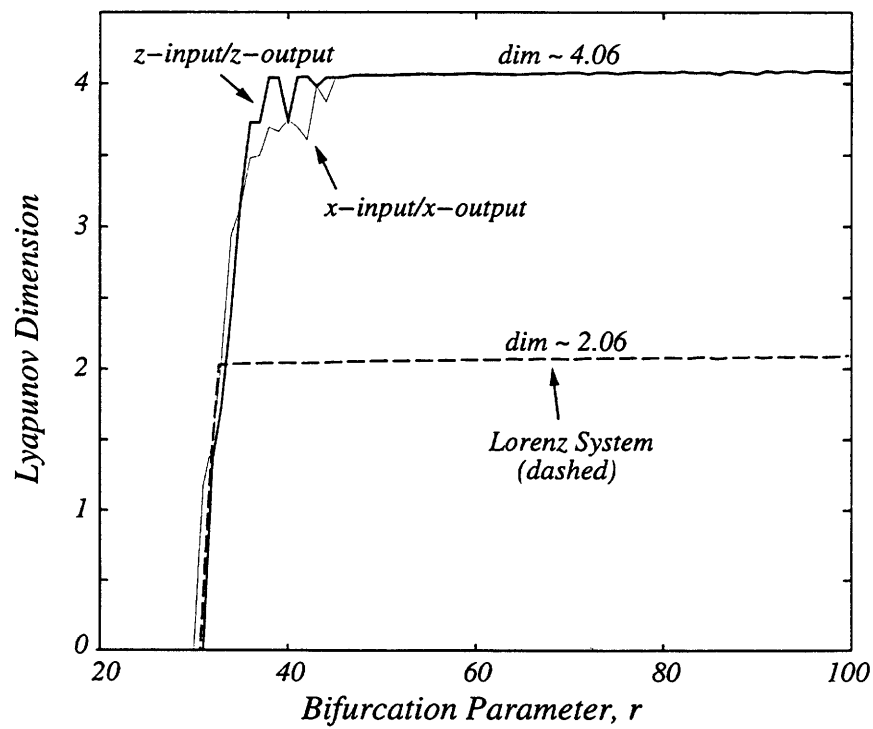


Figure 6-9: Lyapunov Dimension for 5-Dimensional LFBCSs.

z-Input/z-Output LFBCS

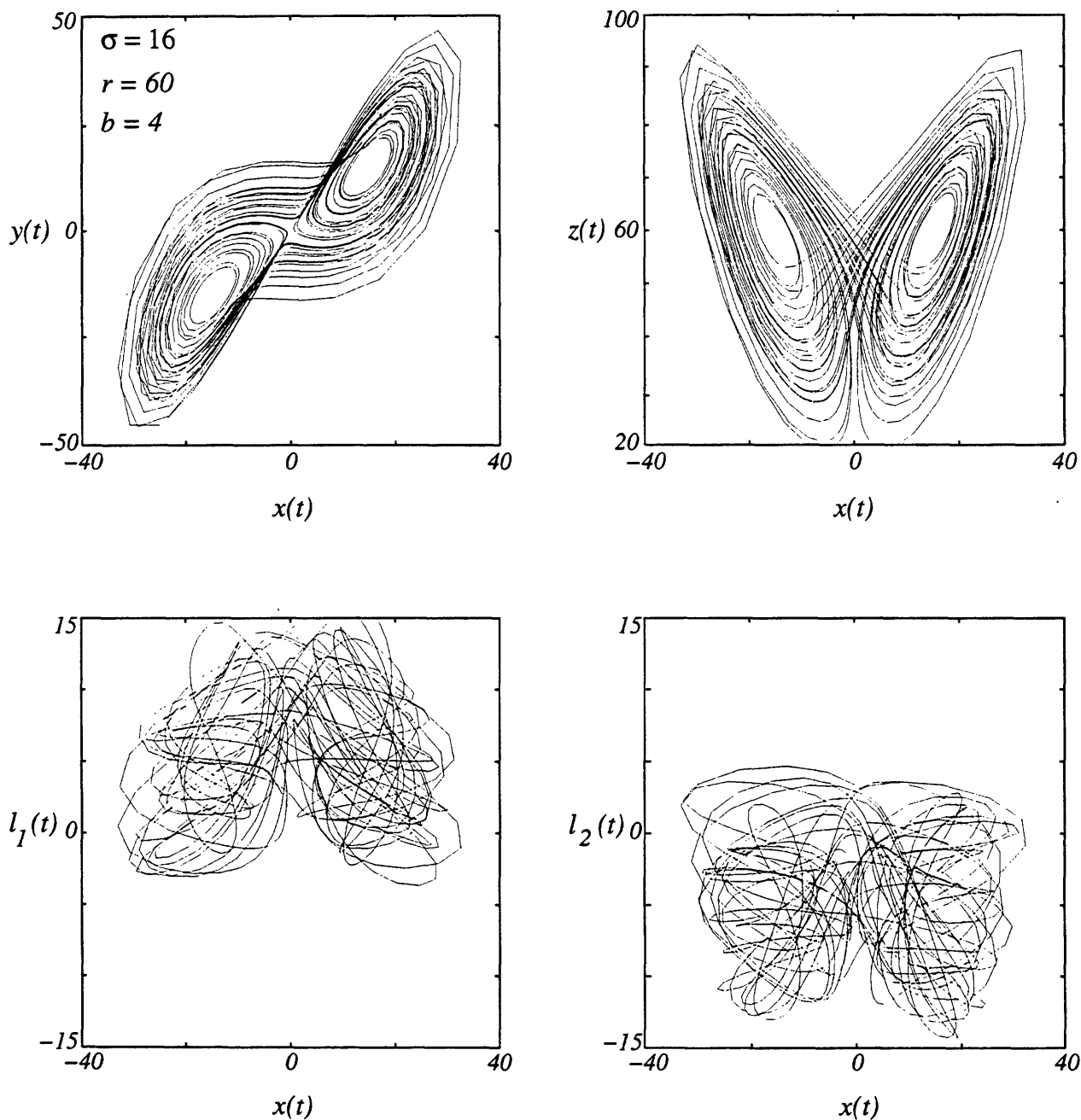


Figure 6-10: *Chaotic Attractor for a 5-Dimensional z-input/z-output LFBCS.*

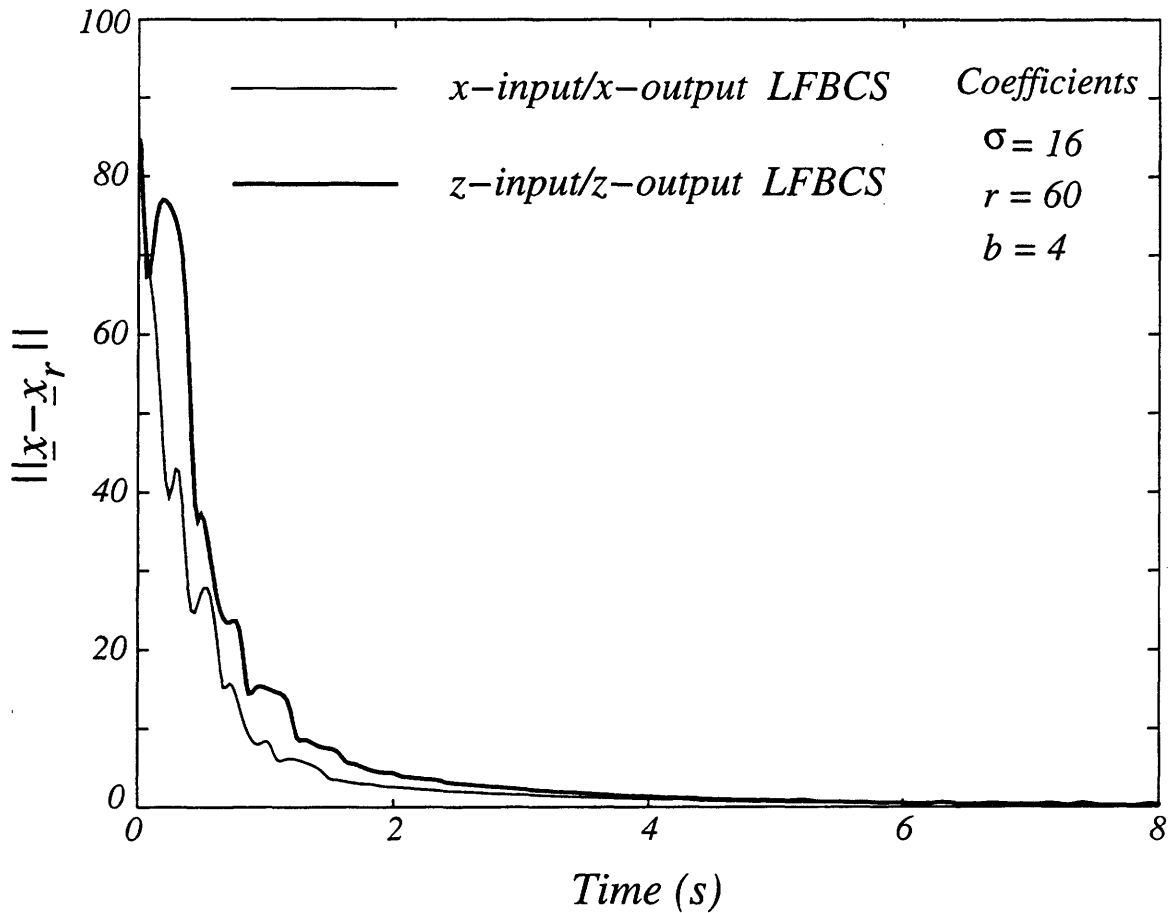


Figure 6-11: *Self-Synchronization in 5-Dimensional LFBCSs.*

- An interesting future experiment would be to switch between the two LFBCS types at the transmitter and to detect the source of the transmitted drive signal by measuring the synchronization error at the corresponding receivers. If the source of the transmitted signal is difficult to detect by unintended listeners, then this approach may be potentially useful for private communications.
- Hardware implementations of LFBCSs should be straightforward and inexpensive. We already know how to implement the Lorenz system with a simple analog circuit (see Chapter 9). Implementing the linear feedback system should be even easier.

While LFBCSs appear to be very promising, they seem to exhibit only a single positive Lyapunov exponent. The creation of additional positive exponents can sig-

nificantly increase the attractor dimension of a chaotic system and may be desirable from certain private communication viewpoints because higher dimensional systems typically give rise to more complex dynamics. The desire to create more complex systems raises two interesting questions:

1. Is it possible to synthesize self-synchronizing chaotic systems by mutually coupling several Lorenz oscillators?
2. Does the coupled system exhibit multiple positive Lyapunov exponents?

As we show in the next chapter, the answer to both of these questions is affirmative.

Chapter 7

Synthesizing Self-Synchronizing Chaotic Arrays

It is well-known that coupling among nonlinear oscillators can produce a wide range of nonlinear dynamical behavior, including periodicity, chaos, hyperchaos, and synchronization. To explore some of the dynamical processes that can occur in these systems, there have been several theoretical, numerical, and experimental investigations of coupled oscillator systems. Kowalski *et al.* [39], for example, has shown numerically that a system consisting of an ensemble of Lorenz oscillators can exhibit mutual synchronization while behaving chaotically. Synchronized chaos has also been investigated in arrays of Rössler oscillators [40, 41], laser systems [4], neural networks [6], and Selkov models [42]. Although significant progress has been made toward understanding these systems, synthesizing self-synchronizing chaotic arrays has not been addressed.

In this chapter, we develop a systematic approach for synthesizing a class of chaotic arrays which possess the self-synchronization property. These arrays are composed of several Lorenz oscillators and a linear feedback system. The linear system provides for both integrated and direct coupling between the individual Lorenz oscillators. The advantages of linearly coupling several Lorenz oscillators are that the resulting chaotic arrays are analytically tractable and have a modular structure which makes them straightforward to implement.

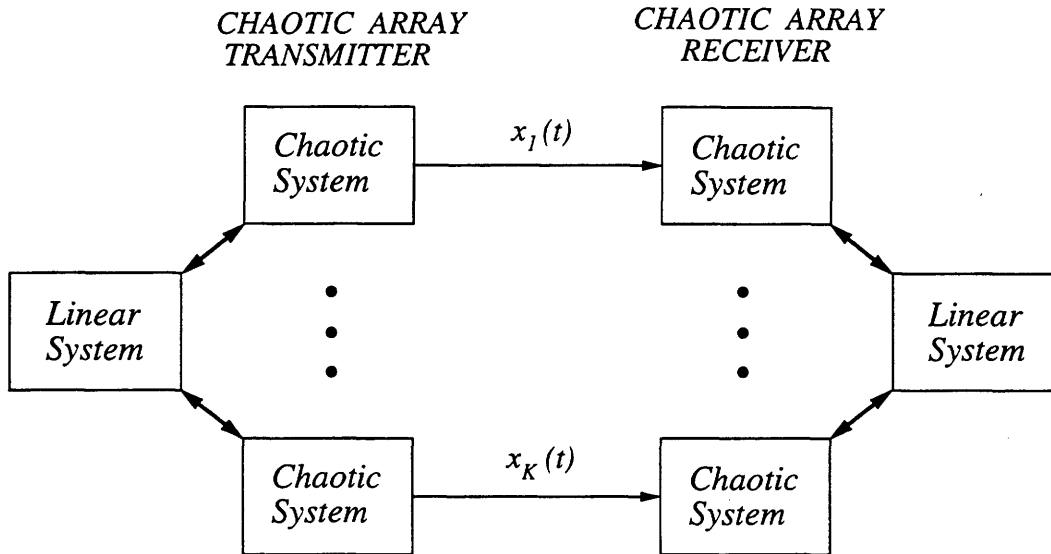


Figure 7-1: *Communicating with Chaotic Arrays.*

Figure 7-1 illustrates a communication scenario in which the transmitter array conveys a *set* of drive signals to an identical receiver array. These drive signals provide a means for establishing and maintaining synchronization between the transmitter and receiver arrays. Although the transmitter and receiver arrays can exhibit very complex dynamics, they will be completely synchronized. A potential drawback of this approach is that the synchronization requires that more than one drive signal be communicated - - one drive signal for each Lorenz oscillator. This requirement increases the complexity of the communication system. There are, however, potential advantages to this approach. The utilization of several drive signals could make it more difficult for an unintended listener to obtain synchronization with the transmitter. Chaotic arrays are also highly modular and easy to modify. Increasing the state space dimension of the array can be achieved by simply adding additional oscillators to the transmitter and receiver.

There are several ways to linearly couple a set of Lorenz oscillators. Our approach is based upon a natural generalization of the z -input/ z -output LFBCSs introduced in Section 6.2. Specifically, the chaotic signals $z(t)$ from each Lorenz oscillator drive the linear system, and the resultant outputs are added to the appropriate oscillator's equation for \dot{z} . This type of array can be represented by a set of state equations of

the form

$$\begin{aligned}
\dot{x}_i &= \sigma_i(y_i - x_i) \\
\dot{y}_i &= r_i x_i - y_i - x_i z_i \\
\dot{z}_i &= x_i y_i - b_i z_i + \nu_i \\
\dot{\mathbf{l}} &= A\mathbf{l} + B\mathbf{z} \\
\nu &= C\mathbf{l} + D\mathbf{z} \ ,
\end{aligned} \tag{7.1}$$

where the subscript “ i ” denotes the individual Lorenz oscillators from the set $i = 1, \dots, K$. The vectors

$$\mathbf{z} = \begin{bmatrix} z_1 \\ \vdots \\ z_K \end{bmatrix} \ , \ \nu = \begin{bmatrix} \nu_1 \\ \vdots \\ \nu_K \end{bmatrix} \ ,$$

denote the inputs and outputs of the linear system, respectively.

In (7.1), the linear system is N -dimensional with K inputs and K outputs. Therefore, the matrices A, B, C , and D have dimension $N \times N$, $N \times K$, $K \times N$, and $K \times K$ respectively. In the single oscillator case, *i.e.*, where $K = 1$, the system (7.1) reduces to the z -input/ z -output LFBCS studied in Section 6.2. In this sense, the chaotic array can be viewed as a straightforward generalization of LFBCSs that allows for multiple Lorenz oscillators to interact through linear feedback. For notational simplicity, we will denote the state variables in (7.1) collectively by the vector $\mathbf{v} = (x_1, y_1, z_1, \dots, x_K, y_K, z_K, \mathbf{l})$ when convenient.

Following the approach outlined in Chapter 6, our first goal is to develop sufficient conditions for which the transmitter equations (7.1) satisfy two requirements: *(i)* there exists an algebraically similar receiver system which possesses the global self-synchronization property, and *(ii)* the transmitter system is globally stable. These requirements are satisfied in Sections 7.1 and 7.2, respectively. In Section 7.3, we summarize the various self-synchronization and global stability conditions for this class of systems and suggest a systematic procedure for synthesizing chaotic arrays. In Section 7.4, we perform a linear stability analysis of the fixed points for a low-order chaotic array. In Section 7.5, we describe the results of several numerical experiments

which demonstrate the nonlinear dynamical behavior of the low-order chaotic array. Section 7.6 summarizes the results of this chapter.

7.1 Conditions for Global Self-Synchronization

The design and implementation of large chaotic arrays is potentially complicated. A significant simplification is achieved by considering a receiver array which has the same algebraic structure as the transmitter. For the Lorenz-based chaotic arrays considered in this chapter, an appropriate set of receiver equations is obtained from the transmitter equations (7.1) by renaming variables $\mathbf{v} \rightarrow \mathbf{v}_r$ and substituting the drive signals $x_i(t)$ for $x_{ir}(t)$ in the equations for \dot{y}_{ir} and \dot{z}_{ir} . In this case, the receiver equations are given by

$$\begin{aligned}
 \dot{x}_{ir} &= \sigma_i(y_{ir} - x_{ir}) \\
 \dot{y}_{ir} &= r_i x_i(t) - y_{ir} - x_i(t) z_{ir} \\
 \dot{z}_{ir} &= x_i(t) y_{ir} - b_i z_{ir} + \nu_{ir} \\
 \dot{\mathbf{l}}_r &= A \mathbf{l}_r + B \mathbf{z}_r \\
 \nu_r &= C \mathbf{l}_r + D \mathbf{z}_r .
 \end{aligned} \tag{7.2}$$

The error system is derived by defining the error variables

$$\begin{aligned}
 e_{xi}(t) &= x_i(t) - x_{ir}(t) \\
 e_{yi}(t) &= y_i(t) - y_{ir}(t) \\
 e_{zi}(t) &= z_i(t) - z_{ir}(t) \\
 \mathbf{e}_l(t) &= \mathbf{l}(t) - \mathbf{l}_r(t) ,
 \end{aligned}$$

and subtracting (7.2) from (7.1) to obtain

$$\begin{aligned}
\dot{e}_{xi} &= \sigma_i(e_{yi} - e_{xi}) \\
\dot{e}_{yi} &= -e_{yi} - x_i(t)e_{zi} \\
\dot{e}_{zi} &= x_i(t)e_{yi} - b_i e_{zi} + C_i e_l + D_i e_z \\
\dot{e}_l &= A e_l + B e_z .
\end{aligned} \tag{7.3}$$

In this system, we denote the K rows of C by C_i and the K rows of D by D_i . The error vector e_z denotes the K error variables corresponding to $e_{zi}(t)$, *i.e.*, $e_z = (e_{z1}, \dots, e_{zK})$.

A set of sufficient conditions for the error system to be globally asymptotically stable at the origin can be derived by considering a Lyapunov function of the form

$$E(\mathbf{e}) = \frac{1}{2} \left(\sum_{i=1}^K \left(\frac{1}{\sigma_i} e_{xi}^2 + e_{yi}^2 + e_{zi}^2 \right) + \mathbf{e}_l^T R \mathbf{e}_l \right) ,$$

where R is a symmetric $N \times N$ positive definite matrix. The time rate of change of $E(\mathbf{e})$ along trajectories is given by

$$\dot{E}(\mathbf{e}) = \sum_{i=1}^K \left\{ \begin{bmatrix} e_{xi} \\ e_{yi} \end{bmatrix}^T \begin{bmatrix} -1 & \frac{1}{2} \\ \frac{1}{2} & -1 \end{bmatrix} \begin{bmatrix} e_{xi} \\ e_{yi} \end{bmatrix} \right\} - \begin{bmatrix} e_z \\ e_l \end{bmatrix}^T T \begin{bmatrix} e_z \\ e_l \end{bmatrix} , \tag{7.4}$$

where the matrix T is given by

$$T = \begin{bmatrix} \Lambda_b - \frac{1}{2}(D + D^T) & -\frac{1}{2}(B^T R + C) \\ -\frac{1}{2}(RB + C^T) & -\frac{1}{2}(RA + A^T R) \end{bmatrix} .$$

Notice that T contains the diagonal matrix $\Lambda_b = \text{diag}(b_1, \dots, b_K)$. The diagonal elements of Λ_b correspond to the set of b parameters for the ensemble of Lorenz oscillators.

Observe that \dot{E} is negative definite if T is positive definite. A sufficient set of conditions for T to be positive definite are given below.

- $RB + C^T = 0$, for some $N \times N$ symmetric positive definite matrix R .
- $RA + A^T R$ is negative definite.

- $\Lambda_b - \frac{1}{2}(D + D^T)$ is positive definite.

The first condition provides a constraint between the allowable B and C matrices. The second condition can always be satisfied if A is a stable matrix. The third condition provides a bound on D . If these conditions are satisfied, then the transmitter and receiver arrays are guaranteed to synchronize regardless of their initial conditions.

7.2 Conditions for Global Stability

A set of sufficient conditions for which all trajectories of the transmitter equations remain bounded can be determined by defining a family of ellipsoids

$$V(\mathbf{v}) = \frac{1}{2} \left(\mathbf{x}^T \Lambda_r \mathbf{x} + \mathbf{y}^T \Lambda_\sigma \mathbf{y} + (\mathbf{z} - 2\mathbf{r})^T \Lambda_\sigma (\mathbf{z} - 2\mathbf{r}) + \mathbf{l}^T P \mathbf{l} \right) = k, \quad (7.5)$$

where P is a symmetric $N \times N$ positive definite matrix and k is a positive scalar. The vectors $\mathbf{x}, \mathbf{y}, \mathbf{z}$, and \mathbf{l} in (7.5) represent the transmitter's state variables and are given by

$$\mathbf{x} = \begin{bmatrix} x_1 \\ \vdots \\ x_K \end{bmatrix}, \quad \mathbf{y} = \begin{bmatrix} y_1 \\ \vdots \\ y_K \end{bmatrix}, \quad \mathbf{z} = \begin{bmatrix} z_1 \\ \vdots \\ z_K \end{bmatrix}, \quad \mathbf{l} = \begin{bmatrix} l_1 \\ \vdots \\ l_K \end{bmatrix}.$$

The diagonal matrices $\Lambda_r = \text{diag}(r_1, \dots, r_K)$ and $\Lambda_\sigma = \text{diag}(\sigma_1, \dots, \sigma_K)$ in (7.5) contain the set of r and σ parameters for the ensemble of Lorenz oscillators. The vector $\mathbf{r} = (r_1, \dots, r_K)$ contains the set of r parameters for each oscillator (the same parameters that correspond to the diagonal elements of Λ_r).

If we impose the restrictions $PB + C^T \Lambda_\sigma = 0$ and $\Lambda_\sigma D = D^T \Lambda_\sigma$, then $\dot{V}(\mathbf{v})$ can be written in the form

$$\dot{V}(\mathbf{v}) = -\mathbf{x}^T \Lambda_\sigma \Lambda_r \mathbf{x} - \mathbf{y}^T \Lambda_\sigma \mathbf{y} - \begin{bmatrix} \mathbf{z} - \mathbf{r} \\ \mathbf{l} - \mathbf{q} \end{bmatrix}^T M \begin{bmatrix} \mathbf{z} - \mathbf{r} \\ \mathbf{l} - \mathbf{q} \end{bmatrix} + c,$$

where the matrix M is given by

$$M = \begin{bmatrix} \Lambda_\sigma(\Lambda_b - D) & 0 \\ 0 & -\frac{1}{2}(PA + A^T P) \end{bmatrix} .$$

Also, the scalar c is given by

$$c = \mathbf{r}^T \Lambda_\sigma(\Lambda_b - D)\mathbf{r} - \mathbf{q}^T \frac{(PA + A^T P)}{2} \mathbf{q} ,$$

and the vector \mathbf{q} is given by

$$\mathbf{q} = -(PA + A^T P)^{-1}(PB - C^T \Lambda_\sigma)\mathbf{r} .$$

If M is positive definite and $c > 0$, then $\dot{V}(\mathbf{v}) = 0$ determines an ellipsoid in state space. Sufficient conditions for M to be positive definite and for $c > 0$ are given below.

- $PB + C^T \Lambda_\sigma = 0$.
- $\Lambda_\sigma D = D^T \Lambda_\sigma$.
- $PA + A^T P$ is negative definite.
- $\Lambda_\sigma(\Lambda_b - D)$ is positive definite.

The first and second conditions are simply the imposed restrictions. The third condition can be satisfied by choosing a stable A matrix such that $PA + A^T P$ is negative definite. The fourth condition provides a bound on D .

If these conditions are satisfied, then $\dot{V} = 0$ determines an ellipsoid of the form

$$\frac{\mathbf{x}^T \Lambda_\sigma \Lambda_r \mathbf{x}}{c} + \frac{\mathbf{y}^T \Lambda_\sigma \mathbf{y}}{c} + \frac{1}{c} \begin{bmatrix} \mathbf{z} - \mathbf{r} \\ \mathbf{l} - \mathbf{q} \end{bmatrix}^T M \begin{bmatrix} \mathbf{z} - \mathbf{r} \\ \mathbf{l} - \mathbf{q} \end{bmatrix} = 1 . \quad (7.6)$$

Since $\dot{V} < 0$ for all \mathbf{v} outside of the ellipsoid (7.6), any ellipsoid from the family (7.5) which contains (7.6) will suffice as a trapping region for the transmitter's flow.

It is also important to determine the appropriate conditions which ensure that the transmitter equations are dissipative. The divergence of the transmitter's vector field is given by

$$\begin{aligned}\nabla \cdot \dot{\mathbf{v}} &= \sum_{i=1}^K \left\{ \frac{\partial \dot{x}_i}{\partial x_i} + \frac{\partial \dot{y}_i}{\partial y_i} + \frac{\partial \dot{z}_i}{\partial z_i} \right\} + \sum_{i=1}^N \frac{\partial \dot{l}_i}{\partial l_i} \\ &= -(\text{tr}(\Lambda_\sigma) + K + \text{tr}(\Lambda_b - D) - \text{tr}(A)) \quad .\end{aligned}$$

The divergence is a negative constant if the condition

$$\text{tr}(\Lambda_\sigma) + K + \text{tr}(\Lambda_b - D) - \text{tr}(A) > 0,$$

is satisfied. This condition alone ensures that the transmitter equations are dissipative with exponentially fast volume contraction. In the next section, we summarize the various self-synchronization and global stability conditions and suggest a straightforward synthesis procedure.

7.3 A Systematic Synthesis Procedure

If K Lorenz oscillators are linearly coupled as defined by equation (7.1), and if the conditions:

$$\begin{array}{l} \text{Self-Synchronization} \\ \text{Global Stability} \\ \text{Dissipative} \end{array} \left\{ \begin{array}{l} 1. \quad RB + C^T = 0, \text{ for some } N \times N \text{ positive} \\ \quad \text{definite matrix } R, \\ 2. \quad RA + A^T R \text{ is negative definite,} \\ 3. \quad \Lambda_b - \frac{1}{2}(D + D^T) \text{ is positive definite,} \\ 4. \quad PB + C^T \Lambda_\sigma = 0, \text{ for some } N \times N \text{ positive} \\ \quad \text{definite matrix } P, \\ 5. \quad \Lambda_\sigma D \text{ is symmetric,} \\ 6. \quad PA + A^T P \text{ is negative definite,} \\ 7. \quad \Lambda_\sigma(\Lambda_b - D) \text{ is positive definite,} \\ 8. \quad \text{tr}(\Lambda_\sigma) + K + \text{tr}(\Lambda_b - D) - \text{tr}(A) > 0, \end{array} \right.$$

are satisfied, then the transmitter array is dissipative and globally stable, and the receiver array possesses the global self-synchronization property. Although satisfying each of these conditions may seem to be a formidable task, the conditions can be significantly reduced by making two simplifying assumptions.

If we choose $P = \sigma R$ and $\Lambda_\sigma = \sigma I$, where I denotes the $K \times K$ identity matrix, then conditions 1 and 4 and conditions 2 and 6 are equivalent. Furthermore, condition 5 will then imply that D is symmetric, and thus, conditions 3 and 7 are equivalent. Also, conditions 2 and 6 imply that A is stable. In this case, condition 8 will be automatically satisfied. As a result of A being stable, there exists a positive definite solution R to the matrix Lyapunov equation

$$RA + A^T R + Q = 0, \quad Q > 0.$$

By choosing any stable A matrix and any symmetric positive definite Q matrix, conditions 2 and 6 can always be satisfied. In light of these simplifications, the following synthesis procedure is suggested.

Synthesis Procedure

1. Choose any stable A matrix and any $N \times N$ symmetric positive definite matrix Q .
2. Solve $RA + A^T R + Q = 0$ for the positive definite solution R .
3. Choose any $N \times K$ matrix B and set $C = -B^T R$.
4. Choose any $K \times K$ symmetric matrix D such that $\Lambda_b - D$ is positive definite.

Comparing this synthesis procedure with the z -input/ z -output LFBCS synthesis procedure (Section 6.2.3) shows that they are consistent.

In the next section, we perform a linear stability analysis of the fixed points for a low-order chaotic array. This analysis provides additional insight into the nonlinear dynamical behavior of this class of systems.

7.4 Linear Stability Analysis

For this analysis, we consider a chaotic array consisting of two Lorenz oscillators and an N -dimensional linear system. The transmitter equations are given by

Oscillator 1:

$$\begin{bmatrix} \dot{x} \\ \dot{y} \\ \dot{z} \end{bmatrix} = \begin{bmatrix} \sigma(y - x) \\ r_1x - y - xz \\ xy - b_1z \end{bmatrix} + \begin{bmatrix} 0 \\ 0 \\ \nu_1 \end{bmatrix},$$

Oscillator 2:

$$\begin{bmatrix} \dot{u} \\ \dot{v} \\ \dot{w} \end{bmatrix} = \begin{bmatrix} \sigma(v - u) \\ r_2u - v - uw \\ uv - b_2w \end{bmatrix} + \begin{bmatrix} 0 \\ 0 \\ \nu_2 \end{bmatrix},$$

Linear System:

$$\begin{aligned} \dot{\mathbf{i}} &= A\mathbf{i} + B \begin{bmatrix} z \\ w \end{bmatrix}, \\ \dot{\boldsymbol{\nu}} &= C\mathbf{i} + D \begin{bmatrix} z \\ w \end{bmatrix}. \end{aligned}$$

To clearly distinguish the state variables of the two oscillators, we have used (x, y, z) to denote the state variables for oscillator 1 and (u, v, w) to denote the state variables for oscillator 2. We have also imposed the restriction $\sigma = \sigma_1 = \sigma_2$ to be consistent with the synthesis procedure developed in Section 7.3. The r and b parameters of the two oscillators are, however, independent.

Inspection of the transmitter equations shows that the origin is always a fixed point. Additional fixed points can be determined by setting the transmitter's vector field equal to zero and solving for the non-trivial stationary points. The equations to

be solved are listed below.

1. $\sigma(y^* - x^*) = 0$,
2. $rx^* - y^* - x^*z^* = 0$,
3. $x^*y^* - b_1z^* + C_1\mathbf{l}^* + D_1 \begin{bmatrix} z^* \\ w^* \end{bmatrix} = 0$,
4. $\sigma(v^* - u^*) = 0$,
5. $ru^* - v^* - u^*w^* = 0$,
6. $u^*v^* - b_2w^* + C_2\mathbf{l}^* + D_2 \begin{bmatrix} z^* \\ w^* \end{bmatrix} = 0$,
7. $A\mathbf{l}^* + B \begin{bmatrix} z^* \\ w^* \end{bmatrix} = 0$.

Equations 1 and 2 determine that $y^*(1 - r_1 + z^*) = 0$. It then follows that either

$$y^* = 0 \quad \text{or} \quad z^* = r_1 - 1 . \quad (7.7)$$

Similarly, equations 4 and 5 determine that $v^*(1 - r_2 + w^*) = 0$, from which it follows that either

$$v^* = 0 \quad \text{or} \quad w^* = r_2 - 1 . \quad (7.8)$$

Equations 3, 6, and 7 can then be combined to obtain

$$\begin{bmatrix} x^{*2} \\ u^{*2} \end{bmatrix} = [\Lambda_b + CA^{-1}B - D] \begin{bmatrix} z^* \\ w^* \end{bmatrix} . \quad (7.9)$$

Observe that the 2×2 matrix $H(0) = -CA^{-1}B + D$ is equivalent to the transfer function of the linear system evaluated at the origin. Therefore, equation (7.9) can

be conveniently written as

$$\begin{bmatrix} x^{*2} \\ u^{*2} \end{bmatrix} = [\Lambda_b - H(0)] \begin{bmatrix} z^* \\ w^* \end{bmatrix}. \quad (7.10)$$

Equations (7.7) through (7.10) provide relationships among the various components of the fixed points. To explicitly solve these equations, we must distinguish between four different types of fixed points which arise from the four possible combinations of stationarity conditions given by equations (7.7) and (7.8). An analysis of each type of fixed point is presented below.

Type 1 Fixed Points: ($y^* = 0, v^* = 0$)

Type 1 fixed points are the most straightforward to analyze. Because $y^* = 0$ and $v^* = 0$, equations 1 and 4 imply that $x^* = 0$ and $u^* = 0$, respectively. It follows from (7.10) that $z^* = 0$ and $w^* = 0$, if the 2×2 matrix $\Lambda_b - H(0)$ is invertible. We then find that $\mathbf{l}^* = 0$ from equation 7. From this analysis, we see that the type 1 fixed point is simply the fixed point at the origin.

To perform a linear stability analysis, it is useful to reorder the transmitter equations so that the state variables in the reordered system can be represented by the vector $\mathbf{v}' = (x, y, z, w, \mathbf{l}, v, u)$. With this reordering of the states, the Jacobian matrix evaluated at the origin is given by

$$J(\mathbf{0}) = \begin{bmatrix} -\sigma & \sigma & 0 & 0 & \mathbf{0}^T & 0 & 0 \\ r_1 & -1 & 0 & 0 & \mathbf{0}^T & 0 & 0 \\ 0 & 0 & -(b_1 - D_{11}) & D_{12} & C_1 & 0 & 0 \\ 0 & 0 & D_{21} & -(b_2 - D_{22}) & C_2 & 0 & 0 \\ \mathbf{0} & \mathbf{0} & B_1 & B_2 & A & \mathbf{0} & \mathbf{0} \\ 0 & 0 & 0 & 0 & \mathbf{0}^T & -1 & r_2 \\ 0 & 0 & 0 & 0 & \mathbf{0}^T & \sigma & -\sigma \end{bmatrix}.$$

The two columns of B are denoted by B_1 and B_2 , and the two rows of C are denoted by C_1 and C_2 . The elements of the 2×2 matrix D are denoted by D_{ij} , accordingly.

A convenient form for $J(\mathbf{0})$ results by reordering the states. Specifically, the upper 2×2 block of $J(\mathbf{0})$ corresponds to states in oscillator 1, whereas the lower 2×2 block corresponds to states in oscillator 2. The central $(N + 2) \times (N + 2)$ block corresponds to states from both oscillators and from the linear system. This block defines the coupling between the two oscillators.

The block diagonal structure of $J(\mathbf{0})$ makes it easy to determine a sufficient condition for the instability of the origin. Evaluating the characteristic polynomial for the upper 2×2 block we obtain

$$\lambda^2 + (\sigma + 1)\lambda + \sigma(1 - r_1) = 0 .$$

Both eigenvalues are in the left-half plane for $r_1 < 1$. For $r_1 > 1$, one eigenvalue is in the right-half plane and the origin is unstable. Similar statements hold true for the lower 2×2 block. For $r_2 < 1$, both eigenvalues are in the left-half plane whereas one eigenvalue is in the right-half plane for $r_2 > 1$. If the central block of $J(\mathbf{0})$ is stable, then the stability of the origin is controlled by the modes of the upper and lower 2×2 blocks. From this analysis, we see that the parameters r_1 and r_2 act as bifurcation parameters because they affect the stability of the origin. We note that it is straightforward to extend this analysis to arrays which contain K coupled Lorenz oscillators.

Type 2 Fixed Points: ($y^* = 0, w^* = r_2 - 1$)

Type 2 fixed points arise by choosing $y^* = 0$ and $w^* = r_2 - 1$ in equations (7.7) and (7.8), respectively. Loosely speaking, these fixed points represent a “cross-product” of the fixed point at the origin for oscillator 1 and the fixed point pair for oscillator 2.

To solve for the remaining components of these fixed points, we substitute $y^* = 0$

into equation 3 and $w^* = r_2 - 1$ into equation 7, and then solve for z^* to obtain

$$z^* = (r_2 - 1) \frac{H_{12}(0)}{b_1 - H_{11}(0)}. \quad (7.11)$$

The scalars $H_{ij}(0) = -C_i A^{-1} B_j + D_{ij}$ in (7.11) correspond to the transfer function between the j^{th} input and i^{th} output of the linear system evaluated at the origin. Using equations 4 and 6, we can then solve for u^* to obtain

$$u^* = \pm \sqrt{(r_2 - 1) \left[b_2 - \left(H_{22}(0) + \frac{H_{12}(0)H_{21}(0)}{b_1 - H_{11}(0)} \right) \right]}. \quad (7.12)$$

The remaining components x^* , v^* , and \mathbf{l}^* are determined as

$$\begin{aligned} x^* &= y^*, \\ v^* &= u^*, \\ \mathbf{l}^* &= -A^{-1}B \begin{bmatrix} z^* \\ r_2 - 1 \end{bmatrix}. \end{aligned}$$

Focusing on equation (7.12), we see that type 2 fixed points exist as a symmetric pair when the term under the radical is positive. This can occur when either:

1. $r_2 > 1$ and $b_2 > H_{22}(0) + \frac{H_{12}(0)H_{21}(0)}{b_1 - H_{11}(0)}$; or
2. $r_2 < 1$ and $b_2 < H_{22}(0) + \frac{H_{12}(0)H_{21}(0)}{b_1 - H_{11}(0)}$.

The existence of type 2 fixed points is controlled by r_2 because b_1 , b_2 , and the linear system are assumed to be fixed. At the critical value of $r_2 = 1$, a bifurcation occurs and a pair of type 2 fixed points are created. Previously, we showed that this same critical value of r_2 produced an unstable mode at the origin. The coincidence of the birth of the fixed point pair with the loss of stability at the origin suggests that a pitchfork bifurcation occurs when $r_2 = 1$. This type of behavior is reminiscent of what occurs at the origin in the Lorenz system and the LFBCSs studied in Chapter 6. Now that we better understand the mechanism which creates the type 2 fixed points, we turn our attention to examining their stability.

Evaluating the Jacobian matrix at the state space location of the type 2 fixed points we obtain

$$J(\mathbf{v}'_0) = \begin{bmatrix} -\sigma & \sigma & 0 & 0 & \mathbf{0}^T & 0 & 0 \\ r^* & -1 & 0 & 0 & \mathbf{0}^T & 0 & 0 \\ 0 & 0 & -(b_1 - D_{11}) & D_{12} & C_1 & 0 & 0 \\ 0 & 0 & D_{21} & -(b_2 - D_{22}) & C_2 & \pm u^* & \pm u^* \\ 0 & 0 & B_1 & B_2 & A & \mathbf{0} & \mathbf{0} \\ 0 & 0 & 0 & \mp u^* & \mathbf{0}^T & -1 & 1 \\ 0 & 0 & 0 & 0 & \mathbf{0}^T & \sigma & -\sigma \end{bmatrix},$$

where the scalar r^* is given by

$$r^* = r_1 - (r_2 - 1) \frac{H_{12}(0)}{b_1 - H_{11}(0)}.$$

Inspection of $J(\mathbf{v}'_0)$ suggests a simple condition which guarantees that these fixed points are unstable. The upper 2×2 block is decoupled from the remaining states, therefore, an unstable mode exists if $r^* > 1$. From this analysis, we conclude that type 2 fixed points are unstable if the inequality

$$r_1 > 1 + (r_2 - 1) \frac{H_{12}(0)}{b_1 - H_{11}(0)}, \quad (7.13)$$

is satisfied. Note that this inequality defines a half-plane in (r_1, r_2) parameter space.

Type 3 Fixed Points: ($v^* = 0, z^* = r_1 - 1$)

Type 3 fixed points arise by choosing $z^* = r_1 - 1$ and $v^* = 0$ in equations (7.7) and (7.8), respectively. They are analogous to type 2 fixed points. For conciseness, we present only the essential existence and stability results below.

The stationarity equations determine w^* as

$$w^* = (r_1 - 1) \frac{H_{21}(0)}{b_2 - H_{22}(0)}, \quad (7.14)$$

and subsequently x^* can be determined as

$$x^* = \pm \sqrt{(r_1 - 1) \left[b_1 - \left(H_{11}(0) + \frac{H_{12}(0)H_{21}(0)}{b_2 - H_{22}(0)} \right) \right]}. \quad (7.15)$$

Once these components have been obtained, the remaining components y^* , u^* , and \mathbf{l}^* are determined as

$$\begin{aligned} y^* &= x^*, \\ u^* &= v^*, \\ \mathbf{l}^* &= -A^{-1}B \begin{bmatrix} r_1 - 1 \\ w^* \end{bmatrix}. \end{aligned}$$

Focusing on equation (7.15), we see that type 3 fixed points exist as a symmetric pair when the term under the radical is positive. This can occur when either:

1. $r_1 > 1$ and $b_1 > H_{11}(0) + \frac{H_{12}(0)H_{21}(0)}{b_2 - H_{22}(0)}$; or
2. $r_1 < 1$ and $b_1 < H_{11}(0) + \frac{H_{12}(0)H_{21}(0)}{b_2 - H_{22}(0)}$.

The existence of type 3 fixed points is controlled by r_1 because b_1 , b_2 , and the linear system are assumed to be fixed. At the critical value of $r_1 = 1$, a bifurcation occurs and a pair of type 3 fixed points are created. This behavior is similar to that which occurs for type 2 fixed points and suggests that a pitchfork bifurcation takes place when $r_1 = 1$. As shown below, linear stability analysis of the type 3 fixed points will define a half-plane in (r_1, r_2) parameter space for which these fixed points are unstable.

Evaluating the Jacobian matrix at the state space location of the type 3 fixed

points we obtain

$$J(\mathbf{v}'_0) = \begin{bmatrix} -\sigma & \sigma & 0 & 0 & \mathbf{0}^T & 0 & 0 \\ 1 & -1 & \mp x^* & 0 & \mathbf{0}^T & 0 & 0 \\ \pm x^* & \pm x^* & -(b_1 - D_{11}) & D_{12} & C_1 & 0 & 0 \\ 0 & 0 & D_{21} & -(b_2 - D_{22}) & C_2 & 0 & 0 \\ \mathbf{0} & \mathbf{0} & B_1 & B_2 & A & \mathbf{0} & \mathbf{0} \\ 0 & 0 & 0 & 0 & \mathbf{0}^T & -1 & r^* \\ 0 & 0 & 0 & 0 & \mathbf{0}^T & \sigma & -\sigma \end{bmatrix},$$

where the scalar r^* is given by

$$r^* = r_2 - (r_1 - 1) \frac{H_{21}(0)}{b_2 - H_{22}(0)}.$$

Because the lower 2×2 block is decoupled from the remaining states, it is clear that an unstable mode exists if $r^* > 1$. From this analysis, we conclude that type 3 fixed points are unstable if the inequality

$$r_2 > 1 + (r_1 - 1) \frac{H_{21}(0)}{b_2 - H_{22}(0)}, \quad (7.16)$$

is satisfied. This inequality also defines a half-plane in (r_1, r_2) parameter space. One might conjecture that the type 4 fixed points exist within the region of (r_1, r_2) parameter space for which both type 2 and type 3 fixed points are unstable. This turns out to be the case as we now show below.

Type 4 Fixed Points: ($z^* = r_1 - 1, w^* = r_2 - 1$)

Type 4 fixed points arise by choosing $z^* = r_1 - 1$ and $w^* = r_2 - 1$ in equations (7.7) and (7.8), respectively. They represent a generalization of the fixed point pair for a single Lorenz oscillator. Conceptually, we can view these fixed points as a “cross-product” of the fixed point pairs for each Lorenz oscillator.

To solve for the remaining components of these fixed points, we need to consider the existence of solutions to equation (7.9), which we reproduced below for convenience.

$$\begin{bmatrix} x^{*2} \\ u^{*2} \end{bmatrix} = \begin{bmatrix} b_1 - H_{11}(0) & -H_{12}(0) \\ -H_{21}(0) & b_2 - H_{22}(0) \end{bmatrix} \begin{bmatrix} r_1 - 1 \\ r_2 - 1 \end{bmatrix}, \quad (7.17)$$

From (7.17), we see that type 4 fixed points exist as quadruplicates (because both x^* and u^* appear quadratically on the left-hand side of (7.17)). As a result, these fixed points will exist if the following two inequalities are satisfied.

$$\begin{aligned} (b_1 - H_{11}(0))(r_1 - 1) - H_{12}(0)(r_2 - 1) &> 0 \\ -H_{21}(0)(r_1 - 1) + (b_2 - H_{22}(0))(r_2 - 1) &> 0 \end{aligned}$$

Solving these inequalities for r_1 and r_2 we obtain

$$r_1 > 1 + (r_2 - 1) \frac{H_{12}(0)}{b_1 - H_{11}(0)}, \quad (7.18)$$

$$r_2 > 1 + (r_1 - 1) \frac{H_{21}(0)}{b_2 - H_{22}(0)}, \quad (7.19)$$

assuming that both $b_1 - H_{11}(0) > 0$ and $b_2 - H_{22}(0) > 0$. If it turns out that either of these assumptions is incorrect, then the direction of the inequality signs “>” in (7.18) and (7.19) will need to be appropriately reversed.

Inequalities (7.18) and (7.19) represent half-planes in (r_1, r_2) space. In the region where these half-planes overlap, four type 4 fixed points will exist. Comparing (7.18) and (7.19) with the instability conditions for type 2 (inequality (7.13)) and type 3 (inequality (7.16)) fixed points shows an exact correspondence. Specifically, the region in (r_1, r_2) parameter space for which type 4 fixed points exist is exactly the same region for which the type 2 and type 3 fixed points are unstable.

The final step in our analysis of the fixed points is to examine the stability of type 4 fixed points. This is most easily accomplished numerically by evaluating the corresponding Jacobian matrix and computing the resulting eigenvalues. In typical

cases, we observe that the type 4 fixed points are unstable for r_1 and r_2 sufficiently large. This comes as no surprise since all of the fixed points in the uncoupled Lorenz oscillators lose stability for $r > r_{Hopf}$. We will demonstrate the behavior of a low-order chaotic array numerically in the next section.

7.5 Numerical Example

For the purpose of demonstration, consider the following 7-dimensional transmitter array.

$$\begin{aligned}
 \dot{x} &= \sigma(y - x) \\
 \dot{y} &= r_1 x - y - xz \\
 \dot{z} &= xy - b_1 z + \nu_1 \\
 \dot{u} &= \sigma(v - u) \\
 \dot{v} &= r_2 u - v - uv \\
 \dot{w} &= uv - b_2 w + \nu_2 \\
 \dot{l} &= -l + \begin{bmatrix} -.36 & .97 \end{bmatrix} \begin{bmatrix} z \\ w \end{bmatrix} \\
 \begin{bmatrix} \nu_1 \\ \nu_2 \end{bmatrix} &= \begin{bmatrix} .36 \\ -.97 \end{bmatrix} l + \begin{bmatrix} .87 & -.10 \\ -.10 & .66 \end{bmatrix} \begin{bmatrix} z \\ w \end{bmatrix}
 \end{aligned}$$

This array consists of two Lorenz oscillators and a one-dimensional linear system. Following the synthesis procedure outlined in Section 7.3, we chose $A = -1$, $Q = 2$, and randomly selected the elements of B and D from the normal distribution $N(0, 1)$. We then set $C = -B^T$ and verified that $\Lambda_b - D$ is positive definite. For the numerical experiments presented below, the Lorenz parameters $\sigma = 16$, $b_1 = 4$, and $b_2 = 4$ are fixed while the bifurcation parameters r_1 and r_2 are varied.

In figure 7-2, we show the stability diagram for this system. The stability diagram illustrates several regions in (r_1, r_2) parameter space where the chaotic array exhibits qualitatively different behavior. For example, the line segments (p, q) and

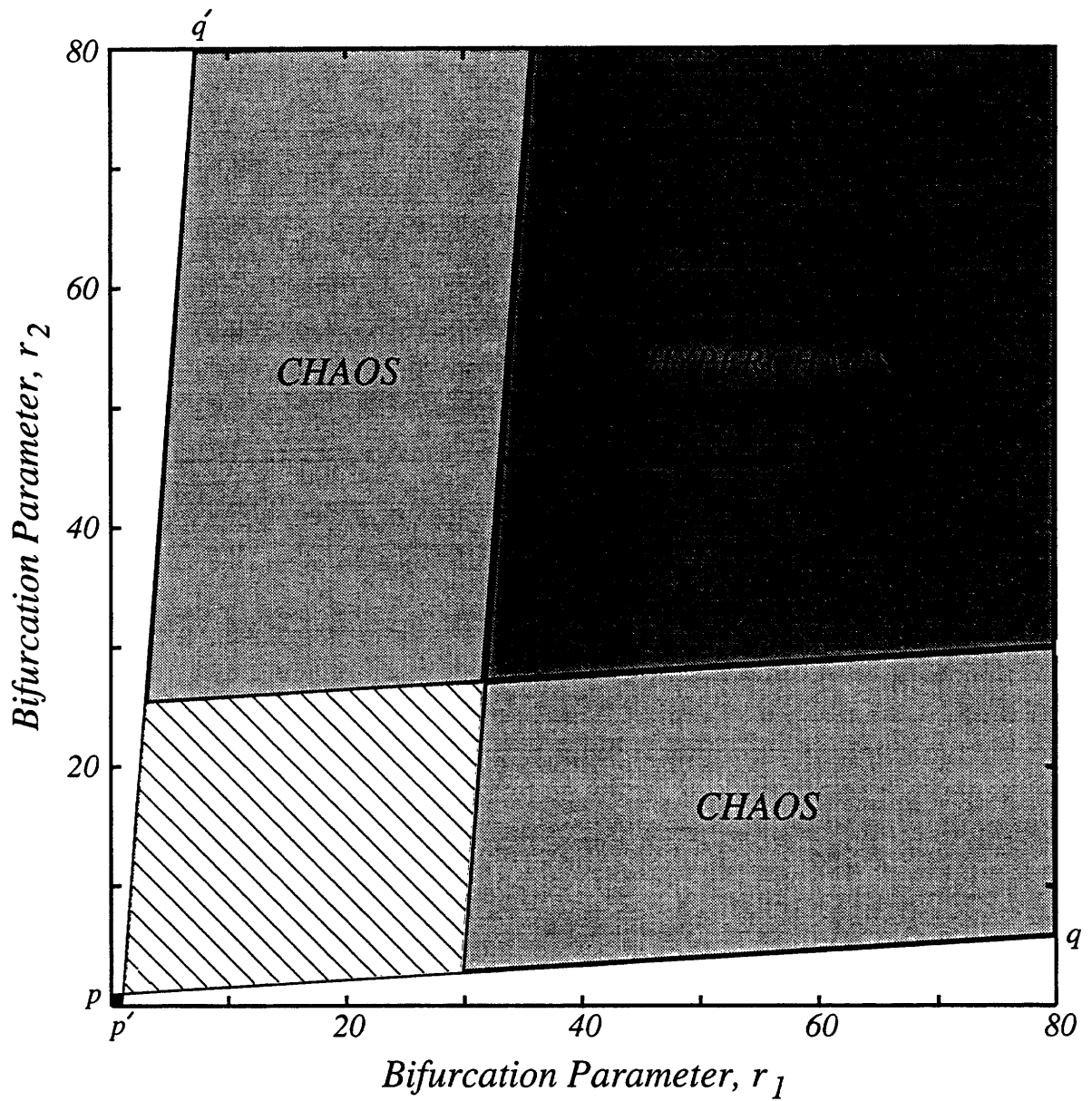
(p', q') correspond to the boundaries where an abrupt change in the stability of type 2 and type 3 fixed points occurs. These same line segments also correspond to the boundaries where type 4 fixed points are either created or destroyed. The linear stability analysis performed in Section 7.4 provides an exact mathematical representation of these boundaries (inequalities (7.18) and (7.19)). The shaded regions of the stability diagram indicate where chaotic motion occurs. The array exhibits a single positive Lyapunov exponent in the regions denoted “CHAOS,” whereas two positive Lyapunov exponents exist in the regions denoted “HYPERCHAOS.”

To visualize the dependence of the Lyapunov exponents on r_1 , we show in figure 7-3 the Lyapunov spectrum as r_1 is varied over the range $20 < r_1 < 80$. The parameter r_2 in this experiment is held fixed at the value $r_2 = 60$. For $r_1 > 33$, two positive exponents exist (hyperchaos region); one corresponds to oscillator 1 and the other corresponds to oscillator 2. Several other important features of the Lyapunov spectrum are listed below.

- An exponent equal to -1 is apparent. This exponent corresponds to the pole of the linear system.
- Two large negative exponents are apparent. These exponents are due to the highly dissipative nature of the chaotic array.
- Two zero exponents are apparent. These exponents correspond to motion tangent to the flow.

For comparison purposes, the computed Lyapunov exponents for a single Lorenz oscillator (dashed lines) are also shown in this figure. Comparing these exponents with the corresponding exponents for the chaotic array suggests a close relationship among them. When an individual Lorenz oscillator is linearly coupled to a second Lorenz oscillator, the Lyapunov exponents show little change.

In figure 7-4, we show the computed Lyapunov dimension as r_1 is varied over the range $20 < r_1 < 80$. Note that there is an abrupt increase in the Lyapunov dimension as the chaotic array enters the hyperchaotic region. As r_1 is increased, the Lyapunov dimension remains nearly constant at a value approximately equal to 5.06.





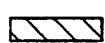

-  9 Unstable Fixed Points, 1 Positive Lyapunov Exponent
-  9 Unstable Fixed Points, 2 Positive Lyapunov Exponents
-  9 Fixed Points, 5 Unstable, 4 Stable
-  5 Fixed Points, 3 Unstable, 2 Stable

Figure 7-2: Stability Diagram for a 7-Dimensional Chaotic Array.

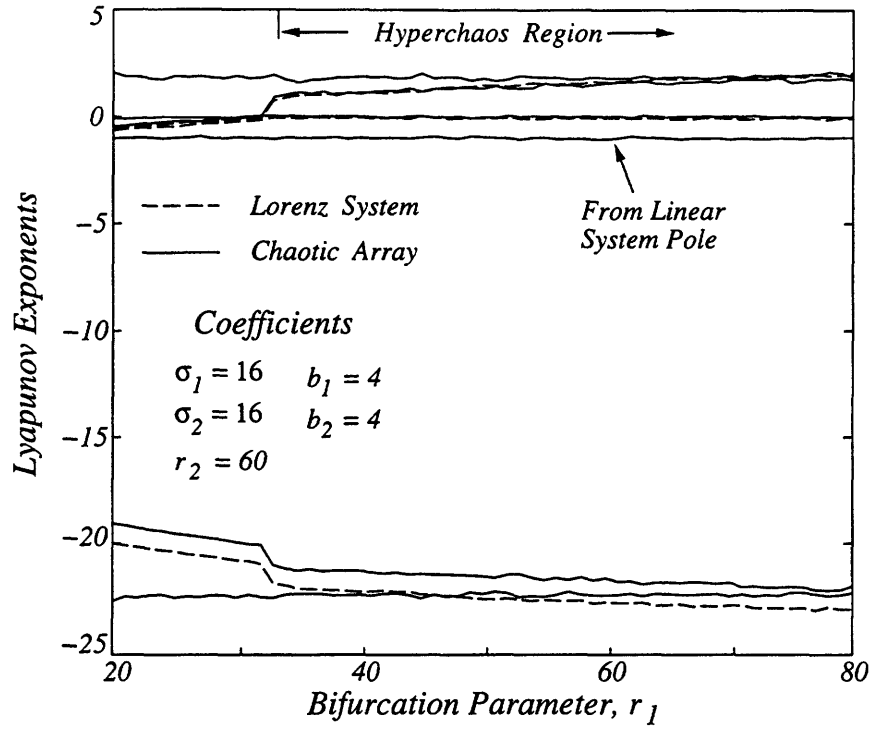


Figure 7-3: Lyapunov Exponents for a 7-Dimensional Chaotic Array.

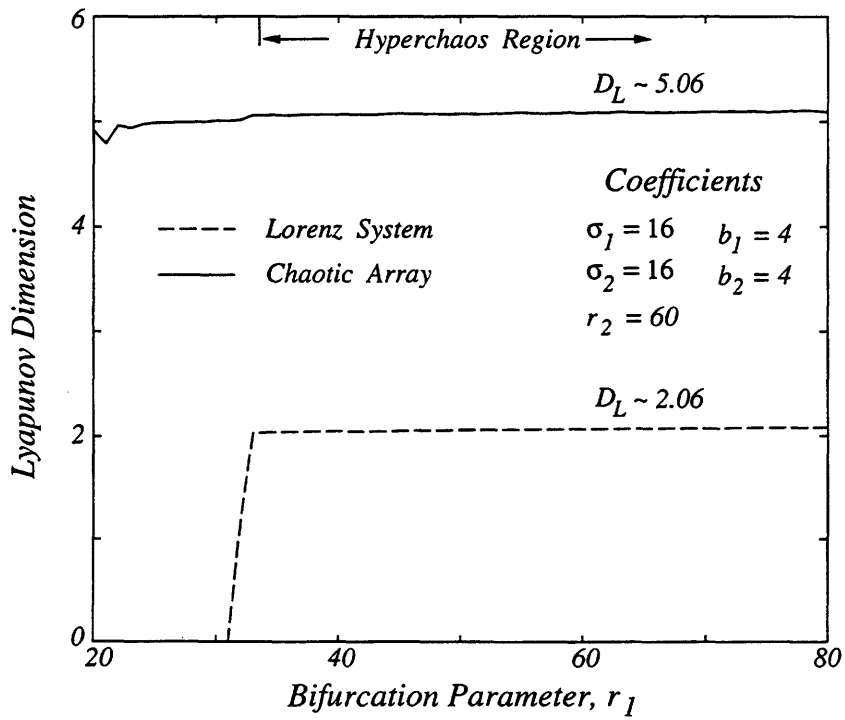


Figure 7-4: Lyapunov Dimension for a 7-Dimensional Chaotic Array.

This relatively large value suggests that the two oscillators in the transmitter array are not synchronized. A numerical calculation of mutual information [4] confirms that the oscillators are operating nearly independent of each other. The Lyapunov dimension of the chaotic array could be increased by adding additional states to the linear system or by adding additional Lorenz oscillators. Using more oscillators has the advantage of introducing additional positive Lyapunov exponents and significantly increasing the complexity of the dynamics, although the implementation would also be more complex.

In figure 7-5, we demonstrate that the transmitter and receiver arrays rapidly synchronize when the receiver is driven by the transmitter signals $x(t)$ and $u(t)$. The curve measures the distance in state space between the transmitter and receiver trajectory when the receiver is initialized in the zero state. In an informal experiment, the transmitter and receiver arrays did not synchronize when only one of the drive links was established.

7.6 Summary

The development of a systematic procedure for synthesizing self-synchronizing chaotic arrays may serve a useful purpose for future communication applications. The methods and results of this chapter, however, could have wider potential. Many physical processes can be modeled by large groups of mutually coupled oscillators [8]. The dynamics within a group can be very complex while the group as a whole can synchronize with other similar groups. The Lorenz-based chaotic arrays investigated in this chapter may lead to models useful for helping us to understand these processes. Some conjectures and insights gained from this work are listed below.

- The individual Lorenz oscillators in a chaotic array seem to operate nearly independent of each other. This conjecture is supported by the linear stability analysis, the Lyapunov spectrum, and the Lyapunov dimension for a low-order chaotic array.

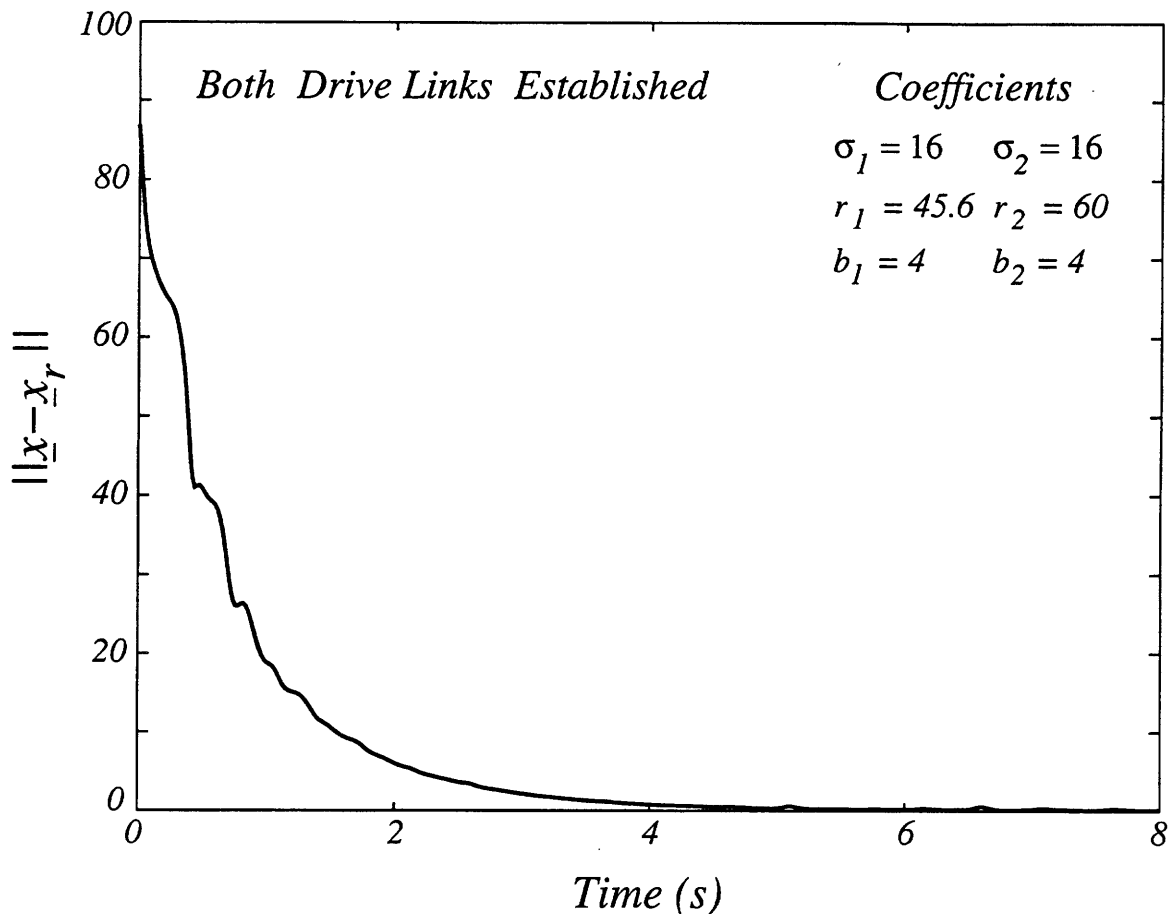


Figure 7-5: *Self-Synchronization in a 7-Dimensional Chaotic Array.*

- It is possible for an array consisting of K Lorenz oscillators to exhibit K positive Lyapunov exponents. This conjecture is based on limited numerical experiments with low-order chaotic arrays.
- If communicating multiple drive signals is not an issue, then the recommended approach for synthesizing a complex transmitter and receiver array is to use as many Lorenz oscillators as possible and to couple them with a first-order linear system. This will produce an array with the most complex dynamics for a given state space dimension.
- If communicating multiple drive signals is a problem, then the dynamics of the transmitter and receiver arrays can be made more complex by using a larger linear system. In the single drive case, the chaotic array reduces to a z -input/ z -

output LFBCS.

- Hardware implementations of chaotic arrays should be straightforward because of their modular structure.

We conclude this chapter by forming a more abstract view of the classes of chaotic systems that we have considered so far. The LFBCSs introduced in Chapter 6 can be viewed as a class of systems which have a linear system and a chaotic system embedded within the same state space. The chaotic arrays developed in this chapter are a generalization of this concept and allow for multiple chaotic systems to be embedded within the system's state space. A further generalization of these concepts would eliminate the necessity of the linear system and allow the chaotic system to occupy the entire state space. In the next chapter, we examine this issue in detail and develop a systematic procedure for synthesizing a more general class of self-synchronizing chaotic systems.

Chapter 8

Synthesizing a General Class of Synchronizing Chaotic Systems

Linear feedback chaotic systems, as discussed in Chapter 6, use a single drive signal for synchronization. The complexity of the dynamics, however, is limited because the nonlinear system component is only three-dimensional. Chaotic arrays, as discussed in Chapter 7, can exhibit more complex dynamics than LFBCSs but multiple drive signals are required for synchronization. This chapter provides a third alternative: a systematic synthesis procedure for chaotic systems that synchronize via a single drive signal and exhibit more complex dynamics than LFBCSs, although somewhat less than chaotic arrays [44].

To develop this new synthesis capability, we begin with a general class of nonlinear systems. For both practical and theoretical simplicity, we will limit consideration to nonlinear systems that can be represented by a set of first-order ordinary differential equations having a quadratic vector field defined on R^N . While this limitation makes the problem more amenable to analysis, it also has the practical advantage of restricting the class of nonlinear systems to those which are relatively easy to implement. Systems having a quadratic term in the vector field can be realized using a single analog multiplier, whereas a cubic or higher-order term would require additional components.

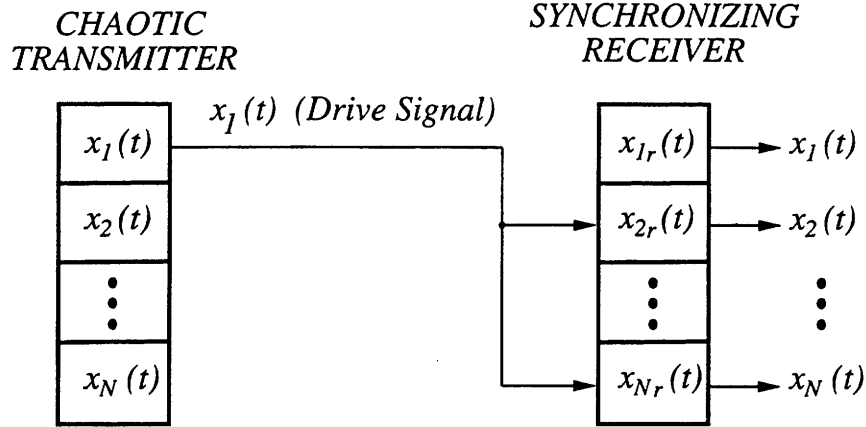


Figure 8-1: *Communicating with a General Class of Synchronizing Chaotic Systems.*

A general nonlinear system with a quadratic vector field is given by

$$\dot{\mathbf{x}} = A\mathbf{x} + (\mathbf{x}^T Q_1 \mathbf{x}, \dots, \mathbf{x}^T Q_N \mathbf{x}) . \quad (8.1)$$

The vector \mathbf{x} denotes the N states (x_1, \dots, x_N) , the A matrix is $N \times N$, and the Q_i , for $i = 1, \dots, N$, are symmetric $N \times N$ matrices. Equation (8.1) will be interpreted as the transmitter system that communicates with the self-synchronizing receiver(s) through the drive signal $x_1(t)$. Figure 8-1 illustrates the approach.

Although our previous synthesis procedures are specific to the Lorenz system, the methodology used in their development is clearly broader. Our approach to synthesis has consistently followed the three step process listed below.

- Determine conditions for the global self-synchronization of the transmitter and receiver systems.
- Determine conditions for the global stability of the transmitter.
- Determine conditions which ensure that the transmitter's fixed points are unstable.

For the classes of chaotic systems considered in Chapters 6 and 7, these steps could be performed in any order. Performing them in the order indicated will, however, considerably simplify our subsequent development of a more general synthesis procedure.

In Section 8.1, we develop sufficient conditions for the transmitter and receiver systems to possess the global self-synchronization property. In Section 8.2, we develop additional conditions to guarantee that the transmitter is globally stable. In Section 8.3, we summarize these conditions and suggest a systematic synthesis procedure. In Section 8.4, we suggest a numerical procedure for studying the stability of the fixed points for this class of systems. In Section 8.5, we demonstrate the synthesis procedure with several numerical examples. In Section 8.6, the results of this chapter are summarized.

8.1 Conditions for Global Self-Synchronization

In our subsequent analysis, we express the transmitter equations (8.1) in the form

$$\dot{\mathbf{x}} = A_0 \mathbf{x} + \mathbf{a}^0 x_1 + (\mathbf{x}^T Q_1 \mathbf{x}, \mathbf{x}^T Q'_2 \mathbf{x}, \dots, \mathbf{x}^T Q'_N \mathbf{x}) + 2A_1 x_1 \mathbf{x} + \mathbf{s}^0 x_1^2 . \quad (8.2)$$

This form results by decomposing the A matrix into $A = A_0 + \mathbf{a}^0 \mathbf{e}_1^T$, where

$$A_0 = \begin{bmatrix} a_{11} & a_{12} & \cdots & a_{1N} \\ 0 & a_{22} & \cdots & a_{2N} \\ \vdots & \vdots & \ddots & \vdots \\ 0 & a_{N2} & \cdots & a_{NN} \end{bmatrix}, \quad \mathbf{a}^0 = \begin{bmatrix} 0 \\ a_{21} \\ \vdots \\ a_{N1} \end{bmatrix}, \quad \mathbf{e}_1 = \begin{bmatrix} 1 \\ 0 \\ \vdots \\ 0 \end{bmatrix} .$$

Also, the matrices Q_i , for $i = 2, \dots, N$, have been decomposed into

$$Q_i = Q'_i + \mathbf{q}_i^0 \mathbf{e}_1^T + \mathbf{e}_1 \mathbf{q}_i^{0T} + \mathbf{e}_1 \mathbf{e}_1^T q_i ,$$

where

$$Q'_i = \begin{bmatrix} 0 & 0 & \cdots & 0 \\ 0 & q_{22}^{(i)} & \cdots & q_{2N}^{(i)} \\ \vdots & \vdots & \ddots & \vdots \\ 0 & q_{N2}^{(i)} & \cdots & q_{NN}^{(i)} \end{bmatrix}, \quad \mathbf{q}_i^0 = \begin{bmatrix} 0 \\ q_{21}^{(i)} \\ \vdots \\ q_{N1}^{(i)} \end{bmatrix}, \quad q_i = q_{11}^{(i)} .$$

For notational simplicity, the vectors \mathbf{q}_i^0 , for $i = 2, \dots, N$ are collected in the matrix $A_1 = [0, \mathbf{q}_2^0, \dots, \mathbf{q}_N^0]^T$ and the scalars q_i , for $i = 2, \dots, N$, are collected in the vector $\mathbf{s}^0 = (0, q_2, \dots, q_N)$.

The transmitter equations have a total of $N^2(N + 1)/2$ free parameters corresponding to the nonlinear terms. If these parameters were selected at random, it is unlikely that the resulting system would possess the self-synchronization property. As we show below, by requiring that a globally self-synchronizing receiver exists, many of the free parameters in the transmitter equations will vanish. Also, a significant analytical simplification is obtained by requiring the transmitter/receiver error dynamics to be linear.

Requirement 1 *The transmitter equations must allow for the existence of a single-input globally self-synchronizing receiver. Moreover, the error dynamics between the transmitter and receiver must be linear.*

By renaming variables in the transmitter (8.2) from $\mathbf{x} \rightarrow \mathbf{x}_r$, an appropriate receiver system can be defined as

$$\dot{\mathbf{x}}_r = A_0 \mathbf{x}_r + \mathbf{a}^0 x_1 + (\mathbf{x}_r^T Q_1 \mathbf{x}_r, \mathbf{x}_r^T Q'_2 \mathbf{x}_r, \dots, \mathbf{x}_r^T Q'_N \mathbf{x}_r) + 2A_1 x_1 \mathbf{x}_r + \mathbf{s}^0 x_1^2. \quad (8.3)$$

Sufficient conditions for the synchronization of the transmitter (8.2) and receiver (8.3) can be determined by forming the error system. The error system is obtained by defining $\mathbf{e} = \mathbf{x} - \mathbf{x}_r$ and subtracting (8.3) from (8.2) to obtain

$$\dot{\mathbf{e}} = (A_0 + 2A_1 x_1) \mathbf{e} + \begin{bmatrix} \mathbf{x}^T Q_1 \mathbf{x} - \mathbf{x}_r^T Q_1 \mathbf{x}_r \\ \mathbf{x}^T Q'_2 \mathbf{x} - \mathbf{x}_r^T Q'_2 \mathbf{x}_r \\ \vdots \\ \mathbf{x}^T Q'_N \mathbf{x} - \mathbf{x}_r^T Q'_N \mathbf{x}_r \end{bmatrix}.$$

If we now make the substitution $\mathbf{x}_r = \mathbf{x} - \mathbf{e}$, we obtain

$$\dot{\mathbf{e}} = (A_0 + 2A_1x_1)\mathbf{e} + \begin{bmatrix} \mathbf{x}^T(Q_1 + Q_1^T)\mathbf{e} - \mathbf{e}^T Q_1 \mathbf{e} \\ \mathbf{x}^T(Q'_2 + Q_2^T)\mathbf{e} - \mathbf{e}^T Q'_2 \mathbf{e} \\ \vdots \\ \mathbf{x}^T(Q'_N + Q_N^T)\mathbf{e} - \mathbf{e}^T Q'_N \mathbf{e} \end{bmatrix} . \quad (8.4)$$

Observe that for linear error dynamics, the matrices Q_1 and Q'_i , for $i = 2, \dots, N$, must be skew-symmetric. Since these matrices are also symmetric by definition, they must be identically zero for linear error dynamics.

Under these requirements, equation (8.4) reduces to

$$\dot{\mathbf{e}} = (A_0 + 2A_1x_1)\mathbf{e} . \quad (8.5)$$

Equation (8.5) is linear in \mathbf{e} , but has a time-dependent coefficient $x_1(t)$. A sufficient condition for this system to be globally asymptotically stable at the origin can be obtained by considering a Lyapunov function of the form

$$E(\mathbf{e}) = \frac{1}{2}\mathbf{e}^T R \mathbf{e} ,$$

where R is a symmetric $N \times N$ positive definite matrix. The time rate of change of $E(\mathbf{e})$ along trajectories is given by

$$\dot{E}(\mathbf{e}) = \mathbf{e}^T \frac{(RA_0 + A_0^T R)}{2} \mathbf{e} + x_1 \mathbf{e}^T (RA_1 + A_1^T R) \mathbf{e} .$$

Observe that \dot{E} is negative definite if the following two conditions are satisfied.

- $RA_1 = -A_1^T R$.
- $RA_0 + A_0^T R$ is negative definite.

Because the first row and column of A_1 is the zero vector, the first condition can be satisfied by choosing R to be a diagonal matrix of the form $R = \text{diag}(p, 1, \dots, 1)$, $p > 0$, and restricting A_1 to be skew-symmetric. This restriction results in a further

reduction in the number of free parameters in the transmitter equations. The second condition can be satisfied by choosing a stable matrix A_0 such that $RA_0 + A_0^T R$ is negative definite.

8.2 Conditions for Global Stability

Requirement 1 reduces the transmitter equations to the form

$$\dot{\mathbf{x}} = A_0 \mathbf{x} + \mathbf{a}^0 x_1 + 2A_1 x_1 \mathbf{x} + \mathbf{s}^0 x_1^2 . \quad (8.6)$$

By requiring the transmitter to be globally stable, further constraints on the algebraic structure of the transmitter can be obtained.

Requirement 2 *All trajectories of the transmitter equations must remain bounded for $t > 0$.*

A sufficient condition for which all trajectories of (8.6) remain bounded can be determined by defining a family of ellipsoids

$$V(\mathbf{x}) = \frac{1}{2}(\mathbf{x} - \mathbf{c})^T P(\mathbf{x} - \mathbf{c}) = k , \quad (8.7)$$

where P is a symmetric $N \times N$ positive definite matrix, \mathbf{c} is a vector which defines the center of the ellipsoids, and k is a positive scalar. As we show below, for k sufficiently large, $V(\mathbf{x})$ will determine a trapping region for the N -dimensional flow.

If we restrict PA_1 to be skew-symmetric, then $\dot{V}(\mathbf{x})$ can be written in the form

$$\begin{aligned} \dot{V}(\mathbf{x}) = & (\mathbf{x} - \mathbf{l})^T \frac{(PA_0 + A_0^T P)}{2} (\mathbf{x} - \mathbf{l}) - \mathbf{l}^T \frac{(PA_0 + A_0^T P)}{2} \mathbf{l} + \\ & \mathbf{x}^T [(P\mathbf{a}^0 - 2A_1^T P\mathbf{c})x_1 + P\mathbf{s}^0 x_1^2] - \mathbf{c}^T (P\mathbf{a}^0 x_1 + P\mathbf{s}^0 x_1^2) , \end{aligned}$$

where the vector \mathbf{l} is given by

$$\mathbf{l} = (PA_0 + A_0^T P)^{-1} A_0^T P \mathbf{c} .$$

Sufficient conditions for $\dot{V} = 0$ to define an ellipsoid in state space are given below.

- $PA_1 = -A_1^T P$.
- $PA_0 + A_0^T P$ is negative definite.
- $\mathbf{s}^0 = \mathbf{0}$.
- $\mathbf{a}^0 = -2A_1 \mathbf{c}$.

The first condition is simply the skew-symmetry restriction on PA_1 . The second condition can be satisfied by choosing a stable matrix A_0 such that $PA_0 + A_0^T P$ is negative definite. Note that the first two conditions are consistent with the self-synchronization conditions. The third condition excludes the quadratic drive term, $x_1^2(t)$, from the transmitter/receiver equations and reduces the number of free parameters which correspond to nonlinear terms to only $(N - 1)(N - 2)/2$. The fourth condition uniquely determines \mathbf{a}^0 in terms of A_1 and \mathbf{c} .

If these conditions are satisfied, then $\dot{V} = 0$ reduces to

$$\frac{(\mathbf{x} - \mathbf{l})^T (PA_0 + A_0^T P)(\mathbf{x} - \mathbf{l})}{\mathbf{l}^T (PA_0 + A_0^T P) \mathbf{l}} = 1 . \quad (8.8)$$

Because $PA_0 + A_0^T P$ is restricted to be negative definite, equation (8.8) defines an ellipsoid in state space. Since $\dot{V} < 0$ for all \mathbf{x} outside of the ellipsoid (8.8), any ellipsoid from the family (8.7) which contains (8.8) will suffice as a trapping region for the N -dimensional flow.

It is also important to determine the conditions which ensure that the transmitter equations (8.6) are dissipative. The divergence of the vector field corresponding to (8.6) is given by

$$\nabla \cdot \dot{\mathbf{x}} = \text{tr}(A) + 2x_1 \text{tr}(A_1) .$$

The condition $\text{tr}(A_1) = 0$ ensures that (8.6) has a constant divergence. The condition $\text{tr}(A) < 0$, together with $\text{tr}(A_1) = 0$, ensures that (8.6) is dissipative with a constant negative divergence. This implies that all volume elements in the transmitter's state space will go to zero exponentially fast at every point in R^N . The practical significance of this property motivates us to add a constant negative divergence requirement.

Requirement 3 *The transmitter equations must have a constant negative divergence.*

As discussed above, this requirement is satisfied if

- $\text{tr}(A_1) = 0$,
- $\text{tr}(A) < 0$.

In the next section, we summarize the various self-synchronization and global stability conditions and suggest a straightforward synthesis procedure.

8.3 A Systematic Synthesis Procedure

In Sections 8.1 and 8.2, we determined sufficient conditions on the algebraic structure of an N -dimensional nonlinear system to ensure that Requirements 1 through 3 are satisfied. These conditions prohibit nonlinearities in the drive equation and require that all remaining nonlinearities consist of cross product terms which include the drive variable. The resulting transmitter can be conveniently expressed as

$$\dot{\mathbf{x}} = (A + 2A_1x_1)\mathbf{x} \quad , \quad (8.9)$$

and the self-synchronizing receiver can be expressed as

$$\dot{\mathbf{x}}_r = (A_0 + 2A_1x_1)\mathbf{x}_r + \mathbf{a}^0x_1 \quad . \quad (8.10)$$

Furthermore, if the conditions:

$$\begin{array}{l}
 \text{Self-Synchronization} \\
 \text{Global Stability} \\
 \text{Constant Negative Divergence}
 \end{array}
 \left\{ \begin{array}{l}
 1. \quad RA_1 = -A_1^T R, \text{ for some } N \times N \text{ positive} \\
 \quad \quad \quad \text{definite matrix } R, \\
 2. \quad RA_0 + A_0^T R \text{ is negative definite,} \\
 3. \quad PA_1 = -A_1^T P, \text{ for some } N \times N \text{ positive} \\
 \quad \quad \quad \text{definite matrix } P, \\
 4. \quad PA_0 + A_0^T P \text{ is negative definite,} \\
 5. \quad \mathbf{a}^0 = -2A_1 \mathbf{c}, \\
 6. \quad \text{tr}(A_1) = 0, \\
 7. \quad \text{tr}(A) < 0,
 \end{array} \right.$$

are satisfied, then the transmitter equations are dissipative and globally stable, and the receiver system will possess the global self-synchronization property. Although satisfying each of these conditions may seem difficult, the conditions can be significantly reduced by making two simplifying assumptions.

If we choose $P = cR$, where c is a positive scalar, then conditions 1 and 3 and conditions 2 and 4 are equivalent. Furthermore, if we choose $R = \text{diag}(p, 1, \dots, 1)$, where p is a positive scalar, then condition 1 implies that A_1 is skew-symmetric and condition 2 implies that A_0 is stable. In this case, conditions 6 and 7 will be automatically satisfied. In light of these simplifications, the following synthesis procedure is suggested.

Synthesis Procedure

1. Choose $R = \text{diag}(p, 1, \dots, 1)$, $p > 0$, and set $P = cR$, $c > 0$.
2. Choose A_1 to be skew-symmetric, where the first row and column of A_1 is the zero vector.
3. Choose any stable A_0 such that $RA_0 + A_0^T R$ is negative definite .
4. Choose the vector \mathbf{c} arbitrarily and set $\mathbf{a}^0 = -2A_1 \mathbf{c}$.

With $A = A_0 + \mathbf{a}^0 \mathbf{e}_1^T$, the transmitter and receiver equations are given by (8.9) and (8.10), respectively.

The stability of the equilibrium points should also be addressed. All of the transmitter's fixed points must be unstable to ensure non-trivial motion. In the next section, linear stability analysis suggests a numerical procedure for studying the stability of the transmitter's fixed points.

8.4 Linear Stability Analysis

Linearizing the vector field of (8.9) about the fixed point \mathbf{x}_0 we obtain

$$\dot{\mathbf{x}} \approx (A + 2A_1 x_{10})\mathbf{x}_0 + J(\mathbf{x}_0)(\mathbf{x} - \mathbf{x}_0) \quad , \quad (8.11)$$

where the Jacobian matrix, $J(\mathbf{x}_0)$, is given by

$$J(\mathbf{x}_0) = A + 2A_1(x_{10}I + \mathbf{x}_0 \mathbf{e}_1^T) \quad . \quad (8.12)$$

While an analytical determination of the fixed points may not be possible, equation (8.11) provides an approach for determining them numerically, *e.g.*, by applying the Newton-Raphson iteration

$$\mathbf{x}_0^{n+1} = \mathbf{x}_0^n - J(\mathbf{x}_0)^{-1}(A + 2A_1 x_{10})\mathbf{x}_0 \quad . \quad (8.13)$$

In practice, convergence to the fixed points is usually rapid. A large number of initial conditions should be tested, however, to ensure that all of the fixed points have been found. Once found, their stability is determined from the eigenvalues of $J(\mathbf{x}_0)$. For example, the origin of (8.9) is always a fixed point and, from (8.12), we observe that the origin's stability is determined by the eigenvalues of A . This provides a simple condition on the eigenvalues of A to ensure that the origin is unstable. *The origin of the transmitter equations (8.9) is unstable if A is an unstable matrix.*

If any of the remaining fixed points are stable, we must adjust the free parameters

in the transmitter equations and observe whether chaotic motion occurs. Fortunately, there is a simple way to vary the transmitter parameters without violating any of the self-synchronization and global stability conditions. We observe that by writing $J(\mathbf{x}_0)$ in the form

$$J(\mathbf{x}_0) = A_0 + \mathbf{a}^0 \mathbf{e}_1^T + 2A_1(x_{10}I + \mathbf{x}_0 \mathbf{e}_1^T) ,$$

and fixing A_0 and A_1 , the eigenvalues of $J(\mathbf{x}_0)$ can be affected by varying \mathbf{a}^0 . Since $\mathbf{a}^0 = -2A_1 \mathbf{c}$, we can adjust \mathbf{a}^0 by varying the \mathbf{c} vector. In typical cases, we have observed numerically that by increasing the magnitude of \mathbf{c} all of the fixed points eventually become unstable. Since the trajectories are bounded, either limit cycles or chaotic motion will result. Furthermore, invariant tori are not possible because of the constant negative divergence requirement. Using specific examples, we will demonstrate this behavior numerically in the next section.

8.5 Numerical Examples

For our first example, we will utilize the synthesis procedure to obtain the Lorenz equations, simultaneously demonstrating that the Lorenz system is only one member of a general class of three-dimensional chaotic systems which possess the self-synchronization property. Subsequent examples will demonstrate the synthesis of higher dimensional chaotic systems.

8.5.1 The Lorenz System

To begin, we must choose the state space dimension N , define $R = \text{diag}(p, 1, \dots, 1)$, $p > 0$, and select an appropriate A_1 . There are exactly $(N-1)(N-2)/2$ independent free parameters in A_1 , reducing to one free parameter for a three-dimensional system.

To illustrate that the Lorenz system is consistent with the synthesis procedure,

we choose $N = 3$, $R = \text{diag}(1/\sigma, 1, 1)$, and A_1 as

$$A_1 = \begin{bmatrix} 0 & 0 & 0 \\ 0 & 0 & -1/2 \\ 0 & 1/2 & 0 \end{bmatrix} .$$

Note that A_1 is skew-symmetric and that $RA_1 = -A_1^T R$. Next, we must choose a stable matrix A_0 such that $RA_0 + A_0^T R$ is negative definite. For the Lorenz system, an appropriate choice is

$$A_0 = \begin{bmatrix} -\sigma & \sigma & 0 \\ 0 & -1 & 0 \\ 0 & 0 & -b \end{bmatrix} ,$$

where $\sigma, b > 0$. Clearly A_0 is a stable matrix, and it is straightforward to verify that $RA_0 + A_0^T R$ is negative definite. Finally, we choose the \mathbf{c} vector as

$$\mathbf{c} = r \begin{bmatrix} 0 \\ 0 \\ 1 \end{bmatrix} ,$$

which determines the center of the ellipsoidal trapping region in state space.

We now have enough information to fully specify the transmitter equations. The vector $\mathbf{a}^0 = -2A_1\mathbf{c}$ is given by

$$\mathbf{a}^0 = \begin{bmatrix} 0 \\ r \\ 0 \end{bmatrix} .$$

The linear coefficient matrix $A = A_0 + \mathbf{a}^0 \mathbf{e}_1^T$ is given by

$$A = \begin{bmatrix} -\sigma & \sigma & 0 \\ r & -1 & 0 \\ 0 & 0 & -b \end{bmatrix} .$$

The transmitter equations are then written as a set of first-order differential equations

$$\begin{aligned} \dot{x}_1 &= \sigma(x_2 - x_1) \\ \dot{x}_2 &= rx_1 - x_2 - x_1x_3 \\ \dot{x}_3 &= x_1x_2 - bx_3 , \end{aligned}$$

which is, of course, the well-known Lorenz system. Choosing different parameters in the synthesis procedure leads to other three-dimensional, non-Lorenz systems. In our next example, we focus on synthesizing a four-dimensional chaotic system.

8.5.2 A Four-Dimensional Synchronizing Chaotic System

In four dimensions, the matrix A_1 contains three free parameters. These parameters may be chosen arbitrarily; suppose that we choose A_1 as

$$A_1 = \begin{bmatrix} 0 & 0 & 0 & 0 \\ 0 & 0 & -1/2 & -1/2 \\ 0 & 1/2 & 0 & 1/2 \\ 0 & 1/2 & -1/2 & 0 \end{bmatrix} .$$

To be consistent with the Lorenz example, A_0 is chosen as

$$A_0 = \begin{bmatrix} -16 & 16 & 0 & 0 \\ 0 & -1 & 0 & 0 \\ 0 & 0 & -4 & 0 \\ 0 & 0 & 0 & -1 \end{bmatrix} .$$

These choices satisfy the synthesis conditions for $R = \text{diag}(1/16, 1, 1, 1)$. Finally, the vector \mathbf{c} is chosen as

$$\mathbf{c} = r \begin{bmatrix} 0 \\ 0 \\ .25 \\ 1 \end{bmatrix},$$

where r is treated as a bifurcation parameter. The vector $\mathbf{a}^0 = -2A_1\mathbf{c}$ is given by

$$\mathbf{a}^0 = r \begin{bmatrix} 0 \\ 1.25 \\ -1 \\ .25 \end{bmatrix},$$

and the linear coefficient matrix $A = A_0 + \mathbf{a}^0\mathbf{e}_1^T$ is given by

$$A = \begin{bmatrix} -\sigma & \sigma & 0 & 0 \\ 1.25r & -1 & 0 & 0 \\ -r & 0 & -b & 0 \\ .25r & 0 & 0 & -1 \end{bmatrix}.$$

The transmitter equations are then written as a set of first-order differential equations

$$\begin{aligned} \dot{x}_1 &= 16(x_2 - x_1) \\ \dot{x}_2 &= 1.25rx_1 - x_2 - x_1x_3 - x_1x_4 \\ \dot{x}_3 &= -rx_1 - 4x_3 + x_1x_2 + x_1x_4 \\ \dot{x}_4 &= .25rx_1 - x_4 + x_1x_2 - x_1x_3. \end{aligned}$$

The nonlinear dynamical behavior of this system is demonstrated in the numerical experiments below.

In figure 8-2, we show the computed Lyapunov exponents for this system as r is

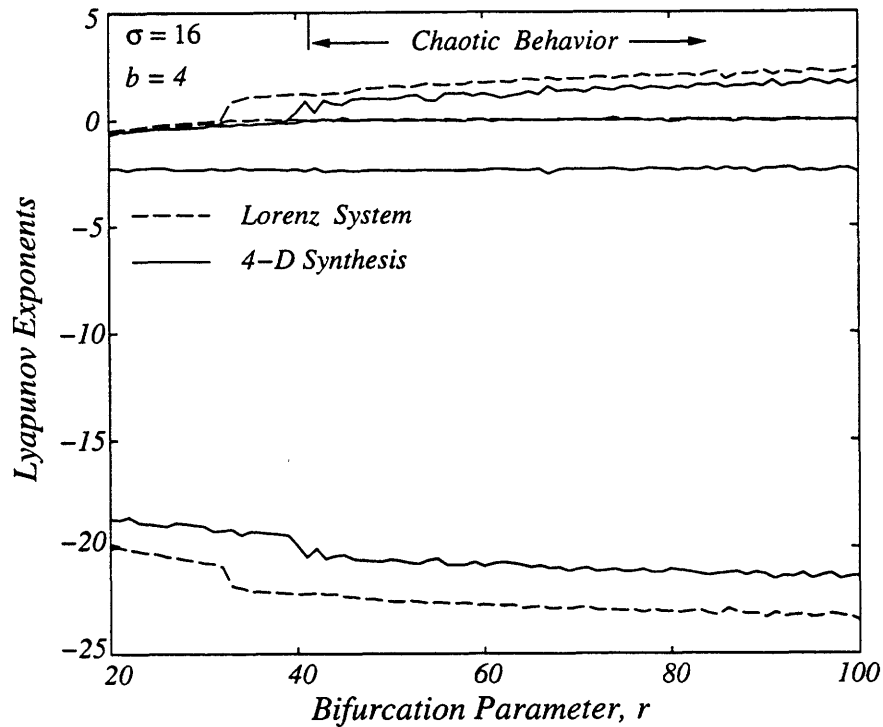


Figure 8-2: *Lyapunov Exponents for a 4-Dimensional Chaotic System.*

varied over the range $20 < r < 100$. The onset of chaotic behavior occurs near $r = 42$, as evidenced by the existence of a positive Lyapunov exponent. Also, two negative exponents are apparent as well as the zero exponent. For comparison purposes, the computed Lyapunov exponents for the Lorenz system are also shown (dashed lines).

In figure 8-3, we show the computed Lyapunov dimension as r is varied over the same range. Note that the Lyapunov dimension increases significantly as r increases. This is in contrast to the Lorenz system, where the attractor dimension is approximately constant at a value near 2.06.

In figure 8-4, we show various projections of the chaotic attractor corresponding to $r = 60$. The (x_1, x_2) projection is similar to the Lorenz attractor as is the (x_1, x_3) projection except, in the latter, one of the “wings” is twisted. The remaining projections illustrate the complicated topology of the chaotic attractor.

The self-synchronizing receiver equations are given by

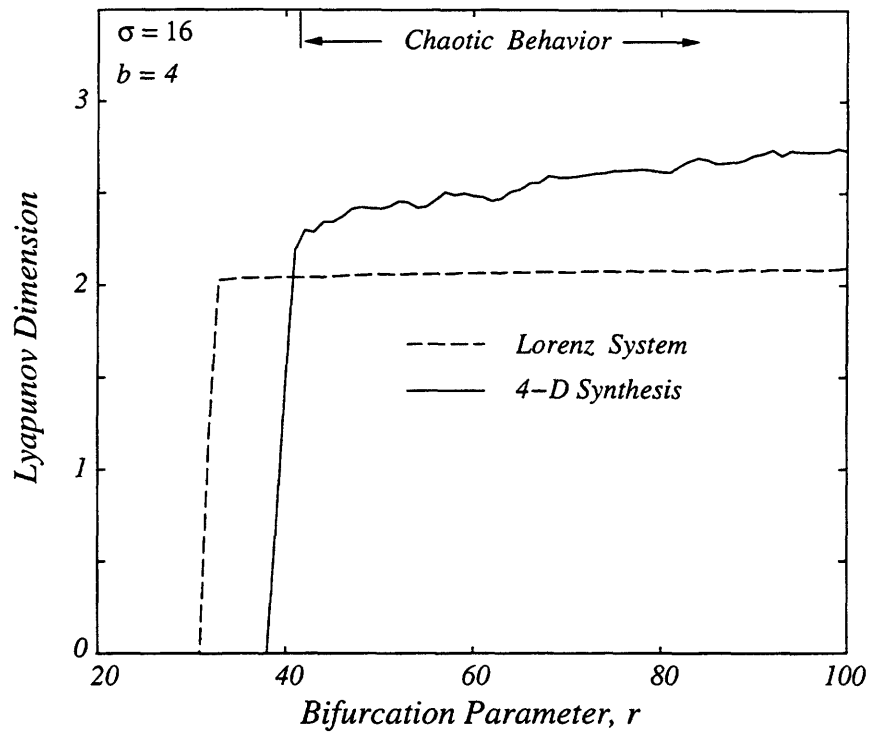


Figure 8-3: *Lyapunov Dimension for a 4-Dimensional Chaotic System.*

$$\begin{aligned} \dot{x}_{1r} &= 16(x_{2r} - x_{1r}) \\ \dot{x}_{2r} &= 1.25rx_1(t) - x_{2r} - x_1(t)x_{3r} - x_1(t)x_{4r} \\ \dot{x}_{3r} &= -rx_1(t) - 4x_{3r} + x_1(t)x_{2r} + x_1(t)x_{4r} \\ \dot{x}_{4r} &= .25rx_1(t) - x_{4r} + x_1(t)x_{2r} - x_1(t)x_{3r} . \end{aligned}$$

In figure 8-5, we illustrate the rapid synchronization between the transmitter and receiver systems. Synchronization is maintained indefinitely, as expected.

8.5.3 A Five-Dimensional Synchronizing Chaotic System

To further emphasize the simplicity and generality of the synthesis procedure, we demonstrate the design of a 5-dimensional chaotic system by starting with the matrix

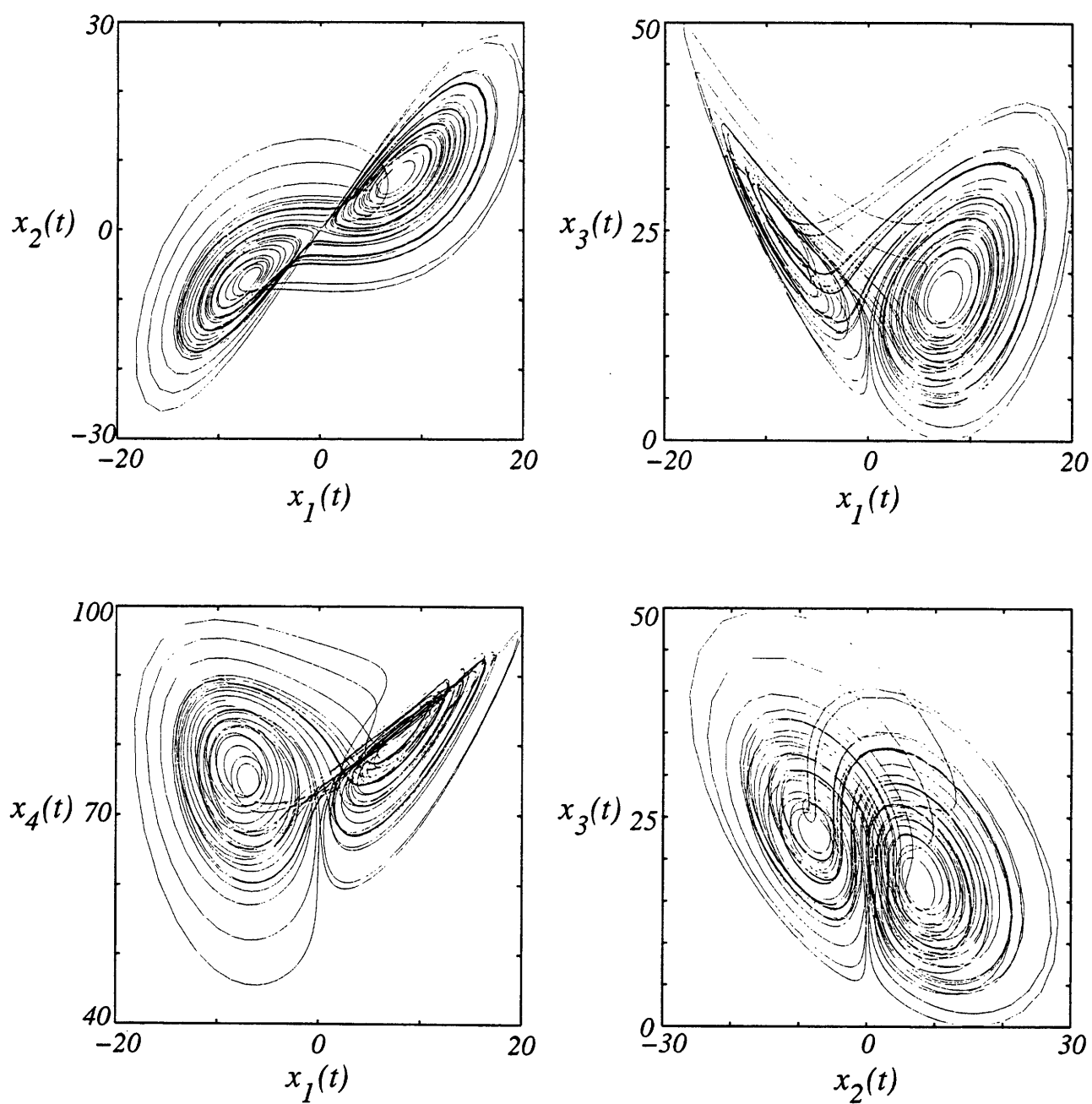


Figure 8-4: *Chaotic Attractor Projections for a 4-Dimensional Chaotic System ($r = 60$).*

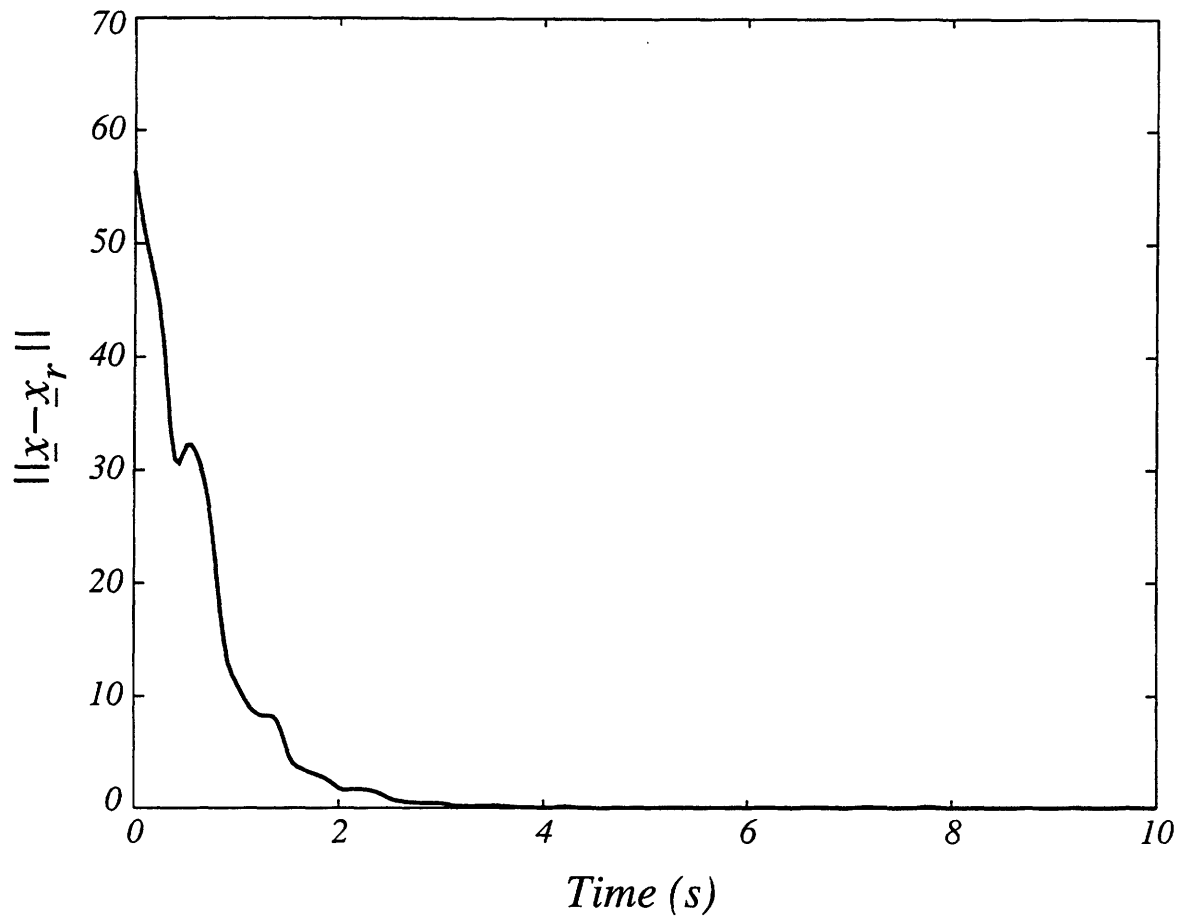


Figure 8-5: *Self-Synchronization in a 4-Dimensional Chaotic System.*

A_1 given by

$$A_1 = \begin{bmatrix} 0 & 0 & 0 & 0 & 0 \\ 0 & 0 & -.56 & -.91 & .36 \\ 0 & .56 & 0 & .36 & .87 \\ 0 & .91 & -.36 & 0 & -.23 \\ 0 & -.36 & -.87 & .23 & 0 \end{bmatrix} .$$

In this case, the six free parameters of A_1 were selected at random from the normal distribution $N(0, 1)$. Next, we choose the stable matrix A_0 as

$$A_0 = \begin{bmatrix} -16 & 16 & 3.66 & 0 & 0 \\ 0 & -1 & .06 & -.80 & 0 \\ 0 & 0 & -4 & -1.07 & 1.55 \\ 0 & 0 & 0 & -1 & .38 \\ 0 & 0 & 0 & 0 & -1 \end{bmatrix} .$$

Note that randomly selected elements have been placed above the main diagonal of A_0 . It is straightforward to verify that these choices satisfy the synthesis conditions for $R = \text{diag}(1/16, 1, 1, 1, 1)$. Finally, we choose the \mathbf{c} vector as

$$\mathbf{c} = r \begin{bmatrix} 0 \\ 0 \\ .04 \\ .58 \\ -.82 \end{bmatrix} ,$$

where r is treated as a bifurcation parameter. The vector $\mathbf{a}^0 = -2A_1\mathbf{c}$ is given by

$$\mathbf{a}^0 = r \begin{bmatrix} 0 \\ 1.68 \\ 1.00 \\ -.35 \\ -.20 \end{bmatrix} ,$$

and the linear coefficient matrix $A = A_0 + \mathbf{a}^0 \mathbf{e}_1^T$ is given by

$$A = \begin{bmatrix} -16 & 16 & 3.66 & 0 & 0 \\ 1.68r & -1 & .06 & -.08 & 0 \\ 1.00r & 0 & -4 & -1.07 & 1.55 \\ -.35r & 0 & 0 & -1 & .38 \\ -.20r & 0 & 0 & 0 & -1 \end{bmatrix} .$$

The transmitter equations are fully determined, and are of the form $\dot{\mathbf{x}} = (A + 2A_1 x_1)\mathbf{x}$.

As an illustration of the nonlinear dynamical behavior exhibited by the transmitter equations, we show in figure 8-6 the computed Lyapunov exponents as r is varied over the range $20 < r < 100$. Several notable features of figure 8-6 are listed below.

- As r increases, all of the fixed points eventually lose stability and the motion is confined to stable limit cycles.
- The limit cycles lose stability near $r = 70$ and a chaotic attractor appears, as evidenced by the existence of a positive Lyapunov exponent.
- Three negative exponents are evident in the chaotic region.

In figure 8-7, we show the Lyapunov dimension as r is varied over the same range. This figure clearly shows the presence of the limit cycle region ($D_L = 1$). After a sequence of bifurcations takes place, the Lyapunov dimension increases sharply as r enters the chaotic region.

In figure 8-8, we show various projections of the chaotic attractor corresponding to $r = 90$. These projections clearly illustrate the extremely complicated topology of the chaotic attractor.

In figure 8-9, we demonstrate that synchronization takes place between the transmitter and receiver systems. Synchronization is rapid and is maintained indefinitely.

It should be emphasized that it is also straightforward to synthesize significantly higher dimensional systems. The relatively low-order designs were chosen to illustrate the synthesis approach, rather than to suggest limitations.

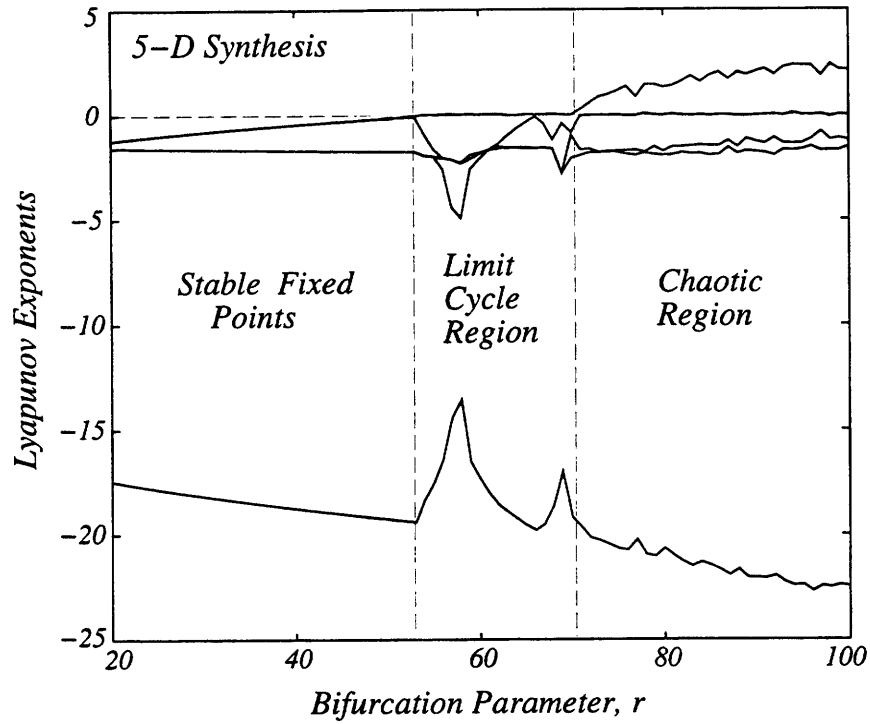


Figure 8-6: Lyapunov Exponents for a 5-Dimensional Chaotic System.

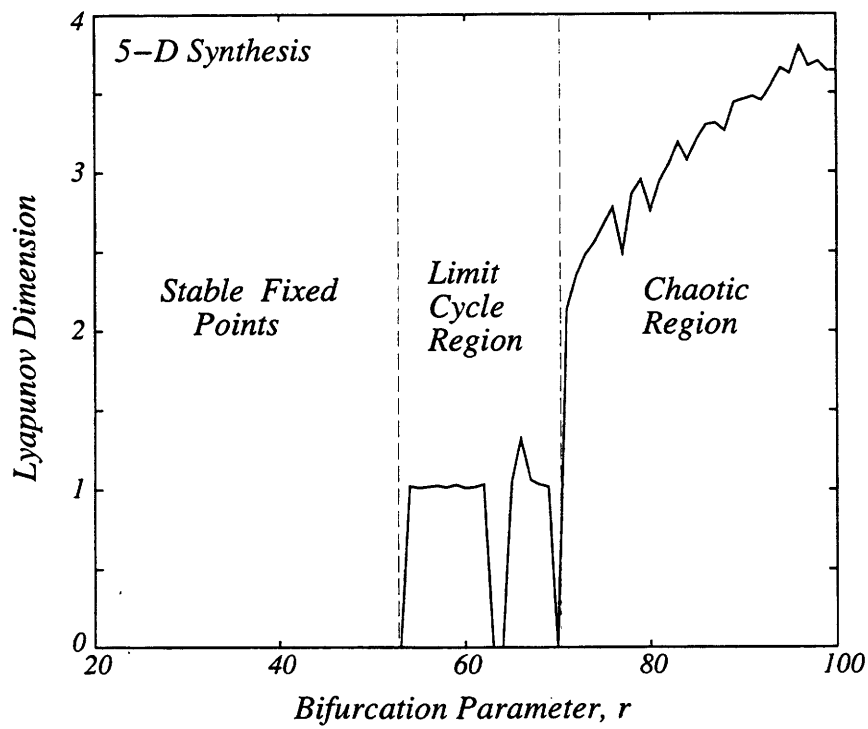


Figure 8-7: Lyapunov Dimension for a 5-Dimensional Chaotic System.

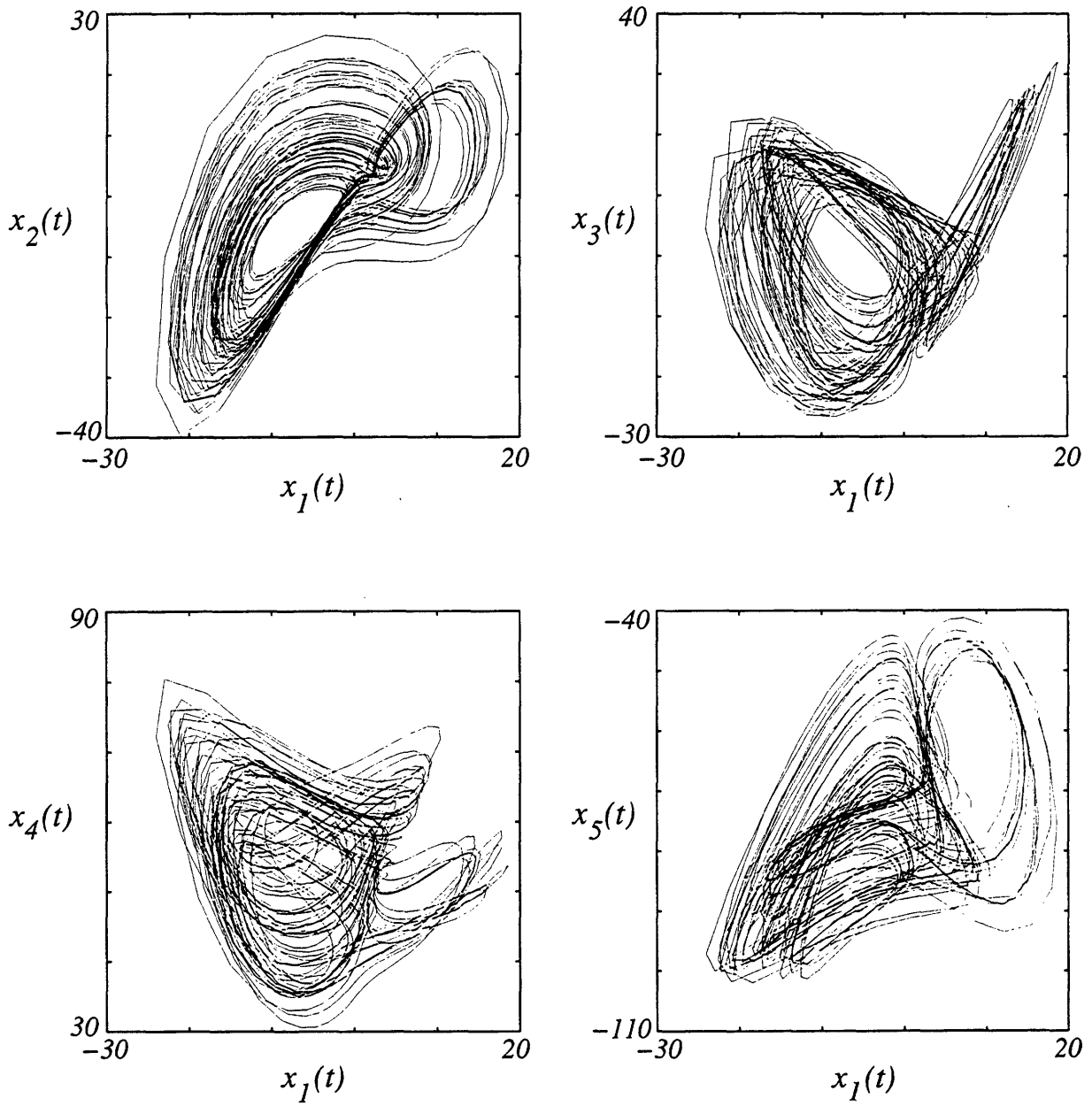


Figure 8-8: *Chaotic Attractor Projections for a 5-Dimensional Chaotic System ($r = 90$).*

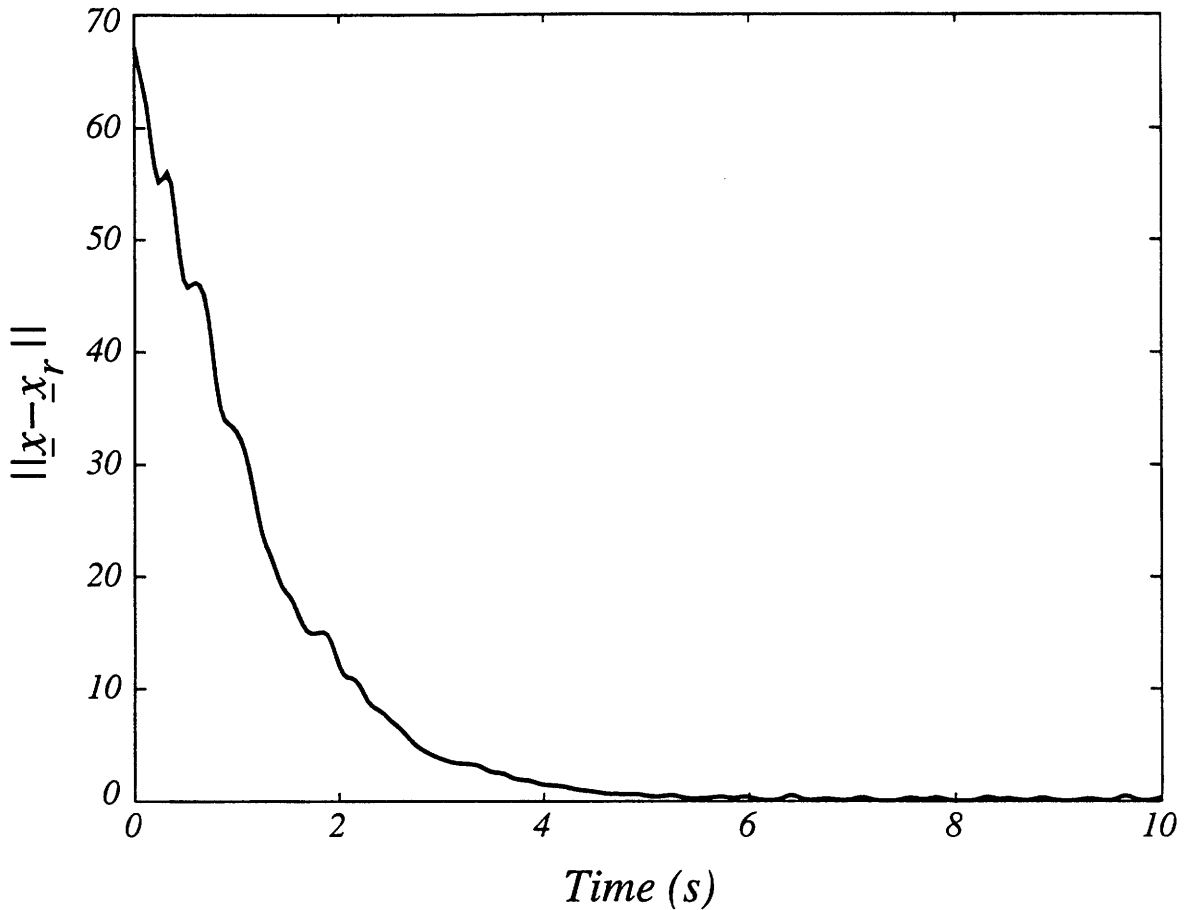


Figure 8-9: *Self-Synchronization in a 5-Dimensional Chaotic System.*

8.6 Summary

In this chapter, a methodology was developed for synthesizing a general class of chaotic systems that possess the self-synchronization property. Some insights gained from this work are listed below.

- The transmitter equations for chaotic systems of this class have the canonical form representation $\dot{\mathbf{x}} = (A + 2A_1x_1)\mathbf{x}$, while the self-synchronizing receiver equations have the representation $\dot{\mathbf{x}}_r = (A_0 + 2A_1x_1)\mathbf{x}_r + \mathbf{a}^0x_1$. For any appropriate choice of A_0 , A_1 , and \mathbf{a}^0 , as specified by the synthesis procedure (Section 8.3), the transmitter equations are dissipative and globally stable, and the receiver system will possess the global self-synchronization property. We showed that the Lorenz system is a member of this more general class of nonlinear

systems.

- While the chaotic behavior exhibited by this class of systems can be very complex, only a single positive Lyapunov exponent has been observed. An interesting future experiment would be to explore the possibility of utilizing the synthesis procedure to obtain a set of transmitter equations which exhibit multiple positive Lyapunov exponents. If this is possible, then it follows that hyperchaotic self-synchronization can be achieved when the receiver is driven by only one transmitter component.
- LFBCSs (Chapter 6) form a subset of the class of chaotic systems considered in this chapter. They can be obtained from the synthesis procedure (Section 8.3) by appropriate choices of A_0 , A_1 , and c .
- Chaotic arrays (Chapter 7), which contain multiple Lorenz oscillators, do not form a subset of the class of chaotic systems considered in this chapter. This follows from the observation that the cross product terms in a chaotic array do not correspond to a single drive variable.

The various synthesis techniques developed in Chapters 6-8 have demonstrated that Lyapunov's direct method provides a general mathematical framework for synthesizing dissipative chaotic systems which possess the self-synchronization property. The flexibility afforded by the various synthesis techniques increases the applicability of synchronized chaotic systems for communications and signal processing.

Having investigated the synthesis problem in some detail, we now turn our attention to the important practical issues associated with implementing a self-synchronizing chaotic system for use in communication applications. In Chapter 9, we discuss the design and implementation of transmitter and receiver circuits that have dynamics governed by the Lorenz system. The Lorenz system is chosen for simplicity; it represents a low-dimensional chaotic system from the general class $\dot{\mathbf{x}} = (A + 2A_1x_1)\mathbf{x}$. We also develop and demonstrate two potential approaches to private communications using the Lorenz-based chaotic circuits.

Chapter 9

Applications of Self-Synchronizing Chaotic Systems

In Chapters 4 and 5, we showed that synchronization in the Lorenz system is robust to wideband perturbation of the drive signal. Chapter 5 also showed that, theoretically, a low-level speech signal could be added to the synchronizing drive signal and accurately recovered at the receiver. These results were based on an analysis of the *exact* Lorenz transmitter and receiver equations.

It is also important to show that a system which exploits the robustness and signal recovery properties can be implemented in practice. When implementing synchronized chaotic systems in hardware, the limitations of available circuit components result in *approximations* of the defining equations. The resulting system performance needs to be re-evaluated to assess any hardware-induced effects or limitations and to ensure that the system is performing within the desired specifications. The purpose of this chapter is to address these applied aspects of synchronized chaotic systems.

In Section 9.1, we implement the Lorenz transmitter and receiver equations with analog circuits. The resulting system performance is assessed. In Section 9.2, we exploit the signal recovery property of the Lorenz system for private communications. Specifically, the Lorenz circuits are used to demonstrate that an actual speech waveform can be privately communicated and recovered with the self-synchronizing receiver circuit. In Section 9.3, we develop an alternative communication approach in-

volving the ability to privately communicate and recover signals that are represented by binary-valued bit streams. The chapter is summarized in Section 9.4.

9.1 Lorenz-Based Circuit Implementations

9.1.1 The Transmitter Circuit

It is well-known that the state variables of the Lorenz system vary widely in amplitude, with values that exceed reasonable power supply limits. To eliminate this problem, we define a transformation of variables as $u = x/10$, $v = y/10$, and $w = z/20$. With this scaling, the Lorenz equations are transformed to

$$\begin{aligned}\dot{u} &= \sigma(v - u) \\ \dot{v} &= ru - v - 20uw \\ \dot{w} &= 5uv - bw \ .\end{aligned}\tag{9.1}$$

This system, which we refer to as the circuit equations, can be readily implemented with an analog circuit; the state variables all have similar dynamic range and circuit voltages remain well within the range of typical power supply limits.

In our notation for the circuit equations, we have established the convention that \dot{u} , \dot{v} , and \dot{w} denote $du/d\tau$, $dv/d\tau$, and $dw/d\tau$ respectively where $\tau = t/T$ is normalized time and T is a time scale factor. This convention provides the flexibility for adjusting the time scale of the signals. It is also convenient to define the normalized frequency $\omega = \Omega T$, where Ω denotes the angular frequency in units of rad/s.

An analog circuit implementation of (9.1) is shown in figure 9-1. The operational amplifiers (1-8) and associated circuitry perform the operations of addition, subtraction, and integration. Analog multipliers implement the nonlinear terms in the circuit equations. A set of state equations which govern the dynamical behavior of the circuit

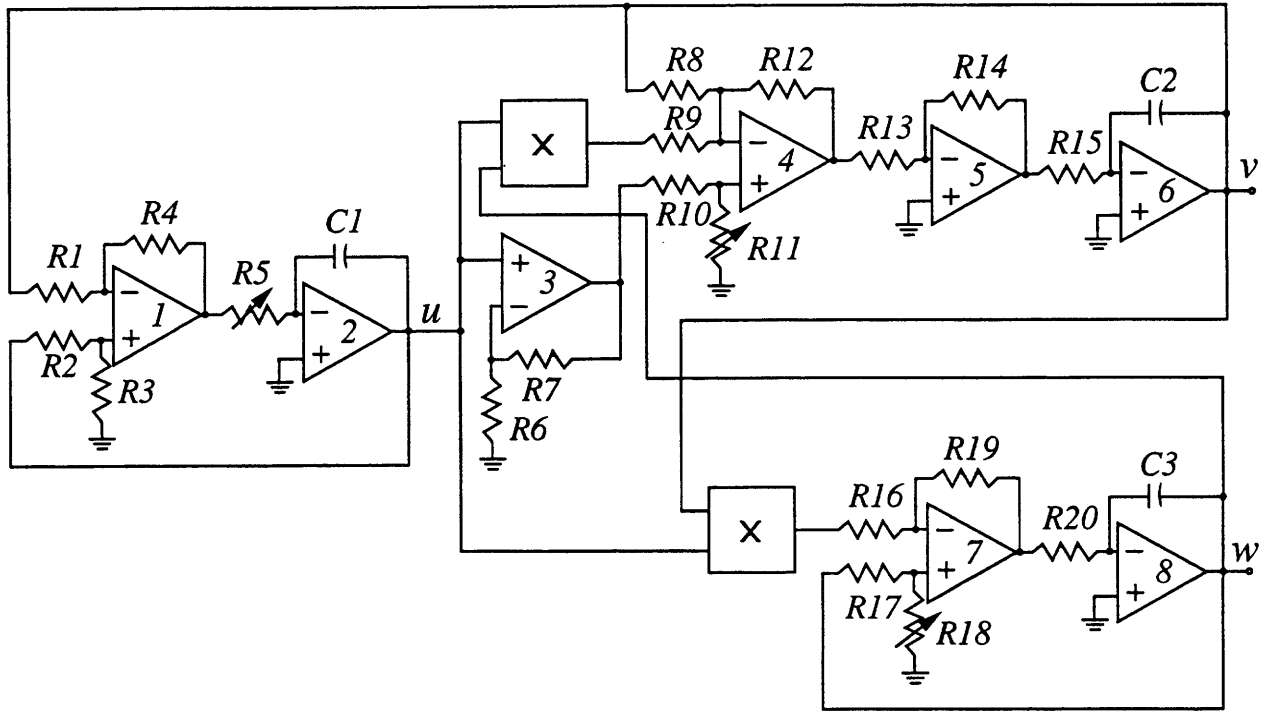


Figure 9-1: Lorenz-Based Chaotic Circuit.

is given by

$$\begin{aligned}
 \frac{du}{dt} &= \frac{1}{R_5 C_1} \left[\frac{R_4}{R_1} v - \frac{R_3}{R_2 + R_3} \left(1 + \frac{R_4}{R_1} \right) u \right] \\
 \frac{dv}{dt} &= \frac{1}{R_{15} C_2} \left[\frac{R_{11}}{R_{10} + R_{11}} \left(1 + \frac{R_{12}}{R_8} + \frac{R_{12}}{R_9} \right) \left(1 + \frac{R_7}{R_6} \right) u - \frac{R_{12}}{R_8} v - \frac{R_{12}}{R_9} uv \right] \\
 \frac{dw}{dt} &= \frac{1}{R_{20} C_3} \left[\frac{R_{19}}{R_{16}} uv - \frac{R_{18}}{R_{17} + R_{18}} \left(1 + \frac{R_{19}}{R_{16}} \right) w \right] .
 \end{aligned} \tag{9.2}$$

The circuit time scale can be adjusted by changing the values of the three capacitors, C_1 , C_2 , and C_3 , by a common factor. If a factor of B increase in signal bandwidth is desired, then it can be achieved by dividing the three capacitor values by the same factor. In addition, the parameters σ , r , and b can be independently varied by adjusting the corresponding resistors R_5 , R_{11} , and R_{18} . For the component values we have chosen (Appendix B), equation (9.2) closely approximates equation (9.1) after rescaling time by a factor of $T = 400 \mu\text{sec}$. The resulting parameters are $\sigma = 16$, $r = 45.6$, and $b = 4$.

To illustrate the chaotic behavior of the transmitter circuit, an analog-to-digital (A/D) data recording system is used to sample the appropriate circuit outputs at a

48 kHz rate and with 16-bit resolution. In figure 9-2(a) and (b), we show a sample function and averaged power spectrum for the circuit waveform $u(t)$. Similarly, figure 9-2(c) and (d) show a sample function of $v(t)$ and its averaged power spectrum. The power spectra are broadband, which is typical of chaotic signals. Figures 9-2(b) and (d) also show the corresponding power spectra from a numerical simulation of the Lorenz equations. As we see, the performance of the circuit and the simulation are consistent.

In figure 9-3(a) and (b), we show the circuit's chaotic attractor projected onto the uv -plane and uw -plane, respectively. This data is obtained from the circuit using the stereo recording capability of the A/D system to simultaneously sample the x -axis and y -axis signals at a 48 kHz rate and with 16-bit resolution. The circuit's chaotic attractor is consistent with numerical simulations.

In figure 9-4(a), we show the autocorrelation functions $R_{uu}(\tau)$ and $R_{vv}(\tau)$ corresponding to the circuit waveforms $u(t)$ and $v(t)$, respectively. The autocorrelation functions are sharply peaked, as expected, by the broadband nature of the chaotic waveforms. The low-level oscillations in $R_{uu}(\tau)$ and $R_{vv}(\tau)$ reflect the oscillatory behavior of trajectories on the Lorenz attractor. On average, it takes approximately .15 msec for a typical trajectory to make a full rotation around one of the wings of the circuit's chaotic attractor. This average time period is consistent with the time period of the oscillations in $R_{uu}(\tau)$ and $R_{vv}(\tau)$. In figure 9-4(b) and (c), we show histograms for the waveforms $u(t)$ and $v(t)$, respectively. Under certain ergodicity assumptions, the histograms can be interpreted as probability densities. In this context, the densities represent the steady-state probabilistic behavior of the circuit waveforms. The densities appear to be unimodal and approximately Gaussian, as indicated by the dashed curve overlays.

In figure 9-5, we show a *Poincaré section* of the chaotic flow (generated from the circuit data). The Poincaré section is defined by $w = (r - 1)/20$ and corresponds to a plane which is oriented with its normal parallel to the w -axis. The curves identify the points of intersection of the Poincaré section with the flow on the chaotic attractor.

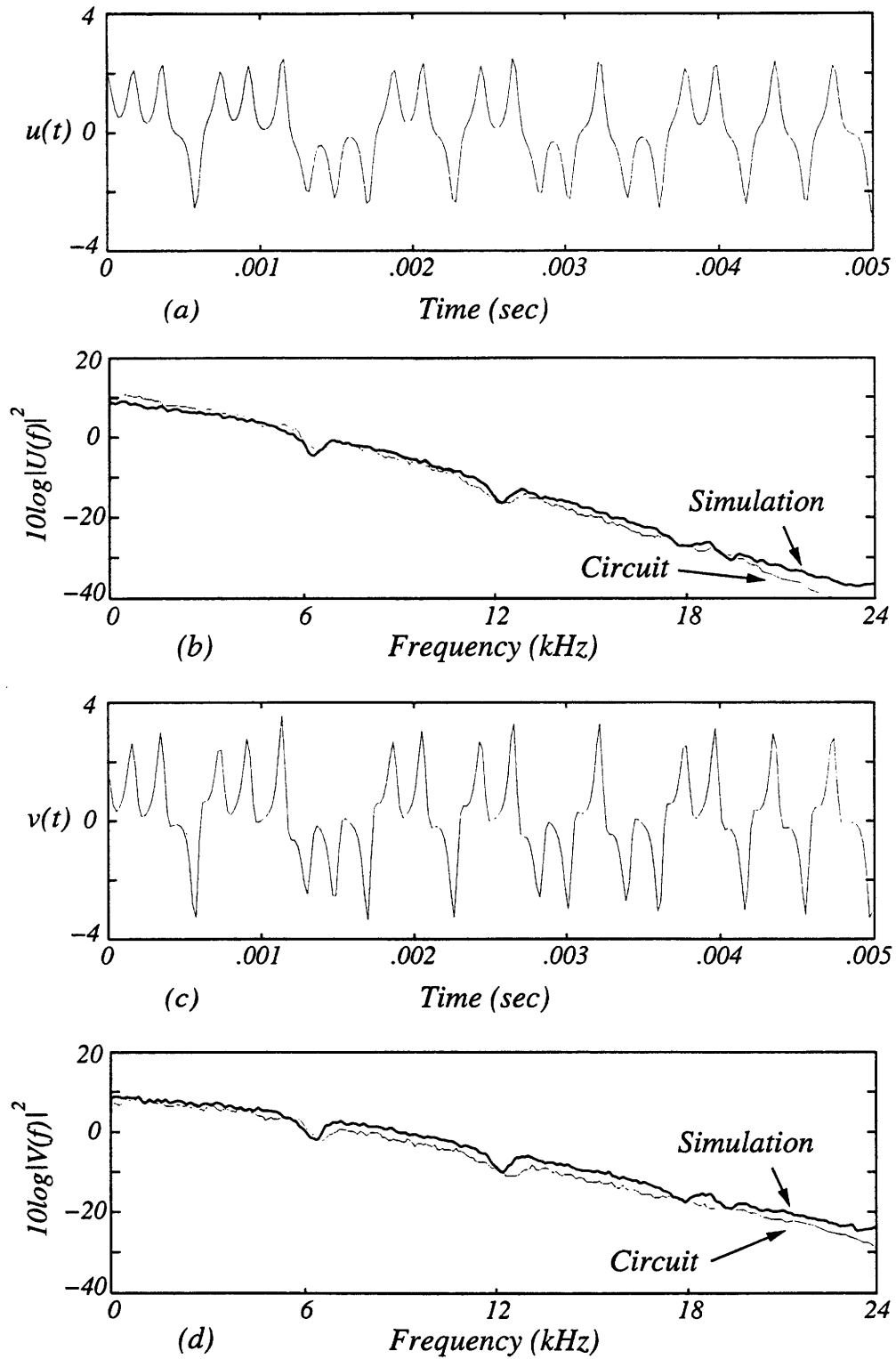


Figure 9-2: *Circuit Data: (a) A sample function of $u(t)$. (b) Averaged power spectrum of $u(t)$. (c) A sample function of $v(t)$. (d) Averaged power spectrum of $v(t)$.*

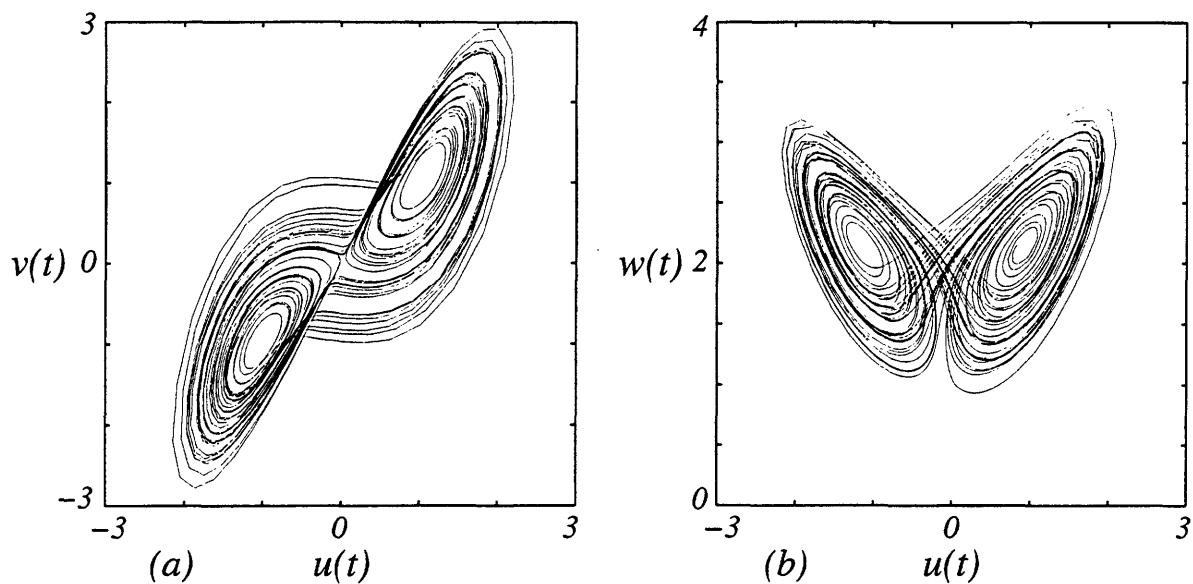


Figure 9-3: *Circuit Data: (a) Chaotic attractor projected onto uv -plane. (b) Chaotic attractor projected onto uw -plane.*

The shape and orientation of the curves imply that the flow is not on a planar surface. This is to be expected since the Lorenz attractor is not a simple geometric object.

As a further demonstration of the transmitter circuit, consider the *first return map* shown in figure 9-6. Because of the highly dissipative nature of the Lorenz system, the dynamics can be described by a one-dimensional map of the form $W_{k+1} = f(W_k)$. This mapping maintains the essential properties of the chaotic flow and is defined by graphing the successive maxima of $w(t)$. Since the slope of the curve $W_{k+1} = f(W_k)$ is always greater than unity in magnitude, chaotic behavior will result for any initial value W_0 .

These circuit experiments illustrate that the performance of the transmitter circuit is consistent with numerical simulations of the Lorenz equations. The hardware-induced effects appear to be minimal. In the next section, the Lorenz receiver equations are implemented with a similar analog circuit.

9.1.2 The Receiver Circuit

The receiver circuit equations are obtained from (9.1) by renaming variables from (u, v, w) to (u_r, v_r, w_r) and then substituting $u(t)$ for $u_r(t)$ in the second and third

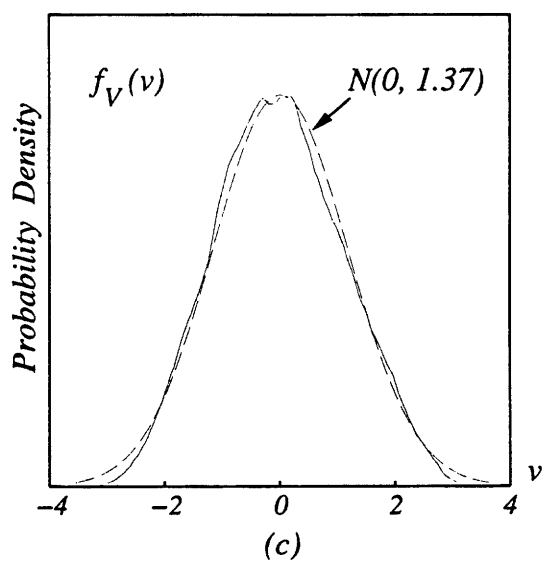
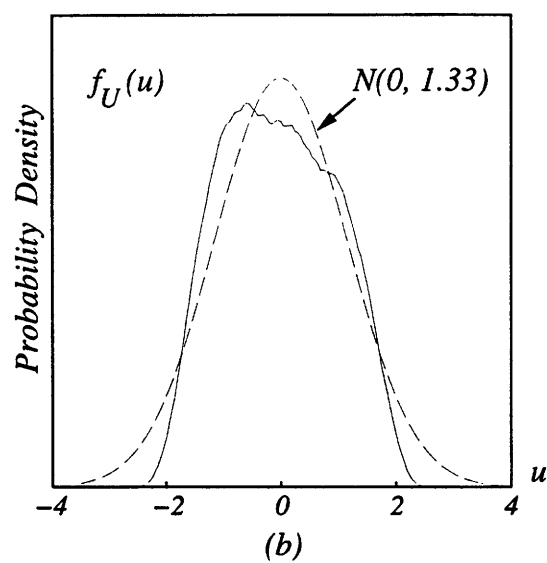
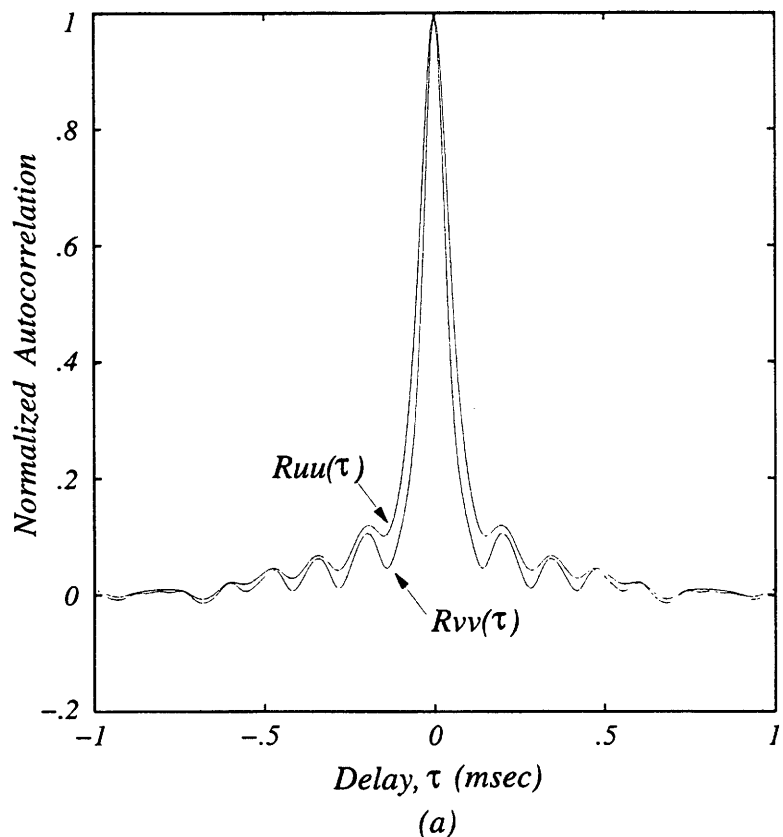


Figure 9-4: Circuit Data: (a) Autocorrelation functions $R_{uu}(\tau)$ and $R_{vv}(\tau)$. (b) Probability density of $u(t)$. (c) Probability density of $v(t)$.

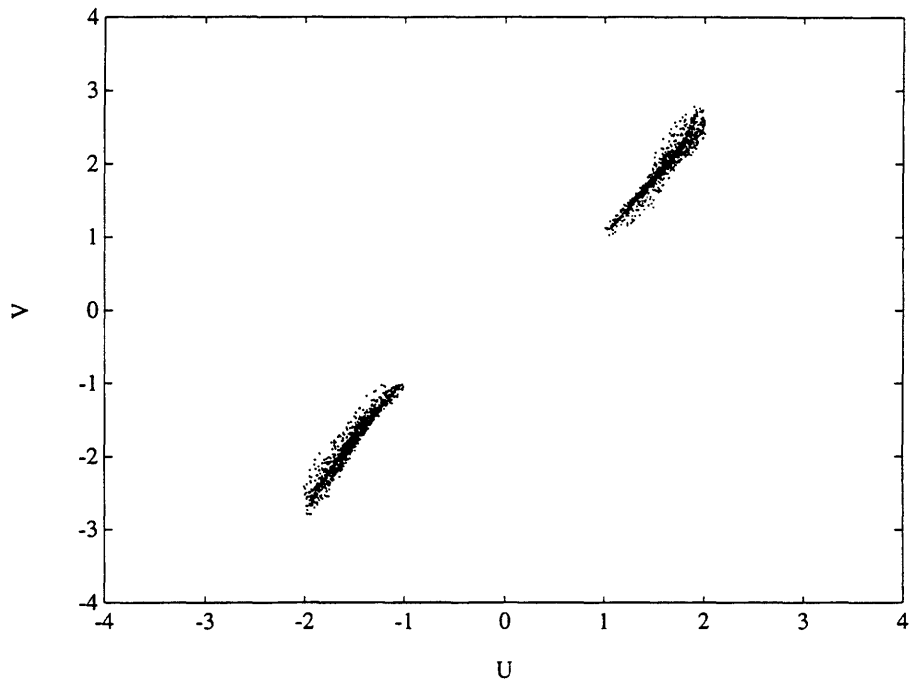


Figure 9-5: *Circuit Data: Poincaré section.*

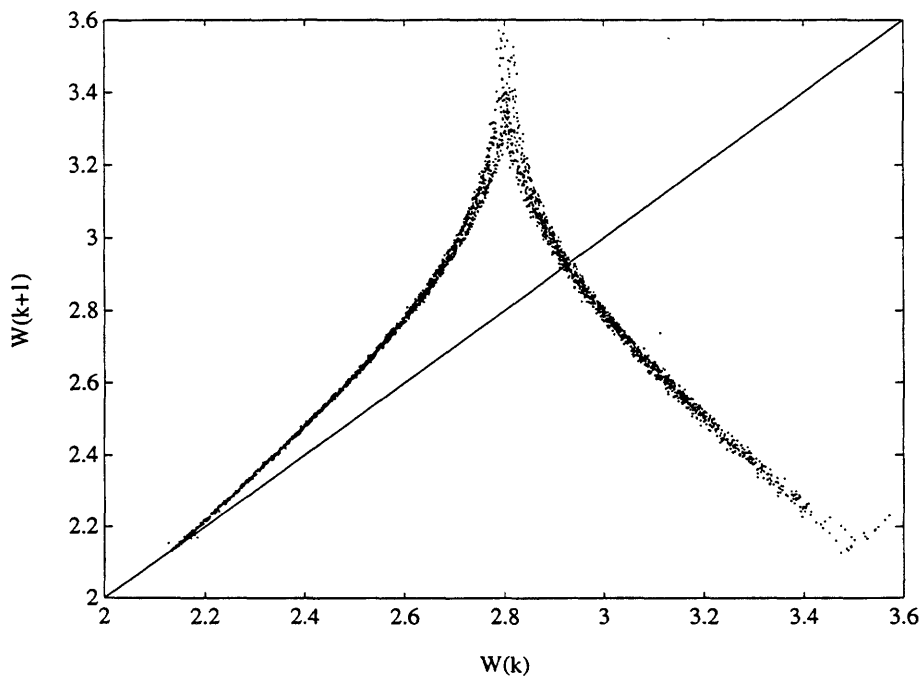


Figure 9-6: *Circuit Data: First return map.*

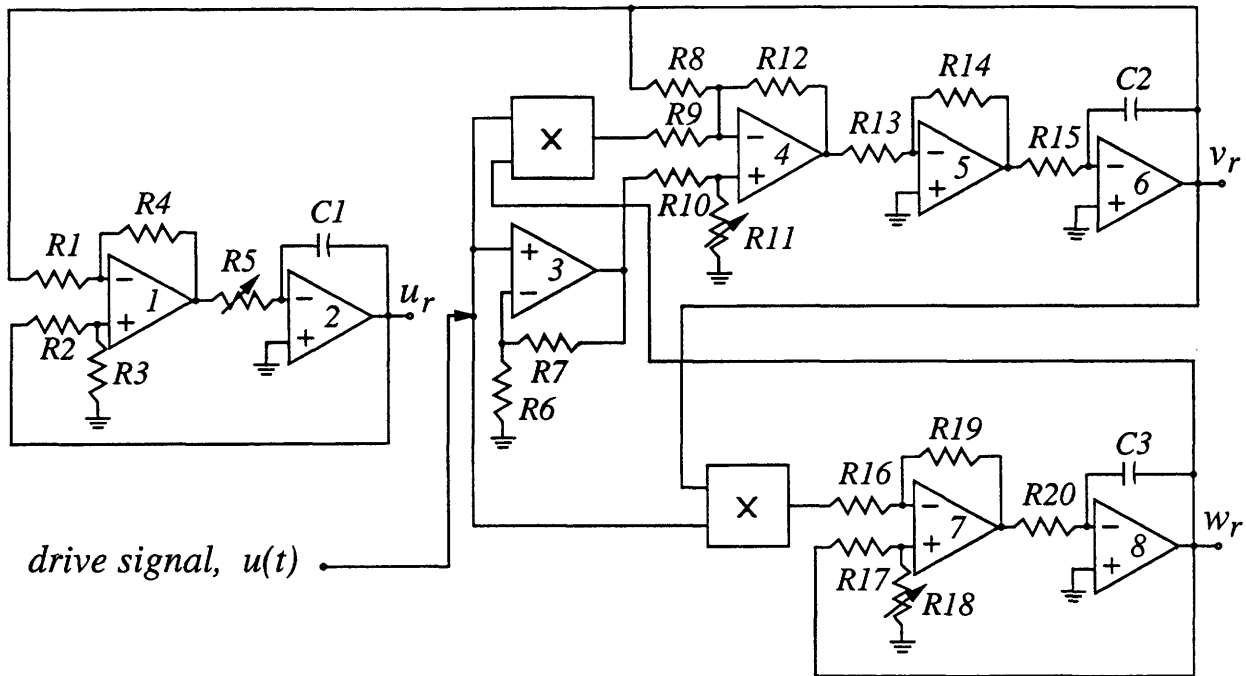


Figure 9-7: Self-Synchronizing Receiver Circuit.

equations. The resulting receiver system is given by

$$\begin{aligned}
 \dot{u}_r &= \sigma(v_r - u_r) \\
 \dot{v}_r &= ru(t) - v_r - 20u(t)w_r \\
 \dot{w}_r &= 5u(t)v_r - bw_r .
 \end{aligned}
 \tag{9.3}$$

The transmitter and receiver circuit equations will synchronize regardless of the initial conditions, provided that $\sigma, b > 0$ (see [31, 32] for an analytical proof).

An analog circuit implementation of the receiver equations (9.3) is shown in figure 9-7. Comparing the receiver circuit with the transmitter circuit (figure 9-1) shows that they are virtually identical. The only difference is that the drive signal $u(t)$ replaces the receiver signal $u_r(t)$ at a key point in the circuit. The practical advantage of this similarity is that the transmitter and receiver circuits are duplicates, which helps them achieve perfect synchronization.

To illustrate the synchronization performance of the receiver circuit, the appropriate transmitter and receiver signals were simultaneously recorded using the stereo recording capability of the A/D system. In figure 9-8(a), a plot of the actual circuit

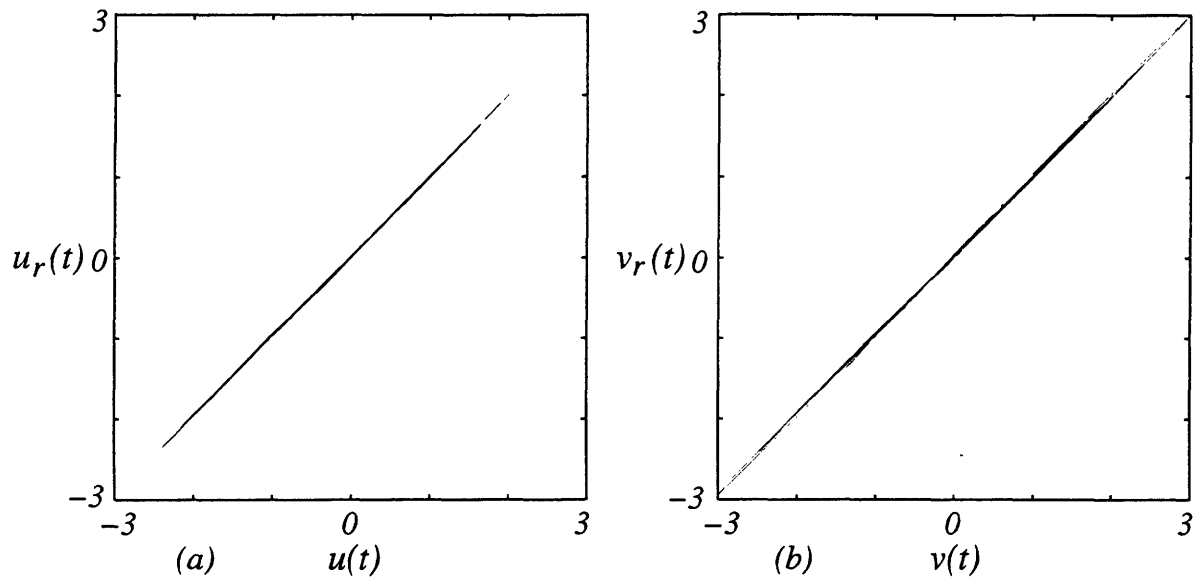


Figure 9-8: *Circuit Data: Synchronization of transmitter and receiver signals.*

outputs $u(t)$ vs. $u_r(t)$ is shown. Figure 9-8(b) shows a similar plot for the circuit outputs $v(t)$ and $v_r(t)$. The 45-degree lines indicate that nearly perfect synchronization is achieved and maintained between the transmitter and receiver. The circuit outputs shown in figure 9-8 reflect a time span of several minutes, indicating considerable stability of the synchronization.

The ability to accurately implement the Lorenz transmitter and receiver equations with simple analog circuits demonstrates the practicality of the Lorenz system. We next address the possibility of utilizing these circuits for practical applications.

9.2 Chaotic Signal Masking and Recovery

In Chapter 5, it was shown that a low-level speech signal could be added to the synchronizing drive signal and accurately recovered at the receiver by subtracting the receiver's regenerated drive signal from the received signal. In the context of private communications, we refer to this concept as *chaotic signal masking and recovery* [9, 10, 30, 31, 32, 33, 34, 45]. This section discusses and demonstrates this concept using the Lorenz circuits.

In Section 9.2.1, we discuss chaotic signal masking and recovery in the context

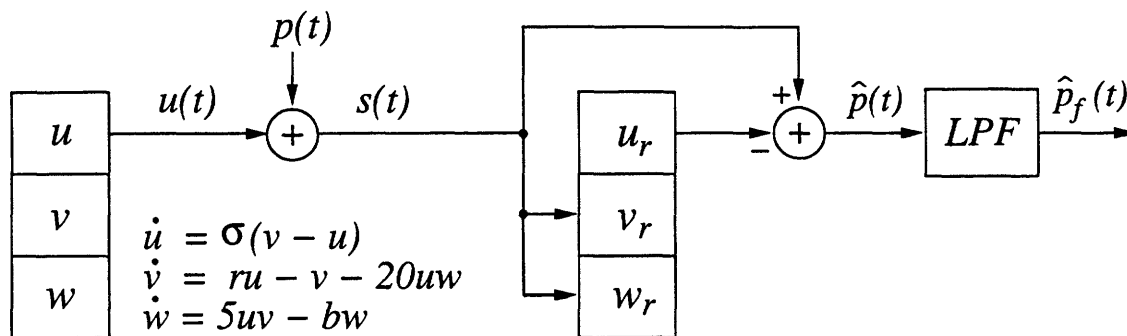


Figure 9-9: *Chaotic Signal Masking and Recovery System.*

of private communications. In Section 9.2.2, we demonstrate this concept using the Lorenz circuits and evaluate the circuit's performance. In Section 9.2.3, we propose the use of an extended Kalman filter for improving the quality of the recovered message.

9.2.1 Concept

In figure 9-9, we illustrate a communication system that is based on chaotic signal masking and recovery. In this figure, a chaotic masking signal $u(t)$ is added to the information-bearing signal $p(t)$ at the transmitter, and at the receiver the masking is removed. For transmission privacy, we assume that, for all frequencies, the spectral density of $p(t)$ is significantly less than the spectral density of $u(t)$. The basic idea is to use the received signal,

$$s(t) = u(t) + p(t) ,$$

at the receiver to recover $p(t)$.

By subtracting the regenerated drive signal $u_r(t)$ from the received signal $s(t)$, the recovered message is

$$\hat{p}(t) = s(t) - u_r(t) = p(t) + [u(t) - u_r(t)] .$$

In this context, $e_u(t)$, the error between $u(t)$ and $u_r(t)$, corresponds directly to the

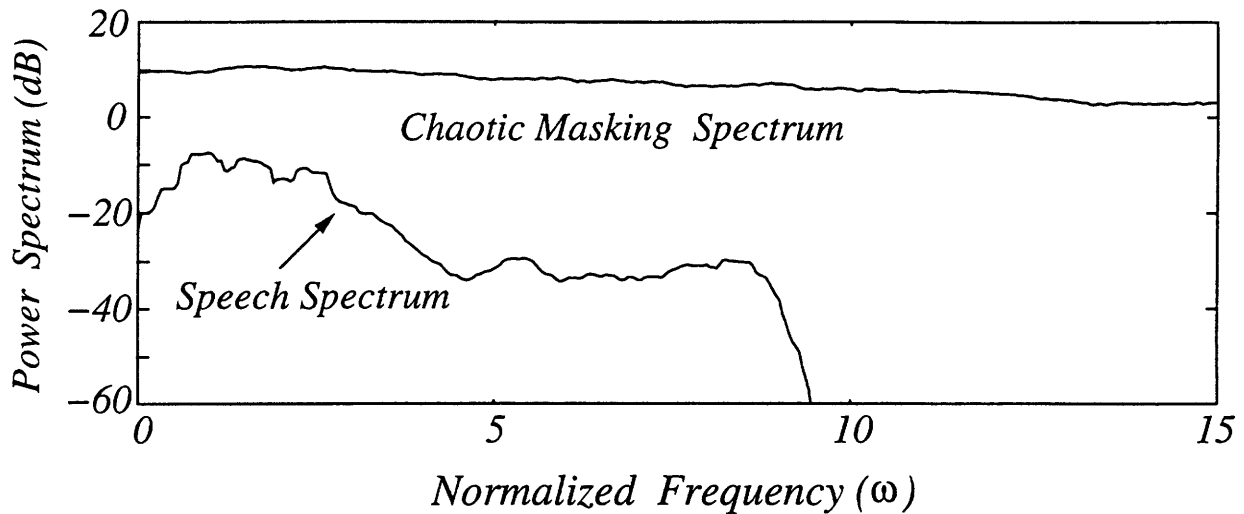


Figure 9-10: *Circuit Data: Power spectra of $u(t)$ and $p(t)$ when the perturbation is a speech signal.*

error in the recovered message. In Chapter 5, we showed that although $e_u(t)$ is not small compared to the message, the message can be recovered because $e_u(t)$ is nearly coherent with the message at low frequencies. In the next section, we demonstrate this effect and the ability to recover the message with the Lorenz receiver circuit.

9.2.2 Circuit Experiment

In this experiment, $p(t)$ is a low-level speech signal (the message to be transmitted and recovered). The normalizing time parameter is $400 \mu\text{sec}$ and the speech signal is bandlimited to 4 kHz or, equivalently, to a normalized frequency ω of 10. Figure 9-10 shows the power spectrum of a representative speech signal and of the circuit waveform $u(t)$. The overall chaos-to-perturbation ratio (CPR) in this experiment is approximately 20 dB.

In figure 9-11, we show the power spectrum of $p(t)$ and $\hat{p}(t)$, where $\hat{p}(t)$ is obtained from both a simulation and from the circuit. The two spectra for $\hat{p}(t)$ are in excellent agreement, indicating that the circuit performs very well. Because $\hat{p}(t)$ includes considerable energy beyond the bandwidth of the speech, the speech recovery can be improved by lowpass filtering $\hat{p}(t)$. We denote the lowpass filtered version of $\hat{p}(t)$ by $\hat{p}_f(t)$. In figure 9-12(a) and (b), we show a comparison of $\hat{p}_f(t)$ from both a simulation

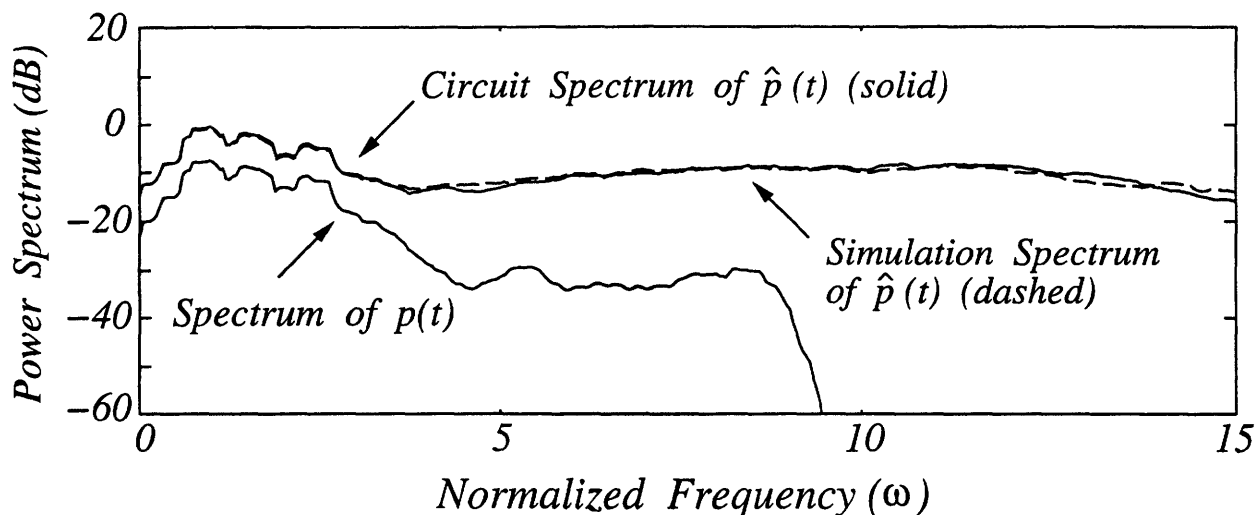


Figure 9-11: *Circuit Data: Power spectra of $p(t)$ and $\hat{p}(t)$ when the perturbation is a speech signal.*

and from the circuit, respectively. Clearly, the circuit performs well and, in informal listening tests, the recovered message is of reasonable quality.

Although $\hat{p}_f(t)$ is of reasonable quality, the low frequency components of the synchronization error cannot be completely removed by lowpass filtering. In the next section, we propose the use of an extended Kalman filter for “on-line” processing of $\hat{p}(t)$; in principle, this can compensate for the message recovery errors, thus improving the quality of the recovered message. Conceptually, the Kalman filter replaces the lowpass filter in figure 9-9 with a more sophisticated algorithm.

9.2.3 Model-Based Signal Recovery

The proposed Kalman filtering approach to signal recovery is statistical and model-based, since it relies on knowledge of an appropriate mathematical description of the transmitter and receiver equations and on the a priori second-order statistics of the message waveform. The basic idea is to use the received signal $s(t)$ and known transmitter/receiver error dynamics to estimate and cancel out the synchronization errors. In principle, an extended Kalman filter which is tuned to the error dynamics between the transmitter and receiver and coupled to the synchronizing receiver can perform the error estimation. The approach is illustrated in figure 9-13. The outputs

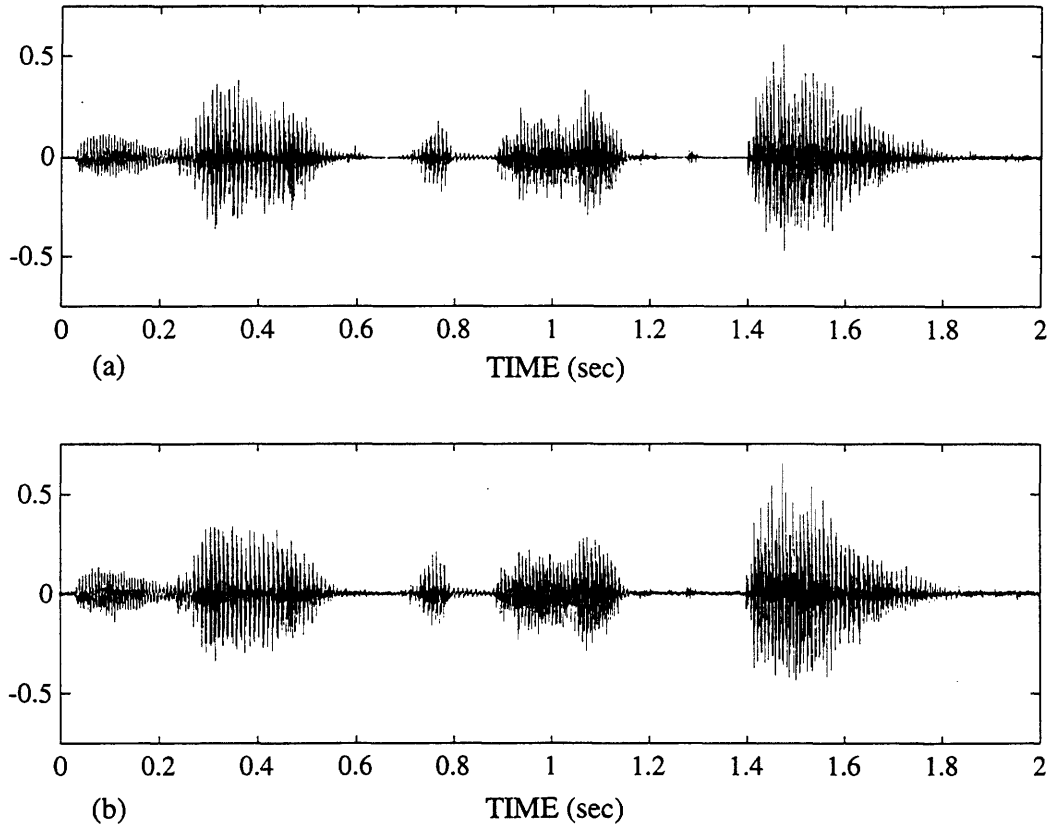


Figure 9-12: (a) *Recovered Speech (simulation)* (b) *Recovered Speech (circuit)*.

$\hat{p}_c(t)$ and $\hat{p}_u(t)$ correspond to the recovered message with and without compensation, respectively.

The received signal $s(t)$ is given by

$$s(t) = u(t) + p(t) + n(t) ,$$

where $n(t)$ is zero-mean white noise. The corresponding transmitter/receiver error dynamics are given by

$$\begin{bmatrix} \dot{e}_u \\ \dot{e}_v \\ \dot{e}_w \end{bmatrix} = \begin{bmatrix} \sigma(e_v - e_u) \\ -e_v + [r - 20(e_w + w_r)](e_u + u_r) \\ 5(e_u + u_r)(e_v + v_r) - be_w \end{bmatrix} + \begin{bmatrix} 0 \\ 20w_r - r \\ -5v_r \end{bmatrix} s(t) . \quad (9.4)$$

For notational simplicity, we refer to the error variables collectively by the vector $\mathbf{e} = (e_u, e_v, e_w)$ and to the receiver variables by the vector $\mathbf{x}_r = (u_r, v_r, w_r)$, when

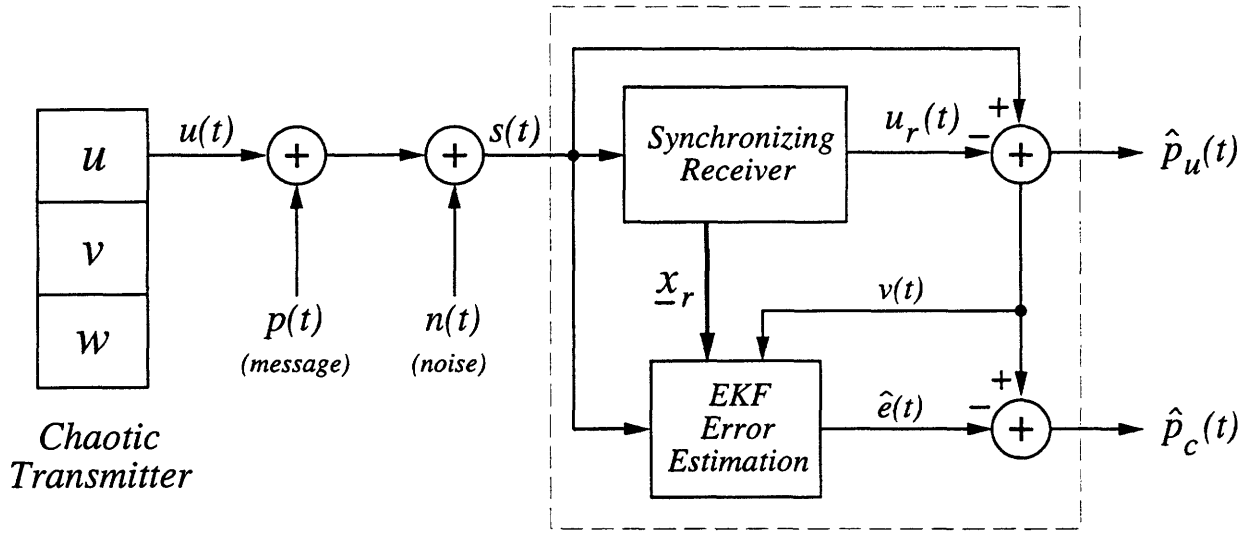


Figure 9-13: Model-Based Signal Recovery.

convenient.

The error system (9.4) depends on the receiver's state estimates \mathbf{x}_r and on the received signal $s(t)$. This system can be written as a probabilistic state model of the form

$$\begin{aligned} \dot{\mathbf{e}}(t) &= \mathbf{f}(\mathbf{e}, \mathbf{x}_r) + B(s(t), \mathbf{x}_r) + \mathbf{w}(t) \\ \nu(t) &= C\mathbf{e} + N(t) \end{aligned} \quad (9.5)$$

where

$$\begin{aligned} \mathbf{f}(\mathbf{e}, \mathbf{x}_r) &= \begin{bmatrix} \sigma(e_v - e_u) \\ -e_v + [r - 20(e_w + w_r)](e_u + u_r) \\ 5(e_u + u_r)(e_v + v_r) - be_w \end{bmatrix} , \\ B(s(t), \mathbf{x}_r) &= \begin{bmatrix} 0 \\ 20w_r - r \\ -5v_r \end{bmatrix} s(t) , \\ C &= \begin{bmatrix} 1 & 0 & 0 \end{bmatrix} , \quad N(t) = p(t) + n(t) . \end{aligned}$$

In this formulation, $B(s(t), \mathbf{x}_r)$ is treated as a deterministic input vector because both

$s(t)$ and \mathbf{x}_r are observed quantities and need not be estimated. The EKF observations are given by $\nu(t) = e_u(t) + N(t)$, as indicated in figure 9-13. For simplicity, we assume that the process noise $\mathbf{w}(t)$ is white and uncorrelated with $N(t)$. We also assume that the message $p(t)$ is a random process with known second-order statistics. With these assumptions, the second-order statistics of the random processes are given by

$$\begin{aligned} E \{ \mathbf{w}(t) \mathbf{w}^T(\tau) \} &= Q \delta(t - \tau) \ , \\ E \{ \mathbf{w}(t) N(\tau) \} &= 0 \ , \\ E \{ N(t) N(\tau) \} &= R_{pp}(t, \tau) + R_{nn}(t, \tau) \ . \end{aligned}$$

Because $p(t)$ is temporally correlated, the observation process $N(t) = p(t) + n(t)$ is also temporally correlated. State estimation techniques can deal with correlated observations by using augmented state space models to account for the “memory” of the observation process. The memory can be incorporated into the system model (9.5) by representing $N(t)$ by a dynamical system of the form

$$\begin{aligned} \dot{\rho}(t) &= F(t)\rho(t) + J(t)\mu_1(t) \\ N(t) &= H(t)\rho(t) + \mu_2(t) \ , \end{aligned} \tag{9.6}$$

where μ_1 and μ_2 are uncorrelated zero-mean Gaussian processes and where

$$E \{ \mu_i(t) \mu_i(\tau)^T \} = S_i(t) \delta(t - \tau) \ .$$

Combining equations (9.5) and (9.6), the overall state model driven by white noise is given by

$$\begin{aligned} \dot{\zeta}(t) &= \Delta(\zeta, \mathbf{x}_r) + \Theta(s(t), \mathbf{x}_r) + \alpha(t) \\ \nu(t) &= W(t)\zeta + \mu_2(t) \ , \end{aligned} \tag{9.7}$$

where

$$\zeta(t) = \begin{bmatrix} \mathbf{e} & \rho \end{bmatrix}^T \ ,$$

$$\Delta(\zeta, \mathbf{x}_r) = \begin{bmatrix} \mathbf{f}(\mathbf{e}, \mathbf{x}_r) \\ F(t)\rho(t) \end{bmatrix}, \quad \Theta(s, \mathbf{x}_r) = \begin{bmatrix} B(s(t), \mathbf{x}_r) \\ 0 \end{bmatrix},$$

$$\alpha(t) = \begin{bmatrix} \mathbf{w}(t) \\ J(t)\mu_1(t) \end{bmatrix}, \quad W(t) = \begin{bmatrix} C & H(t) \end{bmatrix}.$$

This statistical formulation has reduced the signal recovery problem to an estimation problem. The EKF state estimate and covariance equations for the system represented by (9.7) are given by

$$\begin{aligned} \dot{\hat{\zeta}}(t) &= \Delta(\hat{\zeta}, \mathbf{x}_r) + \Theta(s, \mathbf{x}_r) + K(t) [\nu(t) - W(t)\hat{\zeta}] \\ \dot{P}(t) &= D\Delta(\hat{\zeta}, \mathbf{x}_r)P(t) + P(t)D\Delta(\hat{\zeta}, \mathbf{x}_r)^T + Q_1 - P(t)W^T(t)S_2^{-1}(t)W(t)P(t) \\ K(t) &= P(t)W^T(t)S_2^{-1}(t), \end{aligned}$$

where $D\Delta(\hat{\zeta}, \mathbf{x}_r)$ is the linearization of $\Delta(\hat{\zeta}, \mathbf{x}_r)$ and where

$$Q_1 = \begin{bmatrix} Q & 0 \\ 0 & J(t)S_1(t)J^T(t) \end{bmatrix}.$$

Assuming that the message and noise have been accurately modeled, the EKF can provide meaningful estimates of the error signals. These error estimates can then be used to compensate the recovered message $\hat{p}_u(t)$, yielding $\hat{p}_c(t)$ which has improved quality.

While the Kalman filtering approach to signal recovery is an untested idea, it seems promising and merits future research. A limitation, however, is that the presence of additive channel noise will produce message recovery errors that cannot be completely removed; there will always be some error in the recovered message. Because the message and noise are directly added to the synchronizing drive signal, the message-to-noise ratio should be large enough to allow a faithful recovery of the original message. This requires a communication channel which is nearly noise free.

To help overcome this limitation, we developed an alternative approach to private communications based on synchronized chaotic signals and systems. This alternative

approach allows the information-bearing waveform to be exactly recovered at the self-synchronizing receiver(s), even when moderate-level channel noise is present.

9.3 Chaotic Binary Communications

In this section, we discuss a private communication technique called *chaotic binary communications*. This technique utilizes modulation of a transmitter parameter and subsequent detection of synchronization error in the receiver to privately communicate binary-valued bit streams [30, 31, 32, 33, 45].

In Section 9.3.1, we discuss and illustrate the concept. In Section 9.3.2, we perform a synchronization error analysis to quantify the sensitivity of synchronization to parameter modulation at the transmitter. We also propose an optimal detector for recovering the bit streams. In Section 9.3.3, we utilize the Lorenz circuits to demonstrate the technique.

9.3.1 Concept

The concept of chaotic binary communications is to modulate a transmitter parameter with the information-bearing waveform and to transmit the chaotic drive signal. At the receiver, the parameter modulation will produce a synchronization error between the received drive signal and the receiver's regenerated drive signal with an error signal amplitude that depends on the modulation. Using the synchronization error, the modulation can be detected.

This modulation/detection process is illustrated in figure 9-14 for the specific case of implementing the Lorenz system at the transmitter and receiver. To communicate information, we modulate a parameter of the transmitter equations with the information-bearing waveform $p(t)$ while the chaotic drive signal $u(t)$ is transmitted. The noisy received signal $s(t)$ serves as the driving input to the receiver. At the receiver, the parameter modulation is detected by forming the error signal $e(t)$ corresponding to the difference between $s(t)$ and the receiver's regenerated drive signal $u_r(t)$. Assuming that the channel noise $n(t)$ is negligible, the error signal $e(t)$

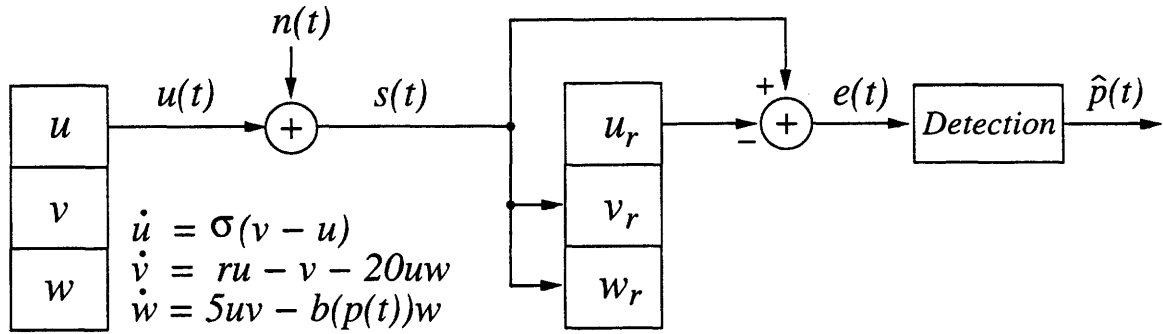


Figure 9-14: *Communicating Binary-valued Bit Streams with Self-Synchronizing Chaotic Systems.*

will have a small average power when the transmitter and receiver parameters are identical. If, however, $p(t)$ is a binary-valued bit stream, with a “1” representing a parameter mismatch between the transmitter and receiver, and a “0” representing no parameter mismatch, then $e(t)$ will be relatively large in amplitude during the time period that a “1” is transmitted and small in amplitude during a “0” transmission. The synchronizing receiver can, therefore, be viewed as a form of matched filter for the chaotic transmitter signal $u(t)$.

In the next section, we numerically examine the sensitivity of the synchronization error $e(t)$ to variations in the transmitter parameters. This analysis determines the preferred Lorenz parameter to modulate with $p(t)$, and suggests an optimal detector for recovering the “0” and “1” transmissions.

9.3.2 Synchronization Error Analysis and Detection

The synchronization error analysis presented in this section focuses on the synchronization properties of the Lorenz transmitter equations

$$\begin{aligned}
 \dot{u} &= \sigma_t(v - u) \\
 \dot{v} &= r_t u - v - 20uw \\
 \dot{w} &= 5uv - b_t w ,
 \end{aligned} \tag{9.8}$$

and the corresponding receiver equations

$$\begin{aligned}
 \dot{u}_r &= \sigma_r(v_r - u_r) \\
 \dot{v}_r &= r_r s(t) - v_r - 20s(t)w_r \\
 \dot{w}_r &= 5s(t)v_r - b_r w_r .
 \end{aligned} \tag{9.9}$$

The received signal $s(t)$ is given by

$$s(t) = u(t) + n(t) ,$$

where $u(t)$ denotes the transmitted drive signal and $n(t)$ denotes the channel noise. The binary signal $p(t)$ influences $u(t)$ by modulating a transmitter parameter ($\sigma_t, r_t,$ or b_t) while the receiver parameters $\sigma_r, r_r,$ and b_r remain fixed. The resulting synchronization error signals are denoted by

$$\begin{aligned}
 e_u(t) &= u(t) - u_r(t) \\
 e_v(t) &= v(t) - v_r(t) \\
 e_w(t) &= w(t) - w_r(t) ,
 \end{aligned}$$

and the parameter mismatch variables are denoted by

$$\begin{aligned}
 \Delta\sigma &= \sigma_t - \sigma_r \\
 \Delta r &= r_t - r_r \\
 \Delta b &= b_t - b_r .
 \end{aligned}$$

The sensitivity of the synchronization errors to the parameter mismatch variables can be examined by forming the error system. By subtracting the receiver equations

(9.9) from the transmitter equations (9.8), the following error system is obtained.

$$\begin{bmatrix} \dot{e}_u \\ \dot{e}_v \\ \dot{e}_w \end{bmatrix} = \begin{bmatrix} -\sigma & \sigma & 0 \\ 0 & -1 & -20s(t) \\ 0 & 5s(t) & -b \end{bmatrix} \begin{bmatrix} e_u \\ e_v \\ e_w \end{bmatrix} + \begin{bmatrix} 0 \\ 20w - r_r \\ -5v \end{bmatrix} n(t) + \begin{bmatrix} (v - u)\Delta\sigma \\ u\Delta r \\ -w\Delta b \end{bmatrix}$$

This error system indicates that if any of the parameter mismatch variables are non-zero, then chaotic driving terms will exist even when $n(t) = 0$. Therefore, the synchronization errors will also be non-zero.

In the specific communication scenario illustrated in figure 9-14, we are particularly interested in the sensitivity of $e_u(t)$ to the parameter mismatch variables. The input signal to the detector $e(t)$ is given by

$$e(t) = e_u(t) + n(t) ,$$

which shows that $e_u(t)$ is important for detecting the “0” and “1” transmissions. To examine this sensitivity, a numerical experiment is performed. All of the receiver parameters are fixed at their nominal values $\sigma_r = 16, r_r = 45.6$, and $b_r = 4$. The transmitter parameters σ_t, r_t , and b_t are independently varied over a range corresponding to a ± 20 percent mismatch from the nominal values implemented at the receiver. Only one transmitter parameter is varied at a time while the other two parameters are held fixed at their nominal values. Numerical integration of the error system is then performed with $n(t) = 0$.

In figure 9-15, we show the normalized synchronization error σ_{eu}/σ_u as a function of the parameter mismatch (percent),

$$\text{Percent Mismatch} = 100 \cdot \frac{\text{Transmitter Value} - \text{Receiver Value}}{\text{Receiver Value}} . \quad (9.10)$$

Note that the synchronization error is most sensitive to r_t and b_t . In private communication applications, it is advantageous to modulate the transmitter parameter with the greatest sensitivity. Small variations in the transmitter parameters are less

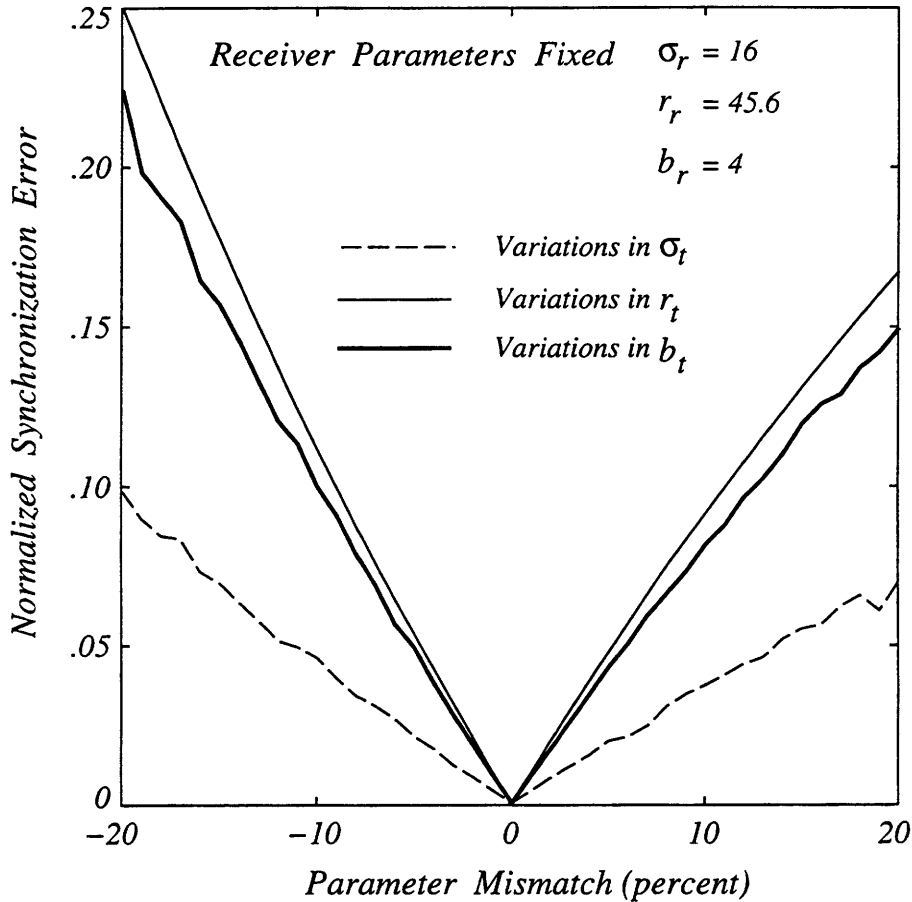


Figure 9-15: *Normalized Synchronization Error vs. Parameter Mismatch (percent).*

detectable by unintended listeners than large variations. Informal experiments suggested that variations in b_t alter the detectable characteristics of the transmitted chaotic signal less than corresponding variations in r_t . This seems plausible because r_t is the bifurcation parameter for the Lorenz system and has a greater influence on the signal levels than equivalent variations in b_t . Based on this synchronization error analysis, b_t was selected as the modulation parameter.

We now turn our attention to detection of the “0” and “1” transmissions. Viewing the detection process as a binary hypothesis testing problem, with H_0 denoting a “0” transmission and H_1 denoting a “1” transmission, we define the two possible outcomes

$$\begin{aligned}
 H_0: e(t) &= e_u^0(t) + n(t) , \\
 H_1: e(t) &= e_u^1(t) + n(t) .
 \end{aligned}
 \tag{9.11}$$

We denote the synchronization error $e_u(t)$ corresponding to hypothesis H_0 by $e_u^0(t)$. Similarly, the synchronization error corresponding to hypothesis H_1 is denoted by $e_u^1(t)$. For simplicity, we will assume that $e_u^0(t)$, $e_u^1(t)$, and $n(t)$ are zero-mean, Gaussian distributed, and wide-sense stationary. These assumptions are roughly justified by numerical experiments.

The variance of $e(t)$, over a bit interval of T_I seconds, is important for detecting the “0” and “1” transmissions. We denote by σ_0^2 and σ_1^2 the variances of $e(t)$ under hypotheses H_0 and H_1 , respectively. We define the sufficient statistic $L(e, t)$ as

$$L(e, t) = \frac{1}{T_I} \int_{t-T_I}^t e^2(\tau) d\tau .$$

An optimal decision rule for selecting the most likely hypothesis is obtained by applying the likelihood ratio test. Assuming Gaussian statistics for the random processes and equal a priori probabilities for H_0 and H_1 , we obtain the decision rule

$$L(e, t) \begin{array}{l} > \\ < \end{array} \begin{array}{l} H_1 \\ H_0 \end{array} \frac{2\sigma_0^2\sigma_1^2}{\sigma_1^2 - \sigma_0^2} \log \left(\frac{\sigma_1}{\sigma_0} \right) = \gamma . \quad (9.12)$$

Equation (9.12) determines an optimal threshold γ for the detection problem. In practice, the sufficient statistic can be computed in real time using commercially available hardware.

In the next section, we utilize the Lorenz transmitter and receiver circuits to demonstrate chaotic binary communications.

9.3.3 Circuit Experiments

In Section 9.1, we pointed out that the parameters of the Lorenz transmitter equations (9.1) can be independently varied by altering the values of appropriate resistors in the circuit implementation. Equation (9.2) indicates that the parameter b is proportional

to

$$b \propto \frac{R_{18}}{R_{17} + R_{18}} \quad (9.13)$$

From (9.13), we see that b can be varied by altering either R_{17} or R_{18} . For implementation purposes, it is preferable to alter R_{18} because a sensitivity analysis of (9.13) shows that b is approximately 3.5 times more sensitive to R_{18} than to R_{17} . In Appendix C, we discuss and illustrate a simple voltage-controlled resistor (VCR) circuit which is used to alter R_{18} in proportion to an applied voltage signal $p(t)$. The VCR circuit is tuned so that for $p(t) = \pm 1$ volt, the resulting variation in b is ± 10 percent from its nominal value of 4.

To illustrate the technique, we use a periodic square-wave for $p(t)$ as shown in figure 9-16(a). The square-wave has a repetition frequency of approximately 110 *Hz* with zero volts representing the zero-bit and one volt representing the one-bit. The square-wave modulates the transmitter parameter b with the zero-bit and one-bit parameters given by

$$\begin{aligned} b(p(t) = 0) &= 4 \quad , \\ b(p(t) = 1) &= 4.4 \quad . \end{aligned}$$

The resulting drive signal $u(t)$ is transmitted and used as the driving input to the synchronizing receiver circuit. For transmission privacy, the parameter modulation should not alter the characteristics of the drive signal in an obvious way. In figure 9-16, we compare the average power spectrum of the drive signal with and without the parameter modulation. There is little change in the power spectrum after the parameter modulation is introduced.

In figure 9-17(a), we reproduce the square-wave $p(t)$ and in figure 9-17(b), we show the synchronization error power $e^2(t)$. The parameter modulation produces significant synchronization error during a "1" transmission and very little error during a "0" transmission. It is plausible that a detector based on the average synchronization

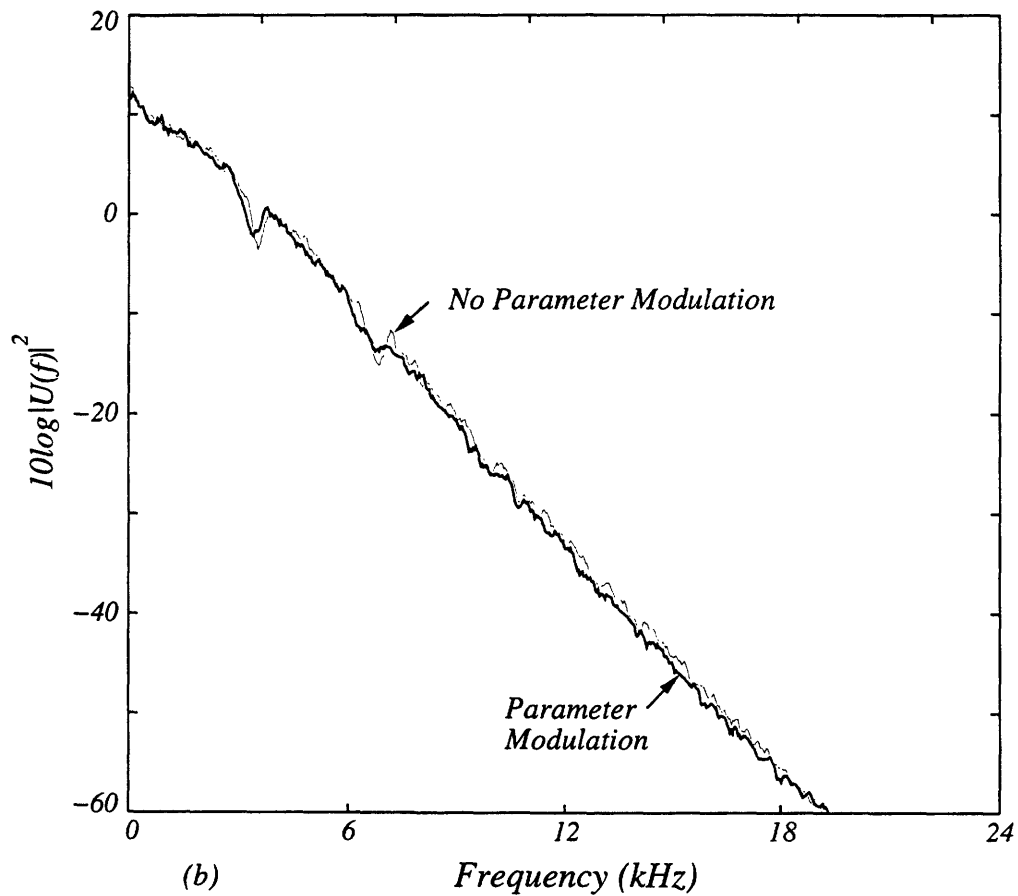
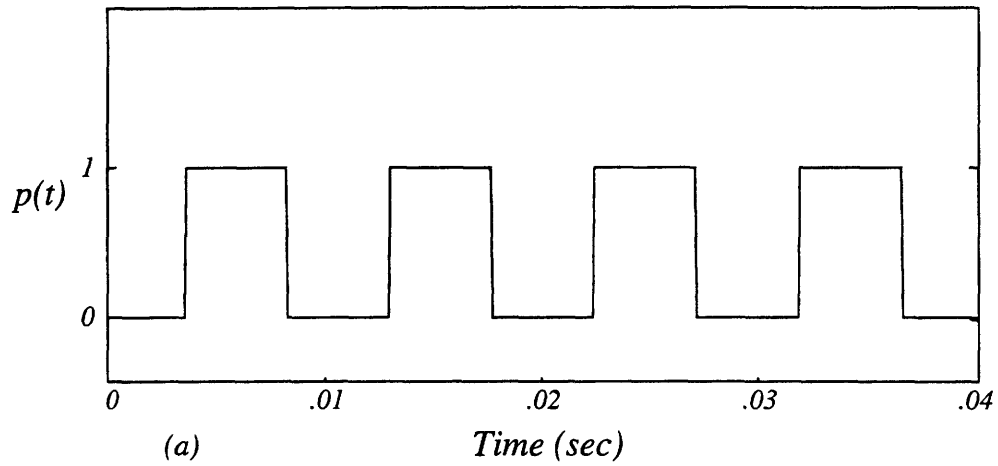


Figure 9-16: Circuit Data: (a) Binary waveform used to modulate the b parameter of the Lorenz transmitter equations. (b) Averaged power spectrum of the drive signal with and without parameter modulation.

error power, followed by a threshold device, could yield reliable performance. A crude approximation to the likelihood function $L(e, t)$ is obtained by using a low-order lowpass filter to perform the integration. Using this simple approach, we illustrate in figure 9-17(c) that the square-wave modulation can be reliably recovered by lowpass filtering the synchronization error power waveform and applying a threshold test. The threshold device used in this experiment consisted of a simple analog comparator circuit.

The allowable data rate of this communication technique is, of course, dependent on the synchronization response time of the receiver system. Although we have used a low bit rate to demonstrate the technique, the circuit time scale can be easily adjusted to allow much faster bit rates. The ability to communicate digital bit streams using this technique does not depend on the periodic nature of the square-wave used to demonstrate the approach. The results apply to aperiodic or random bit streams as well. A similar approach has also been independently shown to work using Chua's circuit [47].

9.4 Summary

The work presented in this chapter has addressed some applied aspects of self-synchronizing chaotic systems. The two most important accomplishments are:

- The implementation of the Lorenz transmitter and receiver systems with a simple analog circuit. The performance of these circuits is excellent, indicating that synchronized chaotic systems can be built with commercially available hardware and perform within desired specifications.
- The development and demonstration of two approaches to private communications using the Lorenz circuit. These results suggest that synchronized chaotic systems may represent a promising class of nonlinear systems for future communication applications.

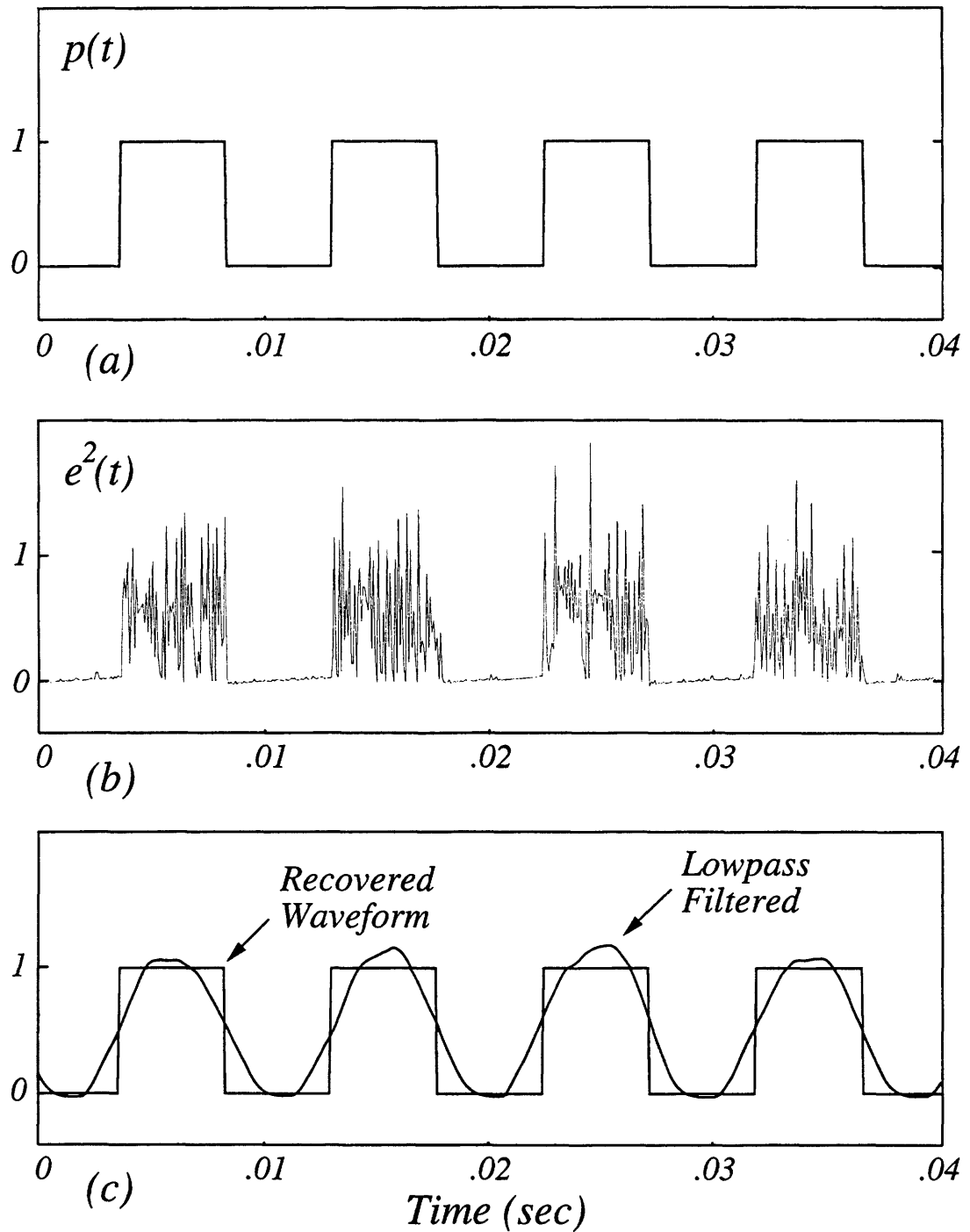


Figure 9-17: Circuit Data: (a) Binary modulation waveform. (b) Synchronization error power. (c) Recovered binary waveform.

Chapter 10

Conclusions and Suggestions for Future Research

Since its discovery in 1990, self-synchronization of chaotic systems has become an extremely active research area. A substantial amount of literature has been published in this emerging field, much of which is experimental in nature. While it appears that potential applications exist for this class of systems, general procedures had not been developed for analyzing and synthesizing chaotic systems which possess the self-synchronization property. This thesis has focused on both of these critical areas.

10.1 Summary and Contributions

We first considered the analysis problem. The notions of conditional Lyapunov exponents and stable response subsystems were used to develop a systematic approach for examining the self-synchronization properties of general nonlinear systems. Although this approach is useful for decomposing any nonlinear system into its stable and unstable components, it has some limitations. Considerable computation is required to determine the conditional Lyapunov exponents and the approach provides little insight into the mechanism underlying the synchronization.

To study self-synchronization of chaotic systems within a clear mathematical framework, we utilized some well-known techniques from nonlinear stability the-

ory. After identifying an equivalence between the concepts of self-synchronization in chaotic systems and asymptotically stable error dynamics between the transmitter and receiver systems, we utilized Lyapunov functions to show that self-synchronization in the Lorenz system does not depend on chaotic behavior. Rather, it is a result of stable error dynamics.

To exploit the self-synchronization properties of the Lorenz system in applications, we examined the sensitivity of synchronization when a perturbation signal is added to the synchronizing drive signal. We showed numerically that the performance of the Lorenz receiver as a nonlinear state estimator compared favorably with two well-known extended Kalman filter algorithms when the perturbation is white noise. Two key features of the synchronization error curves for the Lorenz receiver were identified: *(i)* a threshold effect is evident at a critical value of input chaos-to-perturbation ratio (CPR), and *(ii)* above the threshold, the normalized error in synchronization of each state variable is approximately 10 dB less than the normalized error in the drive signal. We used stochastic calculus to show that the threshold effect was a result of an inherent instability of the second moment equation at low input CPRs. In addition, we developed an equivalent linear time-invariant error model which quantifies and explains the sensitivity of synchronization in the Lorenz system in terms of the spectral characteristics of the perturbation signal. This model provided an explanation of why low-level speech signals or other narrowband perturbations can be accurately recovered at the receiver.

To further enhance the applicability of synchronized chaotic systems for communications, an approach was needed for creating new chaotic systems with the same robust synchronization properties as the Lorenz system. Using Lyapunov's direct method as a basis, we explored various approaches for synthesizing self-synchronizing chaotic systems. We began with the simplest approach, combining the Lorenz system with a linear feedback system. Linear feedback chaotic systems (LFBCSs) allow for more complex dynamics than the Lorenz system while retaining the same self-synchronization properties. Having proposed a systematic synthesis procedure for LFBCSs, we then investigated chaotic arrays consisting of multiple Lorenz oscilla-

tors. The synthesis procedure for the Lorenz-based chaotic arrays is analogous to the synthesis procedure for LFBCSs. Although chaotic arrays exhibited more complex dynamics than LFBCSs, the arrays require multiple drive signals for synchronization (one for each Lorenz oscillator). This tradeoff suggested that it might be possible to develop a more general synthesis procedure. To explore this issue, we started with a very general class of quadratically nonlinear systems and applied the same synthesis methodology. A result of this investigation was a canonical form for a general class of chaotic systems that synchronize via a single drive signal and exhibit more complex dynamics than LFBCSs.

To investigate some applied aspects of self-synchronizing chaotic systems, we implemented the Lorenz system with an analog circuit. We avoided some potential implementation problems by scaling the state variables in the Lorenz equations. Two identical circuits, a Lorenz transmitter and synchronizing receiver, were built using commercially available hardware. After the performance of these circuits was shown to be consistent with the numerical and theoretical predictions, we demonstrated that low-level speech could be added to the synchronizing drive signal, privately communicated, and recovered by the synchronizing receiver. Recognizing a drawback of this approach in realistic communication scenarios, we investigated a second approach to private communications. Instead of adding the information to the drive signal, we investigated the potential for embedding the information in a more abstract way. By modulating a transmitter parameter with a binary-valued bit stream, we demonstrated that it was possible to privately transmit and recover the information with the self-synchronizing receiver circuit. While these results are promising and represent a starting point for utilizing self-synchronizing chaotic systems in communications, much work remains before these approaches can be considered secure or practical.

10.2 Future Research Directions

There are several outstanding issues pertaining to the analysis and synthesis of self-synchronizing chaotic systems which suggest potential future research directions. For

example, the synthesis procedures developed in Chapters 6-8 have not been fully explored. Much work remains for utilizing these procedures to synthesize new self-synchronizing chaotic systems and for examining the chaotic behavior exhibited by these systems. The synthesis procedures provide considerable potential for designing practical chaotic systems which could be implemented in hardware and used for various private communication applications. Another interesting problem for future research is to investigate the potential connections between stability criteria for adaptive control systems and the synthesis procedures proposed in Chapters 6-8.

Although we have focused our synthesis efforts on continuous-time chaotic systems, our methodology is clearly broader. In principle, Lyapunov's direct method could be used as a basis for synthesizing discrete-time systems as well. From a practical perspective, discrete-time systems have certain implementation advantages over their continuous-time counterparts. A related issue for future research involves the possibility of synthesizing discrete-time systems by replacing the derivatives in a set of nonlinear differential equations with an appropriate first difference approximation. This approach has the advantage of allowing the continuous-time theory developed in this thesis to be used for synthesis. The main issue in this case is to determine whether the self-synchronization and global stability properties of the chaotic system are maintained after the discretization. If continuous-time systems can be successfully converted to equivalent discrete-time systems, then digital hardware can be used for the implementations.

Another important issue concerns realistic communication applications for this class of systems. The effects of quantization, gain errors, multipath, and channel fading on the quality of the synchronization need to be addressed. Clearly, these issues would arise in realistic scenarios which utilize chaotic synchronization. A final issue involves transmission privacy. We have not attempted to define optimal communication schemes for achieving privacy, but rather suggested some possible approaches. Intuitively, we believe that the use of high-dimensional chaotic systems may be more private than low-dimensional systems, but much work remains to test this hypothesis.

Appendix A

Linear Stability Analysis of z -Input/ z -Output LFBCSs

The transmitter equations for LFBCSs of this class are given by

$$\begin{aligned}\dot{x} &= \sigma(y - x) \\ \dot{y} &= rx - y - xz \\ \dot{z} &= xy - bz + \nu \\ \dot{\mathbf{i}} &= A\mathbf{i} + Bz \\ \nu &= C\mathbf{i} + Dz \ ,\end{aligned}\tag{A.1}$$

where A is $N \times N$, B is $N \times 1$, C is $1 \times N$, and D is 1×1 .

Inspection of (A.1) shows that the origin in state space is always a fixed point. Two additional fixed points can be determined by setting the transmitter's vector field equal to zero and solving for the non-trivial stationary points. The equations to be solved are listed below¹.

1. $\sigma(y^* - x^*) = 0$,
2. $rx^* - y^* - x^*z^* = 0$,
3. $x^*y^* - bz^* + C\mathbf{i}^* + Dz^* = 0$,

¹State variables with star "*" superscripts denote fixed points in this analysis.

$$4. \mathbf{A}\mathbf{l}^* + \mathbf{B}z^* = 0.$$

Combining equations 1 and 2, we find that $z^* = r - 1$. Equation 4 determines \mathbf{l}^* as

$$\mathbf{l}^* = -\mathbf{A}^{-1}\mathbf{B}(r - 1) ,$$

and x^* is determined from equation 3 as

$$x^* = \pm\sqrt{(r - 1)(\mathbf{C}\mathbf{A}^{-1}\mathbf{B} - D + b)} .$$

The scalar $H(0) = -\mathbf{C}\mathbf{A}^{-1}\mathbf{B} + D$ is equivalent to the transfer function of the linear feedback system evaluated at the origin, and therefore, x^* can be conveniently written as

$$x^* = \pm\sqrt{(r - 1)(b - H(0))} . \quad (\text{A.2})$$

From equation 1, the component y^* is given by $y^* = x^*$.

The term under the radical in (A.2) must be positive for these fixed points to exist. Assuming that $b - H(0) > 0$, the fixed points will exist for $r \geq r_c$, where $r_c = 1$. In the Lorenz system (without feedback) a pair of fixed points exists for $r \geq 1$. This is also the case for z -input/ z -output LFBCSs, assuming that $b - H(0) > 0$. The stability analysis presented below will show that the fixed point pair of the LFBCS is created when the origin loses stability; this is also the case for the Lorenz system without feedback.

Evaluating the Jacobian matrix corresponding to (A.1) at the origin we obtain

$$J(\mathbf{0}) = \begin{bmatrix} -\sigma & \sigma & 0 & \mathbf{0}^T \\ r & -1 & 0 & \mathbf{0}^T \\ 0 & 0 & -(b - D) & C \\ 0 & 0 & B & A \end{bmatrix} .$$

Note that $J(\mathbf{0})$ is block diagonal. If the lower $(N + 1) \times (N + 1)$ block of $J(\mathbf{0})$ is

stable, then the stability of the origin is controlled by the modes of the upper 2×2 block. For $r > 1$, the upper block is unstable, and therefore, the origin is unstable. This critical value of r also corresponds to the creation of the fixed point pair. This analysis suggests that a pitchfork bifurcation occurs at the origin when $r = 1$.

Evaluating the Jacobian matrix at the fixed point pair we obtain

$$J(\mathbf{x}_0) = \begin{bmatrix} -\sigma & \sigma & 0 & \mathbf{0}^T \\ r - z^* & -1 & -x^* & \mathbf{0}^T \\ y^* & x^* & -(b - D) & C \\ \mathbf{0} & \mathbf{0} & B & A \end{bmatrix} .$$

Substituting the coordinates of the fixed point pair into $J(\mathbf{x}_0)$ allows their stability to be examined numerically. As we show below, additional insight into the stability of these fixed points is obtained by examining the eigenvalues of $J(\mathbf{x}_0)$ analytically.

Using the matrix identity

$$\begin{vmatrix} A_{11} & A_{12} \\ A_{21} & A_{22} \end{vmatrix} = |A_{11} - A_{12}A_{22}^{-1}A_{21}| |A_{22}| ,$$

the characteristic polynomial for $J(\mathbf{x}_0)$ is determined as

$$|\lambda I - J(\mathbf{x}_0)| = \prod_{i=1}^N (\lambda - \lambda_i) \begin{vmatrix} \lambda + \sigma & -\sigma & 0 \\ -1 & \lambda + 1 & x^* \\ -x^* & -x^* & \lambda + b - H(\lambda) \end{vmatrix} = 0. \quad (\text{A.3})$$

The eigenvalues λ_i , for $i = 1, \dots, N$, belong to the A matrix and, therefore, represent stable modes. As shown below, the presence of unstable modes can be detected by determining the characteristic polynomial of the 3×3 determinant in (A.3).

The characteristic polynomial for the 3×3 determinant in (A.3) is given by

$$\lambda^3 + (\sigma + b + 1 - H(\lambda))\lambda^2 + (H(0)(1 - r) - (\sigma + 1)H(\lambda) + b(\sigma + r))\lambda + 2\sigma(r - 1)(b - H(0)) = 0 . \quad (\text{A.4})$$

As r is varied, a bifurcation occurs when a root of (A.4) crosses the imaginary axis in the complex plane. When this occurs, the critical value(s) of r can be determined by restricting our attention to solutions of (A.4) for values of $\lambda = jf$, for $f \geq 0$. Substituting $\lambda = jf$ into (A.4) and introducing the notation $H(jf) = H_R(f) + jH_I(f)$, we obtain

$$\begin{aligned} & \left[2\sigma(r-1)(b-H(0)) + fH_I(f)(\sigma+1) - f^2(\sigma+b+1-H_R(f)) \right] + \\ & j \left[f(b(\sigma+r) + H(0)(1-r) - H_R(f)(\sigma+1)) + f^2H_I(f) - f^3 \right] = 0 . \end{aligned}$$

Setting the imaginary part of this expression equal to zero and solving for f in terms of $H_R(f)$ and $H_I(f)$ we obtain the eigenfrequency equation

$$f = \frac{f^3 - f^2H_I(f)}{b(\sigma+r) + H(0)(1-r) - H_R(f)(\sigma+1)} = G'(f) . \quad (\text{A.5})$$

Similarly, by setting the real part equal to zero we obtain an equation for the bifurcation parameter

$$r = 1 + \frac{f^2(\sigma+b+1-H_R(f)) - fH_I(f)(\sigma+1)}{2\sigma(b-H(0))} . \quad (\text{A.6})$$

The eigenfrequency equation (A.5) is written as $f = G'(f)$, where $G'(f)$ is an odd function. Because $G'(f)$ is odd and continuous, it follows that $G'(0) = 0$ and therefore, $f = 0$ is always a solution to (A.5). From (A.6), the corresponding value of r is given by $r = 1$. Recall that this value of r predicts the pitchfork bifurcation at the origin when the origin loses stability and the fixed point pair is created. If the fixed point pair is stable when it is created, then its loss of stability occurs when a complex conjugate pair of eigenvalues ($f > 0$) crosses into the right-half plane. In this case, the loss of stability of the fixed point pair is akin to a Hopf bifurcation. In typical numerical experiments, we have observed that once the fixed point pair loses stability, chaotic motion usually occurs.

Appendix B

Lorenz Transmitter and Receiver Circuit Components

A list of component values used in the Lorenz transmitter and receiver circuits (Section 9.1) are provided below.

Transmitter/Receiver Components

Resistors: (values in kohms, all have 1% precision)

R1 = 100	R11 = 63.4 (nominal)
R2 = 100	R12 = 10
R3 = 100	R13 = 100
R4 = 100	R14 = 100
R5 = 49.9	R15 = 40.2
R6 = 100	R16 = 100
R7 = 100	R17 = 100
R8 = 200	R18 = 66.5 (nominal)
R9 = 10	R19 = 100
R10 = 49.9	R20 = 158

Capacitors: (values in picofarads, all have 5% precision)

C1 = 500 (typical) C2 = 500 (typical) C3 = 500 (typical)

Operational Amplifiers: LF353 **Analog Multipliers:** AD632AD

Appendix C

Voltage-Controlled Resistor Circuit

To vary R_{18} in the circuit implementation of chaotic binary communications (Section 9.3), we use a simple electronic circuit which functions as a voltage-controlled resistor (VCR) as shown in figure C-1. The idea behind the operation of this circuit is to use a voltage-controlled oscillator (VCO) in conjunction with comparators and an analog switch to alternately toggle between R_{10} and R_{11} at a fast rate. The fast switching between R_{10} and R_{11} produces an effective resistance between points a and b which is equal to a weighted average of these two resistors. The weighting depends on the relative duty cycle of $SW1$ and $SW2$ which in turn depends on the control voltage $p(t)$. A linear variation in $p(t)$ produces a linear variation in the duty cycle of $SW1$ and $SW2$ and, thus, $p(t)$ and R_{ab} are linearly related. If points a and b of this circuit replace R_{18} , then b can be electronically controlled by $p(t)$. Resistor R_5 is used to control the gain of the VCR circuit, and is adjusted so that for $p(t) = \pm 1$ volt the resulting deviation in b is ± 10 percent. A list of components used in the implementation of the VCR circuit is provided below.

Voltage-Controlled Resistor Components

Resistors: (values in kohms, all have 1% precision)

$$R1 = 4.7$$

$$R7 = 1$$

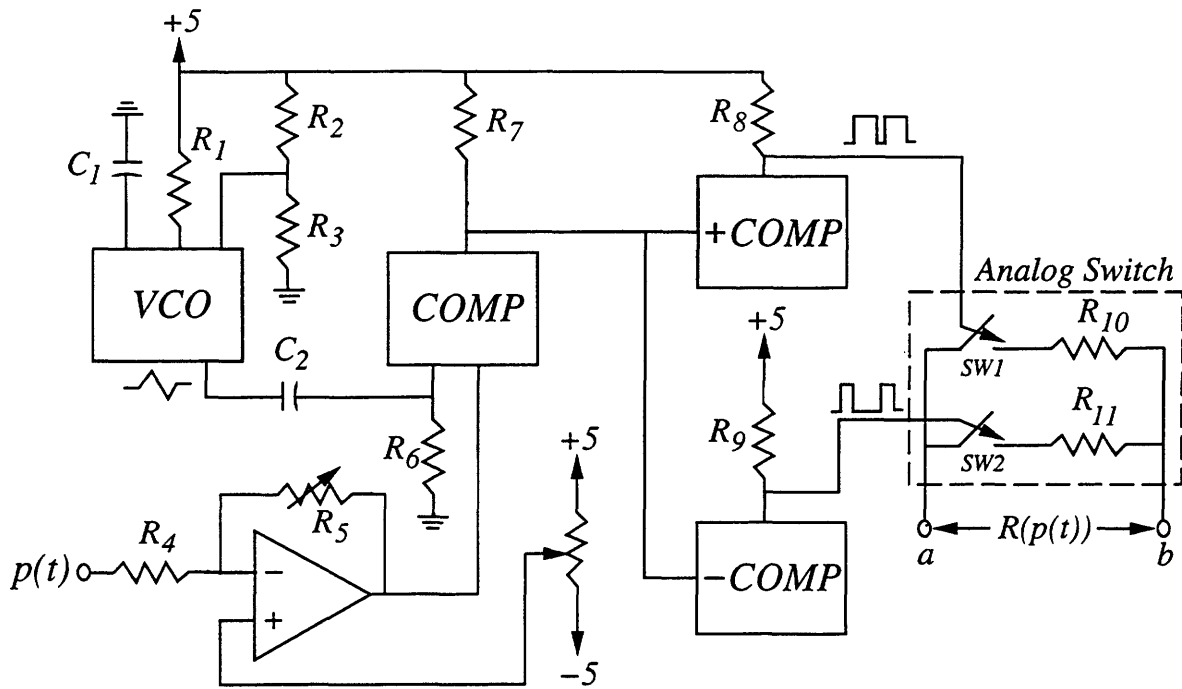


Figure C-1: *Voltage-Controlled Resistor Circuit.*

$R_2 = 10$	$R_8 = 1$
$R_3 = 100$	$R_9 = 1$
$R_4 = 100$	$R_{10} = 82.5$
$R_5 = \text{variable}$	$R_{11} = 53.6$
$R_6 = 5$	

Capacitors: (values in picofarads, all have 5% precision)

$C_1 = 1200$	$C_2 = 10000$
--------------	---------------

Voltage-Controlled Oscillator

LM566

Comparators

LM311

Analog Switch

CD4066

Bibliography

- [1] L. M. Pecora and T. L. Carroll. "Synchronization in Chaotic Systems". *Physical Review Letters*, 64(8):821–824, February 1990.
- [2] T. L. Carroll and L. M. Pecora. "Synchronizing Chaotic Circuits". *IEEE Transactions on Circuits and Systems*, 38(4):453–456, April 1991.
- [3] L. M. Pecora and T. L. Carroll. "Driving Systems with Chaotic Signals". *Physical Review A*, 44(4):2374–2383, August 1991.
- [4] H. G. Winful and L. Rahman. "Synchronized Chaos and Spatiotemporal Chaos in Arrays of Coupled Lasers". *Physical Review Letters*, 65(13):1575–1578, September 1990.
- [5] G. M. Bernstein. "*Nonlinear Oscillations, Synchronization and Chaos*". PhD thesis, University of California, Berkeley, May 1988.
- [6] D. Hansel and H. Sompolinsky. "Synchronization and Computation in a Chaotic Neural Network". *Physical Review Letters*, 68(5):718–721, February 1992.
- [7] A. T. Winfree. "Biological Rhythms and the Behavior of Populations of Coupled Oscillators". *Journal of Theoretical Biology*, 16:15–42, 1967.
- [8] S. H. Strogatz and I. Stewart. "Coupled Oscillators and Biological Synchronization". *Scientific American*, 269(6):102–109, December 1993.
- [9] K. M. Cuomo, A. V. Oppenheim, and S. H. Isabelle. "Spread Spectrum Modulation and Signal Masking Using Synchronized Chaotic Systems". Technical Report 570, MIT Research Laboratory of Electronics, February 1992.
- [10] A. V. Oppenheim, G. W. Wornell, S. H. Isabelle, and K. M. Cuomo. "Signal Processing in the Context of Chaotic Signals". In *Proceedings IEEE ICASSP*, March 1992.
- [11] R. He and P. G. Vaidya. "Analysis and Synthesis of Synchronous Periodic and Chaotic Systems". *Physical Review A*, 46(12):7387–7392, December 1992.
- [12] J. Guckenheimer and P. Holmes. "*Nonlinear Oscillations, Dynamical Systems, and Bifurcations of Vector Fields*". Springer-Verlag, New York, 1983.

- [13] E. N. Lorenz. "Deterministic Nonperiodic Flow". *Journal of the Atmospheric Sciences*, 20:130–141, March 1963.
- [14] P. Berge, Y. Pomeau, and C. Vidal. "Order Within Chaos". Hermann and John Wiley and Sons, Paris, France, 1984.
- [15] D. W. Jordan and P. Smith. "Nonlinear Differential Equations (Second Edition)". Oxford United Press, New York, 1987.
- [16] A. Wolf. "Quantifying Chaos With Lyapunov Exponents". In Chaos, Ed. A. V. Holden, Princeton University Press, Princeton, New Jersey, 1986.
- [17] A. Wolf, J. B. Swift, H. L. Swinney, and J. A. Vastano. "Determining Lyapunov Exponents from a Time Series". *Physica 16D*, 16(3):285–317, July 1985.
- [18] M. Hénon. "A Two-Dimensional Mapping With a Strange Attractor". *Comm. Math. Phys.*, 50:69–77, 1976.
- [19] V. I. Oseledec. "A Multiplicative Ergodic Theorem. Lyapunov Characteristic Numbers for Dynamical Systems". *Trudy Mosk. Mat. Obsc.*, 19:179, 1968.
- [20] J. P. Eckmann and D. Ruelle. "Ergodic Theory of Chaos and Strange Attractors". *Reviews of Modern Physics*, 57(3):617–656, July 1985.
- [21] D. Ruelle. "Chaotic Evolution and Strange Attractors". Cambridge University Press, Cambridge, 1989.
- [22] D. S. Broomhead and G. P. King. "Extracting Qualitative Dynamics from Experimental Data". *Physica*, 20D:217–236, 1986.
- [23] P. Grassberger and I. Procaccia. "Measuring the Strangeness of Strange Attractors". *Physica D*, 9:189, 1983.
- [24] J. L. Kaplan and J. A. Yorke. "Preturbulence: A Regime Observed in a Fluid Flow Model of Lorenz". *Comm. Math. Phys.*, 67:93, 1979.
- [25] P. Frederickson, J. L. Kaplan, E. D. Yorke, and J. A. Yorke. "The Lyapunov Dimension of Strange Attractors". *Journal of Diff. Eqns.*, 49:185–207, March 1983.
- [26] P. Grassberger. "Estimating the Fractal Dimensions and Entropies of Strange Attractors". In Chaos, Ed. A. V. Holden, Princeton University Press, Princeton, New Jersey, 1986.
- [27] T. Matsumoto, L. O. Chua, and K. Tokumasu. "Double Scroll via a Two-Transistor Circuit". *IEEE Transactions on Circuits and Systems*, CAS-33:828–835, 1986.

- [28] T. L. Carroll and L. M. Pecora. "A Circuit for Studying the Synchronization of Chaotic Systems". *International Journal of Bifurcation and Chaos*, 2(3):659–667, 1992.
- [29] T. L. Carroll and L. M. Pecora. "Cascading Synchronized Chaotic Systems". *Physica*, 67D:126–140, 1993.
- [30] K. M. Cuomo and A. V. Oppenheim. "Synchronized Chaotic Circuits and Systems for Communications". Technical Report 575, MIT Research Laboratory of Electronics, November 1992.
- [31] K. M. Cuomo and A. V. Oppenheim. "Chaotic Signals and Systems for Communications". In *Proceedings IEEE ICASSP*, March 1993.
- [32] K. M. Cuomo and A. V. Oppenheim. "Circuit Implementation of Synchronized Chaos with Applications to Communications". *Physical Review Letters*, 71(1):65–68, July 1993.
- [33] K. M. Cuomo, A. V. Oppenheim, and S. H. Strogatz. "Synchronization of Lorenz-Based Chaotic Circuits with Applications to Communications". *IEEE Transactions on Circuits and Systems*, 40(10):626–633, October 1993.
- [34] K. M. Cuomo, A. V. Oppenheim, and S. H. Strogatz. "Robustness and Signal Recovery in a Synchronized Chaotic System". *International Journal of Bifurcation and Chaos*, 3(6), December 1993.
- [35] A. Gelb. "*Applied Optimal Estimation*". The M.I.T. Press, Cambridge Massachusetts, The Analytic Sciences Corporation, 1974.
- [36] R. W. Brockett. "System Theory on Group Manifolds and Coset Spaces". *SIAM Journal on Control*, 10(2):265–284, 1972.
- [37] A. S. Willsky, S. I. Marcus, and D. N. Martin. "On the Stochastic Stability of Linear Systems Containing Colored Multiplicative Noise". *IEEE Transactions on Automatic Control*, 20(5):711–713, October 1975.
- [38] A. S. Willsky and S. I. Marcus. "*Analysis of Bilinear Noise Models in Circuits and Devices*". 1974 IEEE International Symposium on Circuits and Systems, San Francisco, Calif., April 1974.
- [39] J. M. Kowalski, G. L. Albert, and G. W. Gross. "Asymptotically Synchronous Chaotic Orbits in Systems of Excitable Elements". *Physical Review A*, 42(10):6260–6263, November 1990.
- [40] I. Waller and R. Kapral. "Synchronization and Chaos in Coupled Nonlinear Oscillators". *Physics Letters*, 105A(4,5):163–168, October 1984.

- [41] R. R. Klevecz, J. Bolen, and O. Duran. "Self-Organization in Biological Tissues: Analysis of Asynchronous and Synchronous Periodicity, Turbulence and Synchronous Chaos Emergent in Coupled Chaotic Arrays". *International Journal of Bifurcation and Chaos*, 2(4):941–953, 1992.
- [42] P. Badola, V. R. Kumar, and B. D. Kulkarni. "Effects of Coupling Nonlinear Systems with Complex Dynamics". *Physics Letters A*, 155(6,7):365–372, May 1991.
- [43] N. F. Rulkov, A. R. Volkovskii, A. Rodriguez-Lozano, E. Del Rio, and M. G. Velarde. "Mutual Synchronization of Chaotic Self-Oscillations With Dissipative Coupling". *International Journal of Bifurcation and Chaos*, 2(3):669–676, 1992.
- [44] K. M. Cuomo. "Synthesizing Self-Synchronizing Chaotic Systems". *International Journal of Bifurcation and Chaos*, 3(5), October 1993.
- [45] K. M. Cuomo and A. V. Oppenheim. "Communications using Synchronized Chaotic Systems". *U.S. Patent Pending*, Serial No.: 07/989,703, December 1992.
- [46] A. S. Willsky. "Recursive Estimation". Course Notes For 6.433, 1989.
- [47] U. Parlitz, L. Chua, Lj. Kocarev, K. Halle, and A. Shang. "Transmission of Digital Signals by Chaotic Synchronization". *International Journal of Bifurcation and Chaos*, 2(4):973–977, 1992.